

# **Exploring EEG Microstates During Motor Movements: A Study on Tip-pinch and Wrist flexion & extension**

Thesis submitted in partial fulfillment  
of the requirements for the degree of

*Master of Science in **Electronics and Communication Engineering** by Research*

by

SUPREETH S KARAN

20171311

supreeth.karan@research.iiit.ac.in



International Institute of Information Technology

Hyderabad - 500 032, INDIA

June 2023

Copyright © Supreeth S Karan, 2023  
All Rights Reserved

International Institute of Information Technology  
Hyderabad, India

## **CERTIFICATE**

It is certified that the work contained in this thesis, titled “**Exploring EEG Microstates During Motor Movements: A Study on Tip-pinch and Wrist flexion & extension**” by **Supreeth S Karan**, has been carried out under my supervision and is not submitted elsewhere for a degree.

---

Date

---

Adviser: Dr.Kavita Vemuri

I would like to dedicate this thesis to my parents

Shri. C Sudhakaran and Smt. Suneetha

and

My Senior, Ayushi Kumari Agrawal

## Acknowledgments

First and foremost, I thank Lord Ayyappa for constantly showering me with his blessings. I remain perpetually grateful and indebted for His divine grace. Prof. Kavita Vemuri is one of the best guides I've ever had, and I would like to express my most profound admiration and gratitude to her. I can't imagine finishing this project without her. I'll never forget the day she chose me as one of her research students. She has guided me at every stage of my academic life since then. She has always been very encouraging and clearly explained the concepts, and this work is a result of her confidence and belief in me. Her dedication and hard work have been a constant source of motivation for me to continue working freely in research. Having a guide like her is a stroke of luck. I would also like to thank everyone who volunteered to participate in the EEG experiments. They are the reason I could finish this study.

I would also like to thank my parents, Suneetha Menon and Sudhakaran Menon, for their unwavering support throughout my life. During my college years, my parents listened to everything that happened around me, and they deserve special appreciation for always making me feel special and loved. Words cannot adequately convey the depth of my appreciation for the affection and unwavering moral support I have received. They have always kept me going. My mother remained quite interested in my research, receiving daily updates on how the work was progressing and wanting to understand my study's broader ideas and concepts. I would not have accomplished this work without their assistance.

Many enthusiastic people that I met during my time in college helped me either directly or indirectly. Initially, I would like to express my appreciation to my wingmates (Aradhya Tongia, Harsh Sharma, Mudit Agarwal, Prajwal Krishna Maitin, Rishabh Singhal, Shashank Gadila, Sidharth Jain, Yash Chaurasia, Yashas Samaga). My college experience was truly memorable and delightful because of them; we had so much fun together. I enjoyed long, late-night conversations on a variety of topics. I also want to thank Arhant Jain for providing superb research suggestions. His advice helped me complete this project at a breakneck pace. Surendra, who has a cheerful demeanor, is always responsive, and is a well-wisher of mine, deserves my heartfelt gratitude. Because of you guys, I am taking away beautiful memories to remember for the rest of my life.

I want to thank my friend and brother Rishabh Singhal for always being there for me through thick and thin. He made invaluable contributions to my life that I'll never forget and helped me obtain academic success in college. No matter what it is, he makes an effort to research it and offer insightful comments. Our discussions on lifestyle, health, fitness, and investing are memorable. He believes in helping people to improve and was a constant source of inspiration to me. Many of our classmates

found his help cell sessions beneficial for exams when I pushed him to conduct them. He also helped me discover a new version of myself, and I will always be grateful for his presence in my life.

I am deeply thankful to Aradhya Tongia, who has been a great help to me during my college career. I'm glad to remember the wonderful time we had together. Above all, I admire him for his thoughtfulness and for investing time in carefully teaching ideas and concepts to students, including me. I consider myself fortunate to have met him; he exemplifies true friendship — as a lab partner with whom working was a delight, as a tutor who goes above and beyond to help, and as a caring soul who has made my life in college so easy.

I am grateful for Ayushi Agrawal's continued support throughout my research. We were only able to accomplish our research projects with her constant help. She has a wide range of life experiences and is really a kind and giving person. Talking with her opens up a new dimension, allowing us to perceive the world differently. She always encouraged and supported me in my paper writing and looked out for my well-being. She has a pleasing personality that brings people together and makes the lab a pleasant working space. I'll miss our discussions on traveling, soap operas, serials, cuisines, and cars.

I want to express my thanks to my senior, Dhriti Goyal, for her insightful recommendations. Thank you for sharing your experiences with me. I also express my gratitude towards Medha sharma and Naren Akash. A special thanks to my friends and lab members – Dhiraj, Srijia, Sravya, Srinivas, Vivek, Arhant Jain, Bhumika, Nikunj Nawal, Bhaiyya Vaibhaw, Tanvi Narsapur, Ritwik Kadari, Giri Prasath, Srivathsan Bhaskaran, Shantanu Agarwal, Karthik, Akash CR, Divyansh, Amey, Prateek, Prerak and Deepti for making my time at IIIT-H memorable. I am also thankful to my cheerful high school and junior college friends, with whom I still have wonderful memories.

I am grateful to the NBH mess staff, the South mess employees, the mess office, the housekeeping, the security guards, the esteemed Professors, and the College administration. I shall never forget the aroma of The delicious non-vegetarian biryani served at NBH mess Dining Hall; it will always have a special place in my heart. I also thank D. Rohan Reddy, Sourav Karmarkar, Prateek Saxena, Shastri Vaishampayan Mohapatra, Pragati Gupta, Bharath, Arpan, Pratyush, Divyanshu, and Swarnim for being thoughtful of me. They made my final year at IIIT quite memorable and provided me with a wealth of knowledge on various topics. During this time, we had many reading sessions, developed roadmaps for project completion, and had great fun. I am thankful to Rohan and Pragati for proofreading our journal submissions. I also want to express my gratitude to all the well-wishers who have contributed to this work, even anonymously.

## Abstract

The electroencephalography (EEG) technique measures scalp electrical activity with high temporal resolution; required to map the neuronal global functional brain networks supporting motor movements. The time series of the change in electric potential across electrodes is analysed using frequency (and/or) time domain methods. An alternate approach is to represent a dynamic system with states and transitions between them defined using microstates. These are quasi-stable (60-120 ms) scalp potential configurations that represent spontaneous EEG as a sequence of a small number of scalp potential field maps and provide insight into brain health exhibiting sub-second coherent activations of brain. The present study investigates microstates extracted from EEG signals of motor-tasks.

We investigate the extracted microstate parameters (occurrence, duration, coverage and no. of microstate) for Tip-pinch movement (index finger & thumb) and Wrist flexion & extension performed by both hands independently. These movements are selected due to its relevance in benchmarking rehabilitation of paretic arm post-stroke. The data was extracted from 17 electrodes (of a 32 channel EEG system) covering the pre-frontal, frontal, central and motor regions. Twenty-four right-handed and five left-handed healthy male subjects (age = 18-30 years; mean = 24.25 years; SD = 3.96 years) participate in this study.

The approach of analysing each dynamic variable (occurrence, duration, coverage, and number of microstate) values during pre-event, event, and post-event conditions with reported resting state microstates highlights the similarities or differences as a function of motor action. We identified new microstate topographies specific to each motor task. The number of microstates for both motor activities is independent of the handedness of the participant (right-handed and left-handed). Task dependent variation in the topography of the microstates is observed, deviating from the standard maps reported for resting state EEG. The tip-pinch movement for event condition demonstrates higher microstate class stability than Wrist flexion & extension, indicative of lower disruption in the processing for the former action.

The identification of disruptions or novel topologies for a task indicates the potential to function as a physiological marker, even considering the arguments on microstate's state change being discrete or continuous. The findings will serve as a template for future studies analysing data from stroke patients.

# Contents

Chapter	Page
1 Introduction . . . . .	1
1.1 Motor Movements . . . . .	1
1.2 Brain areas linked to motor movement . . . . .	2
1.3 Motor movement related brain activity . . . . .	2
1.4 Objective of the Study . . . . .	4
1.5 Scope of the Study . . . . .	4
1.6 Thesis Organisation . . . . .	5
2 EEG Microstates . . . . .	6
2.1 Introduction to Microstates . . . . .	6
2.1.1 Global Field Power of EEG signals . . . . .	8
2.1.2 How many clusters should be used, and why? . . . . .	8
2.1.3 Why choose EEG Microstates for EEG signal analysis? . . . . .	9
2.1.4 Microstate Variables . . . . .	10
2.2 Clustering algorithms for Microstate Segmentation . . . . .	11
2.2.1 K-means . . . . .	13
2.2.2 Modified K-means . . . . .	13
2.2.3 (Topographic) Atomize and Agglomerative Hierarchical Clustering . . . . .	14
2.3 Effective number of Microstates using measures of fit . . . . .	18
2.3.1 Global Explained Variance . . . . .	18
2.3.2 Cross-Validation Criterion . . . . .	20
2.3.3 Dispersion . . . . .	20
2.3.4 Krzanowski-Lai Criterion . . . . .	21
2.3.5 Normalized Krzanowski-Lai Criterion . . . . .	21
2.4 Microstate Clustering Parameters . . . . .	22
2.4.1 Multiple restarts of the algorithm . . . . .	22
2.4.2 Stopping Criteria:Convergence & Maximum Iterations . . . . .	22
2.5 Backfitting Microstates . . . . .	22
2.6 Temporal smoothing . . . . .	23
2.6.1 Windowed Smoothing . . . . .	23
2.6.2 Small Segment Rejection . . . . .	23
2.7 EEG Microstate Statistics . . . . .	23
2.7.1 Determining Microstate Classes using Microstate Toolbox . . . . .	25
2.8 Microstate analysis of our dataset . . . . .	25
2.8.1 Using Microstate Toolbox . . . . .	25

2.8.2	Using heuristics for determining the dynamic variables of Microstates in Pre-event, Event, and Post-event conditions . . . . .	26
3	Different Time-Frequency methods to analyze EEG . . . . .	28
3.1	Spectral Analysis . . . . .	29
3.2	Fourier Transform . . . . .	29
3.3	Wavelet Transform . . . . .	31
3.4	Hilbert Huang Transform . . . . .	33
3.4.1	Empirical Mode Decomposition . . . . .	33
3.4.2	Hilbert Spectral Analysis . . . . .	34
3.5	Single Frequency Filtering . . . . .	34
3.5.1	Single Frequency Filtering: Analysis of EEG Data . . . . .	35
3.6	Application of Single Frequency Filtering on our dataset . . . . .	37
3.6.1	Amplitude Analysis and Peak Plots (Electrode wise) . . . . .	38
3.6.2	Comparative analysis of 6 specific electrodes of major importance . . . . .	43
4	Decoding Wrist flexion & extension and Tip pinch Movements . . . . .	48
4.1	Background . . . . .	48
4.2	Methodology . . . . .	49
4.2.1	Participants . . . . .	49
4.2.2	Experimental Paradigm . . . . .	50
4.2.3	Pre-processing and Artefact Removal . . . . .	51
4.3	Data Analysis . . . . .	52
4.3.1	Microstate Extraction and Analysis . . . . .	52
4.3.2	Descriptive and Statistical Analysis . . . . .	54
4.4	Results . . . . .	55
4.4.1	The microstate topographies for each hand movement . . . . .	56
4.5	Microstate analysis based on comparing microstate parameters . . . . .	59
4.5.1	Pre-event, event and post-event conditions comparison in Wrist flexion & extension . . . . .	59
4.5.2	Comparison of Left- and right-handed participants for Wrist flexion & extension for NOM values (5 participants in each group) . . . . .	61
4.5.3	Pre-event, event and post-event conditions comparison in Tip-pinch . . . . .	61
4.5.4	Comparison of Left- and right-handed participants for Tip-pinch for NOM values (5 participants in each group) . . . . .	61
4.5.5	Comparing Wrist flexion & extension and Tip-pinch for NOM values . . . . .	61
4.6	Interpretation of Results . . . . .	62
4.6.1	Comparative analysis of the motor task topographies for all hand movements . . . . .	63
4.6.2	Microstate parameters' analysis for all hand movements . . . . .	64
5	Conclusion . . . . .	73
5.1	Findings . . . . .	73
5.1.1	Unique Contributions of this Research . . . . .	74
5.1.2	Limitations and Implications for Future Work . . . . .	74
	Bibliography . . . . .	76

<i>Appendix A: The role of individual physical body measurements and activity on spine kinematics during flexion, lateral bending and twist tasks in healthy young adults - Comparing marker(less) data</i>	
data	123
A.1 Background and Literature Survey	123
A.2 Abstract	127
A.3 Introduction	128
A.4 Measurement Techniques	129
A.5 Scope of the work	130
A.6 Marker-based motion capture system using Opti-track cameras	130
A.6.1 Methodology	131
A.6.1.1 Participants	131
A.6.1.2 Experimental Paradigm	131
A.6.1.3 Data Analysis	131
A.6.1.3.1 Spine Motion Analysis	132
A.6.1.3.2 Knee/Hip Motion Analysis	133
A.6.1.3.3 Statistical Analysis	134
A.6.2 Results	134
A.6.2.1 Descriptive Statistics	134
A.6.2.1.1 Spine Flexion, lateral Bend and Twist Analysis	134
A.6.2.1.2 Hip-knee segment displacement in a squat	135
A.6.2.2 Inferential Statistics	135
A.6.2.2.1 Comparative analysis of Angular Displacement in Spine Flexion	135
A.6.2.2.2 Comparative analysis of Angular Displacement in Spine Lateral Bend	136
A.6.2.2.3 Comparative analysis of Angular Displacement in Spine Side twist	137
A.6.2.2.4 Comparative analysis of Angular Displacement in Squats	137
A.6.2.2.5 Spearman Correlation of BMI, WHR and physical activity level with angular displacements of spinal columns	137
A.6.2.2.6 Seed-based correlation analysis of participants	138
A.7 Marker-less motion capture system using a single RGB camera	138
A.7.1 Methodology	138
A.7.1.1 Experimental paradigm	138
A.7.1.2 Data Extraction	138
A.7.1.3 Data Analysis	139
A.7.2 Results	139
A.7.2.1 Comparative analysis - marker-less & marker-based data	139
A.8 Discussion	140
A.9 Conclusion	143
A.10 Limitations	144

## List of Figures

Figure	Page	
2.1	Microstate Classes A,B,C and D as labelled by Koenig based on spatial similarity on original cluster maps . . . . .	9
2.2	GFP Flow Chart - the microstates & GFP is of 1 participant for the flexion exercise of the left hand . . . . .	11
2.3	Flowchart of Clustering Procedure of Microstates . . . . .	12
2.4	Microstate Analysis . . . . .	27
3.1	Power Spectral Analysis for a motor task performed by a participant. The legend shows the corresponding 17 electrode channels. The high power (peak) in alpha band shows coordination of the visual and the motor cortex to execute the motor task while feeling calm and relaxed. . . . .	30
3.2	2-D peak visualization of the Hilbert Huang Spectrum of channel <b>Fz</b> EEG electrode . .	33
3.3	3-D peak visualisation of the Hilbert Huang Transform of channel <b>Fp1</b> EEG electrode	35
3.4	This is the Peak Signal-to-Noise ratio plots of the four movements executed by an individual. <b>a.</b> Left Wrist flexion & extension <b>b.</b> Right Wrist flexion & extension <b>c.</b> Left tip-Pinch <b>d.</b> Right tip-Pinch . . . . .	36
3.5	3-D peak visualisation of the Single Frequency Filter of channel <b>Fp1</b> EEG electrode .	37
3.6	Comparison of EEG electrodes based on amplitude for <b>Left Wrist flexion &amp; extension</b> movement. This is an electrode-wise (C3, C4, CP1, CP2, CP5, CP6, F3, F4, F7, F8, FC1, FC2, FC5, FC6, FP1, FP2, Fz) illustration of the pre-event, event, and post-event conditions for all 29 participants. . . . .	39
3.7	Comparison of EEG electrodes based on amplitude for <b>Right Wrist flexion &amp; extension</b> movement. This is an electrode-wise (C3, C4, CP1, CP2, CP5, CP6, F3, F4, F7, F8, FC1, FC2, FC5, FC6, FP1, FP2, Fz) illustration of the pre-event, event, and post-event conditions for all 29 participants. . . . .	40
3.8	Comparison of EEG electrodes based on amplitude for <b>Left Tip-pinch</b> movement. This is an electrode-wise (C3, C4, CP1, CP2, CP5, CP6, F3, F4, F7, F8, FC1, FC2, FC5, FC6, FP1, FP2, Fz) illustration of the pre-event, event, and post-event conditions for all 29 participants. . . . .	41
3.9	Comparison of EEG electrodes based on amplitude for <b>Right Tip-pinch</b> movement. This is an electrode-wise (C3, C4, CP1, CP2, CP5, CP6, F3, F4, F7, F8, FC1, FC2, FC5, FC6, FP1, FP2, Fz) illustration of the pre-event, event, and post-event conditions for all 29 participants. . . . .	42
3.10	Amplitude values for <b>Left Wrist flexion &amp; extension</b> . . . . .	44
3.11	Amplitude values for <b>Right Wrist flexion &amp; extension</b> . . . . .	45

3.12	Amplitude values for <b>Left Tip-pinch</b> . . . . .	46
3.13	Amplitude values for <b>Right Tip-pinch</b> . . . . .	47
4.1	EEG recording system Brain Vision actiCHamp amplifier with BrainVision Recorder . . . . .	50
4.2	The 10-20 International System of Electrode Placement . . . . .	51
4.3	Experiment Paradigm Design . . . . .	52
4.4	3D view of location of scalp electrodes . . . . .	53
4.5	Flow Chart representation of Pre-processing steps and Microstate Analysis of the EEG data . . . . .	54
4.6	Electrodes covering the Pre-frontal, Frontal, Central and Motor regions of brain . . . . .	55
4.7	GFP of the active microstates for (a) Left Wrist-flexion & extension (b) Right Wrist-flexion & extension (c) Left Tip-pinch (d) Right Tip-Pinch. . . . .	56
4.8	Left Wrist flexion & extension all participants Global Explained Variance . . . . .	57
4.9	Right Wrist flexion & extension all participants Global Explained Variance . . . . .	57
4.10	Left Tip-pinch all participants Global Explained Variance . . . . .	58
4.11	Right Tip-pinch all participants Global Explained Variance . . . . .	58
4.12	Wrist Flexion & Extension Spider plots for the left and right hand movements. (a) Occurrence (b) Duration (c) Coverage for the left hand & (d) Occurrence (e) Duration (f) Coverage for the right hand . . . . .	60
4.13	Tip-pinch Spider plots for the left and right hand movements. (a) Occurrence (b) Duration (c) Coverage for the left hand & (d) Occurrence (e) Duration (f) Coverage for the right hand . . . . .	62
4.14	Power spectral density for a left-handed and a right-handed participant. (a) left_wrist_flexion_by_left-handed-participant (b) right_wrist_flexion_by_left-handed-participant (c) left_wrist_flexion_by_right-handed-participant (d) right_wrist_flexion_by_right-handed-participant . . . . .	65
4.15	Left Wrist flexion & extension for a group of 5 participants (a) right-handed participant set-1 (b) right-handed participant set-2 (c) left-handed participant set . . . . .	69
4.16	Right Wrist flexion & extension for a group of 5 participants (a) right-handed participant set-1 (b) right-handed participant set-2 (c) left-handed participant set . . . . .	70
4.17	Left Tip-Pinch for a group of 5 participants (a) right-handed participant set-1 (b) right-handed participant set-2 (c) left-handed participant set . . . . .	71
4.18	Right Tip-Pinch for a group of 5 participants (a) right-handed participant set-1 (b) right-handed participant set-2 (c) left-handed participant set . . . . .	72
5.1	Spider plot Occurrence parameter for left Wrist flexion & extension . . . . .	108
5.2	Spider plot Occurrence parameter for right Wrist flexion & extension . . . . .	109
5.3	Spider plot Duration parameter for left Wrist flexion & extension . . . . .	110
5.4	Spider plot Duration parameter for right Wrist flexion & extension . . . . .	111
5.5	Spider plot Coverage parameter for left Wrist flexion & extension . . . . .	112
5.6	Spider plot Coverage parameter for right Wrist flexion & extension . . . . .	113
5.7	Spider plot Occurrence parameter for left tip-pinch . . . . .	114
5.8	Spider plot Occurrence parameter for right tip-pinch . . . . .	115
5.9	Spider plot Duration parameter for left tip-pinch . . . . .	116
5.10	Spider plot Duration parameter for right tip-pinch . . . . .	117
5.11	Spider plot Coverage parameter for left tip-pinch . . . . .	118

5.12 Spider plot Coverage parameter for right tip-pinch . . . . .	119
A.1 (A)Marker placement covering the spine column. A Velcro strip with retro-reflectors affixed was prepared for ease of fixing on the suit. The vectors from the selected base marker are shown in the inset and the estimated angle " $\theta$ " between both positions. (B) The point light capture of the initial position and the flexion exercise. (C) the cartoon representation of the squat exercise and the vector from the spine column to the reflector on the patella of the knee. (D) Approximation of S-shaped spine curvature using vector analysis. Subset images: (i) Last sensor on the lower back as reference (Base) marker (ii) Vectors formed by connecting all the markers with the base marker for the first frame (upright position) (iii) All vectors in the maximum angular displacement frame relative to the first frame in spine flexion exercise (bent position). . . . .	132
A.2 Sample of the temporal sequence of the spine movement of a participant for 3 trials with respect to each frame for marker-based motion capture system. (A) Spine Flexion (B) Spine Lateral Bend - left and right- three trails each (C) Spine Side Twist-clock and anticlock wise -three trails each (D) Squat exercise . . . . .	133
A.3 The angle estimates for the three spine segments and exercises. Flexion: (a) Male participants, (b) Female participants. Lateral Bend: (c) Male Participants, (d) Female participants. Twist: (e) Male participants, (f) Female participants . . . . .	135
A.4 The hip-knee segment angle for (a) male and (b) females. . . . .	136
A.5 Generated 3D Human skeleton for a single participant in spine flexion exercise. (A) Fitted 3D pose from 2D key-points. (B) Consolidated 3D pose visualized in blender tool.	139
A.6 Participant wise distribution of spinal column angles extracted from the RGB camera video for spine flexion exercise in (A) Males (B) Females. . . . .	140
A.7 Participant wise distribution of spinal column angles using marker-based motion capture for spine flexion exercise in (A) Males (B) Females. . . . .	144
A.8 Spinal columns' angle distributions for flexion for male participants based on (A) BMI (B) WHR . . . . .	145
A.9 Spinal columns' angle distributions for flexion for female participants based on (A) BMI (B) WHR . . . . .	145
A.10 Spinal columns' angle distributions for lateral bend for male participants based on (A) BMI (B) WHR . . . . .	145
A.11 Spinal columns' angle distributions for lateral bend for female participants based on (A) BMI (B) WHR . . . . .	146
A.12 Spinal columns' angle distributions for side-twist for male participants based on (A) BMI (B) WHR . . . . .	146
A.13 Spinal columns' angle distributions for side-twist for female participants based on (A) BMI (B) WHR . . . . .	147
A.14 Knee/hip angle distributions for squats for male participants based on (A) BMI (B) WHR	147
A.15 Knee angle distributions for squats for female participants based on (A) BMI (B) WHR	147
A.16 Participant wise distribution of knee/hip angles estimated using marker-less RGB motion capture system for squats exercise in (A) Males (B) Females . . . . .	148
A.17 Spearman's correlation matrix for spine flexion, lateral-bend and physical parameters for males . . . . .	148
A.18 Spearman's correlation matrix for spine side-twist, squats and physical parameters for males . . . . .	149

A.19 Spearman’s correlation matrix for spine flexion, lateral-bend and physical parameters for females . . . . .	149
A.20 Spearman’s correlation matrix for spine side-twist, squats and physical parameters for females . . . . .	150

## List of Tables

Table	Page
2.1	Differences between <b>AAHC</b> and <b>TAAHC</b> algorithms . . . . . 15
2.2	Summary of Clustering Algorithms . . . . . 17
4.1	Microstate topographies for all motor tasks with their corresponding electrodes covering specific cortical areas. It is worth noting that we have specifically mentioned the brain regions that correspond to the conventional Koenig’s orientations while marked a ‘-’ for the ones that don’t. We have mentioned the respective electrodes covering the brain region for the topographies that do not match Koenig’s maps. The symbol ‘x’ denotes unmatched motor-task topographies discovered in our research . . . . . 59
5.1	Dominant/Least Microstate Classes in each state for Wrist flexion & extension and Tip-pinch movements for Occurrence, Duration and Coverage parameters. . . . . 92
5.2	Average NOM values for pre-, event-, and post conditions of both Wrist flexion & extension and Tip-pinch . . . . . 93
5.3	Set of Average NOM values for pre-event, event and post-event conditions for Left-Handed participants for both wrist flexion & extension and tip-pinch . . . . . 94
5.4	Average NOM values for pre-, event-, and post conditions of Left-handed participants executing Tip-pinch movement . . . . . 94
5.5	Average NOM values for pre-, event-, and post conditions of Right-handed(set1) participants executing Tip-pinch movement . . . . . 94
5.6	Average NOM values for pre-, event-, and post conditions of Right-handed(set2) participants executing Tip-pinch movement . . . . . 94
5.7	Average NOM values for pre-, event-, and post conditions of Left-handed participants executing Wrist flexion & extension movement . . . . . 94
5.8	Average NOM values for pre-, event-, and post conditions of Right-handed(set1) participants executing Wrist flexion & extension movement . . . . . 95
5.9	Average NOM values for pre-, event-, and post conditions of Right-handed(set2) participants executing Wrist flexion & extension movement . . . . . 95
5.10	P-values for Occurrence parameter of Microstates for Pre-Event, Event-Post and Pre-Post conditions . . . . . 96
5.11	P-values for Duration parameter of Microstates for Pre-Event, Event-Post and Pre-Post conditions . . . . . 96
5.12	P-values for Coverage parameter of Microstates for Pre-Event, Event-Post and Pre-Post conditions . . . . . 97

5.13	P-values for Occurrence parameter of Microstates for Pre-Event, Event-Post and Pre-Post conditions . . . . .	97
5.14	P-values for Duration parameter of Microstates for Pre-Event, Event-Post and Pre-Post conditions . . . . .	98
5.15	P-values for Coverage parameter of Microstates for Pre-Event, Event-Post and Pre-Post conditions . . . . .	98
5.16	P-values for Occurrence parameter of Microstates for Pre-Event, Event-Post and Pre-Post conditions . . . . .	99
5.17	P-values for Duration parameter of Microstates for Pre-Event, Event-Post and Pre-Post conditions . . . . .	99
5.18	P-values for Coverage parameter of Microstates for Pre-Event, Event-Post and Pre-Post conditions . . . . .	100
5.19	P-values for Occurrence parameter of Microstates for Pre-Event, Event-Post and Pre-Post conditions . . . . .	100
5.20	P-values for Duration parameter of Microstates for Pre-Event, Event-Post and Pre-Post conditions . . . . .	101
5.21	P-values for Coverage parameter of Microstates for Pre-Event, Event-Post and Pre-Post conditions . . . . .	101
5.22	Different MS classes' pre, event, and post condition values for the <b>Occurrence</b> parameter for the Wrist flexion & extension exercise . . . . .	102
5.23	Different MS classes' pre, event, and post condition values for the <b>Duration</b> parameter for the Wrist flexion & extension exercise . . . . .	103
5.24	Different MS classes' pre, event, and post condition values for the <b>Coverage</b> parameter for the Wrist flexion & extension exercise . . . . .	104
5.25	Different MS classes' pre, event, and post condition values for the <b>Occurrence</b> parameter for the Tip-pinch exercise . . . . .	105
5.26	Different MS classes' pre, event, and post condition values for the <b>Duration</b> parameter for the Tip-pinch exercise . . . . .	106
5.27	Different MS classes' pre, event, and post condition values for the <b>Coverage</b> parameter for the Tip-pinch exercise . . . . .	107
5.28	Left Wrist flexion & extension averaged values of <b>Occurrence</b> parameter . . . . .	108
5.29	Right Wrist flexion & extension averaged values of <b>Occurrence</b> parameter . . . . .	109
5.30	Left Wrist Flexion/Extension averaged values of <b>Duration</b> parameter . . . . .	110
5.31	Right Wrist flexion & extension averaged values of <b>Duration</b> parameter . . . . .	111
5.32	Left Wrist flexion & extension averaged values of <b>Coverage</b> parameter . . . . .	112
5.33	Right Wrist flexion & extension averaged values of <b>Coverage</b> parameter . . . . .	113
5.34	Left Tip-pinch averaged values of <b>Occurrence</b> parameter . . . . .	114
5.35	Right Tip-pinch averaged values of <b>Occurrence</b> parameter . . . . .	115
5.36	Left Tip-pinch averaged values of <b>Duration</b> parameter . . . . .	116
5.37	Left Tip-pinch averaged values of <b>Duration</b> parameter . . . . .	117
5.38	Left Tip-pinch averaged values of <b>Coverage</b> parameter . . . . .	118
5.39	Right Tip-pinch averaged values of <b>Coverage</b> parameter . . . . .	119
5.40	Statistically significant Occurrence values for Wrist flexion & extension and Tip-pinch . . . . .	120
5.41	Statistically significant Duration values for Wrist flexion & extension and Tip-pinch . . . . .	121
5.42	Statistically significant Coverage values for Wrist flexion & extension and Tip-pinch . . . . .	122
5.43	Microstate classes with highest parameter values for all hand movements . . . . .	122

A.1	Spearman coefficient ( $\rho$ ) of spine angular displacement with physical activity level for female cohort. The * indicate the statistically significant associations. . . . .	138
A.2	Spearman coefficient ( $\rho$ ) of spine angular displacement with physical activity level for the male cohort. The * indicate the statistically significant associations. . . . .	138
A.3	Spearman coefficient ( $\rho$ ) between marker-based and marker-less RGB systems angles for male and female participants. The number of * indicates statistical significance level ( $p>0.05$ ). . . . .	141

## *Chapter 1*

### **Introduction**

#### **1.1 Motor Movements**

Motor movements are facilitated by the extension or contraction of muscles controlled by the nervous system. They are initiated by signals from the brain, which travel down the spinal cord and into the motor neurons that innervate the muscles (cortico-spinal pathway). These signals trigger the release of neurotransmitters, which stimulate the muscle fibers to contract and produce movement. The study of motor movements is important for understanding the function of the nervous system, muscle health or atrophy as well as for diagnosing and treating disorders that affect movement, such as Parkinson's disease, cerebral palsy, and stroke.

Motor sub-movements are the fundamental components of the Central Nervous System and are detected in a variety of motor movements. Sub-movements are the elements of dynamic coordination that makeup motor behavior and may need complicated patterns of neuromuscular activity to initiate the dynamic process. They are the coordinated, smaller muscle movements that produce a larger, more complex movement. When we execute a movement, such as reaching for a cup or typing on a keyboard, our brain does not only send a single signal to our muscles, but movement is broken down into a sequence of smaller, more precise movements that work together to accomplish the overall movement. Motor primitives are fundamental building blocks of movement that are thought to be pre-wired in the nervous system. Their combination and modification allows for the wide range of movements that humans and animals are capable of. Understanding motor primitives is important for developing prosthetic devices, designing rehabilitation protocols, and studying the neural control of movement.

In our daily life, we execute a series of complex motor actions on a regular basis such as holding items, reaching, grasping things, etc., that are classified as either discrete or rhythmic movements [65]. Discrete movements are learned via experience, whereas rhythmic movements are more likely built in our brain's neural circuits. Different areas in the brain are involved in the execution of rhythmic and discrete movements [163]. Discrete movements require different neurophysiological and theoretical treatment [163], [217]. [66] suggested that sub-movements resemble discrete movements, except that they may have some temporal overlap, and are motor behavior's primitive dynamic elements. Discrete

movements are severely affected in stroke patients than rhythmic, especially if they are visually guided [92]. With effective rehabilitation most stroke affected patients could partially regain muscle strength and movement/control. The wrist and finger movements are considered for motor rehabilitation and therapists consider these as most essential hand movements. Tip pinch is a basic hand skill [34] that is developed through the integration of other motor primitives, such as wrist flexion, finger flexion, and opposition of the thumb. These basic movements are combined in a precise way to produce the tip pinch grip, which is important for activities also requiring fine movements such as writing, drawing, and using small tools. Our study uses EEG to investigate the brain signals for basic motor movements. Towards this, we study two hand motor tasks namely Tip-pinch and Wrist flexion & extension which are discrete in themselves but performed using a visual cue for a rhythmic response in our experimental paradigm. That is, the participants perform a motor task in a time locked 2-sec response window on the onset of a visual cue.

## **1.2 Brain areas linked to motor movement**

The brain regions involved in motor learning include tertiary motor areas (prefrontal cortex, cingulate cortex, pre-supplementary motor area), secondary motor areas and sensory associated areas (SMA proper, pre-motor cortex, inferior frontal cortex), parietal cortex (inferior parietal cortex, superior-posterior parietal cortex), cerebellum, and primary motor areas (primary motor cortex, basal ganglia). Amongst these, the primary motor cortex, the premotor cortex, the supplementary motor area, the basal ganglia, and the cerebellum are cited for motor movement. The primary motor cortex is responsible for the planning and execution of voluntary movements, while the premotor cortex is involved in preparing for movements and in the learning of motor skills. The supplementary motor area is involved in the coordination of more complex motor behaviors. The basal ganglia is involved in the initiation and control of movements, while the cerebellum helps with accuracy and precision.

In summary, motor sequences are attributed to a network consisting of the Supplementary Motor Area (SMA proper), the primary motor cortex, and the basal ganglia [60]. The cortex layer of the brain appears to encode muscle and kinematic synergies relevant to arm and hand motor activities [136], [102], [153]. The macroscale movement details are encoded in the premotor areas, contralateral primary motor cortex, and contralateral somatosensory cortex, all of which have direct connections to the spinal cord. Using the time-domain low frequency EEG signals, the motor tasks of upper limb movements can be decoded [134].

## **1.3 Motor movement related brain activity**

In order to be optimally prepared for processing the incoming stimuli, the brain is intrinsically active in an organised manner while at rest. This understanding of how brain processes information led

to the numerous studies examining the large-scale brain networks at rest, including their temporal dynamics, spatial organisation, and associations with cognitive states [113]. Spontaneous brain activity exhibits distinct spatiotemporal organization at the level of large-scale distributed neuroanatomical systems, however to what extent these are modified to support motor tasks is unclear. Patients with stroke exhibit motor impairments in the upper limb — arm and hand; and the optimal treatment for these patients is still unclear. Understanding how the brain relearns and recovers from injury is poorly understood [32]. Such cases require a deeper understanding of motor neuroscience for designing neurorehabilitation therapies.

Various techniques are utilised to unveil large-scale brain networks, leading to different interpretations of their spatial and temporal organisation. Electroencephalography (EEG) is a non-invasive and relatively inexpensive method of recording and measuring electrical activity in the brain by placing electrodes on the scalp. EEG signals help us in analysing brain & behavior based on the signal frequency classified for different conditions/stimuli such as resting state, cognitive tasks, sleep, physical movements like eye movement, hand movement, or motor activity. Researchers employ EEG to study how the brain functions during different motor tasks [18], [16], [5], [114], [119], [129], [57] by recording the brain's electrical activity through scalp electrodes. EEG (and Magnetoencephalography) can record variations on sub-second time scale and are better suited for examining the temporal dynamics of brain areas/networks and their impact on stimulus processing since these networks must reorganise into varying spatial patterns on sub-second time scale in order to mediate complex mental operations and adapt optimally to the quickly changing information [11]. The brain needs to efficiently process and interpret the time-varying stimulus (sensory inputs), which affects its development and functions [84], to maintain its plasticity which is crucial for cognitive and motor learning [86], [203]. This learning is facilitated by input from higher-level cortical regions to sensory regions [158] leading to neuroplasticity in the brain, and this newly acquired information modifies the neuronal maps, routes, and circuits comprising of billions of neurons and synapses [209], [23]. To learn more about the motor activities that support neuroplasticity, researchers examine brain activations measured using neuroimaging techniques and different signal analysis methods while performing upper limb motor tasks like simple finger tapping, finger flexion, extension, clenching, forearm movement, etc.

In addition to the analysis of the brain activity using time-frequency or frequency-phase analysis, the time series of electric potential change between these may be represented as a dynamic system with states and transitions. This alternative dynamic systems approach — microstate analysis [98] — gives the spatial distribution of the scalp electric potential at each time point resulting from continuous brain activity that can be parsed as quasi-stable(60-120ms) temporal segments in the sub-second range. These periods of quasi-stability of topographies are known as microstates and are better suited for detecting dynamic brain activity changes. Because we know so little about the temporal dynamics of large neural networks, using EEG microstates as a proxy for network activation is advantageous because their time scale coincides with the sub-second range of synchronous firing of these networks.

## 1.4 Objective of the Study

EEG microstates offer a simplified view of the brain's detection of various neural activations occurring at each time instant during movement execution [117]. Our exploratory study investigates the brain activation employing microstate analysis while performing upper-limb movements (functional hand/finger motor-tasks). In addition to the traditionally reported event condition, we compare EEG microstates across pre-event and post-event conditions to broaden the scope of existing research. We also introduce a novel condition-based microstate parameter, Number Of Microstates (NOM) that is magnitude oriented rather than being a classification on frequency, capturing the overall number of microstates across the condition.

Also, very little is known about the differences between left- and right-handed subjects' bilateral activations. We analyze each participant's variation in EEG microstates between the right and the left brain areas (prefrontal, frontal, central, and motor) electrodes for Tip-pinch and Wrist flexion & extension movements done by both hands separately. We extract the statistical parameters/characteristics (occurrence, duration, and coverage) of an individual's brain activations while executing motor tasks. Our findings provide new insights into disruptions in spontaneous dynamic activity in motor tasks and introduce a reference model to analyze upper limb motor skill disorders.

## 1.5 Scope of the Study

This study includes healthy individuals in the 19-25 years age group (all males) and attempts to understand the spatiotemporal characteristics of brain activity. Towards this, a within-subject comparative analysis of the activations in electrodes of twenty-nine subjects for the pre-event, event, and post-event conditions, as well as a microstate level analysis (with respect to microstate parameters—occurrence, duration, coverage, NOM) of both hand movements, is performed. Additionally, as an important addition to motor action research, we looked at the occurrence of EEG microstates in the left- and right-handed people with respect to NOM values by employing a between-subject comparison of the pre-event and post-event brain activity to study hemispheric laterality. We further performed a between-subject analysis of NOM values to see how motor movements done with one hand differed from each other. As NOM is a magnitude-oriented parameter that captures the total number of microstates in a condition, a range of NOM values extracted from healthy controls can be used as a baseline to compare the disruption in the microstates of a stroke patient in the first-level analysis. This can be followed by a second level analysis that examines traditional microstate parameters such as occurrence (a classification of frequency), duration, and coverage to obtain more specific information regarding the distribution and frequencies of these microstates. The original plan was to collect data from stroke patients which could not be done due to the covid pandemic.

In particular we investigate if the four labelled canonical resting-state EEG maps [82] remain intact during the hand/functional motor tasks. The observed task-dependent variance in the microstate topographies of each hand movement results in unaligned partial matches between our sets of topographies and Koenig’s labelled resting-state EEG maps. The additional orientations that emerge in our research provide a deeper understanding of the differences in brain activations of healthy subjects performing different motor tasks, as well as the differences in bilateral activations of left-handed and right-handed subjects performing the Tip-pinch and Wrist flexion & extension tasks. The novel addition was the occurrence of EEG microstates in left- and right-handed people by comparing the pre-event, event and post-event conditions of the task.

Following [179], many EEG channels may be redundant, therefore analysis may not require all 32 channels. Hence, we select a subset of 17 EEG channels covering the prefrontal, frontal, central, and motor areas and extract the temporal and spectral characteristics of the EEG signal. These findings aid in developing a reference model based on the obtained topographical information and the estimated microstate parameters.

## 1.6 Thesis Organisation

- This thesis is divided into five chapters, and each chapter contains sections aligned to it. The contents of *this chapter* cover the elementary introduction on motor movements, brain areas involved in motor movements, brain activity, EEG microstate analysis of motor movements, the objective of the study, and the scope of this study.
- *Chapter 2* discusses **EEG Microstates**, Clustering Algorithms for Microstate segmentations, Microstate Statistics and comparison of the dynamic variables of microstates across Pre-event, Event and Post-event conditions.
- *Chapter 3* talks about the different Time-Frequency methods to analyze EEG signals and includes EEG signal peak analysis using **Single Frequency Filter** and **Hilbert Huang Transform** methods. We also discuss EEGLAB toolbox in addition to Microstate toolbox plugin used for extraction of microstates.
- *Chapter 4* details the decoding of visually cued finger and wrist movements using microstate analysis from the experiments carried out in this study. In addition, this chapter discusses the procedures and findings from this research.
- *Chapter 5* provides the conclusions and summarizes this thesis. It covers practical applications, corresponding limitations, and possible extensions of this work.

## *Chapter 2*

### **EEG Microstates**

This chapter provides an introduction of an EEG signal analysis technique called ‘EEG microstates analysis’ (the transient, patterned, and quasi-stable states), focusing on its embeddedness and dependency on the momentary global functional states of the brain.

#### **2.1 Introduction to Microstates**

Due to the link between brain consciousness activity and the EEG signal, it is possible to identify distinct brain consciousness activity by classifying the EEG signal. The analysis of EEG signal can be performed using Frequency-domain (spectral) analysis, Time-domain (Linear prediction and component) analysis, Time-frequency domain (Wavelet Transform and Hilbert-Huang Transform) analysis, Non-linear methods and Artificial Neural Network methods (RNN and CNN). An alternative method, as introduced by [97], uses states and transitions which can describe the characteristics of the EEG signal. In this dynamical systems approach, state variables are the minimum number of variables needed to completely describe a dynamical system at any given time, while dynamics explain the modification of state characteristics. The states may be viewed in this respect as topographies of electric potential over all EEG electrodes, effectively giving a view of the spatial distribution of the electric potential on the scalp at each time point. This spatial configuration of the electric fields at the scalp characterizes EEG signals. So, studying EEG in this way entails defining momentary states (microstates) of the system based on some variables of interest and then describing variation in the brain activity in terms of how those states have evolved. These microstates carry the basic psychophysiological units of cognition and emotion, and reflect the momentary state of the brain’s global neuronal activity. The functional microstates lasting for shorter durations together constitute basic building blocks of mentation which are stationary or periodically stationary patterns of spatial distribution of the electric potential field of the brain [94] and are considered to be the “atoms of thought”. From a neurophysiological standpoint, phase-locked synchronisation of neural activity is viewed as a crucial method of information integration

in the brain. This phase-locked activity results in steady topography at the sensor level [200] leading to the detection of microstates.

As the temporal scale of EEG microstates corresponds to the sub-second range of synchronized firing of large neural networks, it is possible to detect and quantify the electrical brain activity via microstates as sub-second epochs with stable field topography for the analysis of shorter, transient EEG events. Microstates repeat multiple times in a second, and clustering of these microstates provides a series of short-lasting classes of brain electric states that account for a significant percentage of the data and enables the sequence of states to be analyzed [142]. Hence, microstates provide us the spatial distribution of the scalp electric potential at each time point resulting from continuous brain activity, parsed as quasi-stable(60-120ms) temporal segments, and are better suited for detecting dynamic brain activity changes. Microstate analysis of EEG signals aims at segmenting the time samples and grouping them into microstate classes based on their similar topographies.

Both resting state and task-state brain electrical activity can be described using EEG microstates. The syntax of time series of these microstates is packed with parameters of possible neurophysiological significance [77]. A microstate's average lifespan is regarded as indicative of the stability of its underlying neural assemblies. The frequency with which a given microstate occurs may represent the tendency of its underlying neural generators to get activated. A microstate's coverage and global explained variance (discussed later) are considered to indicate the relative time coverage of its underlying neural generators in comparison to others. The strength or degree of coordination of neurons in underlying neural generators may be reflected in the amplitude of a specific microstate. Lastly, the non-random probabilities of transition from one microstate to the next often suggest an encoded sequential activation of the microstate-generating neuronal assemblies. Previous research has shown that the long-term dependency of the microstate sequence is critically dependent on the variability of the individual microstate duration. Microstate parameters Occurrence, Duration and Coverage can be used to explain the dynamics of the brain [82].

The microstate labels, their duration and specific transitions between states is a function of cognitive conditions, tasks, age and pathologies [12], [99], [127], [77], [33], [116]. A study by [39] used microstate analysis and found smaller variance between the microstates with respect to duration and occurrence. Microstate's statistical characteristics have been shown to be extremely beneficial in providing information on how the brain functions in relation to tasks and other behavioural, sleep, and rest conditions. Most importantly, changes in the temporal dynamics of certain microstates are a marker of disturbances in mental processes linked with neurological and psychiatric disorders [113] and have prompted their use in diagnosing a variety of medical conditions like **sleep disorder** [13], **anxiety disorder** [79], **mood disorder** [184], **bipolar disorder** [95] and **neurogenerative disorder** [61], [126], [133]. Changes in Microstates have been also investigated in case of **schizophrenia** [188], [95], **GTS syndrome** [215], **alzheimer** [180], **parkison** [139], **mild cognitive impairment** [126] and **acute stroke** [193]. Microstates are also recognised as a promising tool for studying the temporal dynamics of the brain during the execution of voluntary or instructed motor tasks [220].

### 2.1.1 Global Field Power of EEG signals

For a given microstate, the percentage of total variance covered is defined as global explained variance (GEV) of that microstate. The variance of EEG activity explained by all four microstates is also known as explained variance. The frequency of occurrence indicates how many times a microstate class is recurring per second, and the global explained variance is the sum of explained variances of each microstate weighted by the global field power(GFP). The integrated electrical activity in a topographical map of electric potential may be quantified using Global field Power by computing a form of spatial standard deviation. The Global Field Power is the root mean of the squared potential differences at all K electrodes divided by the mean of instantaneous potentials across electrodes. It is mainly used to describe global brain activity.

$$GFP = \sqrt{\frac{\sum_{i=1}^N (x_i - \bar{x}_i)^2}{N}} \quad (2.1)$$

where,

$x_i$  is the voltage at electrode i

$\bar{x}_i$  is the average voltage of all electrodes

N is the number of electrodes

During microstate analysis, topographies of the electric field at local maxima of the GFP curve are considered discrete states of the EEG.

### 2.1.2 How many clusters should be used, and why?

Although there may be a large number of potential maps in an EEG signal recording, the majority of the signal is represented by only a few topographies, which generally cover more than 70% of the variance [98]. These four maps topographies span across the specific regions: left occipital to right frontal, right occipital and left frontal, symmetric occipital to prefrontal and symmetric fronto-central to occipital, which are labelled as A, B, C, and D [77]. Most studies of resting-state EEG microstates find this same **set of four cluster maps**, labelled A-D by [83], that serve as canonical "microstate maps" as seen in Figure 2.1.

These maps are stable and do not overlap with other maps for a significant duration. Previous research by [206] found that most segments belonged to a limited number of classes (range: 2-6 classes; mean: 3.7 classes for 90% of analysis of time) and used an agglomerative clustering approach to determine the most dominant classes of centroid locations.

As the cortical potential exhibits distinct patterns that change over time in the spatial domain, several alternative methods for cluster or factor analysis can be used **to determine the most dominant spatial components in map series**. Using data reduction or clustering techniques, EEG microstate analysis

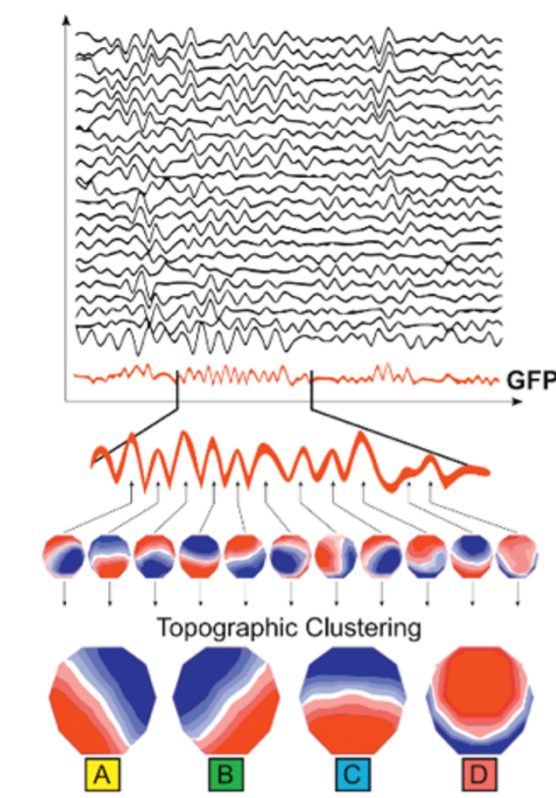


**Figure 2.1** Microstate Classes A,B,C and D as labelled by Koenig based on spatial similarity on original cluster maps

aims to characterize these patterns. The majority of the existing literature on microstate analysis is based on methods developed from classical clustering algorithms such as Modified K-means [142], Atomize and Agglomerate Hierarchical clustering (AAHC) [123], Principal Component analysis(PCA) & Independent Component analysis(ICA). Studies by [178], [181], [182], [30], [218] have incorporated the clustering algorithms in elucidating relationship between microstates against resting-states which were used for analyzing the measured Event Related Potentials extracted using EEG.

### 2.1.3 Why choose EEG Microstates for EEG signal analysis?

Firstly, as spatial EEG signal analysis employing microstates includes signals from all electrodes at the same time, establishing a global representation of functional state makes it better suited for detecting fast and dynamic activity in large-scale neurocognitive networks than other traditional signal analysis methods. Secondly, microstate time series offers many new quantitative approaches for EEG signals and may be neurophysiologically relevant. Parsing the EEG into microstates can also be used to pick periods of interest corresponding to a class of microstates for further analysis, such as time-frequency analysis. So, EEG microstate analysis is a useful, cost-effective, reliable and clinically explicable neurophysiological method for examining large-scale neural networks and time-dependent network activity.

Thirdly, the majority of the signal (often 70-80%) is represented by an astonishingly small number of topographies that do not overlap in time and reveal a global pattern of signal coherence among electrodes throughout the entire scalp. [29] analyzed the EEG data solely based on topographic information. The template maps obtained by them using this information, extracted in response to each stimulus, were very similar to the microstates found in their ERP analysis of the same data. Their findings provide compelling evidence that Event Related Potentials (ERPs) are reliably detectable at a single-trial level when evaluated topographically.

### 2.1.4 Microstate Variables

Global Field Power can be used to determine the total scalp activity of the specified electrode channels. It may be utilised as a parameter for EEG data analysis by either segmenting the data into microstates of information processing or finding latencies and/or identifying the data with the least amount of electric field strength [112]. GFP can be used to detect the brain activity recorded by all the scalp electrodes and the latencies of the evoked potential components are determined using the occurrence times of GFP maxima. When the GFP peaks are extracted and the topography maps are subjected to cluster analysis, the clustering algorithm groups these topographic maps into a small set of classes based on topographic similarity, regardless of the order in which they appear; then, the topography at each GFP peak is labelled as one of these microstate classes, and the EEG signal is re-expressed as a sequence of microstate classes. We have taken as sample from our dataset and extracted GFP and microstates for a participant as an example, Figure 2.2, to illustrate this extraction procedure.

A study by [127], [218] determined different microstate classes using ICA(Independent Component Analysis). The backfitting procedures assigns labels to each EEG sample based on the prototype they are most topographically similar with and further during clustering the microstate classes are generated with their respective labels, and the statistical parameters related to these classes are defined in terms of occurrence, duration, coverage, and transition probabilities.

These Microstate parameters include:

1. The average time it takes for a certain microstate to appear and remain stable [97].
2. The frequency of **Occurrence** of each microstate is defined as the average number of times per second that the microstate becomes dominant during the recording period.
3. **Duration** is defined as the average time in milliseconds that a specific microstate is present.
4. The **Coverage** of a microstate is the proportion of total recording time when the microstate is dominant.
5. The probability of a microstate transitioning to another microstate, as well as the sequence of transitions among microstates, determine the **Transition probabilities**, which are not random and are potentially significant [96].

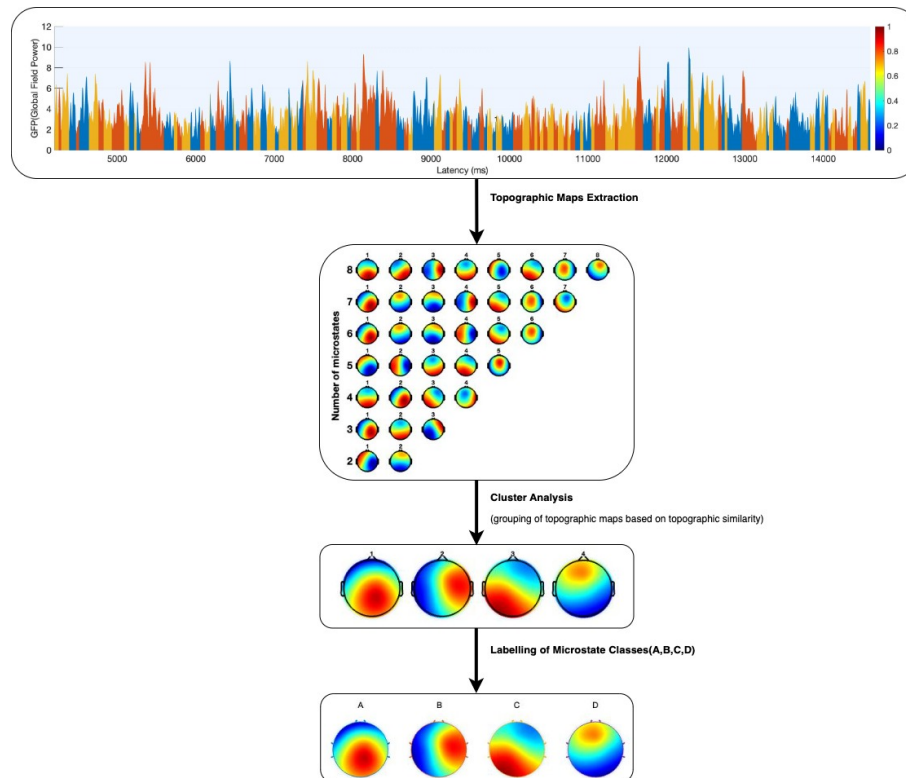


**Figure 2.2** GFP Flow Chart - the microstates & GFP is of 1 participant for the flexion exercise of the left hand

The average GFP during a dominant microstate class defines the amplitude of each microstate [183], [132]. The percentage of overall variation explained by a specific microstate class is defined as the global explained variance of that microstate class [14]. Therefore, Microstate analysis quantifies changes in brain state in terms of changes in these parameters. Further these parameters can be retrieved and used for additional inference and analysis due to their richness in neurophysiological relevant factors.

The further sections discuss about the different clustering algorithms, different measures of fit to determine effective microstates, microstate clustering parameters, assigning of microstate labels (back-fitting), temporal smoothing techniques and calculation of microstate statistics which provides an easy entry point into microstate analysis.

## 2.2 Clustering algorithms for Microstate Segmentation

Various clustering techniques are often used to identify EEG microstates, and the results vary based on the methodology and settings used. In general, different mathematical and statistical approaches exist for data clustering which result in distinct clustering algorithms. The different clustering algorithms and optimal settings for better evaluations are discussed here, as well as various approaches to find the best

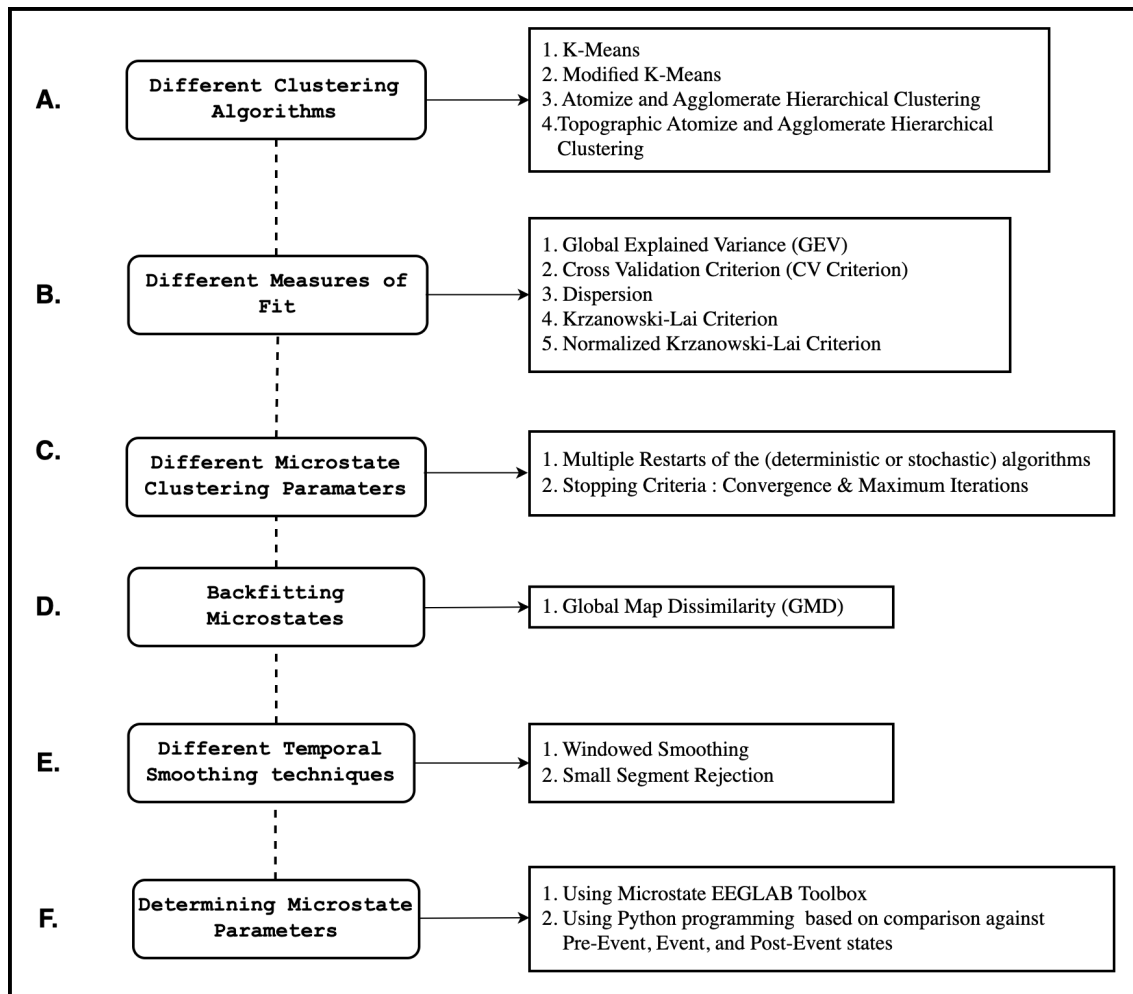


**Figure 2.3** Flowchart of Clustering Procedure of Microstates

solution and evaluating it. Often there is not one true solution that segments the EEG perfectly, so it becomes necessary to decide how many number of microstate clusters are required to achieve the best result. If the same method is applied and run multiple times with the same number of clusters, various segmentations may be generated. To limit variability, we employ distinct algorithm initializations and multiple restarts. Clustering Algorithms such as K-means, Modified K-means, Principal Component Analysis, Hierarchical Clustering, Agglomerative clustering, and Gaussian mixture models can be used to find the prototypical microstate maps. The difficulty with any clustering method is determining the appropriate number of clusters, which involves a trade-off between the number of clusters and their quality, and each of these criterion has its own drawbacks. Based on previous researches, below sections explain the working of these algorithms and mention how effectively they cluster the data in comparison to other techniques in the same field.

### 2.2.1 K-means

K-means clustering is a well-known clustering technique. It is an algorithm used for Unsupervised Machine Learning. It belongs to one of two major types of clustering methods known as partitioning methods, which normally require a user-specified number of clusters. It divides the unlabeled dataset into the determined clusters. Here K defines the number of pre-defined clusters that are to be generated during the process. The number of clusters can also be defined as microstate classes. K-means partitions the EEG signals into fixed number of clusters as determined and redistributes the EEG samples used in iterations until an optimum cluster assignment is found.

[157] stated K-Means clustering as a solution for analysis of spectral microstates maps of EEG as it avoids any arbitrary definition of frequency bands and takes into account power changes in the entire spectrum rather than the independent modulation of oscillations at specific frequencies.

K-cluster centers are defined by the start of the clustering process by choosing K samples at random. The k-means clustering algorithm is a two step process : It first allocates each EEG sample to the cluster with the most similar prototype, and it then recalculates cluster prototypes, which is commonly done by averaging across the newly assigned samples. The algorithm iterates over these two steps until the convergence criteria is reached. Convergence is the point at which it controls the smallest changes in the cluster centres, and convergence criteria is the point at which iteration ends. The procedure is terminated when the redistribution of EEG samples across iterations reaches a predetermined threshold or when a defined number of iterations is reached. The K-means algorithm has the advantages of being simple, easy to use, guaranteed convergence, formation of clusters with different sizes and shapes and efficient to perform.

From a probabilistic point of view K-means is consistent with the propagative model.

$$x_n = a_{ln} + \epsilon_n, \text{ for } n = 1 \dots N, \quad (2.2)$$

where  $a_{ln}$  signifies the topographical map assigned to nth EEG sample.

Modifications to K-means clustering are possible, for instance, by altering how prototypes are initialised or how similarity is calculated.

### 2.2.2 Modified K-means

[141] proposed modified K-means which includes new clustering features. Modified K-means finds the most prototypical topographies and, similar to the standard K-means method, starts by randomly choosing K topographic maps. The modified K-means method requires less iterations than the normal K-means algorithm and has a strong theoretical foundation in the K-means iterative procedure. In comparison to the conventional K-means there are mainly two practical differences. The first is that the prototype microstates' topographical maps are polarity invariant. This means that the samples with

opposite topographical maps (eg.,  $a_k$  and  $-a_k$ ) are grouped in the same cluster. The second difference is, for each time point it models the strength of the microstates.

On the conceptual side, clusters are considered as ‘directions’ in a multidimensional topographical space, and activations measure how far along a microstate-orientation of the EEG signal is at a particular time point. It is easy to understand which EEG signal might draw an asterisk in 2D space when two EEG signals are used. Each line depicts a microstate and along the line, time points with a strong EEG signal are placed. Taking a probabilistic view point, modified K-means is consistent with the generative model.

$$x_n = Az_n + \epsilon_n, \text{ for } n = 1 \dots N, \quad (2.3)$$

with the important constraint at each time point that only one microstate can be functional i.e., all  $K$  elements of  $z_n$  are zero except for one, i.e, the model can be written as

$$x_n = a_{l_n} z_{l_n} + \epsilon_n, \text{ for } n = 1 \dots N. \quad (2.4)$$

Microstate index,  $k$ , is the microstate label of the EEG sample which reduces the orthogonal squared Euclidean distance.

$$l_n = \arg \min_k \{d_k n^2\} \quad (2.5)$$

$$d_k n^2 = x_n^T \cdot x_n - (x_n^T \cdot a_k)^2. \quad (2.6)$$

To prevent short segments, modified K-means algorithm with temporal smoothing microstates label sequences is used.

In order to investigate how cognition and performance are related to skill acquisition, [208] utilizes EEG microstates to identify brain state changes. They use Modified K-means technique for analysis, stating a provision of better understanding of the relationship between cognitive processes, performance and skill acquisition as the rationale.

### 2.2.3 (Topographic) Atomize and Agglomerative Hierarchical Clustering

TAAHC is a microstate analysis algorithm that was developed after the atomize and agglomerate hierarchical clustering algorithm (AAHC). These algorithms differ from conventional hierarchical clustering algorithms. [56] apply AAHC algorithm to cluster the original EEG microstate maps and find it more efficient over the other techniques. AAHC is an iterative classification method. The difference between AAHC and TAAHC Table 2.1 is how they measure the characteristics of their clusters, and the results obtained from these methods differ significantly. As a hierarchical clustering technique, TAAHC can result in increase of size of few clusters which leads to the snowball effect as stated by [124]. The AAHC approach was developed to overcome the snowball effect, which conflicts with the identification

of short periods of steady topography. Contrary to TAAHC, AAHC selects the worst cluster rather than merging clusters and assign each data point to the cluster to which they are most comparable.

[159] provide valuable insights on different types of hierarchical clustering. In hierarchical clustering, pairs of clusters from each data point are merged into a single cluster. Because it is a bottom-up technique, the cluster hierarchy is represented as a tree structure. In contrast to modified K-means, the user doesn't have to enter the number of clusters here. [152] uses TAAHC on the extracted EEG topographies at peaks of GFP to cluster the topographies at local maxima of GFP based on topographic similarity while ignoring the polarity. EEG samples have their own clusters, which is then removed one at a time during the process. In each iteration of the algorithm, it finds the worst cluster and then removes it. These clusters are then reassigned with each of its members to the clusters they are similar with, and the same process continues until there are only two clusters remaining. The lowest sum of correlations between its members and prototype is defined as "worst cluster". TAAHC is polarity invariant when the correlation is expressed in absolute terms. TAAHC can be considered as the specialized K-means since it already comes under specialized hierarchical clustering.

$$CorrSum(k) = \sum_n^N Corr(a_k, x_n) = \sum_n^N \frac{|x_n \cdot a_k|}{||x_n|| \cdot ||a_k||} \text{ for } l_n = k. \quad (2.7)$$

As TAAHC is a stochastic algorithm, to ensure determinism, the clusters are initialized by constructing two-sample clusters from the highest correlated pairs. The TAAHC algorithm accomplishes the following tasks in the toolbox used in this study. Correlations are determined between all sample pairs, with the highest correlated pair allocated to the first cluster and the remaining two samples removed from the existing sample pool. The process is then reiterated on the remaining sample-pool until all pairs are located and the number of clusters is reduced by half. If an odd number of samples are present, they are assigned to their own single-sample cluster.

$$GEV(k) = \sum_n^N GEV_n, \text{ for } l_n = k. \quad (2.8)$$

Members of the removed clusters can join in different clusters in AAHC. The primary difference between TAAHC and AAHC is the quality of the clustering.

AAHC	TAAHC
AAHC uses Global Explained variance (for measuring the quality of clusters)	TAAHC uses Sum of Correlations
AAHC accounts for the strength of maps	TAAHC accounts for the similarities in topographic maps.
Single-member initialization in AAHC is deterministic	Single-member initialization in TAAHC becomes stochastic
It accounts for polarity	It is polarity invariant

**Table 2.1** Differences between AAHC and TAAHC algorithms

Because all clusters have a correlation of 1 with their prototypes and these are initialised by TAAHC when it is stochastic. It is extremely unlikely that two clusters have the identical GFP, implying AAHC determinism. AAHC has been incorporated to the toolbox.

In traditional hierarchical clustering, there are generally two methods for creating similarity measures irrespective of the number of members in the cluster. Either it is Considering the similarity be-

tween cluster prototypes or calculating the average of all pairwise similarities between cluster members. In comparison to traditional hierarchical clustering algorithms, TAAHC methods emphasizes on how similarity is measured or the way it determines the worst cluster. As previously described, TAAHC determines the worst cluster by summing the correlations or GEV determined for each cluster member. Clusters have been awarded for having more data points, even if they are a bad fit. Though AAHC was designed to dissolve the snowball effect, it has unknowingly generated a new type of snowball effect in its approach for determining which cluster to atomize. The impact of these differences has not been studied yet in the recent published papers.

A brief summary of all clustering algorithms is provided in Table 2.2

## Clustering algorithms comparison table

<b>K-means</b>	<b>Modified k-means</b>	<b>Topographic Agglomerative Hierarchical clustering (TAAHC)</b>	<b>Atomize and Agglomerate Hierarchical Clustering (AAHC)</b>	<b>Agglomerative hierarchical clustering</b>
a.) Number clusters (microstate classes) are pre-set by the users	a.) Topographical maps of the prototypical microstates are polarity invariant (samples with proportional and opposite topographical maps are assigned to the same cluster or ignores the polarity of the EEG topography)	a.) The user does not have to pre-set the number of clusters. It is identified as a specialized k-means and hierarchical clustering method; due to the way it models eeg signals	a.) AAHC finds the "worst" cluster, disbands (atomizes) it, and assigns each of its members to the cluster they are most similar to.	a.) Bottom-up hierarchical clustering, since it starts from the bottom with single-member clusters.
b.) Partitioning the EEG samples into the fixed number of clusters, until an optimal cluster assignment has been achieved	b.) Models the activations of the microstates, i.e., the strength of the microstates for each time point.	b.) It starts out with all EEG samples having their own cluster and then one cluster is removed at a time. Each iteration of the algorithm consists of finding the "worst" cluster, and then removing (atomizing) it and reassigning each of its members to the cluster they are most similar to. This process is then continued until there are only two clusters remaining (or a pre-set minimum number of clusters)	b.) In AAHC the worst cluster is defined as the one that has the smallest contribution to the quality of the clustering, as measured by the sum of global explained variance <sup>5</sup> (GEV) of its members The downside of using GEV is that we are not guaranteed to obtain the same segmentation every time the algorithm is run.	b.) The two most similar clusters are merged in each step, meaning that all of their members now belong to the same merged cluster
c.) It is defined by k-cluster centers (choosing k- eeg samples at random). It assigns each EEG sample to the cluster whose prototype it is most similar to. It then recalculates the eeg cluster prototypes. It is often done by averaging over the newly assigned samples.	c.) Faster and slightly better in representing EEG microstates.	c.) TAAC is polarity invariant. It uses a sum of correlations. It accounts for similarities of topography. It becomes stochastic.	c.) members of the removed cluster can join different clusters.	
d.) It takes polarity into account and is suitable to do ERP analysis	d.) Parameter of temporal smoothing microstates label sequences to avoid short segments	d.) polarity invariant	d.) AAHC is deterministic. The AAHC method uses GEV, which weighs the correlation by the global field power to find the worst cluster.	
	e.) Modified K-means seeks to optimize the CV criterion	e.) TAAHC optimizes for Corr Sum(k)	e.) AAHC optimizes for GEV	

**Table 2.2** Summary of Clustering Algorithms

## 2.3 Effective number of Microstates using measures of fit

The most crucial step in cluster analysis is determining the ideal number of groups or clusters which is a major challenge because many number of microstate clusters might explain the EEG data well. They are distinguished by measuring and validating how well the clusters explain the data. A large number of microstate clusters can provide information, making microstate maps which better visualize the data. To capture the main features of the data, all spatial decomposition methods need a certain number of clusters. Study by [199] discusses the issue of how effectively the clusters can measure and validate data. There exists many methods which have been proposed for estimating the number of clusters as mentioned in the following study [115]. So, measures of fit are needed to estimate the apt number of microstates.

Different Microstate segmentations exist in different signal components. When these microstate segmentations are stitched together or combined, they reconstruct the original EEG signal. The quality of these microstate segmentations may be estimated using various measures of fit or approaches. Selecting the number of clusters needed for analysis is a common strategy followed in the microstate analysis procedure. Further calculations are performed on the basis of four metrics of fit before making a qualitative choice. These metrics indicate the quality of the microstates' topographical maps.

These tests are provided in the MATLAB under Microstate EEGLAB toolbox. Users can develop their own custom tests for microstate prototypes selection. Individual developed tests help for analysis since the best prototypes are selected as per the requirements of their experiment design. Cross validation controls segmentations which only consider the neural activity recorded from the brain rather than the unrelated recording noise. Cross validation divides the EEG signal into the two different sets (training set and testing set) for calculating the microstate prototypes and testing how well the prototypes match this information in the original data.

In the below sections we discuss the five measures of fit and provide references for further discussion.

### 2.3.1 Global Explained Variance

Globally explained variance explains how the microstate prototypes fit the whole EEG data signal to which they are assigned to. It assesses the similarities of the microstate prototypes (cluster maps) to the original EEG data. [145] mention using GEV over microstate prototypes to identify how well the global template describes the whole dataset. GEV is used to calculate the optimum and effective number of cluster maps. It is a commonly used parameter that assesses how closely the microstates sequences approximate the original EEG dataset [123]. It also computes the percentage of data variation explained by a given set of microstate maps.

If the value of GEV is higher it is considered to be better. Greater the value of GEV more similarities exist between the maps and the EEG data. GEV can be calculated as Equation 2.9:

$$GEV_n = \frac{(Corr(x_n, a_{ln}) \cdot GFP_n)^2}{\sum_{n_1}^N GFP_{n_1}^2} \quad (2.9)$$

Where  $GFP_n$  is the global field power, calculated as the standard deviation across all electrodes of the EEG for the  $n^{\text{th}}$  time sample. GEV is the squared correlation between the EEG sample and its microstate prototype weighted by the EEG sample's fraction of the total squared GFP shown in Equation 2.10:

$$GEV_n = Corr(x_n, a_{ln})^2 \cdot \frac{GFP_n^2}{\sum_{n_1}^N GFP_{n_1}^2} \quad (2.10)$$

The GEV is calculated by adding all of the GEV values of the members in the specified cluster. The GEV measure of fit of the data is obtained by adding all of the GEV samples in the segmentation. The total global explained variance is the sum of GEV values across all microstate maps. Global Explained variance of microstates (in %) were calculated along with Fisher LSD tests by [151] for single word priming.

Many studies have considered GEV (Global Explained Variance) as a parameter that provides information about the variation and presence of the particular microstate map during different experimental tasks. Study by [13] found GEV and Coverage to be dependent on each other and had shown very similar results for EEG microstates of wakefulness and NREM (non-rapid eye movement). The longer time a map occupies over a particular epoched data, the more variance it explains. [36] examined how well microstate were present in different auditory and visual tasks using GEV and found for all conditions the GEV was more than 80%. The Explained variance varies with the number of microstates considered during the clustering. According to [172] they found 80% of variance when 15 microstates are considered. In all of their experimental conditions they found as the number of microstates increases, global explained variance also increases. Post-hoc analysis of their study revealed lower explained variance during eyes-open conditions against eyes-closed conditions, regardless of task. Study by [201] investigated the temporal characteristics of resting EEG microstates in schizophrenia and their association with prior symptoms. The temporal characteristic global explained variance in their study explains more than 80% of the variance. [27] identified seven state-specific networks/clusters/microstates that provided the best explanation for the data and accounted for 84.8% of the global explained variance. However, conventional maps A,B,C,D together explain around 60% of the variance, and in addition to these conventional maps, alternative maps E-G explain an additional 25% of the variance. Studies conducted by [113] and [77] found 80% of the variance in resting EEG conditions. Four Microstate classes explain nearly 80% of the variance of EEG brain activity.

After the extraction of the microstate prototypes/microstate classes, these were compared against the predefined [113] classes of microstate maps. Koenig labelled these maps as A, B, C, and D. The nomenclature was based on the topographies' spatial similarities, which closely resembled the maps.

As represented by [77] Figure 2.1 resting state data has been represented by four prototypical microstate classes and this seems to account for most of the variance (>70%).

Most studies have described around four topographies account for most of the variance (>70%) the four are: the right-frontal left-posterior(A), left-frontal right-posterior(B), midline frontal-occipital (C) and midline frontal topographies (D).

### 2.3.2 Cross-Validation Criterion

The Cross-Validation criterion (CV) was introduced by Pascual-Marqui in 1995. [15] apply Cross-Validation criterion to identify the number of clusters and claim that increasing the number of clusters beyond the one proposed by the cross-validation or other optimization criterion will not lead to new microstates that survive the statistical tests. This measure is related to the residual noise, and the goal is therefore to obtain a low value of CV.

$$CV = \hat{\sigma}^2 \cdot \left( \frac{C - 1}{C - K - 1} \right)^2, \quad (2.11)$$

where  $\hat{\sigma}^2$  is an estimator of variance of the residual noise which is calculated as :

$$\hat{\sigma}^2 = \frac{\sum_n^N x_n^T x_n - (a_{l_n}^T x_n)^2}{N(C - 1)} \quad (2.12)$$

### 2.3.3 Dispersion

The average distance between the cluster members of the same cluster can be calculated by using the technique called Dispersion. Dispersion reflects the compactness of a cluster when employed at the intra-cluster level and reveals the separation when measured at the inter-cluster level. Given K clusters, the microstates should be segmented into, the sum of squares between the members of each microstate cluster can be represented as  $W_k$  :

$$S_k = \sum_n^N \sum_{n'}^N \|x_n - x_{n'}\|^2, \quad l_n = k \wedge l_{n'} = k \quad (2.13)$$

$$W_k = \sum_k^K \frac{S_k}{2N_k} \quad (2.14)$$

$W_k$  is an error measure. As the number of clusters increases, dispersion monotonically decreases since the cluster prototypes can then be closer to its members. Therefore, it usually selects as many clusters as it wants and this by itself is not a good measure of fit.

The sum of squares obtained in Equation 2.13 takes polarity into account, hence it is not a polarity invariant measure. As a result, it is not an appropriate fit measure for polarity-invariant techniques like modified K-means and (T)AAHC.

### 2.3.4 Krzanowski-Lai Criterion

Krzanowski and Lai established the KL criteria in 1988 as a method of determining how many clusters to utilize based on the dispersion measure. [15] utilize the quality measure given by the Krzanowski-Lai criterion to set the optimal number of clusters such that an increase does not result in a significant gain in global quality. The optimal number of clusters indicates high KL values. The "elbow(L-corner)" pattern of the curve is used to determine the ideal number of clusters. When  $W_k$  drops monotonically, an "elbow" appears, after which the curve flattens. The elbow indicates that adding more clusters would have little impact at this point. The KL criteria is the detection of such an elbow by examining variations in  $W_k$ . Changes in  $W_k$  can be observed as:

$$DIFF(K) = (K - 1)^{2/C}W_K - 1 - K^{2/C}W_K \quad (2.15)$$

$$KL(K) = \left[ \frac{DIFF(K)}{DIFF(K + 1)} \right] \quad (2.16)$$

When a L-corner in the  $W_k$  curve occurs, the Krzanowski-Lai criteria attains high values. In the toolbox  $KL(K)$  is set to zero when  $W_k - W_{k-1}$  is positive.

KL is not a polarity invariant measure since it is based on  $W_k$ . For polarity invariant methods such as K-means and (T)AAHC, KL would not be a suitable measure of fit. KL can only be used in finding the L-corner in the curve, adjustments can be made based on finding the elbow in the curve of the measure optimized for by the chosen method/algorithm.

### 2.3.5 Normalized Krzanowski-Lai Criterion

Normalized Krzanowski-Lai criterion  $KL_{norm}$  was introduced by [123]. It calculates/computes the quality measure of the segmentation known as Dispersion(W).  $W$  tends to zero as the quality of the clustering improves, just as GEV approaches to one. The Normalized Krzanowski-lai criterion is defined as:

$$D_K = K^{2/C}W_K - (K + 1)^{2/C}W_{K+1} \quad (2.17)$$

$$KL_{norm}(K) = \frac{D_{K-1} - D_K}{(K - 1)^{2/C}W_{K-1}}. \quad (2.18)$$

The primary difference between Krzanowski-Lai and Normalized Krzanowski-Lai criterion is that the first one calculates the ratio of change in the dispersion function, whereas the latter finds the difference in the change of dispersion. Since  $KL_{norm}$  is not a polarity invariant measure, hence it might not be a suitable measure of fit for polarity-invariant methods such as modified K-means and (T)AAHC.

## 2.4 Microstate Clustering Parameters

The below sub sections briefly define the settings of clustering algorithms and their relevance.

### 2.4.1 Multiple restarts of the algorithm

Using deterministic approaches like K-means and Modified K-means run the risk of getting inferior results. Therefore, to make the algorithm stochastic, a common approach is to select random EEG samples. On multiple runs of this stochastic algorithm, multiple segmentations of the same dataset can be tested, and the best ones can be selected based on the Global Explained Variance. The only downside of this stochasticity is that after every run of the algorithm it does not guarantee to obtain the same segmentation.

By default, in our study for the analysis we have used **10** restarts in the toolbox. The number of restarts to utilize is a trade-off between computing time and the probability of convergence on the same optimal solution.

### 2.4.2 Stopping Criteria: Convergence & Maximum Iterations

Algorithms such as K-means consists of several steps in iterations. The iterations are limited to the value of stopping criteria which is based on the convergence threshold which is set to  $10^6$  in the toolbox. To ensure the trade-off between computation time and precision of the segmentation, the maximum number of repetitions before stopping must be defined. In the toolbox the default maximum number of iterations is set to **1000**.

## 2.5 Backfitting Microstates

Based on the chosen clustering method, computation performed for the following microstate analysis follows a “winner takes all” approach introduced by [142] known as back-fitting. Averaging trials cannot lower noise levels in spontaneous EEG recordings. Time samples of maximum GFP time curve are considered since they contain the “cleanest representations” of the microstate and after obtaining prototypes it is then relevant to see which microstate prototype they are most topographically similar with. Global Map dissimilarity is a measure used to calculate the similarities of the prototype’s topographies.

The GMD is invariant to the strength of the signal and instead compares how similar the topographical maps appear. For two EEG samples,  $x_n$  and  $x'_n$  GMD is calculated as :

$$GMD = \frac{\left\| \frac{x_n}{GFP_n} \right\| - \left\| \frac{x'_n}{GFP'_n} \right\|}{\sqrt{C}} \quad (2.19)$$

By normalising using GFP, two EEG samples from the same microstate but with differing strengths produce a minimal GMD distance.

## 2.6 Temporal smoothing

Short microstate segments appear after clustering and backfitting which primarily exist due to the nature of spontaneous EEG signals where the noise can't be averaged as like ERP's. This is where temporal smoothing comes in, since it not only allocates EEG data to microstate classes based on topographical similarities, but also groups them based on the microstate labels of preceding samples and the next EEG sample. The majority of clustering techniques in microstate analysis ignore temporal order. As a result, the temporal smoothing will be performed as a processing step after the microstate segmentation has been completed.

### 2.6.1 Windowed Smoothing

There are different variations of temporal smoothing. Windowed smoothing was the one of the variations introduced by [142]. The smoothing of microstate segments is performed by updating the microstate labels with a distance measure. It is a trade-off between optimizing the best to fit to data and temporal smoothness of the labels. With the additional parameter of temporal smoothness, Distance measure expressed in Equation 2.6 changes to the following distance measure as:

$$d_{kn}^2 = x_n^T \cdot x_n - (x_n^T \cdot a_k)^2 - \lambda \cdot b_{kn}, \quad (2.20)$$

where  $b_{kn}$  is the number of samples with the microstate label  $k$  in a window around the  $n$ 'th sample, and  $\lambda$  indicates how much to weight smoothness.

Two parameters are to be set by the user in this particular smoothing process i.e.,  $\lambda$  and width of the window. As suggested by [142] the value of  $\lambda$  is set to 5 and three samples for window width. However EEG data differs among datasets owing to a variety of reasons, such as different recording circumstances, varying sampling frequency, and other difficulties. There are chances of having dissimilarities among the same task data sets. Cross validation can be used to find the optimal smoothing settings.

### 2.6.2 Small Segment Rejection

From all the microstates segments extracted with different durations, in this toolbox there is a set of minimum duration microstate segments that are allowed to last. As evaluated by GMD (Global Map Dissimilarity), the algorithms continually scan over the microstate segments to the next most likely microstate class. The process is in cycle until it finds no microstate segments which is smaller than the set threshold.

## 2.7 EEG Microstate Statistics

After the extraction process of microstate prototypes, the prototypes are then backfitted to individual participant's EEG data. Examining the EEG data in the form of microstates provides different tem-

poral/statistical parameters. These parameters give significant information for the study of large-scale brain networks, and variations in these microstate parameters can reflect cognitive capacity of an individual [166].

Study by [113] suggests that EEG microstates are related with large scale brain networks and that their features may be utilised to analyse the functioning of big scale brain networks. These statistical factors can be categorized into activation strength, spatial configuration, and temporal features of microstates. The average GFP of all EEG data assigned to microstate k defines the strength of the given microstate k's average global activation.

$$GFP_k = \frac{1}{N_k} \sum_n^N GFP_n, \text{ for } l_n = k, \quad (2.21)$$

where  $N_k$  is the number of samples assigned to cluster k.

The average GEV and the average spatial correlation define upto what extent the microstate prototypes can explain the data. GEV looks at both the strength of the EEG and spatial fit(between microstate prototype maps and their assigned EEG samples), whereas the average spatial correlation only looks at the spatial fit.

$$GEV_k = \frac{1}{N_k} \sum_n^N GEV_n, \text{ for } l_n = k \quad (2.22)$$

$$Corr_k = \frac{1}{N_k} \sum_n nNCorr(a_k, x_n), \text{ for } l_n = k \quad (2.23)$$

$$= \frac{CorrSum(k)}{N_k} \quad (2.24)$$

The temporal dynamics of microstates are described in terms of parameters such as Occurrence, Duration and Coverage. The toolbox by default calculates these parameters by using the run-length encoding. Run-length encoding is a lossless data compression algorithm that compresses data by eliminating repeated and consecutive data, which is referred to as runs.

- **"Occurrence"** is the number of occurrences of the microstates of a given class per second.
- **"Duration"** is the average duration of the given microstate in milliseconds.
- **"Coverage"** is the fraction of total recording time that the microstate is dominant, this statistic may alternatively be read as a percentage of the total analysis time.
- **"Transition probabilities"** is an additional parameter. It is used to measure how microstates of one class are followed by microstates of another.

### **2.7.1 Determining Microstate Classes using Microstate Toolbox**

The microstate toolbox includes MATLAB functions that accept a variety of parameters as inputs. This aids in the analysis of EEG and ERP spontaneous data. Microstate toolbox provides a GUI (Graphical User Interface) for performing microstate analysis on a small sample of spontaneous EEG data.

The EEG data is parsed into different microstate classes using microstate analysis procedure. The study focuses on the spatio-temporal properties of the EEG time series data using microstate prototypes. The EEG data is classified into as few microstate prototypes as possible after loading a dataset into the toolbox, accounting for a set of microstate prototypes that offers as much variance in the EEG data as possible. GFP is computed for that specific data, and only that data is chosen with the GFP peaks set at a threshold, as a data reduction step. This helps in the reduction of EEG data entering pre-processing by removing low signal-to-noise-ratio maps. The data are now subjected to the clustering procedure, in which the clustering algorithm divides the data into small groups based on topographic similarities. The microstate prototype is then calculated for each microstate class. The topography of each sample is labelled to indicate which classes they belong to, and the EEG signal is therefore represented as a series of microstate classes. The toolbox may be used to generate statistics for these classes, which can then be analyzed for empirical studies.

## **2.8 Microstate analysis of our dataset**

Out of the total 29 male subjects who participated in our study, twenty-four were right-handed and the remaining five were left-handed (age = 18-30 years; mean = 24.25 years; SD = 3.96 years). We conducted 2 kinds of analysis, a within-subject analysis of all 29 participants for microstate parameters, and a between-subject analysis to compare participants based on their handedness. Due to the skewed distribution of the participants, for the latter analysis, we randomly picked right-handed individuals to form two groups of five each, which we then compared to the left-handed group. We chose methods and settings based on the previous literature and to the best of our knowledge for analysing our EEG dataset.

### **2.8.1 Using Microstate Toolbox**

When provided an EEG cleaned signal, the Microstates toolbox plugin in EEGLAB toolbox helps in the extraction of the microstate maps and their statistical parameters. The EEG signal is split into 1000 GFP peaks during the microstate calculation procedure, and signal segments of 60-120 ms length are then considered for cluster analysis. Modified k-means clustering technique (faster and slightly better in representing polarity invariant EEG microstates) is then used to form four (ensures a good balance between the goodness of fit and the number of clusters for generating feasible topographies with good spatial correlation) microstate classes based on the topographic similarities. Labels are allocated to these classes and are backfitted to the EEG data using only global explained variance (GEV) and cross

validation (CV) criteria as they are polarity invariant, unlike other criteria. This process is shown in Figure 2.4.

Global field power is extracted for the three groups (one left-handed group, and 2 right-handed groups) for the respective motor movements performed using both left and right hand independently. Also, GFP of the active microstates in the complete time range across all 29 participants for both the movements are extracted.

For each individual, first 1000 peaks are extracted with a 10ms distance between the peaks. GFP peaks exceeding 1 times of standard deviation are excluded and these 6\*1000 electric potential topographies undergo further clustering. The GFP peak plots for both tip-pinch and Wrist flexion & extension exercises for all 29 participants as well as left-handed and right-handed groups are discussed later in detail in chapter 4.

## **2.8.2 Using heuristics for determining the dynamic variables of Microstates in Pre-event, Event, and Post-event conditions**

At the start of the toolbox initialization, MATLAB constructs an EEG struct and saves all the labels in a (17 \* (total no. of frames of a participant)) matrix format stored as microstate.fit.labels. In addition to extracting the window lengths of 2s each before (pre-event) as well as after (post-event) executing the movement, a window length of 2s for executing the tip pinch movement while 3s for executing the Wrist flexion & extension is also extracted. For each window, all the contiguous identical labels forming a segment, along with the count of their associated frames, are sampled (divided by 500 and multiplied by 1000) to determine whether they meet the requirements of being a microstate (60ms <= segment length <= 120ms). Then, for all microstate classes present in the window, the microstate parameters such as occurrence, duration, coverage, and count of microstates are computed. This process is performed for the pre-event, event, and post-event conditions in each trial of each participant for each exercise.

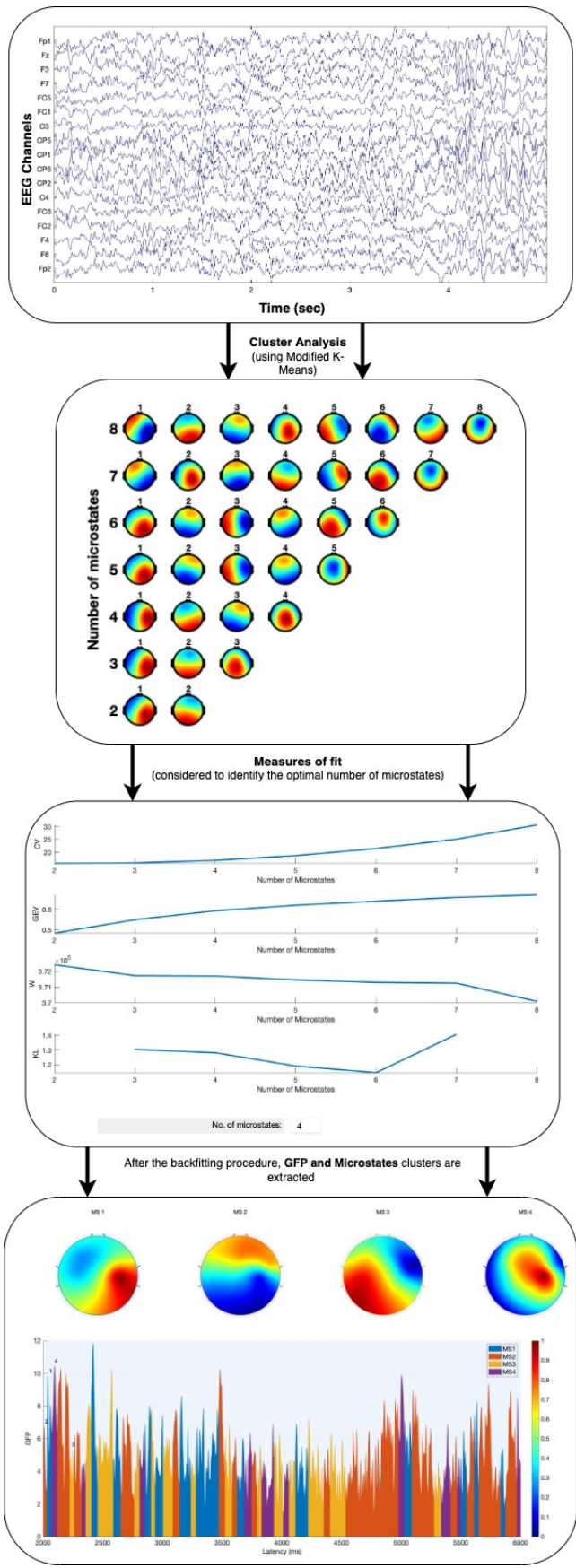


Figure 2.4 Microstate Analysis

## *Chapter 3*

### **Different Time-Frequency methods to analyze EEG**

In this chapter we discuss the different time-frequency approaches for analyzing EEG data. EEG signal exhibits significant complex behavior with strong non-linear and dynamic properties. Understanding and analyzing the behavior and dynamics of brain activations necessitates the use of a variety of linear and nonlinear signal processing techniques, as well as decoding their relationship to physiological events. These signal analysis methods are crucial for brain-computer interface study, which has applications in medical diagnosis such as

- identifying Sleep Apnea syndrome by analysing EEG signals using techniques like Wavelet Transforms and neural networks [187]
- detecting epileptic EEG signals using Discrete Wavelet Transforms coefficients with neural networks [186]
- analyzing effect of reflexology on EEG signals [130], [76] using nonlinear features and modeling techniques
- analyzing the variability and increase in alpha phase synchrony during meditation [63]
- identifying higher degree of gamma band synchrony in musicians [7]
- detecting unique bands for different musical signal stimuli by considering power at each band of each electrode as features [106].

For feature extraction, EEG signals are analysed in the time domain, frequency domain and time-frequency domain. Feature extraction methods are classified into three categories: spectral estimation methods, family of transforms, and time domain decomposition. Spectral Analysis of EEG provides us with the quantification and analysis of the event-related brain oscillatory responses. Frequency phase analysis is now becoming increasingly popular and some of the common methods like Wavelet-Transforms(WT), Fast-Fourier Transforms(FFT) and Hilbert-Huang Transforms(HHT) have been used in many researches. Time domain decomposition methods entail segmenting signals into non overlapping segments. Primary methods for time domain decompositions include windowing techniques which

segments the signal into partially overlapping windows, event related decomposition which segments based on event parameter knowledge, waveform decomposition which segments based on wave peaks, and statistical methods which calculate the mean and variance for each segment. In this study, we have used Single Frequency Filter (SFF) and Hilbert-Huang Transform(HHT) to analyze the EEG data. Sections that follow provide an overview of the fundamental techniques used in EEG signal analysis.

### 3.1 Spectral Analysis

Spectral quantification of non-stationary EEG data is complex due to their dynamic nature. EEG signals which describe the brain activity reflect a variety of cognitive function and sensorimotor information of the brain. EEG signals are known to have a linear mixture of basic vibrations that pulsate at a certain frequency bands and decompose each frequency component to represent its amplitude and power. The primary frequencies of human EEG waves (Brain waves) are oscillating electrical voltages in the brain that measure a few millionths of a volt [1]. These brain waves are labelled as alpha  $\alpha$  (8-13Hz.,) wave, beta  $\beta$  (13-30Hz.,) wave, gamma  $\gamma$  (30-50Hz.,) wave, delta  $\delta$  (1-4Hz.,) wave, and theta  $\theta$  (4-8Hz.,) wave based on the range of their oscillating frequencies.

There are different approaches to spectral signal analysis of EEG data which include PSD(Power Spectral Density) techniques, Atomic Decompositions, Time-Frequency(t-f) distributions and, Continuous and Discrete Wavelet approaches. EEG recordings with varying velocities and frequencies can be used to assess various brain states. The amount of power in a certain frequency band of a signal and its spatial distribution determines the underlying brain activities. We have plotted the power spectral density for a sample from our dataset as an example to illustrate this in Figure 3.1.

Since EEG signals are non-stationary in nature, power spectral density only reflects the frequency component of the signal and its power distribution over frequency.

### 3.2 Fourier Transform

In the early 1900's, the most extensively used frequency analysis method to determine frequency components in EEG signals is the Fourier transform. An infinite sum of periodic complex exponential functions can be expressed as any periodic function. Because of its computing speed, the Fourier transform was chosen for real-time monitoring and analysis of a variety of physiological data. Rhythmic activity in the EEG signal can be determined using the Fourier transform which enables the separation of distinct EEG oscillations. An EEG signal can be decomposed into a set of sinusoidal functions of different frequencies, amplitudes and phases using Fourier analysis and into a complex exponential function as :

$$X(f) = \int_{-\infty}^{\infty} x(r)e^{-2j\pi ft} dt \quad (3.1)$$

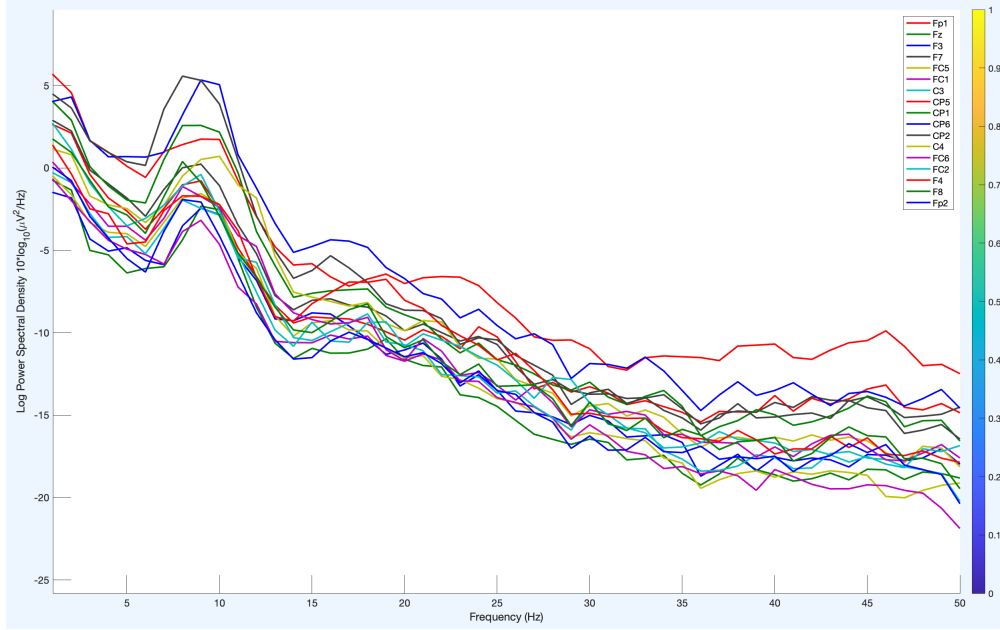


**Figure 3.1** Power Spectral Analysis for a motor task performed by a participant. The legend shows the corresponding 17 electrode channels. The high power (peak) in alpha band shows coordination of the visual and the motor cortex to execute the motor task while feeling calm and relaxed.

$$x(t) = \int_{-\infty}^{\infty} X(f)e^{2j\pi ft}df \quad (3.2)$$

In the above equation,  $t$  signifies time,  $f$  signifies frequency, and  $x$  is the signal under consideration. Note that here  $x$  denotes the signal in the time domain and  $X$  denotes the signal in the frequency domain. Equation 3.1 is referred as the Fourier Transform of  $x(t)$ , whereas Equation 3.2 is known as the inverse Fourier transform of  $X(f)$ , which is equal to  $x(t)$ .

Fourier transforms are commonly used to analyze stationary signals; however, EEG signals are non-stationary, and the frequency component of the signal changes with time, hence Fourier transforms are not regarded as an efficient technique for obtaining precise EEG signal properties. Suppose if the time window in the time series of the signal is assumed to be stationary then the Fourier transform can be used on that part of the signal which lead to the development of a new idea known as STFT.

STFT is a windowed Fourier transform which is applied on the signal in stages across a few seconds time window with a fixed window length. Short Time Fourier Transform allows us to examine time-localized frequency information of windowed frequency components, whereas Fourier transform only gives us the averaged frequency information of the entire signal. Different types of window used are :

- Hamming Window
- Triangular Window
- Rectangular Window.

For windowing the signals, a window function “w” is chosen. The window’s width must be equal to the signal segment in which stationarity holds true.

$$STFT_x^{(w)}(t, f) = \int_t x(t)^* w^*(t - t') e^{-2j\pi ft} dt \quad (3.3)$$

The equation above is the Fourier transform of the signal multiplied by a window function. In the above equation, the signal is denoted by  $x(t)$ , the window function is represented by  $w(t)$ , and \* denotes the complex conjugate.

[42] studied the EEG signals obtained from writing and found the specific patterns in the spectrogram using STFT, [176] developed a framework with STFT and CNN for classification of motor imagery, [144] predicted Epileptic seizure using STFT technique, [175] analyzed the background activity using STFT in Autism disease. STFT has better temporal and frequency localization properties compared with the Fourier Transform. Temporal changes of power spectrum in prediction of finger movements for motor execution and motor imagery was calculated using STFT [62] and Power Spectral Density of EEG signals centered at 1s length finger movement Peak was calculated using Fourier Transform [104].

STFT works on fixed basis functions and uses fixed-size time shifted windows which limits the number of non-stationary characteristics and therefore it has a tradeoff between time and frequency resolution which leads to the uncertainty involved in data analysis. In Fourier Transform if small window size is considered it results in poor frequency resolution and large window size results in imprecise temporal localization. Fourier Transform provides perfect frequency resolution however no temporal information is provided when used for infinite-length window. STFT has higher temporal resolution along with stationarity, however with small window and less frequency resolution. To overcome these limitations Wavelet Transform could be used to improve the time frequency representation and resolution.

### 3.3 Wavelet Transform

The mathematical approaches for signal processing employing Wavelet transform can also be used to analyze EEG data. It is the improved version of the Fourier Transform. Wavelet transform is a new multi-resolution time-frequency analysis method. Since EEG signals are non-stationary in nature, Wavelet transforms can be applied to extract the features from the raw data. Analysis of wavelet transforms uses small waves and functions recognized as wavelets which are described as a local wavelike

function. On the signal a wavelet can be stimulated at different places, and it can be expanded or compressed as per requirements and the wavelet transform measures the matching of the signal on a local basis with the wavelets [10]. Any general function can be expressed as an infinite series of wavelets since wavelet transform is a spectral estimation technique and the signal can be represented in both time and frequency domains in the form of wavelet coefficients.

Wavelet transform allows to decompose the complex information of signal into elementary forms and scales; and subsequently reconstructs it with high precision [177]. It overcomes the limitations of STFT in terms of window size selection and also solves the resolution problem associated with STFT. Time-frequency representation of signal can be done in a more flexible way using wavelet transforms with the use of variable sized window techniques. In STFT, the signal is multiplied by a function similar to the window function in the STFT and for each segment of the time-domain signal the transform is calculated independently. As opposed to the STFT approach, in Wavelet transform the original EEG signal is represented by secured and simple building blocks [2] known as wavelets with defined duration and energy. Frequency component can be altered in Wavelet transform using different sized windows. Higher frequency can be achieved using narrower window whereas wider window gives low frequency. By this, the optimum time-frequency resolution can be gained across all frequencies, and it removes the need of the signal to be stationary. The Wavelet transform is classified into two categories: Continuous Wavelet transform and Discrete Wavelet transform. Continuous wavelet transform is an alternative method of transformation in comparison to STFT and is complex to implement than Discrete Wavelet transform. Discrete Wavelet Transform is analyzed at different scales with respect to time and; in Continuous Wavelet Transform time-varying window sizes are selected according to the different spectral components. The Discrete Wavelet transform has been found to provide a quick computation, reducing the amount of time and resources required. It is the most commonly used method for EEG based epilepsy diagnosis application [78]. Continuous Wavelet transform is better for diagnosing diseases, motor skills, and decoding finger movements on EEG that have complex spectral and temporal pattern. [161] found Continuous Wavelet transform serves as an effective method for feature extraction since it retains phase information and fine-frequency modulations. [88] used Continuous Wavelet transform for extraction of spatio-temporal features and recognizing twenty directions of wrist movements from EEG signals which are suitable for analyzing the non-stationary biomedical signals and [214] investigated six motor functions which comprise grasp-and-lift events and classified them combining common spatial pattern (CSP) and Continuous Wavelet transform (CWT).

There are four distinct frequency bands(alpha, beta, gamma, delta) that allow us to identify the instantaneous source strength of a particular microstate in EEG. Study by [67] used Discrete Wavelet transform to separate the beta band of EEG signal to extract features and investigated the performance of Probabilistic Neural Network for building a better classifier for left and right hand movements. Features were extracted from alpha and beta bands since they contain more information using DWT by [204] for classification of different finger movements. Pain perception was also investigated by [52] using

EEG when presented with heat, bristles and pinch stimuli, using dual feature extraction methods (Power spectral density (PSD) and Discrete Wavelet transform (DWT)).

### 3.4 Hilbert Huang Transform

Hilbert Huang Transform is applied on non-stationarity and nonlinear signals. This technique is used to obtain instantaneous frequency data. HHT follows a two-step procedure for the analysis of the input signal. When an input signal is given to the system, HHT first decomposes the input signal into a finite number of Intrinsic Mode Functions using Empirical Mode Decomposition and then the Hilbert spectrum is obtained by applying Hilbert Transform over Intrinsic Mode Functions. [109] used HHT analysis since it provides a thorough understanding of the time frequency structure of EEG signal. [105] used HHT analysis for Clinical Alcoholic EEG signal. The authors highlight the significance of HHT in providing characteristic vector of the EEG signal for alcoholism, frequency characteristics, amplitude characteristics, time dependent temporal spatial-frequency correlation, and correlation of multiple channel EEG signal. As an illustrative example, Figure 3.2 exhibits a sample Hilbert spectrum of our EEG data obtained from the Fz electrode.

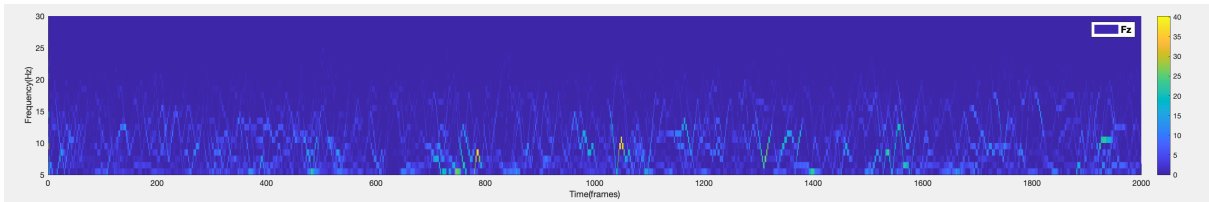


**Figure 3.2** 2-D peak visualization of the Hilbert Huang Spectrum of channel **Fz** EEG electrode

Adaptive decomposition of the IMF's can be done using HHT which provides enhanced time-frequency resolution compared to other methods such as Wavelet Transform, Short time Fourier Transform and S-Transform. The HHT algorithm is composed of two major components:

1. Empirical Mode Decomposition (EMD) - EMD is a data adaptive multiresolution technique which decomposes signal into meaningful components known as Intrinsic mode functions, where each component carries lower-frequency oscillations.
2. Hilbert Spectral Analysis (HSA) - In HSA, instantaneous frequency and amplitude of different Intrinsic mode functions can be determined by using Hilbert Transform.

#### 3.4.1 Empirical Mode Decomposition

Empirical Mode Decomposition method was proposed by [68]. EMD is a significant part of Hilbert Transform. It is an adaptive time-frequency data analysis method which breaks down nonlinear and non-stationary signals into Intrinsic Mode Functions (IMFs) and after decomposing it into IMF, the

Hilbert transform is applied which produces an orthogonal pair for each IMF. These components (IMF) on a whole form the orthogonal basis for the given original signal. High frequency, most oscillatory components are typically present in first Intrinsic Mode Functions. As a result, it can be rejected to eliminate high-frequency components (eg., random noise). For High quality seismic records and its processing, EMDs are required.

Intrinsic mode functions are characterized as simple oscillations, which contain same number of extreme and zero-crossings. During the signal decomposition, IMF first finds all local extrema, then connects all local maxima by natural cubic spline line in the upper part of the envelope. Same is applied for the lower envelope such that both upper and lower envelope cover the whole signal. Since IMF contains oscillatory components, it has to satisfy the following conditions:

1. The number of extrema and zero crossings must either be the same or differ by one.
2. The envelope created by the local peaks and minima must have a mean value of zero at any point.

### **3.4.2 Hilbert Spectral Analysis**

After obtaining the intrinsic mode function components, Hilbert Transform is applied over each IMF component which computes the instantaneous frequency. Intrinsic mode functions represent a generalized Fourier expansion. Efficiency of expansion is greatly influenced by variable amplitude and instantaneous frequency which also helps in accommodation of nonlinear and non-stationary data. The restriction of the constant amplitude and fixed frequency of the Fourier expansion has been overcome with the help of variable amplitude and frequency representation. This frequency-time distribution is referred to as "Hilbert Spectrum". Localized characteristics of an EEG signal can be identified using the Hilbert Spectrum as shown in the 3-D peak visualization as an example Figure 3.3 of a trial performed by a participant in our experiment. Localized characteristics of an EEG signal can be identified using the Hilbert Spectrum.

[195] extracted features from the analytic Intrinsic Mode Functions of EEG signals and fed them to the LS-SVM classifier for the classification of Motor Imagery Tasks. The authors found their method helpful in classifying the physiological and pathological states of the brain using EEG signals.

## **3.5 Single Frequency Filtering**

SFF method is a novel technique which was used for voice detection by [4] and was applied on EEG signals for the first time by [73]. An illustration of employing SFF on EEG signal is shown in the 3-D peak visualisation example Figure 3.5 of a trial performed by a participant in our experiment. Single frequency filtering gets its name from the fact that the energy is extracted at a single frequency. SFF's time frequency representation has less frequency dispersion compared to STFT's time frequency representation, according to [198]. SFF time frequency representation is known to give the improved

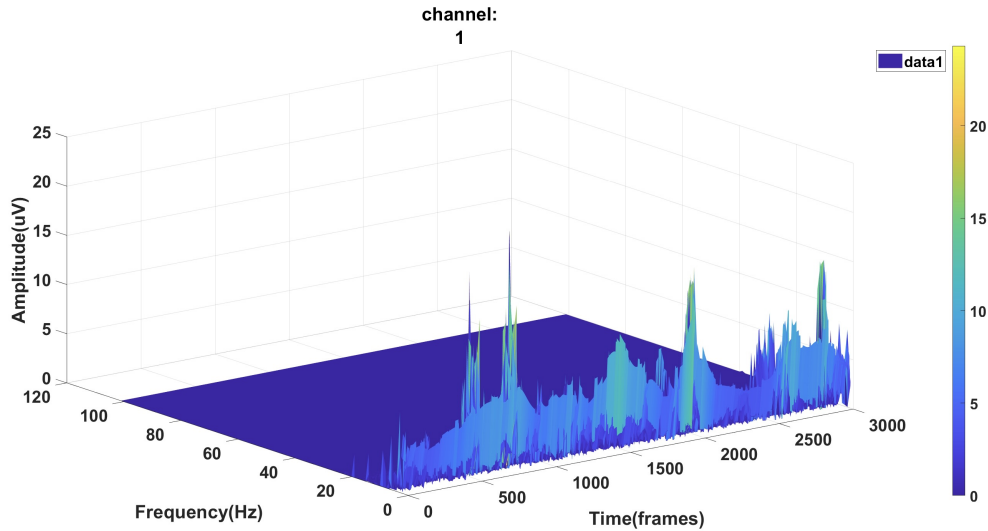


**Figure 3.3** 3-D peak visualisation of the Hilbert Huang Transform of channel **Fp1** EEG electrode

time-frequency localization. In comparison to the STFT approach, SFF has very little dispersion over the whole frequency range. The amplitude envelope of the signal is derived at each frequency with great temporal and spectral resolution using SFF.

### 3.5.1 Single Frequency Filtering: Analysis of EEG Data

Neuronal activity can be identified by the small variations in the voltage fluctuations of the EEG measurements. Visual inspection of EEG recordings may be inaccurate due to the presence of artifacts, and thus requires different signal processing analysis mechanisms to extract features following recognition of different functional states of brain using statistical tests. In the time-frequency domain, the SFF technique may be used to analyze non-stationary EEG data. Non stationary speech and non-speech discrimination was done by [4], using SFF algorithm. In speech signals, both time and frequency are interdependent. The power distribution of these signals is also non-uniform across all frequencies. Hence, the signal-to-noise  $S^2(f)/N^2(f)$  ratio will vary at different frequencies, where  $S(f)$  and  $N(f)$  denote the signal and noise amplitudes. The average signal-to-noise  $S^2(f)/N^2(f)$  ratio throughout a frequency range produced by the authors' technique is much larger than the ratio of total signal power over the whole frequency range. In some frequency regions, the signal-to-noise ratio is higher, whereas in others, it is lower. The signal-to-noise ratio in the time and frequency domains is greater due to SFF's high resolution [4]. To visually represent Peak signal-to-noise-ratio, Figure 3.4 shows an example plotted for an individual performing all exercises in our experimental setup.

Each frequency component has a high temporal and spectral resolution; therefore, the amplitude envelope was extracted at each frequency. There is an extension to the SFF called Single frequency filter bank (SFFB) that can be used to decompose the EEG signals into different frequency bands. A

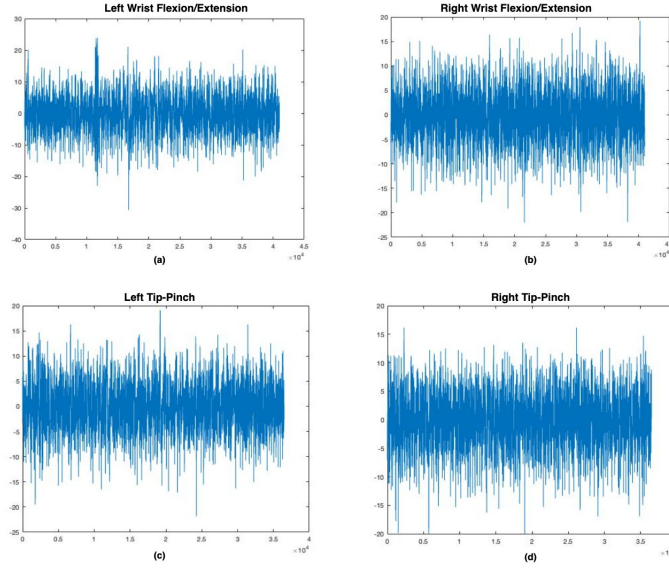


**Figure 3.4** This is the Peak Signal-to-Noise ratio plots of the four movements executed by an individual. **a.** Left Wrist flexion & extension **b.** Right Wrist flexion & extension **c.** Left tip-Pinch **d.** Right tip-Pinch

filter bank is an array of band-pass filters used in signal processing to separate an input signal into numerous components [143]. SFFB has the benefit of separating the signal under consideration into two or more signals in the frequency domain with good spectro-temporal resolution [74].

The transfer function of Single frequency filtering was given by:

$$H(z) = 1/(1 - az^{-1}) \quad (3.4)$$

where  $a$  indicates the location of the pole and determines the bandwidth of the single-frequency filter.

Equally spaced frequency-modulated single-frequency filters form the core of the single-frequency filter banks, and the transfer function for the frequency modulated SFF was given by:

$$H_k(z) = 1/(1 - a_k z^{-1}) \quad (3.5)$$

where,  $a_k = a * exp(-j\omega_k k)$ ,  $\omega_k = (2 * \pi * \tilde{\omega}_k) / fs$

$\tilde{\omega}_k$ :  $k^{\text{th}}$  frequency component of the signal

fs : Sampling rate

Thus, the signal is divided into  $M$  frequency components, and a single frequency filter bank is given by:

$$SF_{filterbank} = [(H_1(w)H_2...H_k(w))]^T \quad (3.6)$$

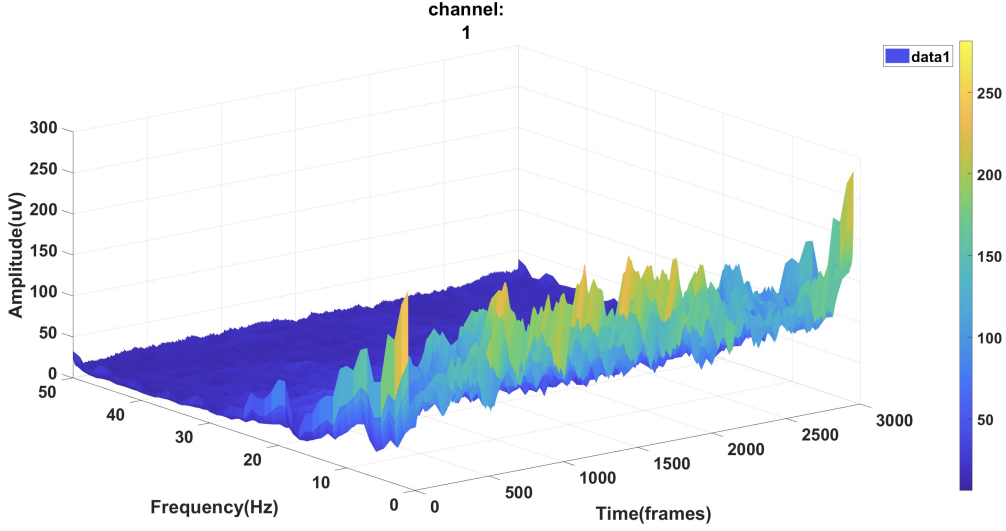


**Figure 3.5** 3-D peak visualisation of the Single Frequency Filter of channel **Fp1** EEG electrode

where  $k = 1, 2, 3, \dots, M$

The  $k^{\text{th}}$  filter response  $y_k[n]$ , and the corresponding envelope of each filtered component  $m_k[n]$  were given by:

$$y_k[n] = \sum_{i=0}^N h_k[i]^* x[n - i] \quad (3.7)$$

$$m_k[n] = (y_{kR}^2[n] + y_{kI}^2[n])^{1/2} \quad (3.8)$$

$Y_{kR}[n]$  and  $Y_{kI}[n]$  are the real and imaginary parts of the filtered component  $y_k$ . EEG signal is represented by  $x[n]$  and  $n$  is the discrete-time variable.

### 3.6 Application of Single Frequency Filtering on our dataset

To extract the changes in the signal caused by performing the Wrist flexion & extension and Tip-pinch motor movements in our study, high temporal resolution is required, rather than the specific functions showing the change. As a result, we used a single-frequency filter bank to achieve higher resolution than typical bandpass filtering, short-time FFT, or continuous wavelet transform analysis with a sliding window. Towards this, we picked  $a = 0.995$  so that filter bandwidth is equivalent to 0.001Hz and frequency components from 1Hz to 50Hz were decomposed with a frequency resolution of 1Hz. The amplitudes of the power spectrum density plots were retrieved for each trial.

### **3.6.1 Amplitude Analysis and Peak Plots (Electrode wise)**

Applying Single Frequency Filtering, amplitude and peak analysis of each electrode across three conditions (pre-event, event, and post-event) has been defined in this section. The analysis were performed for both Wrist flexion & extension and Tip-pinch hand movements. Time-locked trials related to these movements of 6 and 7 seconds were collected using the Experiment paradigm by extracting 2 seconds previous to the movement (preparation condition), 2 seconds after the movement (post-event,/degradation condition), and 2 seconds window of the movement (event condition) in case of Tip-Pinch movement and 3 seconds window of the movement (event condition) in case of Wrist flexion & extension movement (event condition). Following that, the epoched EEG data was subjected to time-frequency analysis using the single frequency filtering (SFF) technique. The comparison of electrodes' amplitude for hand movements such as Left Wrist flexion & extension, Right Wrist flexion & extension, Left Tip-pinch, and Right Tip-pinch along with the electrodes namely C3, C4, CP1, CP2, CP5, CP6, F3, F4, F7, F8, FC1, FC2, FC5, FC6, Fp1, Fp2, Fz. For each condition (pre-event, event, and post-event), the highest amplitude was collected from the trials conducted of each movement of the 17 chosen channels. The maximum amplitude of all electrode trails were considered further and was investigated for descriptive analysis for each individual.

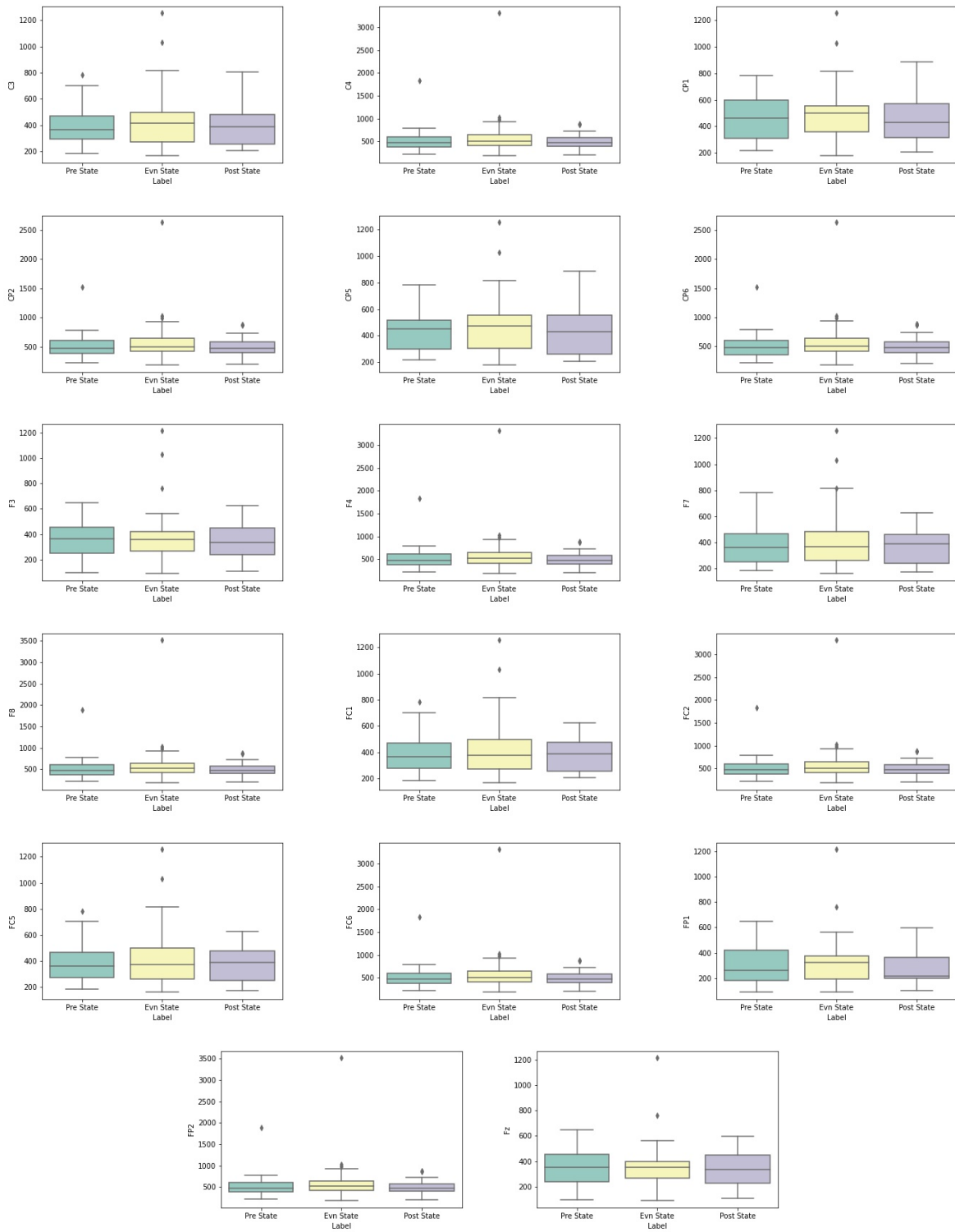


**Figure 3.6** Comparison of EEG electrodes based on amplitude for **Left Wrist flexion & extension** movement. This is an electrode-wise (C3, C4, CP1, CP2, CP5, CP6, F3, F4, F7, F8, FC1, FC2, FC5, FC6, FP1, FP2, Fz) illustration of the pre-event, event, and post-event conditions for all 29 participants.

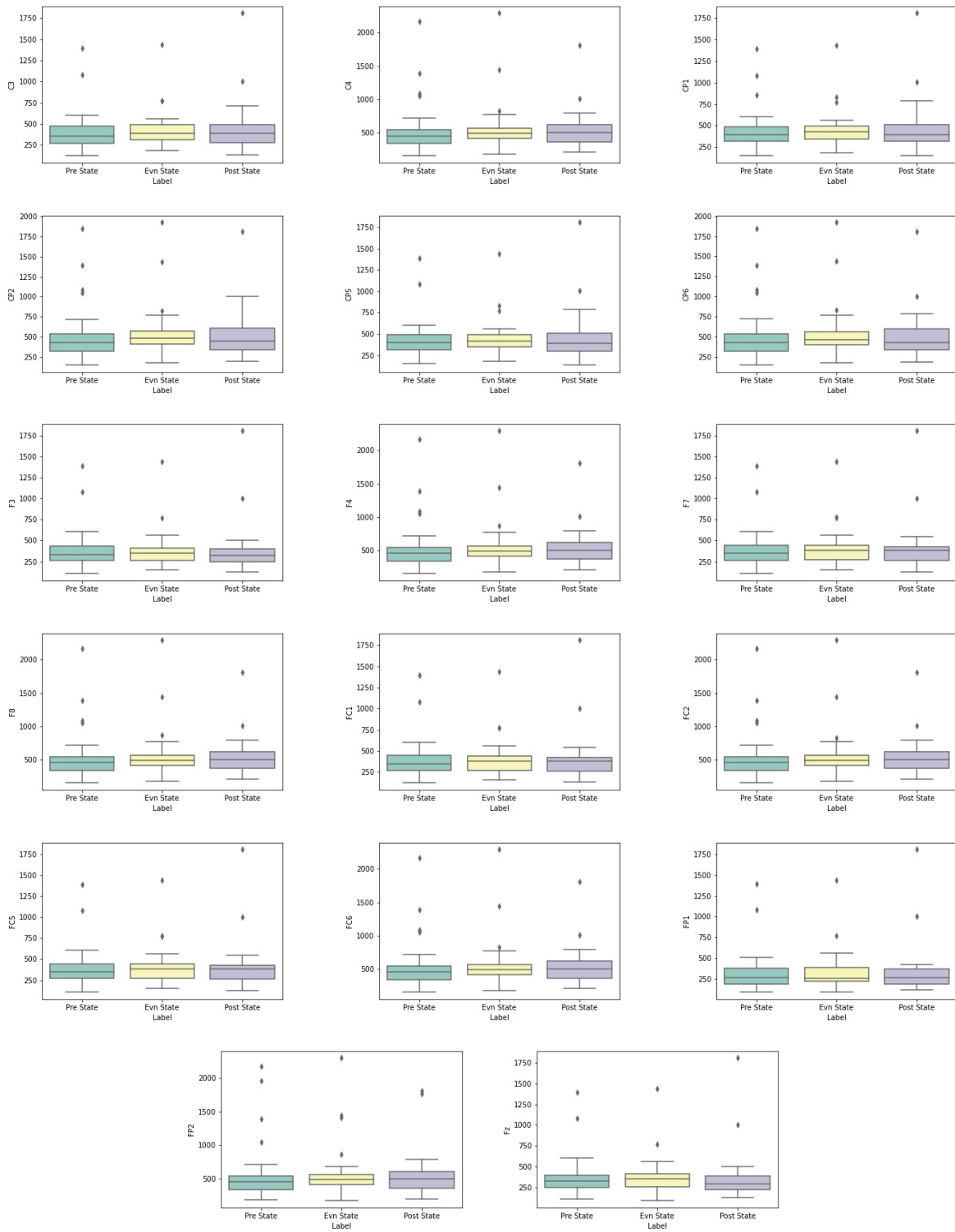


**Figure 3.7** Comparison of EEG electrodes based on amplitude for **Right Wrist flexion & extension** movement. This is an electrode-wise (C3, C4, CP1, CP2, CP5, CP6, F3, F4, F7, F8, FC1, FC2, FC5, FC6, FP1, FP2, Fz) illustration of the pre-event, event, and post-event conditions for all 29 participants.

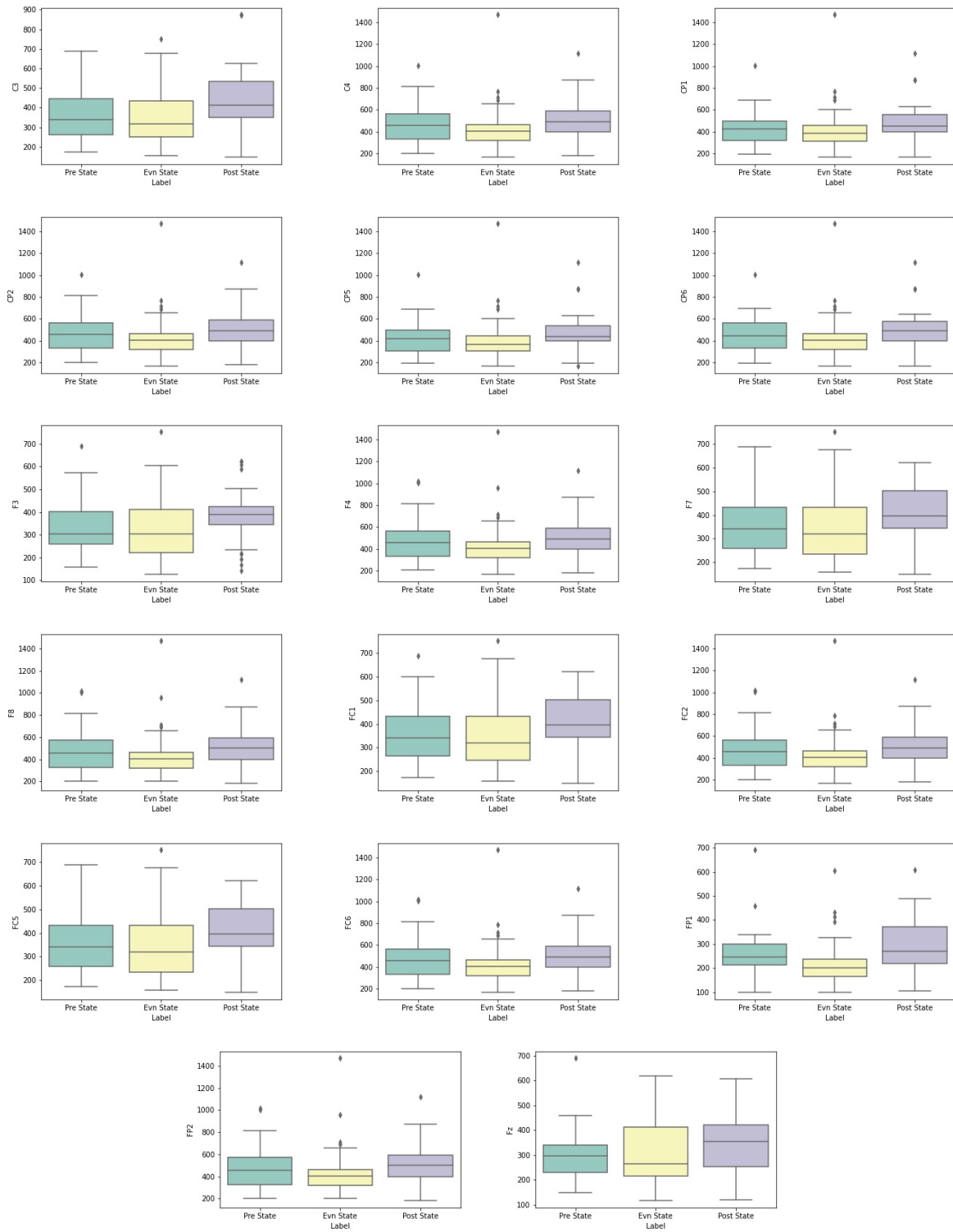


**Figure 3.8** Comparison of EEG electrodes based on amplitude for **Left Tip-pinch** movement. This is an electrode-wise (C3, C4, CP1, CP2, CP5, CP6, F3, F4, F7, F8, FC1, FC2, FC5, FC6, FP1, FP2, Fz) illustration of the pre-event, event, and post-event conditions for all 29 participants.

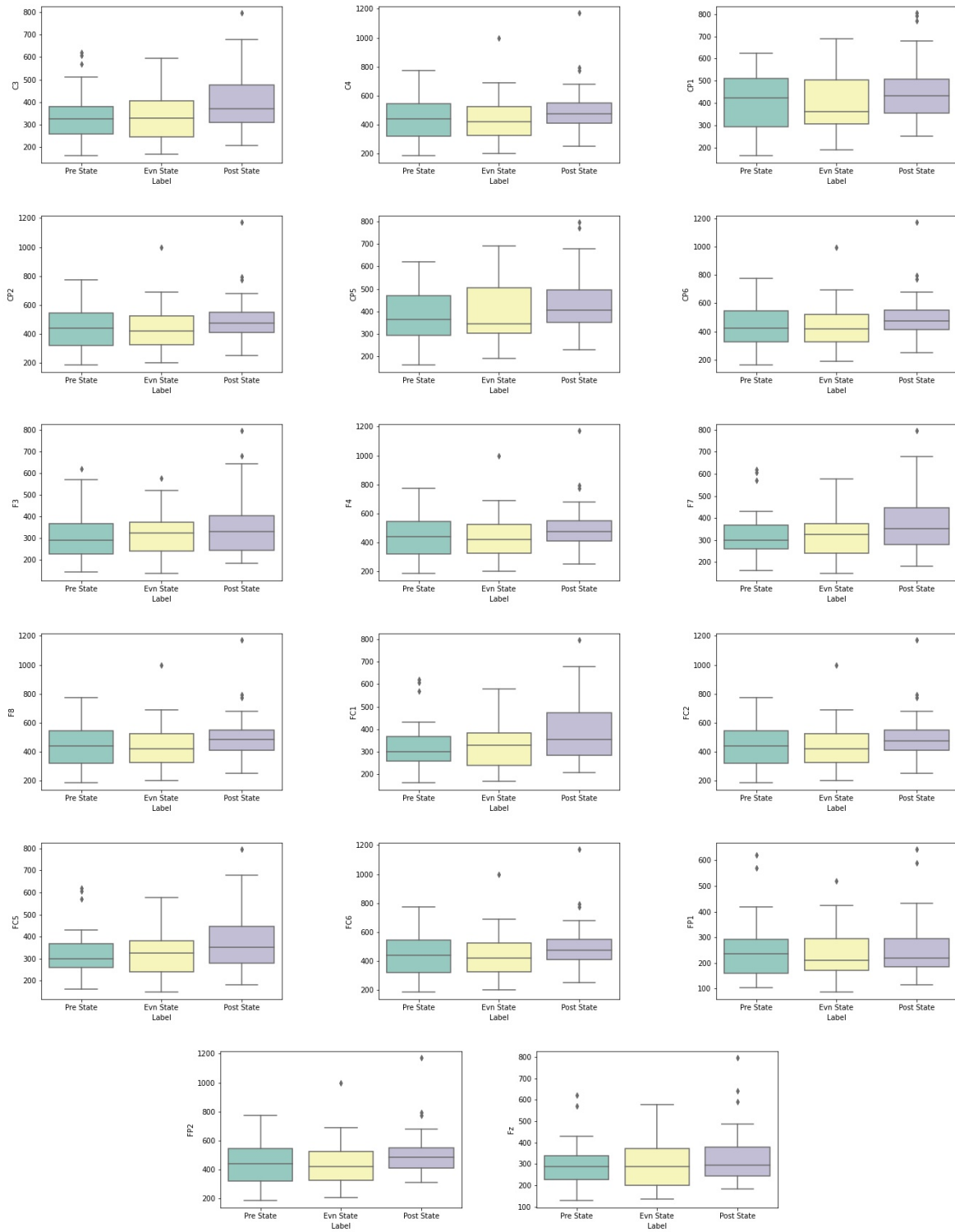


**Figure 3.9** Comparison of EEG electrodes based on amplitude for **Right Tip-pinch** movement. This is an electrode-wise (C3, C4, CP1, CP2, CP5, CP6, F3, F4, F7, F8, FC1, FC2, FC5, FC6, FP1, FP2, Fz) illustration of the pre-event, event, and post-event conditions for all 29 participants.

### **3.6.2 Comparative analysis of 6 specific electrodes of major importance**

For all motor tasks, the EEG signals from the 17 electrodes placed on the ipsilateral side of the brain show more fluctuations, while the signals from the electrodes placed on the contralateral side of the brain are comparable and the difference is too small to tell. This small difference could be because the participants are young and healthy. We carefully examine and pick six electrode channels by visual inspection. The selected electrodes cover the central (C3,C4), centro-parietal (CP5,CP6), and frontal (F3,F4) parts of the brain. We consider only the EEG signals of the participants whose peak amplitudes are between -2 standard deviations and +2 standard deviations. The peak plots for Wrist flexion & extension are depicted across pre-event, event, and post-event conditions in Figure 3.10 (left) and Figure 3.11 (right). The same is depicted for Tip-pinch Figure 3.12 (left) and Figure 3.13 (right).

We use the aforementioned electrode channels selection for outlier removal. However, if we exclude the data of an outlier for a single motor task from all the motor tasks for coherence, it leads to data sparsity. Thus, we decide only to remove outlier(s) from their corresponding task. This exclusion criterion results in different number of participants for each motor task's final analysis. As a result, this misalignment leads to incoherence in any inter task analysis. Therefore, we do not explore any comparison of peak plots across exercises further.

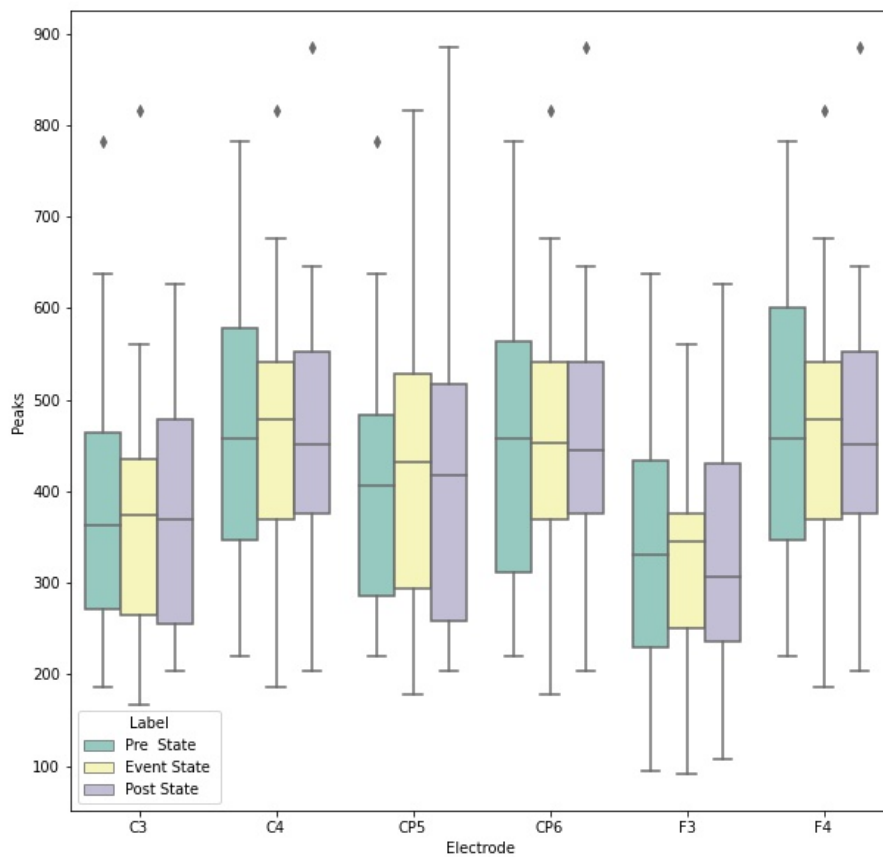


**Figure 3.10** Amplitude values for **Left Wrist flexion & extension**

This is an electrode wise comparison of the amplitude values across pre-event, event, and post-event states for C3, C4, CP5, CP6, F3 and F4 electrodes for all 29 participants.

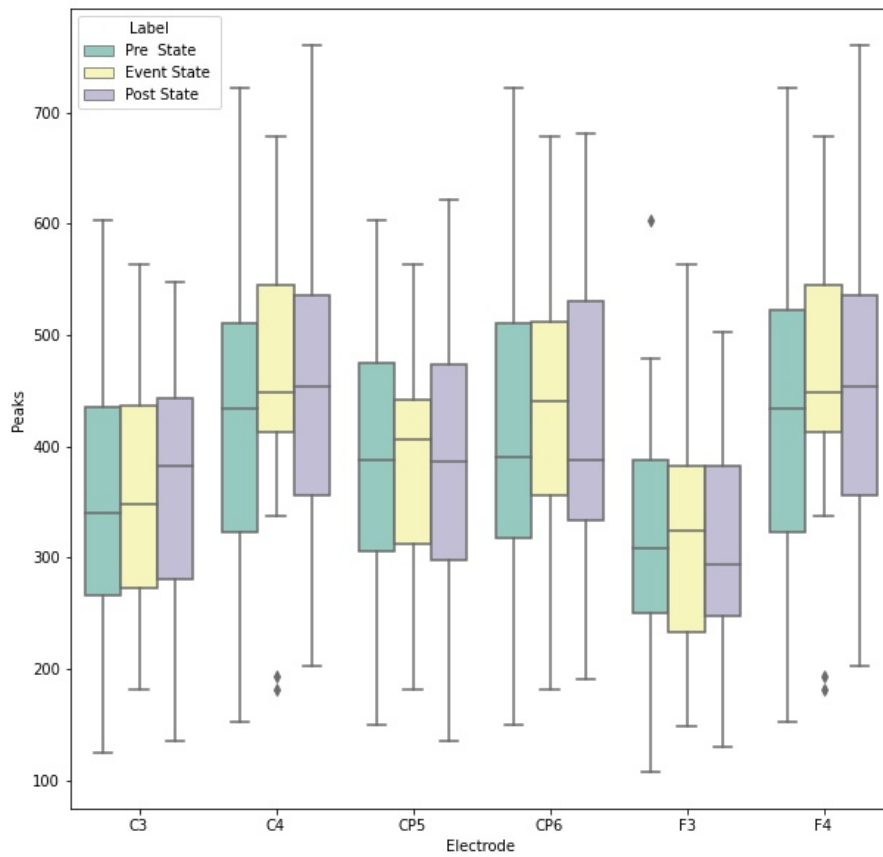


**Figure 3.11** Amplitude values for **Right Wrist flexion & extension**

This is an electrode wise comparison of the amplitude values across pre-event, event, and post-event states for C3, C4, CP5, CP6, F3 and F4 electrodes for all 29 participants.

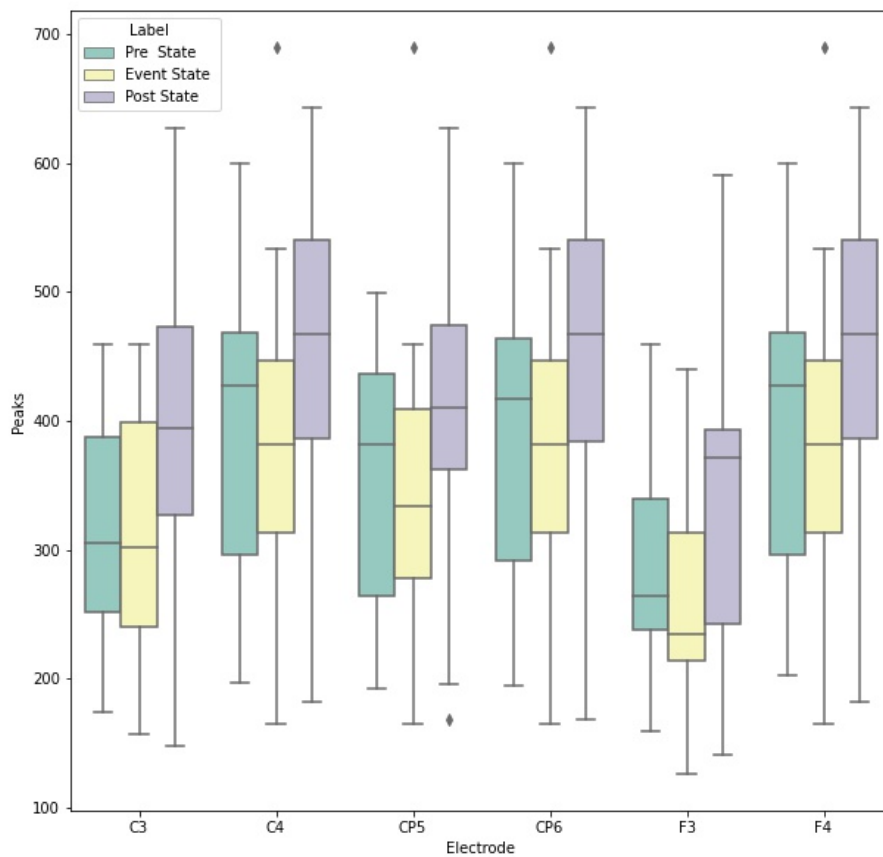


**Figure 3.12** Amplitude values for **Left Tip-pinch**

This is an electrode wise comparison of the amplitude values across pre-event, event, and post-event states for C3, C4, CP5, CP6, F3 and F4 electrodes for all 29 participants.

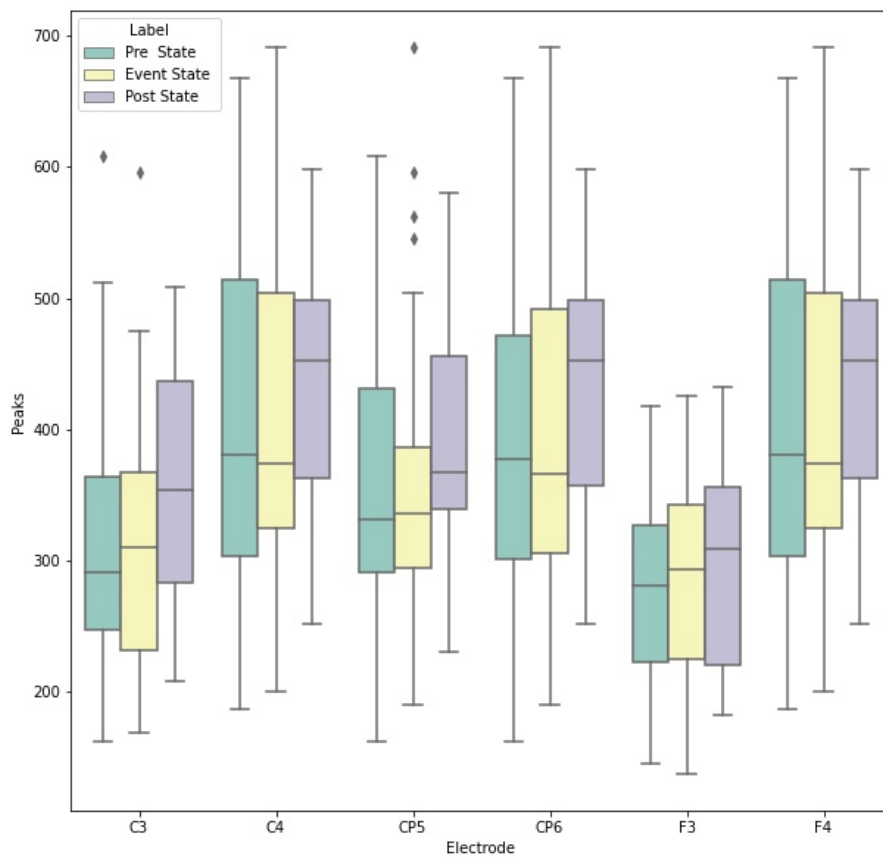


**Figure 3.13** Amplitude values for **Right Tip-pinch**

This is an electrode wise comparison of the amplitude values across pre-event, event, and post-event states for C3, C4, CP5, CP6, F3 and F4 electrodes for all 29 participants.

## Chapter 4

### Decoding Wrist flexion & extension and Tip pinch Movements

#### 4.1 Background

Similar to [117] which showed that EEG microstates help us in identifying brain networks and their temporal activation by comparing resting state with motor tasks (reaching and grasping), we have investigated the microstates extracted from EEG signals of motor tasks. Our study extends the existing research on motor action and underlying inter and intra hemispheric responses by reporting findings from an EEG experiment with a paradigm employing a tip pinch (pincer grasp) and a Wrist flexion & extension movement. The focus of our exploratory study is to investigate the role of EEG microstates in upper limb motor movements and to map the neural activations supporting these two exercises performed using left and right hands separately. Though studies using EEG microstates analysis providing evidence of their benefits in motor control studies [108], [117], [32], [69] have been reported, most of the studies either employ it in resting state [202], [35], [79], [147], imagined movements [45] or in tasks performed with controlled sensory modalities. Our study compares EEG microstates across pre-event, event, and post-event conditions, analogous to [25], who found pre-stimulus microstates for distinguishing cognitive brain activity and whose findings provide the first causal evidence for the task and area specificity of pre stimulus EEG microstates.

As microstates are discrete epochs of topographic stability that last 60 - 120ms before quickly shifting to a new topography that lasts the same amount of time, some of the microstate's temporal parameters, such as the average duration for which a given microstate remains stable, the frequency of occurrence for each microstate independent of its individual duration, the time for which a given microstate is dominant, and the microstate's transition probabilities, provide a detailed understanding of microstate features. EEG signals captured for movements have consistent changes in 8-12 Hz (alpha band). Identifying markers or task-specific activations requires a consideration of task-dependent changes. Our study analyses microstates from EEG signals of functional hand/finger motor-tasks and their characteristics during the execution of cue-driven Wrist flexion & extension and Tip-pinch, for both left- and right-handed people. The results of this research enhance our knowledge of the functional and temporal structure underlying the activation of motor primitives during upper limb movements as well as sheds

light on the temporal organisation of EEG microstates across the three conditions (pre-event, event, & post-event) for all motor tasks. These findings may help us better understand how to use this information to (re)learn a motor activity based on the amount of information processing taking place in the brain during these motor actions.

## 4.2 Methodology

In this study, participants were instructed to perform two motor tasks (Wrist flexion & extension and Tip-pinch) using their right and left hands, according to a predefined motor paradigm.

### 4.2.1 Participants

For the present study Ethics approval was taken from the Ethics Committee of the International Institute of Information Technology, Hyderabad. After receiving detailed information about the study, each subject gave informed consent, was credited with an honorarium (INR 300), and was notified that they might exit if they felt uncomfortable during the experiment. Spontaneous EEG data was collected using Brain Vision Acti Champ System Figure 4.1 from Twenty-nine healthy male subjects — Twenty-five right-handed (one participant's data got corrupted when transferring to the analysis machine) and five left-handed (age = 18-30 years; mean = 24.25 years; SD = 3.96 years) volunteers who participated in the study. EEG data of the participants was collected independently for the two mentioned motor tasks. During the EEG recordings, all of the subjects were in a normal neurological condition and were not undergoing any pharmacological therapy. Also, none of them were diagnosed with neurological problems, cognitive disorders or receiving any medical treatment. The actiCAP's electrodes were placed according to the 10/20 international system.

The Brain Vision Acti Champ System is highly scalable modular solution for recording brain signals which has channels ranging from 32-160 in number. Along with this it also enables integration of more than 8 extra inputs of physiological sensors that can be used with a variety of biosignal sensors (GSR, EOG, temperature, blood pulse and photosensor) and offers an exceptionally high sampling rate (up to 100 kHz). It allows for easy setup with external devices (eg., TMS-EMG(Transcranial Magnetic Simulation-Electromyography)). With the help of Brain Vision Recorder software, users can now perform the following functions such as baseline corrections, artifact rejection, online segmentation and averaging on the collected EEG data. Combination of the active electrodes based with Ag/AgCl sensors provides lower noise levels where the Impedance conversion occurs at the electrode level. There are different EEG standard electrode configurations for recording neuronal activity from inferior surfaces of the brain such as basal temporal lobe, temporal pole, orbito-frontal cortex, basal occipital and cerebellar areas. The different EEG configurations are EEG25(Minimum 10-20 configuration including inferior electrodes), EEG33(Additional 10-10 electrodes within the major squares), EEG35(Additional supraorbital electrodes for better EOG separation), EEG37(Wider inferior coverage at interlaced 20%

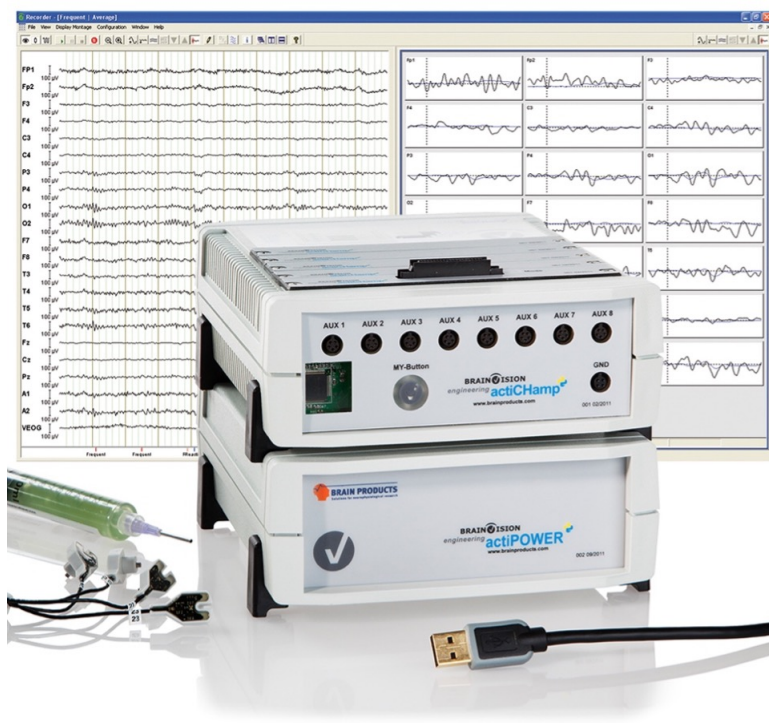


**Figure 4.1** EEG recording system Brain Vision actiCHamp amplifier with BrainVision Recorder

distances), EEG41(Improved frontal and occipital coverage), EEG43(Inferior chain with 5 electrodes including A1/A2), EEG64-256. In our study, we placed the electrodes according to the 10/20 international system. Placement of the Electrodes on the actiCAP and their representation is as shown in Figure 4.2.

#### 4.2.2 Experimental Paradigm

Before the start of the experiment participants were asked to sit in a comfortable and in a relaxed position. In brain-related research, stability of mind is a critical element that plays a significant role in obtaining accurate, error-free data. Study by [Bullock,2019] suggests Stress relief therapies such as meditation and yoga help in keeping mind calm.

In the present study, there exists two different hand motor tasks. The participants were instructed to complete two motor tasks: a Tip-pinch and a Wrist flexion & extension, using the right and left hand independently, on a motor paradigm designed with the Open Sesame software [110]. Open Sesame software is a program useful for building experiments for psychology and neuroscience related studies. It provides a robust GUI (graphical user interface) that helps in designing experiments compared to python which involves programming complicated tasks. Extending the paradigm used by [73], the design as shown in Figure 4.3 included a 2-minute relaxation period followed by performing the first motor task, a Tip pinch, in a 2-seconds window with a 6-seconds rest in between trials. The second task

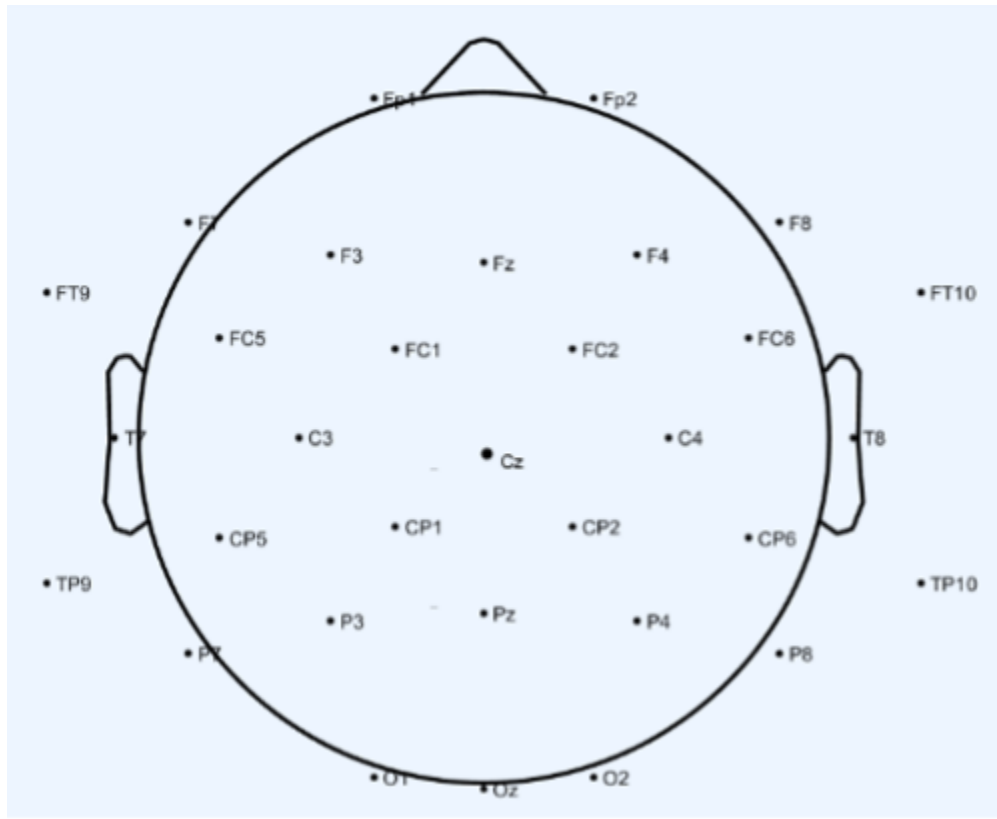


**Figure 4.2** The 10-20 International System of Electrode Placement

was to perform a Wrist flexion & extension in a 3-seconds window with a 6-seconds rest. Both motor tasks were performed using right and left hands independently. On the display of a visual cue ('+' sign) for 2 seconds in the case of Tip-pinch while 3 seconds in the case of Wrist Flexion & Extension in each trial, the participant performed the corresponding task for ten trials.

### 4.2.3 Pre-processing and Artefact Removal

EEG signal processing was performed in MATLAB, 2021b software using the EEGLAB toolbox to process time-series EEG data [31]. Selected electrodes such as (Fp1, Fp2, F7, F3, Fz, F4, F8, FC5, C3, Cp5, Fc1, Fc2, Cp1, Cp2, Fc6, C4, Cp6) corresponding to pre-frontal, frontal, central and motor region areas were considered in this study as shown in Figure 4.6. Three-dimensional image of the scalp EEG electrode placement is as shown below Figure 4.4.

Average referencing was used to cancel the outward positive currents with the inward negative currents. The baseline noise was eliminated by subtracting the mean from the raw signal [207]. EEG signals were bandpass filtered in the 1-50 Hz cut-off frequency range, which reduces filtering artefacts at epoch boundaries, and then sampled at 500 Hz frequency.

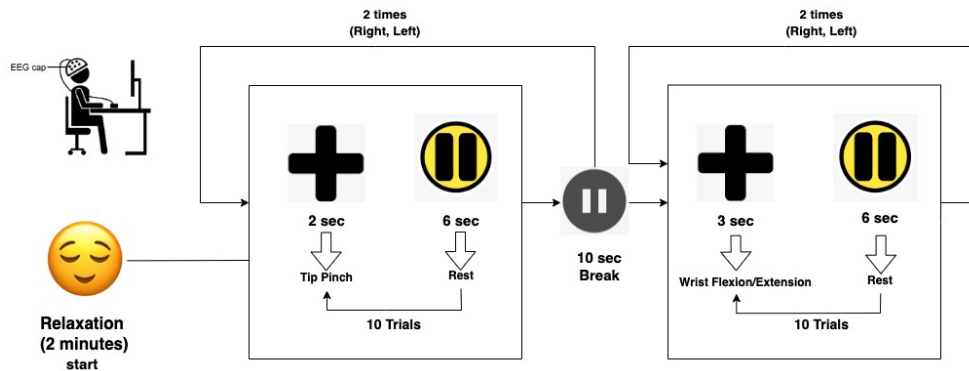


**Figure 4.3** Experiment Paradigm Design

The Experiment design involves a 2-min relaxation prior to the start of the experiment followed by Tip-pinch 2-sec and Wrist flexion & extension 3-sec with a 6-sec gap between the trails.

Sinusoidal artefacts were removed to reduce the alternating current (AC) power line fluctuations and from other power sources as they are a common source of noise in electrophysiological data. Independent Component Analysis was performed to reduce artefacts associated to eye blinks and physiological activity (pulse rate). Independent Components (ICs) with high artefact probability were eliminated using visual inspection and the MARA algorithm [73]. A flow chart representation of the pre-processing is provided in Figure 4.5.

## 4.3 Data Analysis

For both motor movements, time-locked trials of 6 seconds for Tip-pinch; while 7 seconds for Wrist flexion & extension were obtained by extracting 2 seconds before the movement (pre/preparation condition), a 2-second window for Tip-pinch and a 3-second window for Wrist flexion & extension movement (event execution condition), and 2 seconds after the movement (post/degradation condition). In the pre-condition an individual is invoked by a specific functional reaction for the upcoming task. Here the brain prepares the individual accordingly to perform the given task. In the case of event condition the individual performs the task and in the post-condition is a period which lasts for some time which involves thinking even after execution of the event.

### 4.3.1 Microstate Extraction and Analysis

The Microstate EEGlab toolbox [148] in the MATLAB was used to examine the characteristics of event time-locked microstates in the pre-event, event and post-event conditions as it provides complete transparency of the exact method applied with respect to all the steps of analysis and allows the integration of widely used clustering algorithm available in open-source EEG analysis.

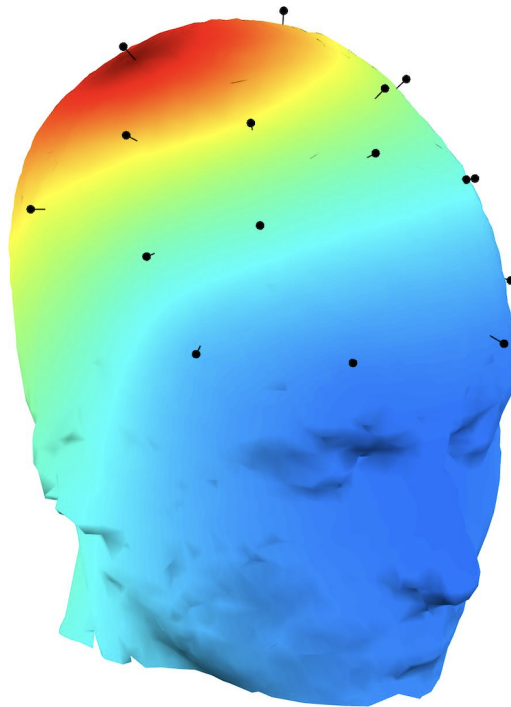


**Figure 4.4** 3D view of location of scalp electrodes

The toolkit assigns a microstate label to each frame of the pre-processed EEG sample after artifact removal. To extract the microstate parameters, we first selected four clusters to explain the EEG data samples [113], [12], [13], [82] as it ensured a good balance between the goodness of fit and the number of clusters and generated feasible topographies with good spatial correlation. After segmenting the recorded EEG time samples into four microstate classes [12], [13] the segments (series of frames) were extracted with the same microstate label with their duration, occurrence, and temporal coverage characteristics. Only the segments of length/duration 60-120 milli-seconds [113] were identified as microstates.

We then determined the number of microstates present in each condition (pre-event, event, post-event) for each trial. Finally, before applying the descriptive and statistical analysis, the NOM of each participant's trial were averaged out for each condition. The occurrence, duration and coverage parameters for all the microstate classes were calculated for each condition for all participants for the statistical analysis. For the spider plot analysis, the values of each parameter were first averaged over all trials for each condition for each participant, and then across all participants. A schematic representation of the microstate extraction procedure is shown in the flowchart Figure 4.5.

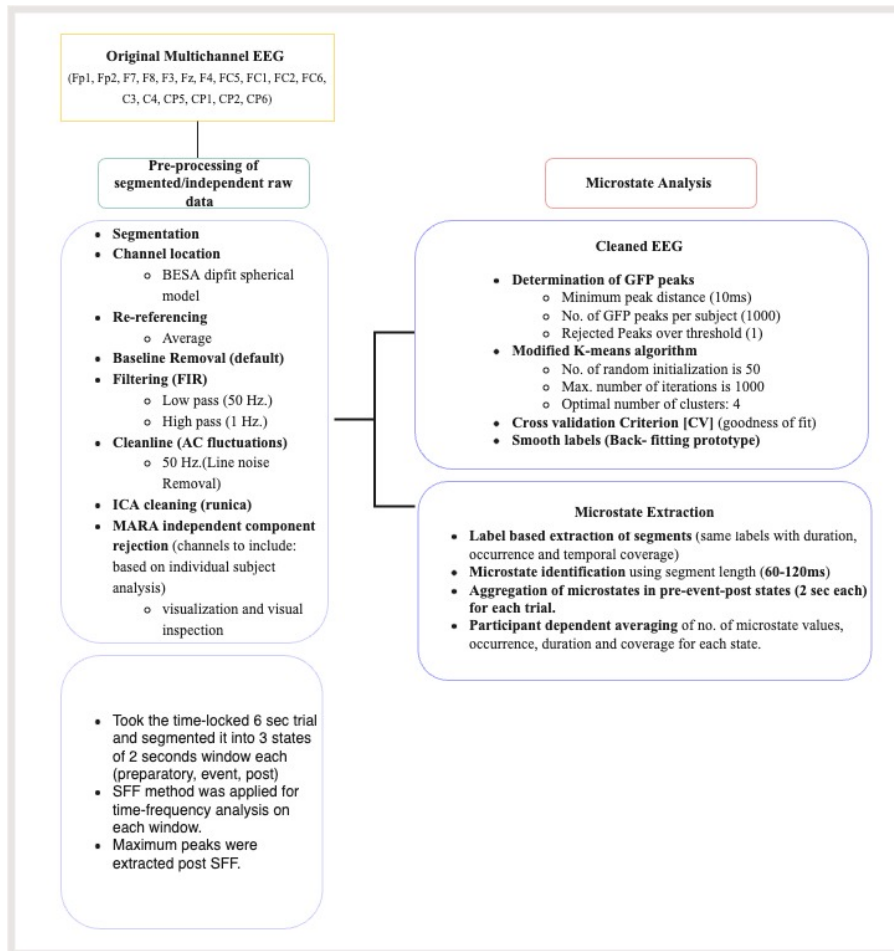
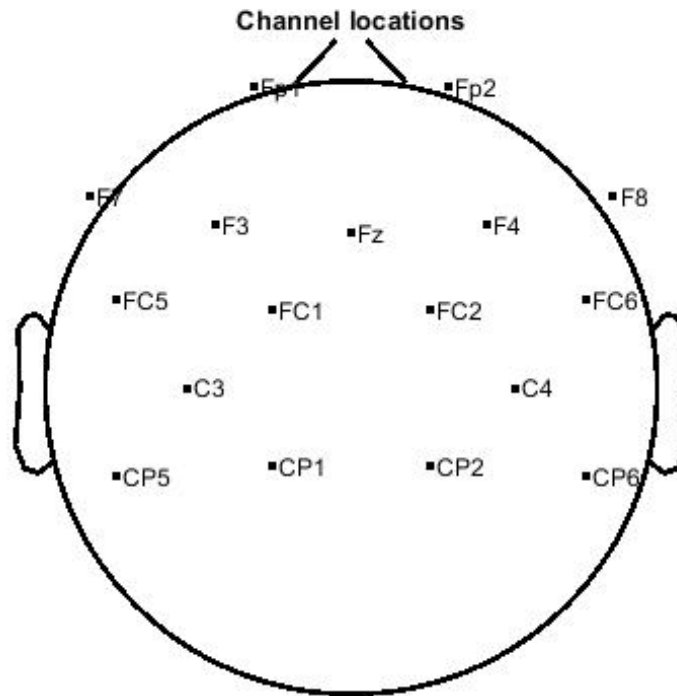


**Figure 4.5** Flow Chart representation of Pre-processing steps and Microstate Analysis of the EEG data

Global field power (GFP) [100] of the active microstates in the complete time range across all individuals for both the movements, done with the right and left hand separately, is shown in Figure 4.7 which visualises the microstate segmentation. GFP peaks along with the respective active global maps were extracted for both the motor tasks performed by all participants. The microstate classes were present throughout the whole signal and were evident across the entire range with varying intensities and activations. These microstate classifications account for significant percentages of the topographic variance and overall variance of the data. A thousand peaks [125] were obtained for each participant, and the maps were active for a total time of  $6 * 10^4$  ms.

### 4.3.2 Descriptive and Statistical Analysis

Shapiro-Wilk test was applied to check the normality of the microstate parameter values. Based on the distribution of the data, the non-parametric Wilcoxon signed rank test, or the parametric Student's paired t-test was used to obtain the condition-wise differences (pre-event vs event vs post-event) for all



17 of 17 electrode locations shown

**Figure 4.6** Electrodes covering the Pre-frontal, Frontal, Central and Motor regions of brain  
Pictorial representation of EEG montage as shown in EEGLAB

microstate parameters. To compare the left-handed and right-handed participant groups on NOM values for both the motor movements, the non-parametric Mann-Whitney U test or the Parametric Student's t-test was used. The statistical significance level for all tests was set at  $p < 0.05$ . To avoid Type I error, Bonferroni correction ( $p < 0.016$ ) was applied on the respective tests.

## 4.4 Results

We first present the microstate parameter values for the complete data set followed by statistical analysis with respect to the NOM, occurrence, duration and coverage in the pre-event, event, and post-event conditions for all twenty-nine participants. To analyse the role of handedness, two sets of right-handed participant group having five participants each were randomly picked and compared to a set of 5 left-handed cohort.

The Shapiro-Wilk test was significant for the NOM parameter for all three conditions in the left Wrist-flexion & extension, left Tip-pinch, and right Tip-pinch performed by all participants ( $p < 0.05$ ). Only for the event—post-event condition of the right Wrist-flexion & extension, Shapiro-Wilk was not

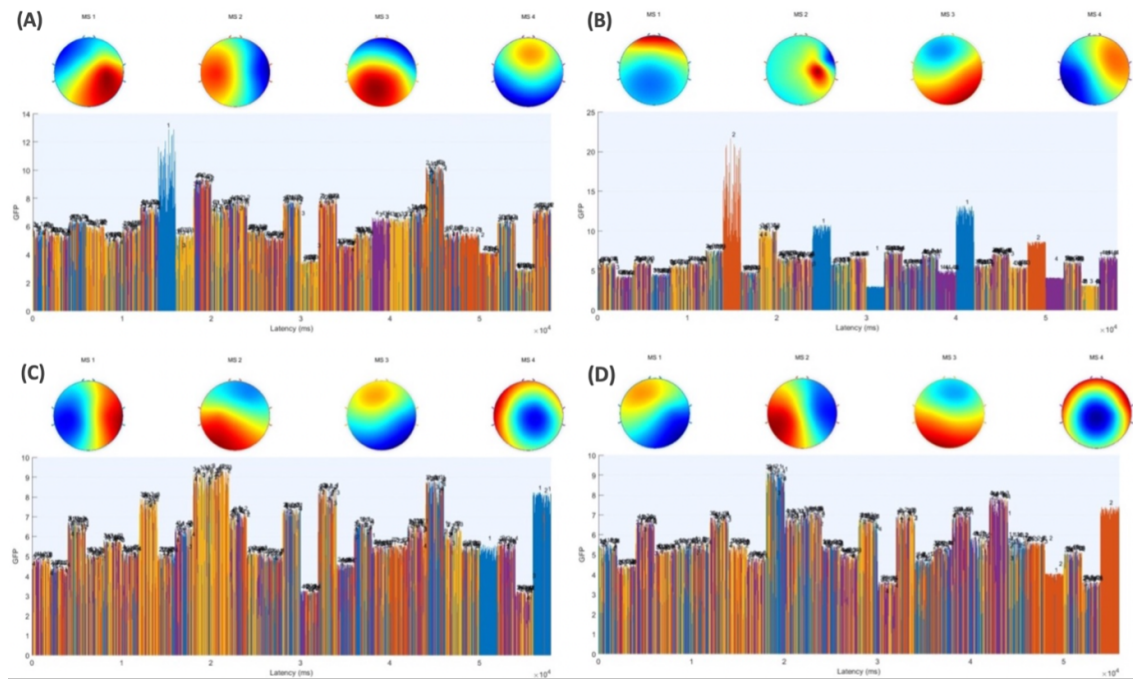


**Figure 4.7** GFP of the active microstates for (a) Left Wrist-flexion & extension (b) Right Wrist-flexion & extension (c) Left Tip-pinch (d) Right Tip-Pinch.

significant. For the three groups (handedness) of five participants each, data was non-parametric for 23 out of 36 sets of NOM values (3 conditions \* 4 movements \* 3 sets = 36).

Similarly, the Shapiro-Wilk test was significant for the occurrence, duration, and coverage parameters for only some of the conditions in all motor tasks (4 movements \* 3 conditions \* 4 microstate classes = total 48 sets of values for each parameter). Only  $MT_{MS2}$  of the pre-event—event condition for the right tip-pinch was significant ( $p < 0.05$ ) for occurrence parameter.  $MT_{MS3}$  of the pre-event—event condition for the left tip-pinch and  $MT_{MS3}$  of the event—post-event condition for the right tip-pinch were significant ( $p < 0.05$ ) for duration parameter. For coverage, only  $MT_{MS3}$  of the pre-event—post-event condition for left Wrist-flexion & extension was significant.

#### 4.4.1 The microstate topographies for each hand movement

As some of our extracted motor task topographies are different from the reported resting-state topographies, we have used the representation  $RS_{MSa-d}$  to refer to the resting-state microstate maps A, B, C, and D while  $MT_{MS1-4}$  to refer to the obtained motor-task-state microstate classes MS1, MS2, MS3 and MS4 respectively. As mentioned in section 4.3.1, GFP was extracted for all microstate classes for each exercise.  $MT_{MS1}$  has the maximum amplitude for Left Wrist flexion & extension, whereas  $MT_{MS2}$  has the highest amplitude for Right Wrist flexion & extension as shown in Figure 4.7A,B. For Left Tip-pinch shown in Figure 4.7C and Right Tip-pinch in Figure 4.7D, no microstate class with the highest GFP amplitude value is distinguishable.

The microstate topographies  $MT_{MS1}$ ,  $MT_{MS2}$ ,  $MT_{MS3}$ ,  $MT_{MS4}$  for the corresponding hand movements performed by all 29 individuals are a mix of non-canonical task specific topographies and resting-state (canonical) Koenig's maps that persisted in the motor task state. These microstate prototypes account for 75.1% variance for left Wrist flexion & extension Figure 4.8 and 73.6% variance for right Wrist flexion & extension Figure 4.9 while 75.6% variance for left Tip-pinch Figure 4.10 and 75.3% for right Tip-pinch Figure 4.11. The topographies obtained for the motor tasks are shown in the following Table 4.1.

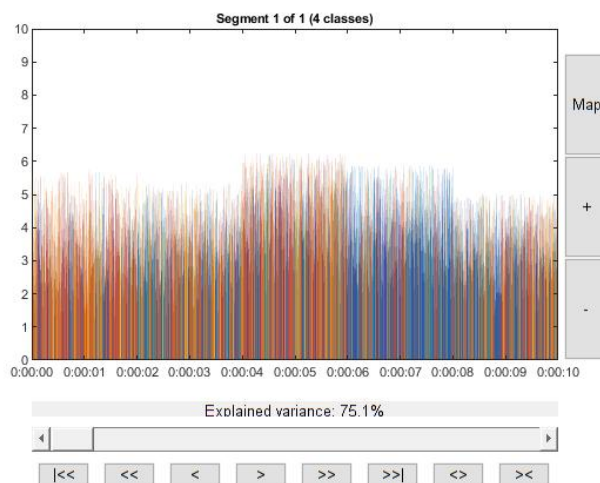


**Figure 4.8** Left Wrist flexion & extension all participants Global Explained Variance

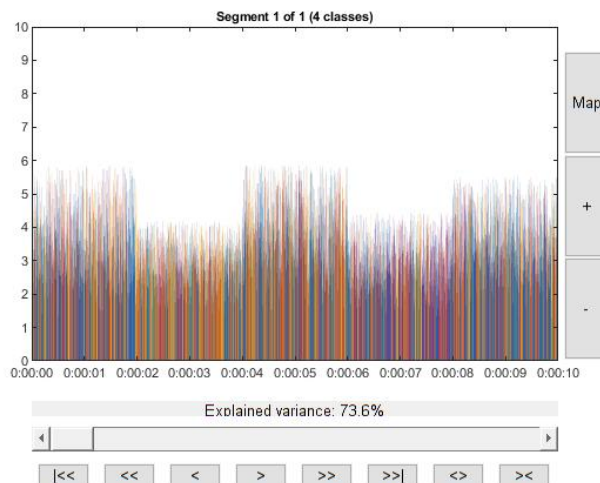


**Figure 4.9** Right Wrist flexion & extension all participants Global Explained Variance

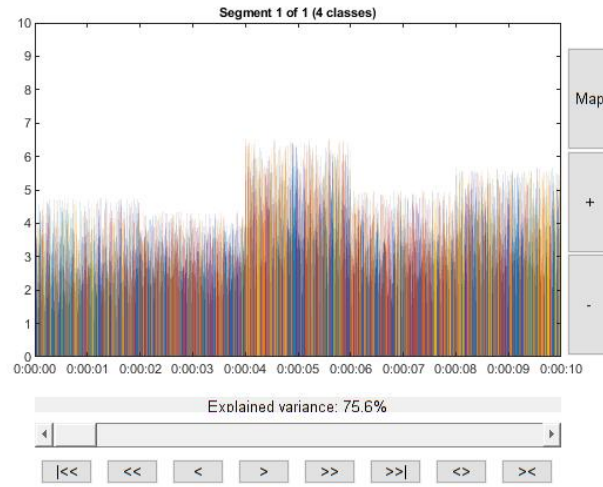


**Figure 4.10** Left Tip-pinch all participants Global Explained Variance

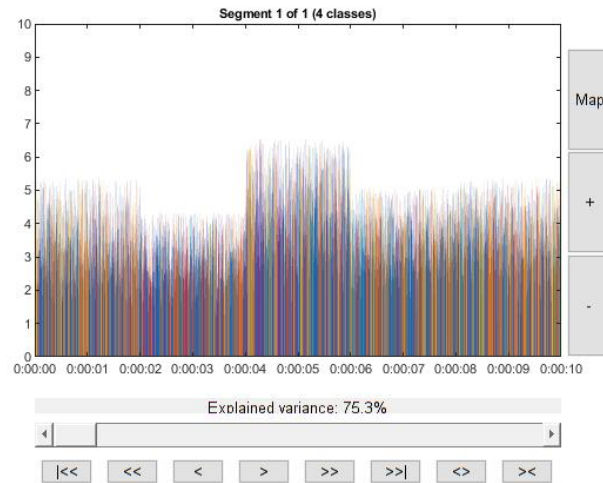


**Figure 4.11** Right Tip-pinch all participants Global Explained Variance

Motor-task	Microstate topographies	Regions of the brain	Electrodes	Similar to Koenig's resting state maps
Left wrist flexion/extension	$MT_{MS1}$	Left anterior to right posterior.	-	$RS_{MSb}$
	$MT_{MS2}$	-	F4, F8, FC6, C4, CP6, F3, F7, FC5, C3, CP5	x
	$MT_{MS3}$	Midline frontal to occipital.	-	$RS_{MSc}$
	$MT_{MS4}$	Midline occipital to frontal.	CP5, CP6, Fz	Partially to $RS_{MSd}$
Right wrist flexion/extension	$MT_{MS1}$	Midline occipital to frontal.	-	$RS_{MSd}$
	$MT_{MS2}$	Right anterior to centro-parietal.	FC6, C4	x
	$MT_{MS3}$	Left anterior to right posterior.	-	$RS_{MSb}$
	$MT_{MS4}$	Left posterior to right anterior.	-	$RS_{MSa}$
Left tip-pinch movement	$MT_{MS1}$	-	FC5, C3, CP5, F4, F8, FC6, C4, CP6	x
	$MT_{MS2}$	Right anterior to left posterior.	-	$RS_{MSa}$
	$MT_{MS3}$	Right posterior to left anterior.	-	$RS_{MSb}$
	$MT_{MS4}$	Right centro-parietal to left temporal and frontal.	C4, CP2, FC2, F7, FC5	x
Right tip-pinch movement	$MT_{MS1}$	Right posterior to left anterior.	-	$RS_{MSb}$
	$MT_{MS2}$	-	F4, F8, FC6, CP6, C4, CP1, FC5, C3, CP5	x
	$MT_{MS3}$	Midline frontal to occipital	-	$RS_{MSc}$
	$MT_{MS4}$	Centro-parietal to temporal and frontal orientations.	FC1, FC2, CP1, CP2, C3, C4, F7, FP1, FP2, F8	x

**Table 4.1** Microstate topographies for all motor tasks with their corresponding electrodes covering specific cortical areas. It is worth noting that we have specifically mentioned the brain regions that correspond to the conventional Koenig's orientations while marked a '-' for the ones that don't. We have mentioned the respective electrodes covering the brain region for the topographies that do not match Koenig's maps. The symbol 'x' denotes unmatched motor-task topographies discovered in our research

## 4.5 Microstate analysis based on comparing microstate parameters

### 4.5.1 Pre-event, event and post-event conditions comparison in Wrist flexion & extension

The spider plots Figure 4.12 and Figure 4.13 illustrate differences in pre-event, event and post-event condition values for each microstate characteristics for all exercises. For each microstate class, Figure 5.1.2 shows the p-values, means/ranks and their t/u scores (based on the parametricity of the data) for the microstate parameters for each state-group pair (pre-event—event, event—post-event, and pre-event—post-event).

**OCCURRENCE:** For left-hand movement, the event condition had higher occurrence values than pre-post condition, while pre-post values were comparable. For all microstate classes, the **Student's t-test** was significant for the groups pre-event—event and event—post-event Table 5.40. However, only  $MT_{MS1}$  and  $MT_{MS2}$  were significant ( $p < 0.016$ ) for the pre-event—post-event group pair. A similar pattern was seen with the right-hand, with differences being significant in the groups pre-event—event and event—post-event but not in the pre-event—post-event group pair Table 5.40.

**DURATION:** For left-hand movement, the event condition had higher duration values than the other two conditions. For all microstate classes, the **Student's test** was significant for pre-event—event and event—post-event Table 5.41. A similar pattern was seen with the right-hand, where the group differences in pre-event—event and event—post-event were significant Table 5.41.

**COVERAGE:** A similar trend was also observed for coverage values, with higher values in the event conditions than the other two conditions for left-hand movement. For all microstate classes, the **Student's t-test** was significant for groups pre-event—event and event—post-event, however only  $MT_{MS1}$  was significant for the pre-event—post-event group pair Table 5.42. A similar pattern was seen with the right-hand, where the group differences in pre-event—event and event—post-event were significant for all microstate classes, however only  $MT_{MS3}$  was found significant in pre-event—post-event group pair Table 5.42.

**NOM:** The event condition had significantly higher NOM values than the other two conditions for Wrist-flexion & extension done with the left-hand, whereas the pre-event and post-event conditions had comparable NOM values Table 5.2. The **Wilcoxon signed rank test** was significant for the pre-event—event ( $m1=4.276$ ,  $m2=9.172$ ,  $W=0$ ,  $p<.001$ ,  $N=29$ ,  $z\text{-score}=-4.703$ ) and, event—post-event ( $m1=9.172$ ,  $m2=4.310$ ,  $W=435$ ,  $p<.001$ ,  $N=29$ ,  $z\text{-score}=4.703$ ) while not significant for the pre-event—post-event group pair. A similar pattern was observed in the movement performed with the right-hand Table 5.2, where **Wilcoxon signed rank test** was significant for the groups pre-event—event ( $m1=4.138$ ,  $m2=8.862$ ,  $W=0$ ,  $p<.001$ ,  $N=29$ ,  $z\text{-score}=-4.703$ ) and, event—post-event ( $m1=8.862$ ,  $m2=4.414$ ,  $W=435$ ,  $p<.001$ ,  $N=29$ ,  $z\text{-score}=4.703$ , effect) while not significant for the pre-event—post-event group pair.

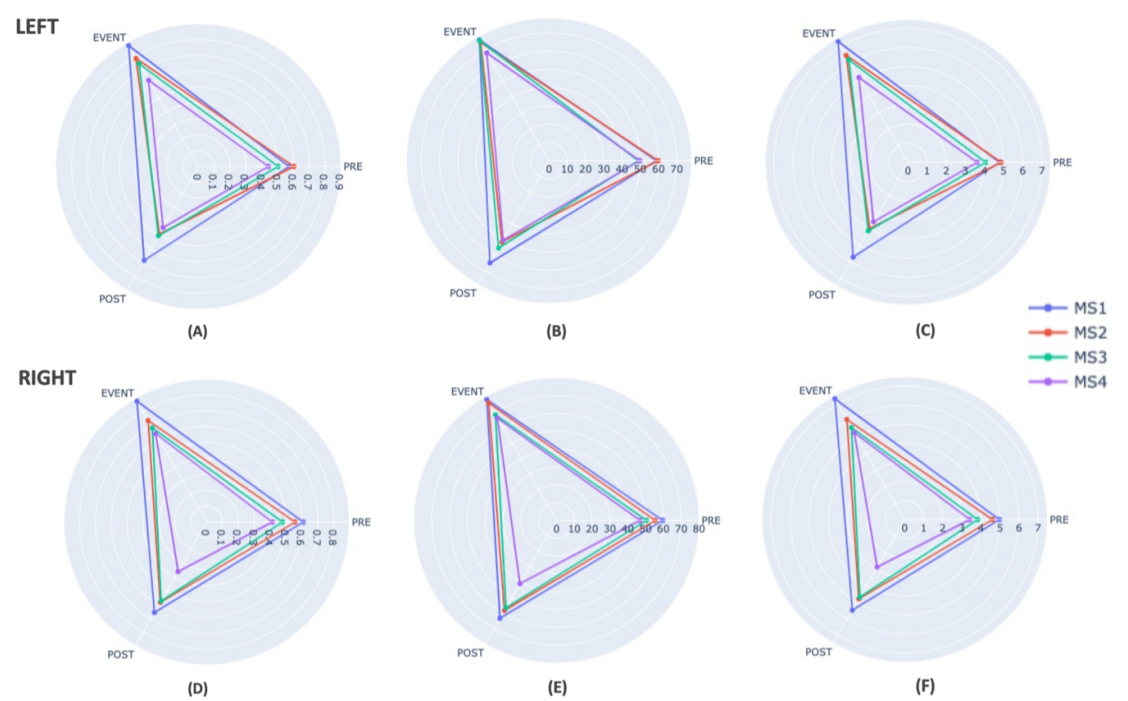


**Figure 4.12** Wrist Flexion & Extension Spider plots for the left and right hand movements.  
 (a) Occurrence (b) Duration (c) Coverage for the left hand &  
 (d) Occurrence (e) Duration (f) Coverage for the right hand

#### **4.5.2 Comparison of Left- and right-handed participants for Wrist flexion & extension for NOM values (5 participants in each group)**

Our dataset consisted of five left-handed participants and twenty-four right-handed participants. For comparing the flexion movement of left-handed and right-handed participants, ten right-handed participant's data were randomly picked and divided into two groups (Set-1 and Set-2). The **Mann-Whitney test** did not show significant effect of handedness for NOM values Table 5.3, Table 5.8, Table 5.9.

#### **4.5.3 Pre-event, event and post-event conditions comparison in Tip-pinch**

**OCCURRENCE, DURATION & COVERAGE** : For the left-hand, the occurrence, duration, and coverage values for all three conditions were comparable Figure 4.13. There was no significant difference in pre-event—event, event—post-event, as well as pre-event—post-event groups across all microstate classes. For the right Tip-pinch movement, however, the group difference in  $MT_{MS1}$  for the pre-event—event group pair was significant for occurrence and coverage parameters whereas the group difference in  $MT_{MS4}$  was significant for the event—post-event group pair for all parameters Table 5.40, Table 5.41, Table 5.42.

**NOM**: For tip-pinch performed with the left-hand, all three condition NOM values were comparable Table 5.2. The **Wilcoxon signed rank test** was not significant for any group pair. In the case of Tip-pinch performed with the right-hand, the Wilcoxon signed rank test was significant only for event—post-event group pair ( $m1=4.793$ ,  $m2=4.172$ ,  $W=140$ ,  $p=0.002$ ,  $N=29$ ,  $z\text{-score}=3.006$ ) and not significant for the other two groups.

#### **4.5.4 Comparison of Left- and right-handed participants for Tip-pinch for NOM values (5 participants in each group)**

The participant grouping to test the effect of handedness for Tip-pinch movement was similar to the Wrist flexion & extension movement. The left-handed participant group had comparable NOM values with both the right-handed participant's groups (Set-1 and Set-2) and hence the Mann-Whitney test was not significant Table 5.3, Table 5.5, Table 5.6.

#### **4.5.5 Comparing Wrist flexion & extension and Tip-pinch for NOM values**

A between subject analysis of all 29 participants using non-parametric **Mann-Whitney U test** for the motor-tasks performed with the left-hand for NOM parameter showed significant differences between the left Wrist-flexion & extension and left tip-pinch movement ( $U\text{-mean}=420.5$ ,  $p\text{-value}<.001$ ,  $n1=29$ ,  $n2=29$ ,  $z\text{-score}=6.53$ ,  $\text{effect-size}:1$ , two-tailed). Similar result was observed for the right Wrist flexion

& extension and right tip-pinch (U-mean=420.5, p-value<.001, n1=29, n2=29, z-score=6.44, effect-size:0.9, two-tailed).

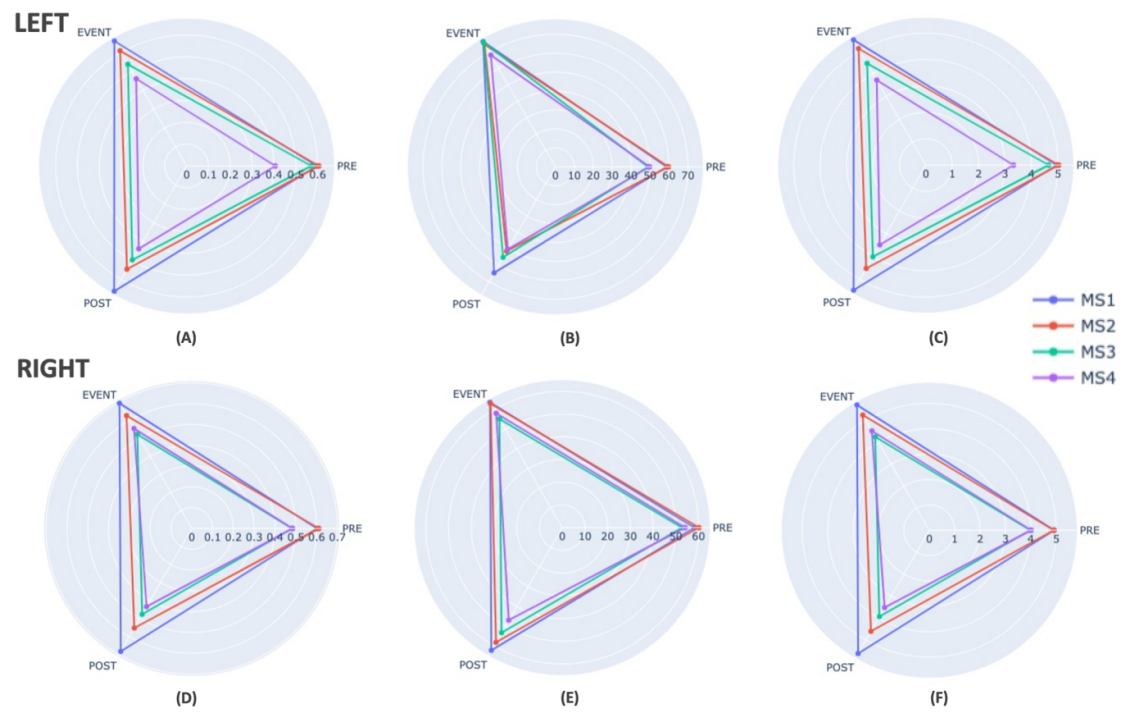


**Figure 4.13** Tip-pinch Spider plots for the left and right hand movements.  
 (a) Occurrence (b) Duration (c) Coverage for the left hand &  
 (d) Occurrence (e) Duration (f) Coverage for the right hand

## 4.6 Interpretation of Results

Resting-state microstates are conventionally labelled as microstate class A — left occipital to right frontal orientation ( $RS_{MSa}$ ), B — right occipital to left frontal ( $RS_{MSb}$ ), C — symmetric occipital to prefrontal orientation ( $RS_{MSc}$ ) and D — symmetric but with a frontocentral to occipital axis ( $RS_{MSd}$ ) [83]. Each microstate class is linked to a specific functional brain area network, such as Microstate class A (left posterior–right anterior orientation:  $RS_{MSa}$ ) for Auditory, class B (right posterior–left anterior orientation:  $RS_{MSb}$ ) for visual, class C (anterior–posterior orientation:  $RS_{MSc}$ ) for Saliency and class D (central maximum:  $RS_{MSd}$ ) for attention networks [12], [28], [27]. These microstates help us in identifying brain networks and their temporal activation by comparing resting state with motor tasks (reaching and grasping) [117]. All four microstate classes are evident across the entire signal range with varying intensities and demonstrate the activations in different brain regions corresponding to the respective upper limb motor movement carried out in our study. Comparing the established resting state topographies or canonical maps established in literature to our motor-task topographies based on the

spatial configuration of the potential distribution, revealed shared and task-specific maps, implying that only a few resting state topographies persisted during motor tasks performed in our experiment.

#### 4.6.1 Comparative analysis of the motor task topographies for all hand movements

For the Left Wrist flexion & extension, our  $MT_{MS1}$  corresponds to  $RS_{MSb}$ ,  $MT_{MS3}$  to  $RS_{MSc}$  and  $MT_{MS4}$  partially to  $RS_{MSd}$ , Figure 4.7A.  $MT_{MS2}$  is distinct from the resting-state maps indicating that electrodes capturing the frontal, central and centro-parietal bilateral regions show higher signal strength during this task. For the Right Wrist flexion & extension,  $MT_{MS1}$  corresponds to  $RS_{MSd}$ ,  $MT_{MS3}$  to  $RS_{MSb}$ , and  $MT_{MS4}$  to  $RS_{MSa}$  with inverted polarity.  $MT_{MS2}$  emerged as task-specific map for this task, as seen in the Figure 4.7B. The electrodes encompassing the anterior and posterior regions of the brain show reversed signal strength as indicated from  $MT_{MS4}$ , and some electrodes covering ipsilateral centro-parietal region show more signal strength. Comparison of the task-specific topographies of the Left with the Right Wrist flexion & extension movement shows the common and laterality-specific topographies. While  $MT_{MS2}$  of the right is a laterality-specific topography,  $MT_{MS1}$  of the left is comparable to  $MT_{MS3}$  of the right,  $MT_{MS2}$  of the left partially matches  $MT_{MS4}$  of the right,  $MT_{MS3}$  of the left is  $MT_{MS1}$  of the right with inverted polarity, and  $MT_{MS4}$  of the left corresponds to  $MT_{MS1}$  of the right, but with varying intensities.

For the Left tip-pinch movement,  $MT_{MS2}$  corresponds to  $RS_{MSa}$  and  $MT_{MS3}$  corresponds to  $RS_{MSb}$  with inverted polarity as shown in Figure 4.7C.  $MT_{MS1}$  and  $MT_{MS4}$  are task-specific maps for this movement demonstrating that few electrodes capturing the ipsi-lateral temporal and fronto-central regions show higher signal strength. For the right Tip-pinch movement,  $MT_{MS3}$  corresponds to  $RS_{MSc}$  and,  $MT_{MS1}$  corresponds to  $RS_{MSb}$  with inverted polarity Figure 4.7D.  $MT_{MS2}$  and  $MT_{MS4}$  task-specific topographies for this movement which demonstrate that some electrodes covering the bilateral pre-frontal, frontal, fronto-central, central and centro-parietal regions show higher signal strength. Left and right tip-pinch topographies are more similar than those of wrist movement. The  $MT_{MS1}$  of the left tip-pinch movement corresponds to the  $MT_{MS2}$  of the right Tip-pinch movement with inverted polarity, the  $MT_{MS2}$  of the left partially matches the  $MT_{MS3}$  of the right, and the  $MT_{MS3}$  and  $MT_{MS4}$  of the left respectively match the  $MT_{MS1}$  and  $MT_{MS4}$  of the right.

The respective electrodes positioned in the anterior and posterior regions of the brain show reversed brain signal strength during the movements than what it was at rest, as indicated by  $MT_{MS3}$  of the left- and  $MT_{MS1}$  of the right Tip-pinch movement.

In addition to the standard microstate classes, the task-specific maps  $MT_{MS1}$  (left tip-pinch),  $MT_{MS2}$  (left Wrist flexion & extension and right Tip-pinch), and  $MT_{MS4}$  (left- and right Tip-pinch), are also present during the movement execution. It is worth noting that the  $MT_{MS4}$  of both tip-pinch movements is quite distinct from the topographies of Wrist flexion & extension movement but closer to the novel class E found by [146] for grasping movement.

## 4.6.2 Microstate parameters' analysis for all hand movements

As the spider plots Figure 4.12, Figure 4.13 represent, except for the left Tip-pinch, in which  $MT_{MS2}$  has a slightly longer duration Table 5.1 than  $MT_{MS1}$  during task performance, respective  $MT_{MS1}$  has the greatest occurrence, coverage, and duration during and after the execution of the respective motor task Table 5.43. However, in the preparation phase,  $MT_{MS2}$  has higher occurrence, duration, and coverage in the left Wrist flexion & extension and the left- and right Tip-pinch while  $MT_{MS1}$  has more occurrence, longer duration, and greatest coverage in the case of right Wrist flexion & extension Table 5.1.

The dominance of  $MT_{MS1}$  in all microstate parameters during the preparatory phase of right Wrist flexion & extension movement rather than  $MT_{MS2}$ , which is dominant in the case of left Wrist flexion & extension, may be attributed to the higher number of self-reported right-handed participants (twenty-five out of twenty-nine). The subjects anticipated the right Wrist flexion & extension movement performed with their dominant right-hand with fewer microstates (mean  $NOM_{right\_wrist-flexion/extension} = 4.138$ ) than their non-dominant left-hand (mean  $NOM_{left\_wrist-flexion/extension} = 4.276$ ). This is further supported by the observation that for right Wrist flexion & extension,  $MT_{MS1}$  (Koenig's resting state topography  $RS_{MSd}$  as reported in Table 4.1), persisted across all conditions for all parameters. The need for a relatively greater number of microstates to anticipate the left Wrist flexion & extension movement performed using non-dominant left-hand, i.e., starting to prepare earlier than with their dominant hand, may be used to explain the dominance of  $MT_{MS2}$ , which is a task-specific topography that emerged during the preparatory phase of the left Wrist flexion & extension movement, for all microstate parameters. This preparatory anticipatory motor imagery may have triggered one's motor visual memory or imagery, leading to an early onset of  $MT_{MS2}$  in pre-event condition followed by  $MT_{MS1}$  (Koenig's resting state topography  $RS_{MSb}$  as reported in Table 4.1) which persisted in event and post-event conditions. It is also worth noting that the significant differences in the occurrences of  $MT_{MS1}$  and  $MT_{MS2}$  between pre-event and post-event conditions of left Wrist flexion & extension may suggest post-motor movement analysis by the participants with their non-dominant hand. This is corroborated by the lack of any statistically significant difference in the occurrence of microstates for any condition of the right Wrist flexion & extension movement. The PSD (Power-Spectral Density) is shown for a left-handed Figure 4.14 (A),(B) and a right-handed participant Figure 4.14 (C),(D). For both participants, there is a high signal intensity in case of using their non-dominant hand which can be attributed to their handedness as they have to put more cognitive effort in executing the motor task [138]. This is also supported by studies employing other techniques like fMRI [26]. Since variations in power of different brain areas may imply distinct brain activities, critical information stored in the spatial distribution of brain power is necessary. Study by [80] indicated that in their comparative analysis, Power Spectral Density techniques are more reliable and consistent in obtaining the EEG spectral patterns connected to motor imagery. However, another finding of our study shows that NOM is independent of the subjects' handedness for both motor tasks (as reported in subsection 4.5.2 and subsection 4.5.4), suggesting that more research is needed to make inferences from these findings.

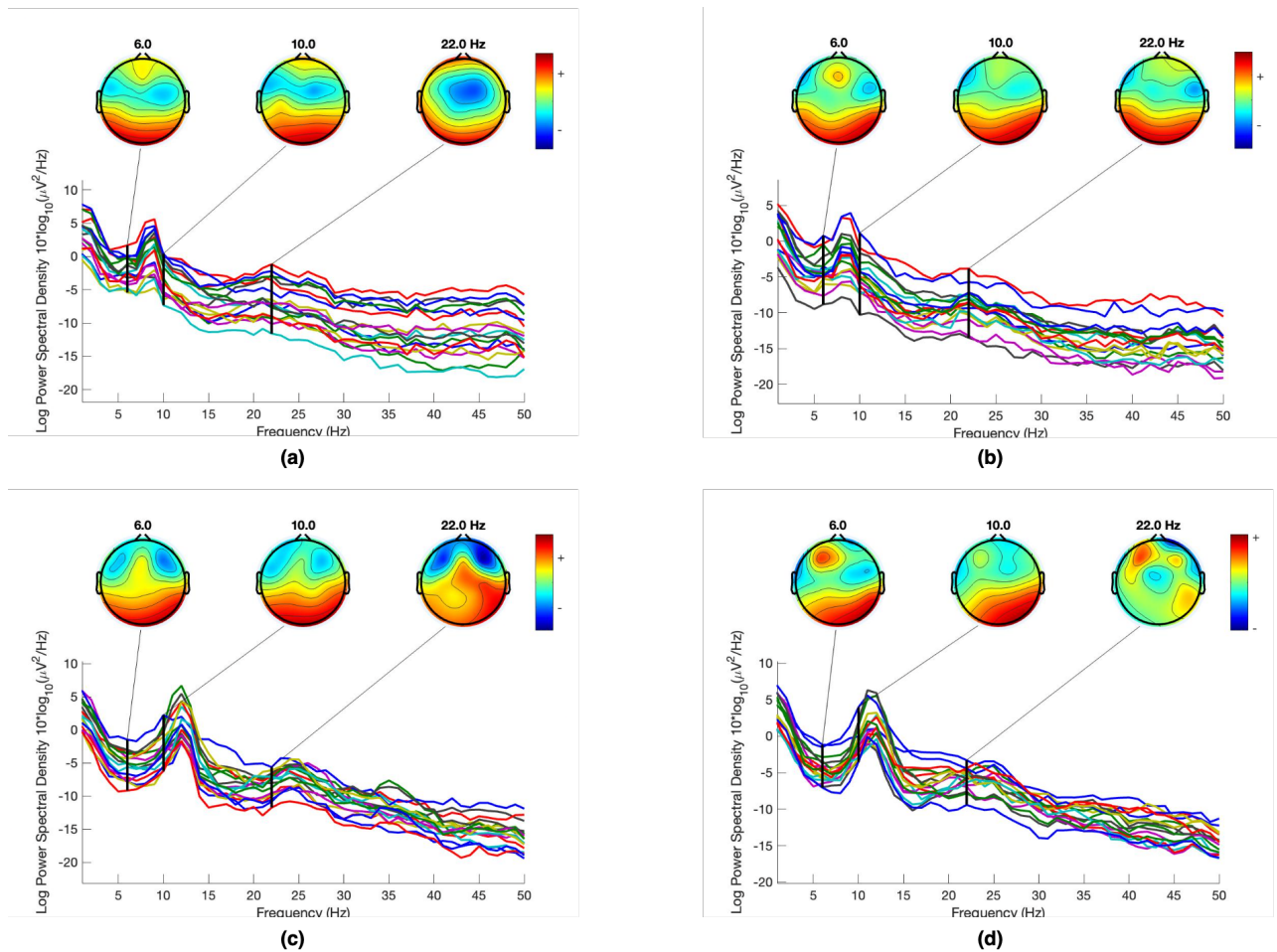


**Figure 4.14** Power spectral density for a left-handed and a right-handed participant. (a) left\_wrist\_flexion\_by\_left-handed-participant (b) right\_wrist\_flexion\_by\_left-handed-participant (c) left\_wrist\_flexion\_by\_right-handed-participant (d) right\_wrist\_flexion\_by\_right-handed-participant

In contrast to the Wrist flexion & extension movements,  $MT_{MS2}$  is prominent during the preparatory phases of the left and right tip-pinch movements, indicating that the participants' handedness probably has no impact on their preparedness for the tip-pinch task. Similar result is also observed for NOM parameter where tip-pinch has significantly fewer number. of microstates than Wrist flexion & extension in the event condition for both left- and right-hand movements subsection 4.5.4. It might be because wrist movement is generally performed with the dominant hand, but tip-pinching is frequently utilised in many daily tasks [34] regardless of handedness. However, the significant differences in  $MT_{MS4}$ , similar to the class D microstate [27] comprising of brain areas attributed to central executive control appeared during the event condition for all microstate parameters in case of the right tip-pinch movement, between event and post-event conditions require further investigation.

For both left and right Wrist flexion & extension movements, pre-event and post-event conditions had mostly comparable values for the occurrence, duration and coverage parameters Figure 4.12, whereas

the event condition had significantly higher values than other two conditions. The statistical tests showed significant differences in these motor tasks between the pre-event—event and event—post-event condition groups for all 29 participants for all parameters Table 5.40, Table 5.41, Table 5.42. Similarly for NOM, event condition had the maximum number of microstates, as mentioned in subsection 4.5.1. These significantly higher values during the execution than pre and post motor task can be explored further as potential markers.

In the comparative analysis of the pre-event—post-event condition for left- and right-Tip-pinch and left Wrist flexion & extension movements,  $MT_{MS2}$  is found to occur more frequently and for a longer duration before the execution, whereas  $MT_{MS1}$  is observed to occur more frequently following the execution of the exercise. Additionally, the mean coverage of  $MT_{MS1}$  before and after performing these motor tasks is significantly different only in case of left Wrist flexion & extension. For the right Wrist flexion & extension,  $MT_{MS3}$  has significantly more coverage following the task completion. The statistically comparable values of all parameters Figure 4.13 and Table 5.40, Table 5.41, Table 5.42 across all three conditions, suggest that there are no differences in the state of microstates before, during or after performing the left pinch movement. For the right Tip-Pinch movement,  $MT_{MS1}$  occurs more frequently and has greater coverage in the event condition than in the other two conditions. Likewise,  $MT_{MS4}$  (a task-specific topography) is observed to occur significantly more frequently, for a longer duration, and with greater coverage in the event condition compared to the other two conditions. These findings are in line with our prior observation that event condition has highest NOM values amongst all conditions for tip-pinch subsection 4.5.3. It is interesting to note that there are significant differences in microstates between the basic left- and right- tip pinch movements. However, given the sample size constraints, interpreting these findings with caution is critical as when checked for groupwise differences based on the handedness of the participants, the nonparametric Mann-Whitney test of NOM found no significant differences between left- and right-handed participants in any of the four movements Table 5.2 suggesting that disruption in total no. of microstates is independent of the dexterity of the participants.

---

Microstates can be utilized to explore different brain activation patterns and identify different intensities of brain during motor tasks. It also provides insights into the functional connectivity and communication between these regions during motor tasks.

#### 1. **Left vs Right Wrist flexion & extension** : Activations of brain region electrodes based on Microstate Montages

- **MS1** : For left Wrist flexion & extension, contralateral (right posterior region) electrodes seemed to have more high electrical activations as opposed to right Wrist flexion & extension where the (frontal cortical region) electrodes Fp1, Fp2, F3, F4, F7 & F8 seemed to have more high activations.

- **MS2** : For left Wrist flexion & extension, ipsilateral (left temporal region) electrodes seemed to have more high electrical activations than the right Wrist flexion & extension where ipsilateral (right central and parietal region) electrode C4 seemed to have more high activations.
- **MS3** : For both left and right Wrist flexion & extension, the posterior part of the brain seemed to have higher activations. In case of left Wrist flexion & extension, the left posterior (ipsilateral region) electrode had higher intensity activations and the frontal cortical region electrodes F3, F4 & Fz had distributed low intensity/energy activations while in case of right flexion, the right posterior (ipsilateral region) electrode had higher intensity activations and the left anterior part region electrode F7, F3, & Fp1 had more low intensity activations.
- **MS4** : For both left and right Wrist flexion & extension, the overall intensity of the high activations was less. In case of left Wrist flexion & extension, the frontal part of the brain electrodes Fp1, Fp2, F3, F4 & Fz seemed to have more high activations while right anterior (ipsilateral region) electrodes F8, F4, & Fp2 seemed to have more high activations in case of right Wrist flexion & extension.

## 2. **Left vs Right Tip-Pinch** : Activations of brain region electrodes based on Microstate Montages

- **MS1** : For left tip-pinch, contralateral (right temporal region) electrodes T5, P3 seemed to have more high activations than for right tip pinch which seemed to have high activations in the left anterior cortical region electrodes F7, F3, & Fp1. The left tip pinch had higher intensity activations than the right tip pinch.
- **MS2** : For left tip-pinch, posterior part of the brain ( occipital lobe & parietal lobe) electrodes O1, O2 & Pz seemed to have more high activations as compared to right tip-pinch which seemed to have higher activation in contralateral (left) temporal cortical region electrodes T6 & P4.
- **MS3** : The left tip-pinch seemed to have lesser intensity high activations than the right tip-pinch. In case of left tip pinch, ipsilateral (left anterior region) electrodes Fp1, F3, & F7 seemed to have high activations as compared to right tip-pinch which seemed to have distributed high activations in the posterior region electrodes O1, O2, P3, Pz, & P4.
- **MS4** : For both left and right tip-pinch, the frontal cortical region electrodes Fp1, Fp2, F3, F4, F7, & F8 seemed to have high activations. In case of left tip-pinch, the ipsilateral (left

frontal and temporal regions) electrodes F3, C3, F4, & C4 seemed to have high activation as compared to right tip pinch which seemed to have more distributed high activations in frontal electrodes F3, F4, F7 & F8 and temporal electrodes.

---

The GFP peak plots for comparing left-handed group of participants (5) with two right-handed groups of participants (5 each) are shown in Figure 4.15, Figure 4.16, Figure 4.17 and Figure 4.18 for Wrist flexion & extension and Tip-pinch exercises. From these topographical maps, we observe that for any motor movement, topographies between any two groups of participants exhibit observable differences invariant of the handedness of the participants in the group. This suggests idiosyncratic behavior in topographies with respect to participants. We also observe that these inter-group differences are relatively less in case of Tip-pinch movements. Overall, extraction of microstate maps for these exercises leads us to observe no generalizable patterns with respect to handedness of participants. This is also supported by our findings in case of NOM microstate parameter.

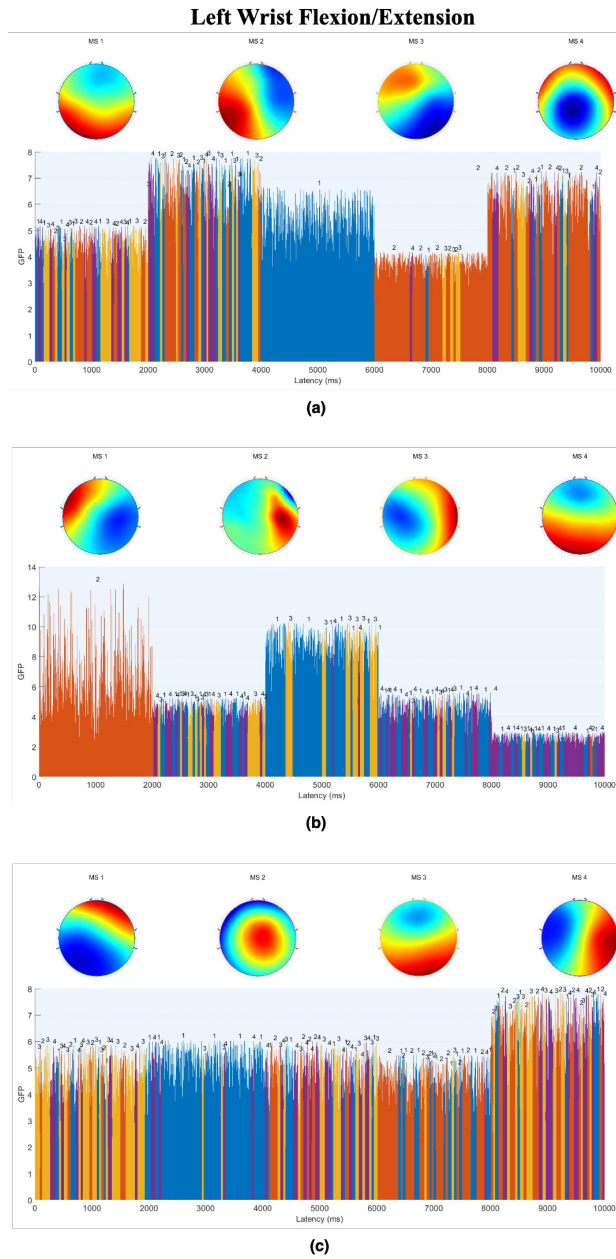


**Figure 4.15** Left Wrist flexion & extension for a group of 5 participants (a) right-handed participant set-1 (b) right-handed participant set-2 (c) left-handed participant set

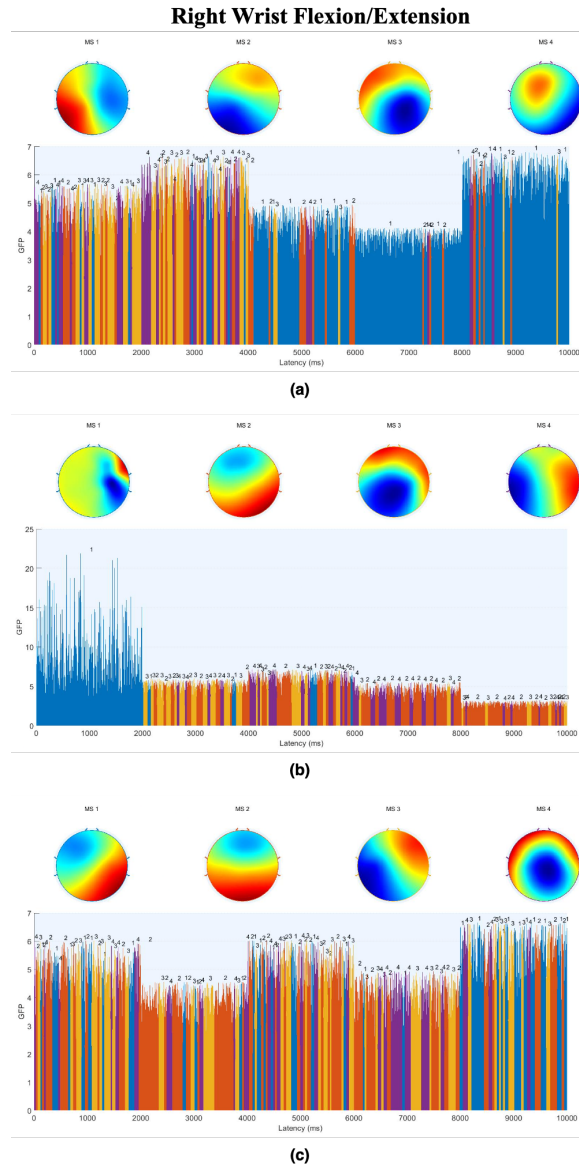


**Figure 4.16** Right Wrist flexion & extension for a group of 5 participants (a) right-handed participant set-1 (b) right-handed participant set-2 (c) left-handed participant set

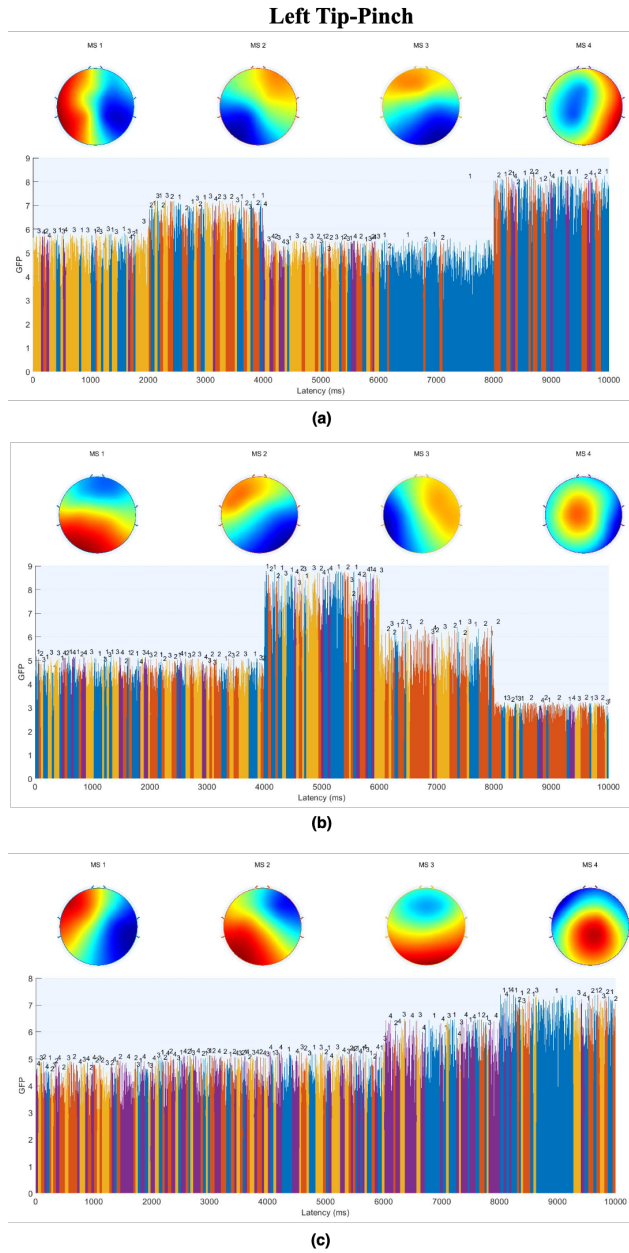


**Figure 4.17** Left Tip-Pinch for a group of 5 participants **(a)** right-handed participant set-1 **(b)** right-handed participant set-2 **(c)** left-handed participant set

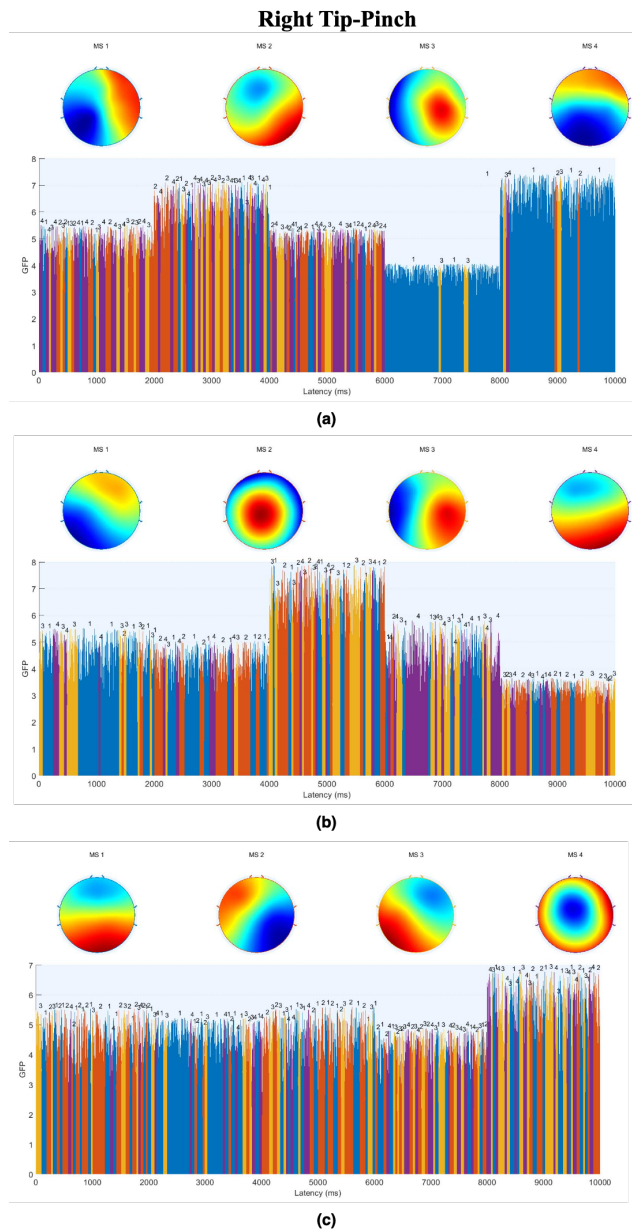


**Figure 4.18** Right Tip-Pinch for a group of 5 participants **(a)** right-handed participant set-1 **(b)** right-handed participant set-2 **(c)** left-handed participant set

## *Chapter 5*

### **Conclusion**

#### **5.1 Findings**

In this work, we analyse the brain's electrical activity of motor action executed when cued by a visual stimuli. The actions were Wrist flexion & extension and Tip-pinch (index & thumb) by each hand separately. These simple motor movements are critical to understand functionality of the motor cortex in particular. The participants were healthy young adults. The EEG signals from 17 electrodes channels was analysed for microstates. The study found that both right and left hand movements have a Global Explained Variance of over 70% across all four microstate classes. We determine whether the established canonical resting-state EEG maps labelled by Koenig persist during motor tasks. For each motor movement, we investigate the effects of microstate parameters (occurrence, duration, coverage, and the number of microstate values) between and within each of the three conditions (pre-event, event and post-event). The NOM microstates for both motor tasks is independent of the handedness. This is also corroborated by our findings from the comparative analysis of the topographical maps of left-handed and right-handed participants. We observe task-dependent variation in microstate topographies, deviating from resting-state EEG maps. These sets of topographies differ by laterality as well. The Tip-pinch movement shows higher microstate class stability than Wrist flexion & extension in the event condition (during the execution of the task), indicative of lower disruption due to processing for this motor task. In addition to this, we also report the statistical significance analysis of the microstate parameters.

By comparing the topographies and parameters of these motor tasks, the study provides new insights into the brain's neuronal networks and identifies disruptions in microstates during the processing of motor tasks. These findings can be used as a reference model to compare with a patient dataset of motor movements and resting state.

### **5.1.1 Unique Contributions of this Research**

Our work has following main contributions:

- We add to the existing literature by exploring upper-limb movements using EEG microstates by examining Wrist flexion & extension motor task.
- We compare EEG microstates across pre-event and post-event conditions, in addition to the traditionally reported event-condition, which extends the scope of existing research.
- We introduce a novel condition based microstate parameter number of microstates (NOM), which is defined as a classification on magnitude rather than frequency (per second), capturing the overall number of microstates across the condition.

These findings provide new insights to the field of spontaneous dynamic activity, allowing for a more accurate classification of disorders related to upper limb motor movements.

### **5.1.2 Limitations and Implications for Future Work**

The study was exploratory in nature, and data was only obtained from healthy individuals, and allowed for the development of a reference model to compare with motor activities performed by stroke or upper limb injury patients. Second, only younger-aged males got recruited for this study. For a more generalised result, it is necessary to generate models as a function of age. In addition, the distribution of right- and left-handed individuals was highly skewed as it was not the initial scope of the study. Third, the microstate transition probabilities have not been examined in our research. Looking into this might yield useful information on the systematic deviation of these probabilities from randomness during upper limb motor movements as well as handedness-specific variations in the deviation patterns of these probabilities. The experiment was initially designed to collect data from stroke patients, but due to covid pandemic we had to restrict the collection to participants within the campus. In the future, we would like to extend our study to post-stroke patients by utilising the current results as a pre-defined model. Additionally, using EEG source imaging, combined EEG-fMRI for source localization or using source-space microstate analysis [194] offers insights on the upper limb motor movement-specific brain regions that are functionally inter-related (neural networks).

## Related Publications

- Supreeth S Karan, Harsh Sharma, Ayushi Kumari Agrawal, Kavita Vemuri. "Investigation of microstates from EEG signals of tip-pinch and wrist flexion/extension movement." accepted as an abstract in **Society of Applied Neuroscience, 2022**
- Supreeth S Karan, Harsh Sharma, Ayushi Kumari Agrawal, Kavita Vemuri. "EEG microstate analysis of tip-pinch and wrist flexion/extension movement" (under review in a journal).
- Harsh Sharma, Supreeth S. Karan, Ayushi Kumari Agrawal, Kavita Vemuri. "The role of individual physical body measurements and activity on spine kinematics during flexion, lateral bending and twist tasks in healthy young adults – Comparing marker(less) data." accepted in **Biomedical Signal Processing and Control, 2023**.

## Bibliography

- [1] P. A. Abhang, B. W. Gawali, and S. C. Mehrotra. Technological basics of eeg recording and operation of apparatus. *Introduction to EEG-and Speech-Based Emotion Recognition*, pages 19–50, 2016.
- [2] A. S. Al-Fahoum and A. A. Al-Fraihat. Methods of eeg signal features extraction using linear analysis in frequency and time-frequency domains. *International Scholarly Research Notices*, 2014, 2014.
- [3] W. J. Anderst, W. F. Donaldson III, J. Y. Lee, and J. D. Kang. Continuous cervical spine kinematics during in vivo dynamic flexion-extension. *The Spine Journal*, 14(7):1221–1227, 2014.
- [4] G. Aneeja and B. Yegnanarayana. Single frequency filtering approach for discriminating speech and non-speech. *IEEE/ACM Transactions on Audio, Speech, and Language Processing*, 23(4):705–717, 2015.
- [5] S. Baillet, J. C. Mosher, and R. M. Leahy. Electromagnetic brain mapping. *IEEE Signal processing magazine*, 18(6):14–30, 2001.
- [6] C. M. Bauer, F. M. Rast, M. J. Ernst, S. Oetiker, A. Meichtry, J. Kool, S. M. Rissanen, J. H. Suni, and M. Kankaanpää. Pain intensity attenuates movement control of the lumbar spine in low back pain. *Journal of Electromyography and Kinesiology*, 25(6):919–927, 2015.
- [7] J. Bhattacharya and H. Petsche. Phase synchrony analysis of eeg during music perception reveals changes in functional connectivity due to musical expertise. *Signal processing*, 85(11):2161–2177, 2005.
- [8] J. E. Bible, D. Biswas, C. P. Miller, P. G. Whang, and J. N. Grauer. Normal functional range of motion of the cervical spine during 15 activities of daily living. *Clinical Spine Surgery*, 23(1):15–21, 2010.
- [9] F. Bogo, A. Kanazawa, C. Lassner, P. Gehler, J. Romero, and M. J. Black. Keep it smpl: Automatic estimation of 3d human pose and shape from a single image. In *Computer Vision–ECCV 2016: 14th European Conference, Amsterdam, The Netherlands, October 11-14, 2016, Proceedings, Part V 14*, pages 561–578. Springer, 2016.
- [10] K. R. Borisagar, R. M. Thanki, B. S. Sedani, K. R. Borisagar, R. M. Thanki, and B. S. Sedani. Fourier transform, short-time fourier transform, and wavelet transform. *Speech enhancement techniques for digital hearing aids*, pages 63–74, 2019.
- [11] S. L. Bressler. Large-scale cortical networks and cognition. *Brain Research Reviews*, 20(3):288–304, 1995.
- [12] J. Britz, D. Van De Ville, and C. M. Michel. Bold correlates of eeg topography reveal rapid resting-state network dynamics. *Neuroimage*, 52(4):1162–1170, 2010.

- [13] V. Brodbeck, A. Kuhn, F. von Wegner, A. Morzelewski, E. Tagliazucchi, S. Borisov, C. M. Michel, and H. Laufs. Eeg microstates of wakefulness and nrem sleep. *Neuroimage*, 62(3):2129–2139, 2012.
- [14] V. Brodbeck, A. Kuhn, F. von Wegner, A. Morzelewski, E. Tagliazucchi, S. Borisov, C. M. Michel, and H. Laufs. EEG microstates of wakefulness and NREM sleep. *NeuroImage*, 62(3):2129–2139, Sept. 2012.
- [15] D. Brunet, M. M. Murray, and C. M. Michel. Spatiotemporal analysis of multichannel eeg: Cartool. *Computational intelligence and neuroscience*, 2011:1–15, 2011.
- [16] B. Burle, L. Spieser, C. Roger, L. Casini, T. Hasbroucq, and F. Vidal. Spatial and temporal resolutions of eeg: Is it really black and white? a scalp current density view. *International Journal of Psychophysiology*, 97(3):210–220, 2015.
- [17] Z. Cao, T. Simon, S.-E. Wei, and Y. Sheikh. Realtime multi-person 2d pose estimation using part affinity fields. In *Proceedings of the IEEE conference on computer vision and pattern recognition*, pages 7291–7299, 2017.
- [18] A. J. Casson, D. C. Yates, S. J. Smith, J. S. Duncan, and E. Rodriguez-Villegas. Wearable electroencephalography. *IEEE engineering in medicine and biology magazine*, 29(3):44–56, 2010.
- [19] A. Castelli, G. Paolini, A. Cereatti, and U. Della Croce. A 2d markerless gait analysis methodology: Validation on healthy subjects. *Computational and mathematical methods in medicine*, 2015, 2015.
- [20] E. Ceseracciu, Z. Sawacha, and C. Cobelli. Comparison of markerless and marker-based motion capture technologies through simultaneous data collection during gait: proof of concept. *PloS one*, 9(3):e87640, 2014.
- [21] N. Chidi-Ogbolu and K. Baar. Effect of estrogen on musculoskeletal performance and injury risk. *Frontiers in physiology*, page 1834, 2019.
- [22] G. Christe, L. Redhead, T. Legrand, B. M. Jolles, and J. Favre. Multi-segment analysis of spinal kinematics during sit-to-stand in patients with chronic low back pain. *Journal of biomechanics*, 49(10):2060–2067, 2016.
- [23] S. J. Colcombe, A. F. Kramer, K. I. Erickson, P. Scalf, E. McAuley, N. J. Cohen, A. Webb, G. J. Jerome, D. X. Marquez, and S. Elavsky. Cardiovascular fitness, cortical plasticity, and aging. *Proceedings of the National Academy of Sciences*, 101(9):3316–3321, 2004.
- [24] R. J. Cotton. Kinematic tracking of rehabilitation patients with markerless pose estimation fused with wearable inertial sensors. In *2020 15th IEEE International Conference on Automatic Face and Gesture Recognition (FG 2020)*, pages 508–514. IEEE, 2020.
- [25] P. Croce, F. Zappasodi, S. Spadone, and P. Capotosto. Magnetic stimulation selectively affects pre-stimulus eeg microstates. *Neuroimage*, 176:239–245, 2018.
- [26] M. Crotti, K. Koschutnig, and S. C. Wriessneger. Handedness impacts the neural correlates of kinesthetic motor imagery and execution: A fmri study. *Journal of Neuroscience Research*, 100(3):798–826, 2022.

- [27] A. Custo, D. Van De Ville, W. M. Wells, M. I. Tomescu, D. Brunet, and C. M. Michel. Electroencephalographic resting-state networks: source localization of microstates. *Brain connectivity*, 7(10):671–682, 2017.
- [28] A. Custo, S. Vulliemoz, F. Grouiller, D. Van De Ville, and C. Michel. Eeg source imaging of brain states using spatiotemporal regression. *Neuroimage*, 96:106–116, 2014.
- [29] M. De Lucia, C. M. Michel, S. Clarke, and M. M. Murray. Single subject eeg analysis based on topographic information. *International Journal of Bioelectromagnetism*, 9(3):168–171, 2007.
- [30] M. De Lucia, C. M. Michel, and M. M. Murray. Comparing ica-based and single-trial topographic erp analyses. *Brain topography*, 23:119–127, 2010.
- [31] A. Delorme and S. Makeig. Eeglab: an open source toolbox for analysis of single-trial eeg dynamics including independent component analysis. *Journal of neuroscience methods*, 134(1):9–21, 2004.
- [32] L. Dipietro, M. Plank, H. Poizner, and H. Krebs. Eeg microstate analysis in human motor corrections. In *2012 4th IEEE RAS & EMBS International Conference on Biomedical Robotics and Biomechatronics (BioRob)*, pages 1727–1732. IEEE, 2012.
- [33] N. M. Drissi, A. Szakács, S. T. Witt, A. Wretman, M. Ulander, H. Ståhlbrandt, N. Darin, T. Hallböök, A.-M. Landtblom, and M. Engström. Altered brain microstate dynamics in adolescents with narcolepsy. *Frontiers in human neuroscience*, 10:369, 2016.
- [34] M. T. Duruöz. *Hand function: a practical guide to assessment*. Springer, 2014.
- [35] D. F. D’Croz-Baron, M. Baker, C. M. Michel, and T. Karp. Eeg microstates analysis in young adults with autism spectrum disorder during resting-state. *Frontiers in human neuroscience*, 13:173, 2019.
- [36] D. F. D’Croz-Baron, L. Bréchet, M. Baker, and T. Karp. Auditory and visual tasks influence the temporal dynamics of eeg microstates during post-encoding rest. *Brain Topography*, 34:19–28, 2021.
- [37] D. D. D’Lima, B. J. Fregly, S. Patil, N. Steklov, and C. W. Colwell Jr. Knee joint forces: prediction, measurement, and significance. *Proceedings of the Institution of Mechanical Engineers, Part H: Journal of Engineering in Medicine*, 226(2):95–102, 2012.
- [38] D. D. D’Lima, S. Patil, N. Steklov, S. Chien, and C. W. Colwell Jr. In vivo knee moments and shear after total knee arthroplasty. *Journal of biomechanics*, 40:S11–S17, 2007.
- [39] M. Ertl, M. Schulte, and M. Dieterich. Eeg microstate architecture does not change during passive whole-body accelerations. *Journal of neurology*, 267:76–78, 2020.
- [40] R. F. Escamilla. Knee biomechanics of the dynamic squat exercise. *Medicine & science in sports & exercise*, 33(1):127–141, 2001.
- [41] N. R. Evans, G. Hooper, R. Edwards, G. Whatling, V. Sparkes, C. Holt, and S. Ahuja. A 3d motion analysis study comparing the effectiveness of cervical spine orthoses at restricting spinal motion through physiological ranges. *European Spine Journal*, 22:10–15, 2013.

- [42] C. C. W. Fadzal, W. Mansor, L. Khuan, and A. Zabidi. Short-time fourier transform analysis of eeg signal from writing. In *2012 IEEE 8th International Colloquium on Signal Processing and its Applications*, pages 525–527. IEEE, 2012.
- [43] M. Feng, L. Liang, W. Sun, G. W. Liu, X. Yin, T. Han, X. Wei, and L. Zhu. Measurements of cervical range of motion using an optical motion capture system: Repeatability and validity. *Experimental and therapeutic medicine*, 18(6):4193–4202, 2019.
- [44] A. C. Fry, J. C. Smith, and B. K. Schilling. Effect of knee position on hip and knee torques during the barbell squat. *The Journal of Strength & Conditioning Research*, 17(4):629–633, 2003.
- [45] Y. Fu, J. Chen, and X. Xiong. Calculation and analysis of microstate related to variation in executed and imagined movement of force of hand clenching. *Computational Intelligence and Neuroscience*, 2018, 2018.
- [46] T. Fujimori, M. Iwasaki, Y. Nagamoto, T. Ishii, M. Kashii, T. Murase, T. Sugiura, Y. Matsuo, K. Sugamoto, and H. Yoshikawa. Kinematics of the thoracic spine in trunk rotation: in vivo 3-dimensional analysis. *Spine*, 37(21):E1318–E1328, 2012.
- [47] E. Fujita, H. Kanehisa, Y. Yoshitake, T. Fukunaga, and H. Nishizono. Association between knee extensor strength and emg activities during squat movement. *Medicine and science in sports and exercise*, 43(12):2328–2334, 2011.
- [48] C. P. Gabel, H. R. Mokhtarinia, J. Hoffman, J. Osborne, E.-L. Laakso, and M. Melloh. Does the performance of five back-associated exercises relate to the presence of low back pain? a cross-sectional observational investigation in regional australian council workers. *BMJ open*, 8(8):e020946, 2018.
- [49] S. Ganesan, A. S. Acharya, R. Chauhan, and S. Acharya. Prevalence and risk factors for low back pain in 1,355 young adults: a cross-sectional study. *Asian spine journal*, 11(4):610, 2017.
- [50] F. Ghezelbash, A. Shirazi-Adl, N. Arjmand, Z. El-Ouaaid, and A. Plamondon. Subject-specific biomechanics of trunk: musculoskeletal scaling, internal loads and intradiscal pressure estimation. *Biomechanics and modeling in mechanobiology*, 15:1699–1712, 2016.
- [51] F. Ghezelbash, A. Shirazi-Adl, A. Plamondon, N. Arjmand, and M. Parnianpour. Obesity and obesity shape markedly influence spine biomechanics: a subject-specific risk assessment model. *Annals of biomedical engineering*, 45:2373–2382, 2017.
- [52] S. Ghosh, M. Laha, A. Konar, and A. K. Nagar. Decoding of subjective pain-sensitivity by brain signal analysis using a general type-2 fuzzy classifier. In *2020 IEEE Symposium Series on Computational Intelligence (SSCI)*, pages 3099–3106. IEEE, 2020.
- [53] S. P. Gombatto, D. R. Collins, S. A. Sahrman, J. R. Engsborg, and L. R. Van Dillen. Patterns of lumbar region movement during trunk lateral bending in 2 subgroups of people with low back pain. *Physical Therapy*, 87(4):441–454, 2007.

- [54] J. Gorsuch, J. Long, K. Miller, K. Primeau, S. Rutledge, A. Sossong, and J. J. Durocher. The effect of squat depth on multiarticular muscle activation in collegiate cross-country runners. *The Journal of Strength & Conditioning Research*, 27(9):2619–2625, 2013.
- [55] V. Graci, L. R. Van Dillen, and G. B. Salsich. Gender differences in trunk, pelvis and lower limb kinematics during a single leg squat. *Gait & posture*, 36(3):461–466, 2012.
- [56] F. Gu, A. Gong, Y. Qu, H. Xiao, J. Wu, W. Nan, C. Jiang, and Y. Fu. Research on top archer’s EEG microstates and source analysis in different states. *Brain Sciences*, 12(8):1017, July 2022.
- [57] Y. Gu, K. Dremstrup, and D. Farina. Single-trial discrimination of type and speed of wrist movements from eeg recordings. *Clinical neurophysiology*, 120(8):1596–1600, 2009.
- [58] L. Guidetti, U. Placentino, and C. Baldari. Reliability and criterion validity of the smartphone inclinometer application to quantify cervical spine mobility. *Clinical spine surgery*, 30(10):E1359–E1366, 2017.
- [59] R. Hale, J. G. Hausselle, and R. V. Gonzalez. A preliminary study on the differences in male and female muscle force distribution patterns during squatting and lunging maneuvers. *Computers in biology and medicine*, 52:57–65, 2014.
- [60] U. Halsband and R. K. Lange. Motor learning in man: a review of functional and clinical studies. *Journal of Physiology-Paris*, 99(4-6):414–424, 2006.
- [61] F. Hatz, M. Hardmeier, N. Benz, M. Ehrensperger, U. Gschwandtner, S. Rüegg, C. Schindler, A. U. Mon-sch, and P. Fuhr. Microstate connectivity alterations in patients with early alzheimer’s disease. *Alzheimer’s research & therapy*, 7:1–11, 2015.
- [62] T. Hayashi, H. Yokoyama, I. Nambu, and Y. Wada. Prediction of individual finger movements for motor execution and imagery: An eeg study. In *2017 IEEE International Conference on Systems, Man, and Cybernetics (SMC)*, pages 3020–3023. IEEE, 2017.
- [63] R. Hebert, D. Lehmann, G. Tan, F. Travis, and A. Arenander. Enhanced eeg alpha time-domain phase synchrony during transcendental meditation: Implications for cortical integration theory. *Signal Processing*, 85(11):2213–2232, 2005.
- [64] A. Hernandez, K. Gross, and S. Gombatto. Differences in lumbar spine and lower extremity kinematics during a step down functional task in people with and people without low back pain. *Clinical Biomechanics*, 47:46–52, 2017.
- [65] N. Hogan and D. Sternad. On rhythmic and discrete movements: reflections, definitions and implications for motor control. *Experimental brain research*, 181:13–30, 2007.
- [66] N. Hogan and D. Sternad. Dynamic primitives of motor behavior. *Biological cybernetics*, 106:727–739, 2012.
- [67] A. Hossain, M. W. Rahman, and M. A. Riheen. Left and right hand movements eeg signals classifica-tion using wavelet transform and probabilistic neural network. *International Journal of Electrical and Computer Engineering*, 5(1):92–101, 2015.

- [68] N. E. Huang, Z. Shen, S. R. Long, M. C. Wu, H. H. Shih, Q. Zheng, N.-C. Yen, C. C. Tung, and H. H. Liu. The empirical mode decomposition and the hilbert spectrum for nonlinear and non-stationary time series analysis. *Proceedings of the Royal Society of London. Series A: mathematical, physical and engineering sciences*, 454(1971):903–995, 1998.
- [69] L. Hussain, W. Aziz, S. Saeed, S. A. Shah, M. S. A. Nadeem, I. A. Awan, A. Abbas, A. Majid, and S. Z. H. Kazmi. Complexity analysis of eeg motor movement with eye open and close subjects using multiscale permutation entropy (mpe) technique. *Biomedical Research (0970-938X)*, 28(16), 2017.
- [70] D. Ignasiak, A. Rüeger, and S. J. Ferguson. Multi-segmental thoracic spine kinematics measured dynamically in the young and elderly during flexion. *Human movement science*, 54:230–239, 2017.
- [71] T. Ishii, Y. Mukai, N. Hosono, H. Sakaura, R. Fujii, Y. Nakajima, S. Tamura, M. Iwasaki, H. Yoshikawa, and K. Sugamoto. Kinematics of the cervical spine in lateral bending: In vivo: Three-dimensional analysis. *Spine*, 31(2):155–160, 2006.
- [72] T. Ishii, Y. Mukai, N. Hosono, H. Sakaura, Y. Nakajima, Y. Sato, K. Sugamoto, and H. Yoshikawa. Kinematics of the upper cervical spine in rotation: In vivo: Three-dimensional analysis. *Spine*, 29(7):E139–E144, 2004.
- [73] A. Jain, K. Gurugubelli, A. K. Vuppala, and K. Vemuri. Decoding self-automated and motivated finger movements using novel single-frequency filtering method—an eeg study. *Biomedical Signal Processing and Control*, 72:103284, 2022.
- [74] M. H. Javid, K. Gurugubelli, and A. K. Vuppala. Single frequency filter bank based long-term average spectra for hypernasality detection and assessment in cleft lip and palate speech. In *ICASSP 2020-2020 IEEE International Conference on Acoustics, Speech and Signal Processing (ICASSP)*, pages 6754–6758. IEEE, 2020.
- [75] S. K. Jun, X. Zhou, D. K. Ramsey, and V. N. Krovi. A comparative study of human motion capture and computational analysis tools. In *The 2nd International Digital Human Modeling Symposium*. Citeseer, 2003.
- [76] N. Kannathal. Analysis of eeg signals with and without reflexology using fft and auto regressive modelling techniques. *CHINESE CLINICAL MEDICINE*, 1:12–20, 2006.
- [77] A. Khanna, A. Pascual-Leone, C. M. Michel, and F. Farzan. Microstates in resting-state eeg: current status and future directions. *Neuroscience & Biobehavioral Reviews*, 49:105–113, 2015.
- [78] A. Khosla, P. Khandnor, and T. Chand. A comparative analysis of signal processing and classification methods for different applications based on eeg signals. *Biocybernetics and Biomedical Engineering*, 40(2):649–690, 2020.
- [79] M. Kikuchi, T. Koenig, T. Munesue, A. Hanaoka, W. Strik, T. Dierks, Y. Koshino, and Y. Minabe. Eeg microstate analysis in drug-naive patients with panic disorder. *PloS one*, 6(7):e22912, 2011.
- [80] D.-W. Kim and C.-H. Im. Eeg spectral analysis. *Computational EEG analysis: Methods and applications*, pages 35–53, 2018.

- [81] S. Kim, M. Miller, A. Tallarico, S. Helder, Y. Liu, and S. Lee. Relationships between physical characteristics and biomechanics of lower extremity during the squat. *Journal of Exercise Science & Fitness*, 19(4):269–277, 2021.
- [82] T. Koenig, D. Lehmann, M. C. Merlo, K. Kochi, D. Hell, and M. Koukkou. A deviant eeg brain microstate in acute, neuroleptic-naive schizophrenics at rest. *European archives of psychiatry and clinical neuroscience*, 249:205–211, 1999.
- [83] T. Koenig, L. Prichep, D. Lehmann, P. V. Sosa, E. Braeker, H. Kleinlogel, R. Isenhardt, and E. R. John. Millisecond by millisecond, year by year: normative eeg microstates and developmental stages. *Neuroimage*, 16(1):41–48, 2002.
- [84] B. Kolb and R. Gibb. Brain plasticity and behaviour in the developing brain. *Journal of the Canadian Academy of Child and Adolescent Psychiatry*, 20(4):265, 2011.
- [85] N. Kolotouros, G. Pavlakos, D. Jayaraman, and K. Daniilidis. Probabilistic modeling for human mesh recovery. In *Proceedings of the IEEE/CVF international conference on computer vision*, pages 11605–11614, 2021.
- [86] M. G. Lacourse, J. A. Turner, E. Randolph-Orr, and S. L. Schandler. Cerebral and cerebellar sensorimotor plasticity following motor imagery-based mental practice of. *Journal of Rehabilitation Research & Development*, 41(4):505–524, 2004.
- [87] R. A. Laird, J. Gilbert, P. Kent, and J. L. Keating. Comparing lumbo-pelvic kinematics in people with and without back pain: a systematic review and meta-analysis. *BMC musculoskeletal disorders*, 15(1):1–13, 2014.
- [88] H. Lakany and B. Conway. Classification of wrist movements using eeg-based wavelets features. In *2005 IEEE Engineering in Medicine and Biology 27th Annual Conference*, pages 5404–5407. IEEE, 2006.
- [89] C. Lansade, S. Laporte, P. Thoreux, M.-A. Rousseau, W. Skalli, and F. Lavaste. Three-dimensional analysis of the cervical spine kinematics: effect of age and gender in healthy subjects. *Spine*, 34(26):2900–2906, 2009.
- [90] D. J. Larson, Y. Wang, D. P. Zwambag, and S. H. Brown. Characterizing local dynamic stability of lumbar spine sub-regions during repetitive trunk flexion-extension movements. *Frontiers in Sports and Active Living*, 1:48, 2019.
- [91] A. Leardini, F. Biagi, A. Merlo, C. Belvedere, and M. G. Benedetti. Multi-segment trunk kinematics during locomotion and elementary exercises. *Clinical Biomechanics*, 26(6):562–571, 2011.
- [92] P. Leconte, J.-J. Orban de Xivry, G. Stoquart, T. Lejeune, and R. Ronsse. Rhythmic arm movements are less affected than discrete ones after a stroke. *Experimental brain research*, 234:1403–1417, 2016.
- [93] R. Y. Lee and T. K. Wong. Relationship between the movements of the lumbar spine and hip. *Human movement science*, 21(4):481–494, 2002.
- [94] D. Lehmann. Microstates of the brain in eeg and erp mapping studies. In *Brain Dynamics: Progress and Perspectives*, pages 72–83. Springer, 1989.

- [95] D. Lehmann, P. L. Faber, S. Galderisi, W. M. Herrmann, T. Kinoshita, M. Koukkou, A. Mucci, R. D. Pascual-Marqui, N. Saito, J. Wackermann, et al. Eeg microstate duration and syntax in acute, medication-naïve, first-episode schizophrenia: a multi-center study. *Psychiatry Research: Neuroimaging*, 138(2):141–156, 2005.
- [96] D. Lehmann, P. L. Faber, S. Galderisi, W. M. Herrmann, T. Kinoshita, M. Koukkou, A. Mucci, R. D. Pascual-Marqui, N. Saito, J. Wackermann, G. Winterer, and T. Koenig. EEG microstate duration and syntax in acute, medication-naïve, first-episode schizophrenia: a multi-center study. *Psychiatry Research: Neuroimaging*, 138(2):141–156, Feb. 2005.
- [97] D. Lehmann, H. Ozaki, and I. Pal. Eeg alpha map series: brain micro-states by space-oriented adaptive segmentation. *Electroencephalography and clinical neurophysiology*, 67(3):271–288, 1987.
- [98] D. Lehmann, R. D. Pascual-Marqui, and C. Michel. Eeg microstates. *Scholarpedia*, 4(3):7632, 2009.
- [99] D. Lehmann, R. D. Pascual-Marqui, W. K. Strik, and T. Koenig. Core networks for visual-concrete and abstract thought content: a brain electric microstate analysis. *Neuroimage*, 49(1):1073–1079, 2010.
- [100] D. Lehmann and W. Skrandies. Reference-free identification of components of checkerboard-evoked multichannel potential fields. *Electroencephalography and clinical neurophysiology*, 48(6):609–621, 1980.
- [101] G. Lemmers, M. Heijmans, A. Scafoglieri, R. Buyl, J. Staal, M. Schmitt, and E. Cattrysse. Three-dimensional kinematics of the cervical spine using an electromagnetic tracking device. differences between healthy subjects and subjects with non-specific neck pain and the effect of age. *Clinical Biomechanics*, 54:111–117, 2018.
- [102] A. Leo, G. Handjaras, M. Bianchi, H. Marino, M. Gabiccini, A. Guidi, E. P. Scilingo, P. Pietrini, A. Bicchi, M. Santello, et al. A synergy-based hand control is encoded in human motor cortical areas. *Elife*, 5:e13420, 2016.
- [103] G. Li, S. Wang, P. Passias, Q. Xia, G. Li, and K. Wood. Segmental in vivo vertebral motion during functional human lumbar spine activities. *European spine journal*, 18:1013–1021, 2009.
- [104] K. Liao, R. Xiao, J. Gonzalez, and L. Ding. Decoding individual finger movements from one hand using human eeg signals. *PloS one*, 9(1):e85192, 2014.
- [105] C.-F. Lin, S.-W. Yeh, Y.-Y. Chien, T.-I. Peng, J.-H. Wang, and S.-H. Chang. A hht-based time frequency analysis scheme for clinical alcoholic eeg signals. In *WSEAS international conference. Proceedings. Mathematics and computers in science and engineering*, number 9. World Scientific and Engineering Academy and Society, 2009.
- [106] W.-C. Lin, H.-W. Chiu, and C.-Y. Hsu. Discovering eeg signals response to musical signal stimuli by time-frequency analysis and independent component analysis. In *2005 IEEE Engineering in Medicine and Biology 27th Annual Conference*, pages 2765–2768. IEEE, 2006.
- [107] R. List, T. Gülay, M. Stoop, and S. Lorenzetti. Kinematics of the trunk and the lower extremities during restricted and unrestricted squats. *The Journal of Strength & Conditioning Research*, 27(6):1529–1538, 2013.

- [108] W. Liu, X. Liu, R. Dai, and X. Tang. Exploring differences between left and right hand motor imagery via spatio-temporal eeg microstate. *Computer Assisted Surgery*, 22(sup1):258–266, 2017.
- [109] L. Losonczi, L. Bako, S.-T. Brassai, and L.-F. Marton. Hilbert-huang transform used for eeg signal analysis. In *The international conference interdisciplinarity in engineering INTER-ENG*, page 361. Elsevier Limited, 2012.
- [110] S. Mathôt, D. Schreij, and J. Theeuwes. Opensesame: An open-source, graphical experiment builder for the social sciences. *Behavior research methods*, 44:314–324, 2012.
- [111] D. Mehta, O. Sotnychenko, F. Mueller, W. Xu, M. Elgharib, P. Fua, H.-P. Seidel, H. Rhodin, G. Pons-Moll, and C. Theobalt. Xnect: Real-time multi-person 3d motion capture with a single rgb camera. *Acm Transactions On Graphics (TOG)*, 39(4):82–1, 2020.
- [112] C. Michel, D. Brandeis, W. Skrandies, R. Pascual, W. Strik, T. Dierks, H. Hamburger, and W. Karniski. Global field power: A "time-honoured" index for eeg/ep map analysis. 1993.
- [113] C. M. Michel and T. Koenig. Eeg microstates as a tool for studying the temporal dynamics of whole-brain neuronal networks: a review. *Neuroimage*, 180:577–593, 2018.
- [114] C. M. Michel, M. M. Murray, G. Lantz, S. Gonzalez, L. Spinelli, and R. G. De Peralta. Eeg source imaging. *Clinical neurophysiology*, 115(10):2195–2222, 2004.
- [115] G. W. Milligan and M. C. Cooper. An examination of procedures for determining the number of clusters in a data set. *Psychometrika*, 50:159–179, 1985.
- [116] P. Milz, P. L. Faber, D. Lehmann, T. Koenig, K. Kochi, and R. D. Pascual-Marqui. The functional significance of eeg microstates—associations with modalities of thinking. *Neuroimage*, 125:643–656, 2016.
- [117] J. Minguillon, E. Pirondini, M. Coscia, R. Leeb, J. Millán, D. Van De Ville, and S. Micera. Modular organization of reaching and grasping movements investigated using eeg microstates. In *2014 36th Annual International Conference of the IEEE Engineering in Medicine and Biology Society*, pages 2093–2096. IEEE, 2014.
- [118] P. J. Moga. Skin distraction at select landmarks on the spine midline in the upright and fully flexed postures. *Journal of bodywork and movement therapies*, 14(1):13–18, 2010.
- [119] M. Mohseni, V. Shalchyan, M. Jochumsen, and I. K. Niazi. Upper limb complex movements decoding from pre-movement eeg signals using wavelet common spatial patterns. *Computer methods and programs in biomedicine*, 183:105076, 2020.
- [120] A. J. Moreno, G. Utrilla, J. Marin, J. J. Marin, M. B. Sanchez-Valverde, and A. C. Royo. Cervical spine assessment using passive and active mobilization recorded through an optical motion capture. *Journal of chiropractic medicine*, 17(3):167–181, 2018.
- [121] L. Mündermann, S. Corazza, A. M. Chaudhari, T. P. Andriacchi, A. Sundaresan, and R. Chellappa. Measuring human movement for biomechanical applications using markerless motion capture. In *Three-dimensional image capture and applications VII*, volume 6056, pages 246–255. SPIE, 2006.

- [122] M. G. Muriuki, R. M. Havey, L. I. Voronov, G. Carandang, M. R. Zindrick, M. A. Lorenz, L. Lomasney, and A. G. Patwardhan. Effects of motion segment level, pfirrmann intervertebral disc degeneration grade and gender on lumbar spine kinematics. *Journal of Orthopaedic Research*, 34(8):1389–1398, 2016.
- [123] M. M. Murray, D. Brunet, and C. M. Michel. Topographic erp analyses: a step-by-step tutorial review. *Brain topography*, 20(4):249–264, 2008.
- [124] M. M. Murray, D. Brunet, and C. M. Michel. Topographic ERP analyses: A step-by-step tutorial review. *Brain Topography*, 20(4):249–264, Mar. 2008.
- [125] C. S. Musaeus, K. Engedal, P. Høgh, V. Jelic, A. R. Khanna, T. W. Kjær, M. Mørup, M. Naik, A.-R. Oeksengaard, E. Santarnecchi, et al. Changes in the left temporal microstate are a sign of cognitive decline in patients with alzheimer’s disease. *Brain and Behavior*, 10(6):e01630, 2020.
- [126] C. S. Musaeus, M. S. Nielsen, and P. Høgh. Microstates as disease and progression markers in patients with mild cognitive impairment. *Frontiers in neuroscience*, 13:563, 2019.
- [127] F. Musso, J. Brinkmeyer, A. Mobascher, T. Warbrick, and G. Winterer. Spontaneous brain activity and eeg microstates. a novel eeg/fmri analysis approach to explore resting-state networks. *Neuroimage*, 52(4):1149–1161, 2010.
- [128] G. Nagymáté and R. M. Kiss. Application of optitrack motion capture systems in human movement analysis: A systematic literature review. *Recent Innovations in Mechatronics*, 5(1.):1–9, 2018.
- [129] H. Namazi and T. S. Ala. Decoding of simple and compound limb motor imagery movements by fractal analysis of electroencephalogram (eeg) signal. *Fractals*, 27(03):1950041, 2019.
- [130] K. Natarajan, R. Acharya U, F. Alias, T. Tiboleng, and S. K. Puthusserypady. Nonlinear analysis of eeg signals at different mental states. *Biomedical engineering online*, 3:1–11, 2004.
- [131] S. Negrini, B. Piovanelli, C. Amici, V. Cappellini, G. Bovi, M. Ferrarin, F. Zaina, A. Borboni, et al. Trunk motion analysis: a systematic review from a clinical and methodological perspective. *European Journal of Physical and Rehabilitation Medicine*, 52(4):583–592, 2016.
- [132] K. Nishida, Y. Morishima, M. Yoshimura, T. Isotani, S. Irisawa, K. Jann, T. Dierks, W. Strik, T. Kinoshita, and T. Koenig. EEG microstates associated with salience and frontoparietal networks in frontotemporal dementia, schizophrenia and alzheimer’s disease. *Clinical Neurophysiology*, 124(6):1106–1114, June 2013.
- [133] K. Nishida, Y. Morishima, M. Yoshimura, T. Isotani, S. Irisawa, K. Jann, T. Dierks, W. Strik, T. Kinoshita, and T. Koenig. Eeg microstates associated with salience and frontoparietal networks in frontotemporal dementia, schizophrenia and alzheimer’s disease. *Clinical neurophysiology*, 124(6):1106–1114, 2013.
- [134] P. Ofner, A. Schwarz, J. Pereira, and G. R. Müller-Putz. Upper limb movements can be decoded from the time-domain of low-frequency eeg. *PloS one*, 12(8):e0182578, 2017.
- [135] N. O. Onyemaechi, G. E. Anyanwu, E. N. Obikili, O. Onwuasoigwe, and O. E. Nwankwo. Impact of overweight and obesity on the musculoskeletal system using lumbosacral angles. *Patient preference and adherence*, pages 291–296, 2016.

- [136] S. A. Overduin, A. d'Avella, J. Roh, J. M. Carmena, and E. Bizzi. Representation of muscle synergies in the primate brain. *Journal of Neuroscience*, 35(37):12615–12624, 2015.
- [137] M. O. Oyakhire, L. E. Oghenemavwe, and C. E. Agi. Influence of age, body mass index and waist-hip ratio on the human spine; a radiographic study of adult male subjects in port harcourt-nigeria. 2021.
- [138] J. Packheiser, J. Schmitz, Y. Pan, Y. El Basbasse, P. Friedrich, O. Güntürkün, and S. Ocklenburg. Using mobile eeg to investigate alpha and beta asymmetries during hand and foot use. *Frontiers in neuroscience*, 14:109, 2020.
- [139] A. Pal, M. Behari, V. Goyal, and R. Sharma. Study of eeg microstates in parkinson's disease: a potential biomarker? *Cognitive Neurodynamics*, 15:463–471, 2021.
- [140] E. Papi, A. M. Bull, and A. H. McGregor. Spinal segments do not move together predictably during daily activities. *Gait & Posture*, 67:277–283, 2019.
- [141] R. Pascual-Marqui, C. Michel, and D. Lehmann. Segmentation of brain electrical activity into microstates: model estimation and validation. *IEEE Transactions on Biomedical Engineering*, 42(7):658–665, July 1995.
- [142] R. D. Pascual-Marqui, C. M. Michel, and D. Lehmann. Segmentation of brain electrical activity into microstates: model estimation and validation. *IEEE Transactions on Biomedical Engineering*, 42(7):658–665, 1995.
- [143] S. R. Penedo, M. L. Netto, and J. F. Justo. Designing digital filter banks using wavelets. *EURASIP Journal on Advances in Signal Processing*, 2019:1–11, 2019.
- [144] P. Peng, Y. Song, L. Yang, and H. Wei. Seizure prediction in eeg signals using stft and domain adaptation. *Frontiers in Neuroscience*, 15:1880, 2022.
- [145] C. Pierpaolo, T. Franca, T. Gabriella, F. Patrique, C. Silvia, and Z. Filippo. Brain electrical microstate features as biomarkers of a stable motor output. *Journal of Neural Engineering*, 19(5):056042, 2022.
- [146] E. Pirondini, M. Coscia, J. Minguillon, J. d. R. Millán, D. Van De Ville, and S. Micera. Eeg topographies provide subject-specific correlates of motor control. *Scientific reports*, 7(1):1–16, 2017.
- [147] E. Pirondini, N. Goldshuv-Ezra, N. Zinger, J. Britz, N. Soroker, L. Y. Deouell, and D. Van De Ville. Resting-state eeg topographies: Reliable and sensitive signatures of unilateral spatial neglect. *NeuroImage: Clinical*, 26:102237, 2020.
- [148] A. T. Poulsen, A. Pedroni, N. Langer, and L. K. Hansen. Microstate eeglab toolbox: An introductory guide. *BioRxiv*, page 289850, 2018.
- [149] M. R. Pourahmadi, R. Bagheri, M. Taghipour, I. E. Takamjani, J. Sarrafzadeh, and M. A. Mohseni-Bandpei. A new iphone application for measuring active craniocervical range of motion in patients with non-specific neck pain: a reliability and validity study. *The Spine Journal*, 18(3):447–457, 2018.
- [150] S. C. Puthenveetil, C. P. Daphalapurkar, W. Zhu, M. C. Leu, X. F. Liu, A. M. Chang, J. K. Gilpin-Mcminn, P. H. Wu, and S. D. Snodgrass. Comparison of marker-based and marker-less systems for low-cost human

- motion capture. In *International Design Engineering Technical Conferences and Computers and Information in Engineering Conference*, volume 55867, page V02BT02A036. American Society of Mechanical Engineers, 2013.
- [151] G. Python, R. Fargier, and M. Laganaro. When wine and apple both help the production of grapes: Erp evidence for post-lexical semantic facilitation in picture naming. *Frontiers in human neuroscience*, 12:136, 2018.
- [152] S. Qiu, S. Wang, W. Peng, W. Yi, C. Zhang, J. Zhang, and H. He. Continuous theta-burst stimulation modulates resting-state eeg microstates in healthy subjects. *Cognitive Neurodynamics*, pages 1–11, 2021.
- [153] M. Rana, M. S. Yani, S. Asavasopon, B. E. Fisher, and J. J. Kutch. Brain connectivity associated with muscle synergies in humans. *Journal of Neuroscience*, 35(44):14708–14716, 2015.
- [154] A. Ranavolo, R. Don, F. Draicchio, M. Bartolo, M. Serrao, L. Padua, G. Cipolla, F. Pierelli, S. Iavicoli, and G. Sandrini. Modelling the spine as a deformable body: Feasibility of reconstruction using an opto-electronic system. *Applied Ergonomics*, 44(2):192–199, 2013.
- [155] M. S. S. RESHMA, M. Sirajudeen, T. Chinnakalai, M. Suhail, N. al Hussinan, and P. Pillai. Reliability of the flexible ruler in measuring lumbar lordosis among children. *Journal of Clinical and Diagnostic Research*, 14:YC01–YC04, 2020.
- [156] J. V. Robertson and A. Roby-Brami. The trunk as a part of the kinematic chain for reaching movements in healthy subjects and hemiparetic patients. *Brain research*, 1382:137–146, 2011.
- [157] J. Rodriguez-Larios. *Capturing EEG Spectral Microstates Through K Means Clustering*. 2019.
- [158] P. R. Roelfsema, A. van Ooyen, and T. Watanabe. Perceptual learning rules based on reinforcers and attention. *Trends in cognitive sciences*, 14(2):64–71, 2010.
- [159] L. Rokach and O. Maimon. *Clustering methods.*, 2005.
- [160] A. Saifuddin, S. Blease, and E. MacSweeney. Axial loaded mri of the lumbar spine. *Clinical radiology*, 58(9):661–671, 2003.
- [161] J. B. Salyers, Y. Dong, and Y. Gai. Continuous wavelet transform for decoding finger movements from single-channel eeg. *IEEE Transactions on Biomedical Engineering*, 66(6):1588–1597, 2018.
- [162] S. P. Savic, G. Devedzic, B. Ristic, A. Matic, N. Prodanovic, and R. Stojanovic. Clinical application of a portable motion capture system: A methodology. In *2018 7th Mediterranean Conference on Embedded Computing (MECO)*, pages 1–4. IEEE, 2018.
- [163] S. Schaal, D. Sternad, R. Osu, and M. Kawato. Rhythmic arm movement is not discrete. *Nature neuroscience*, 7(10):1136–1143, 2004.
- [164] A. Schinkel-Ivy and J. D. Drake. Which motion segments are required to sufficiently characterize the kinematic behavior of the trunk? *Journal of Electromyography and Kinesiology*, 25(2):239–246, 2015.
- [165] A. Schinkel-Ivy, B. C. Nairn, and J. D. Drake. Evaluation of methods for the quantification of the flexion-relaxation phenomenon in the lumbar erector spinae muscles. *Journal of Manipulative and Physiological Therapeutics*, 36(6):349–358, 2013.

- [166] F. Schlegel, D. Lehmann, P. L. Faber, P. Milz, and L. R. Gianotti. Eeg microstates during resting represent personality differences. *Brain topography*, 25:20–26, 2012.
- [167] S. Schmid, B. Bruhin, D. Ignasiak, J. Romkes, W. R. Taylor, S. J. Ferguson, R. Brunner, and S. Lorenzetti. Spinal kinematics during gait in healthy individuals across different age groups. *Human movement science*, 54:73–81, 2017.
- [168] S. Schmid, L. Connolly, G. Moschini, M. L. Meier, and M. Senteler. Skin marker-based subject-specific spinal alignment modeling: A feasibility study. *Journal of Biomechanics*, 137:111102, 2022.
- [169] A. Schmitz, M. Ye, G. Boggess, R. Shapiro, R. Yang, and B. Noehren. The measurement of in vivo joint angles during a squat using a single camera markerless motion capture system as compared to a marker based system. *Gait & posture*, 41(2):694–698, 2015.
- [170] S. A. Scholtes, S. P. Gombatto, and L. R. Van Dillen. Differences in lumbopelvic motion between people with and people without low back pain during two lower limb movement tests. *Clinical Biomechanics*, 24(1):7–12, 2009.
- [171] J. A. Sedrez, T. S. Furlanetto, G. M. Gelain, and C. T. Candotti. Validity and reliability of smartphones in assessing spinal kinematics: a systematic review and meta-analysis. *Journal of Manipulative and Physiological Therapeutics*, 43(6):635–645, 2020.
- [172] B. A. Seitzman, M. Abell, S. C. Bartley, M. A. Erickson, A. R. Bolbecker, and W. P. Hetrick. Cognitive manipulation of brain electric microstates. *Neuroimage*, 146:533–543, 2017.
- [173] P. Severijns, T. Overbergh, S. Schmid, L. Moke, and L. Scheys. Spinal palpation error and its impact on skin marker-based spinal alignment measurement in adult spinal deformity. *Frontiers in Bioengineering and Biotechnology*, 9:687323, 2021.
- [174] P. Severijns, T. Overbergh, A. Thauvoeye, J. Baudewijns, D. Monari, L. Moke, K. Desloovere, and L. Scheys. A subject-specific method to measure dynamic spinal alignment in adult spinal deformity. *The Spine Journal*, 20(6):934–946, 2020.
- [175] A. Sheikhani, H. Behnam, M.-R. Mohammadi, and M. Noroozian. Analysis of eeg background activity in autism disease patients with bispectrum and stft measure. In *Proceedings of the 11th WSEAS International Conference on COMMUNICATIONS*, 2007.
- [176] T. H. Shovon, Z. Al Nazi, S. Dash, and M. F. Hossain. Classification of motor imagery eeg signals with multi-input convolutional neural network by augmenting stft. In *2019 5th International Conference on Advances in Electrical Engineering (ICAEE)*, pages 398–403. IEEE, 2019.
- [177] M. Sifuzzaman, M. R. Islam, and M. Z. Ali. Application of wavelet transform and its advantages compared to fourier transform. 2009.
- [178] W. Skrandies. Data reduction of multichannel fields: global field power and principal component analysis. *Brain topography*, 2:73–80, 1989.
- [179] J. Sleight, P. Pillai, and S. Mohan. Classification of executed and imagined motor movement eeg signals. *Ann Arbor: University of Michigan*, 110, 2009.

- [180] U. Smailovic and V. Jelic. Neurophysiological markers of alzheimer's disease: quantitative eeg approach. *Neurology and therapy*, 8:37–55, 2019.
- [181] K. M. Spencer, J. Dien, and E. Donchin. A componential analysis of the erp elicited by novel events using a dense electrode array, 1999.
- [182] K. M. Spencer, J. Dien, and E. Donchin. Spatiotemporal analysis of the late erp responses to deviant stimuli. *Psychophysiology*, 38(2):343–358, 2001.
- [183] V. Strelets, P. Faber, J. Golikova, V. Novototsky-Vlasov, T. Koenig, L. Gianotti, J. Gruzelier, and D. Lehmann. Chronic schizophrenics with positive symptomatology have shortened EEG microstate durations. *Clinical Neurophysiology*, 114(11):2043–2051, Nov. 2003.
- [184] W. Strik, T. Dierks, T. Becker, and D. Lehmann. Larger topographical variance and decreased duration of brain electric microstates in depression. *Journal of Neural Transmission/General Section JNT*, 99:213–222, 1995.
- [185] M. J. Stuart, D. A. Meglan, G. E. Lutz, E. S. Growney, and K.-N. An. Comparison of intersegmental tibiofemoral joint forces and muscle activity during various closed kinetic chain exercises. *The American journal of sports medicine*, 24(6):792–799, 1996.
- [186] A. Subasi. Eeg signal classification using wavelet feature extraction and a mixture of expert model. *Expert Systems with Applications*, 32(4):1084–1093, 2007.
- [187] D. P. Subha, P. K. Joseph, R. Acharya U, and C. M. Lim. Eeg signal analysis: a survey. *Journal of medical systems*, 34:195–212, 2010.
- [188] K. Sueyoshi and T. Sumiyoshi. Electrophysiological evidence in schizophrenia in relation to treatment response. *Frontiers in Psychiatry*, 9:259, 2018.
- [189] P. S. Sung, K. F. Spratt, and D. G. Wilder. A possible methodological flaw in comparing dominant and nondominant sided lumbar spine muscle responses without simultaneously considering hand dominance. *Spine*, 29(17):1914–1922, 2004.
- [190] C. T. Swain, D. G. Whyte, C. L. Ekegren, P. Taylor, K. McMaster, C. L. Dow, and E. J. Bradshaw. Multi-segment spine kinematics: Relationship with dance training and low back pain. *Gait & posture*, 68:274–279, 2019.
- [191] E. E. Swartz, R. Floyd, and M. Cendoma. Cervical spine functional anatomy and the biomechanics of injury due to compressive loading. *Journal of athletic training*, 40(3):155, 2005.
- [192] A. Tafazzol, N. Arjmand, A. Shirazi-Adl, and M. Parnianpour. Lumbopelvic rhythm during forward and backward sagittal trunk rotations: combined in vivo measurement with inertial tracking device and biomechanical modeling. *Clinical Biomechanics*, 29(1):7–13, 2014.
- [193] L. Tait, F. Tamagnini, G. Stothart, E. Barvas, C. Monaldini, R. Frusciante, M. Volpini, S. Guttman, E. Coulthard, J. T. Brown, et al. Eeg microstate complexity for aiding early diagnosis of alzheimer's disease. *Scientific reports*, 10(1):1–10, 2020.

- [194] L. Tait and J. Zhang. + microstate: A matlab toolbox for brain microstate analysis in sensor and cortical eeg/meg. *Neuroimage*, 258:119346, 2022.
- [195] S. Taran, V. Bajaj, D. Sharma, S. Siuly, and A. Sengur. Features based on analytic imf for classifying motor imagery eeg signals in bci applications. *Measurement*, 116:68–76, 2018.
- [196] S. Taweetanalarp and N. Purepong. Comparison of lumbar spinal angle between normal body mass index and overweight young adults. *Journal of physical therapy science*, 27(7):2343–2346, 2015.
- [197] W. R. Taylor, T. Consmüller, and A. Rohlmann. A novel system for the dynamic assessment of back shape. *Medical engineering & physics*, 32(9):1080–1083, 2010.
- [198] R. Thirumuru, K. Gurugubelli, and A. K. Vuppala. Novel feature representation using single frequency filtering and nonlinear energy operator for speech emotion recognition. *Digital Signal Processing*, 120:103293, 2022.
- [199] R. Tibshirani and G. Walther. Cluster validation by prediction strength. *Journal of Computational and Graphical Statistics*, 14(3):511–528, 2005.
- [200] E. Tognoli and J. S. Kelso. The metastable brain. *Neuron*, 81(1):35–48, 2014.
- [201] M. I. Tomescu, T. A. Rihs, R. Becker, J. Britz, A. Custo, F. Grouiller, M. Schneider, M. Debbané, S. Eliez, and C. M. Michel. Deviant dynamics of eeg resting state pattern in 22q11. 2 deletion syndrome adolescents: a vulnerability marker of schizophrenia? *Schizophrenia research*, 157(1-3):175–181, 2014.
- [202] M. I. Tomescu, T. A. Rihs, M. Roinishvili, F. I. Karahanoglu, M. Schneider, S. Menghetti, D. Van De Ville, A. Brand, E. Chkonia, S. Eliez, et al. Schizophrenia patients and 22q11. 2 deletion syndrome adolescents at risk express the same deviant patterns of resting state eeg microstates: a candidate endophenotype of schizophrenia. *Schizophrenia Research: Cognition*, 2(3):159–165, 2015.
- [203] L. G. Ungerleider, J. Doyon, and A. Karni. Imaging brain plasticity during motor skill learning. *Neurobiology of learning and memory*, 78(3):553–564, 2002.
- [204] C. Vigneshwari, V. Vimala, S. V. Vignesh, and G. Sumithra. Analysis of finger movements using eeg signal. *International Journal of Emerging Technology and Advanced Engineering*, 3(1):583–588, 2013.
- [205] J. M. Vital, J. Sénégas, C. Garnier, and H. Bouloussa. Kinematics of the spine. *Spinal Anatomy: Modern Concepts*, pages 457–484, 2020.
- [206] J. Wackermann, D. Lehmann, C. Michel, and W. Strik. Adaptive segmentation of spontaneous eeg map series into spatially defined microstates. *International Journal of Psychophysiology*, 14(3):269–283, 1993.
- [207] M. Wairagkar, Y. Hayashi, and S. J. Nasuto. Exploration of neural correlates of movement intention based on characterisation of temporal dependencies in electroencephalography. *PloS one*, 13(3):e0193722, 2018.
- [208] P. Walia, Y. Fu, J. Norfleet, S. D. Schwaizberg, X. Intes, S. De, L. Cavuoto, and A. Dutta. Error-related brain state analysis using electroencephalography in conjunction with functional near-infrared spectroscopy during a complex surgical motor task. *Brain Informatics*, 9(1), Dec. 2022.

- [209] J. Wall, J. Xu, and X. Wang. Human brain plasticity: an emerging view of the multiple substrates and mechanisms that cause cortical changes and related sensory dysfunctions after injuries of sensory inputs from the body. *Brain Research Reviews*, 39(2-3):181–215, 2002.
- [210] D. A. Wallace, G. J. Salem, R. Salinas, and C. M. Powers. Patellofemoral joint kinetics while squatting with and without an external load. *Journal of Orthopaedic & Sports Physical Therapy*, 32(4):141–148, 2002.
- [211] B. K. Weeks, C. P. Carty, and S. A. Horan. Effect of sex and fatigue on single leg squat kinematics in healthy young adults. *BMC musculoskeletal disorders*, 16:1–9, 2015.
- [212] J. Widmer, P. Fornaciari, M. Senteler, T. Roth, J. G. Snedeker, and M. Farshad. Kinematics of the spine under healthy and degenerative conditions: a systematic review. *Annals of biomedical engineering*, 47:1491–1522, 2019.
- [213] K. W. Wong, J. C. Leong, M.-k. Chan, K. D. Luk, and W. W. Lu. The flexion–extension profile of lumbar spine in 100 healthy volunteers. *Spine*, 29(15):1636–1641, 2004.
- [214] N. Yahya, H. Musa, Z. Y. Ong, and I. Elamvazuthi. Classification of motor functions from electroencephalogram (eeg) signals based on an integrated method comprised of common spatial pattern and wavelet transform framework. *Sensors*, 19(22):4878, 2019.
- [215] D. Yan, J. Liu, M. Liao, B. Liu, S. Wu, X. Li, H. Li, W. Ou, L. Zhang, Z. Li, et al. Prediction of clinical outcomes with eeg microstate in patients with major depressive disorder. *Frontiers in Psychiatry*, 12:695272, 2021.
- [216] J. W. Youdas, T. R. Garrett, S. Harmsen, V. J. Suman, and J. R. Carey. Lumbar lordosis and pelvic inclination of asymptomatic adults. *Physical therapy*, 76(10):1066–1081, 1996.
- [217] H. Yu, D. Sternad, D. M. Corcos, and D. E. Vaillancourt. Role of hyperactive cerebellum and motor cortex in parkinson’s disease. *Neuroimage*, 35(1):222–233, 2007.
- [218] H. Yuan, V. Zotey, R. Phillips, W. C. Drevets, and J. Bodurka. Spatiotemporal dynamics of the brain at rest—exploring eeg microstates as electrophysiological signatures of bold resting state networks. *Neuroimage*, 60(4):2062–2072, 2012.
- [219] B. L. Zeller, J. L. McCrory, W. Ben Kibler, and T. L. Uhl. Differences in kinematics and electromyographic activity between men and women during the single-legged squat. *The American journal of sports medicine*, 31(3):449–456, 2003.
- [220] L. Zhang, T. Shen, R. Zhang, and Y. Hu. Altered electroencephalography microstates during the motor preparation process for voluntary and instructed action. *Engineered Science*, 18:159–167, 2022.
- [221] X. Zhu and G. Shin. Kinematics and muscle activities of the lumbar spine during and after working in stooped postures. *Journal of electromyography and kinesiology*, 23(4):801–806, 2013.
- [222] D. P. Zwambag, S. M. Beaudette, D. E. Gregory, and S. H. Brown. Development of a novel technique to record 3d intersegmental angular kinematics during dynamic spine movements. *Annals of Biomedical Engineering*, 46:298–309, 2018.

## Supplementary Tables

**Dominant and Least Microstate classes for Microstate Parameters**

Microstate Parameters	States	Wrist Flexion/Extension left	Wrist Flexion/Extension right	Tip-pinch Left	Tip-pinch Right
<i>Dominant Microstate class</i>					
Occurrence	Event	MS1	MS1	MS1	MS1
	Pre-event	MS2	MS1	MS2	MS2
	Post-event	MS1	MS1	MS1	MS1
Duration	Event	MS1	MS1	MS2	MS2
	Pre-event	MS2	MS1	MS2	MS2
	Post-event	MS1	MS1	MS1	MS1
Coverage	Event	MS1	MS1	MS1	MS1
	Pre-event	MS2	MS1	MS2	MS1
	Post-event	MS1	MS1	MS1	MS1
<i>Least Microstate class</i>					
Occurrence	Event	MS4	MS4	MS4	MS3
	Pre-event	MS4	MS4	MS4	MS3, MS4
	Post-event	MS4	MS4	MS4	MS4
Duration	Event	MS4	MS4	MS4	MS3
	Pre-event	MS3	MS4	MS4	MS3
	Post-event	MS4	MS4	MS3	MS4
Coverage	Event	MS4	MS4	MS4	MS3
	Pre-event	MS4	MS4	MS4	MS3
	Post-event	MS4	MS4	MS4	MS4

**Table 5.1** Dominant/Least Microstate Classes in each state for Wrist flexion & extension and Tip-pinch movements for Occurrence, Duration and Coverage parameters.

Participant ID	Wrist flexion & extension (left)	Wrist flexion & extension (right)	Tip-pinch left	Tip-pinch right
1	4,9,5	4,11,4	4,5,5	4,6,5
2	3,10,5	5,10,5	5,4,4	4,6,5
3	5,11,5	5,10,5	4,5,5	4,5,4
4	5,9,5	4,9,5	5,5,4	4,5,5
5	4,8,5	3,8,4	4,5,4	5,3,4
6	6,10,5	4,10,6	4,5,5	4,4,4
7	5,11,4	5,9,5	3,4,4	5,5,3
8	3,8,4	4,6,4	4,5,5	7,5,5
9	5,10,5	4,6,4	5,3,5	3,4,3
10	3,7,3	3,8,4	4,4,4	4,4,4
11	3,9,4	3,8,4	3,4,3	4,4,4
12	3,9,4	4,9,4	4,4,3	4,5,4
13	4,8,5	4,7,5	5,4,6	4,6,5
14	5,9,4	4,8,5	5,5,4	5,4,4
15	4,9,4	5,9,4	5,5,4	4,5,3
16	5,9,4	4,8,5	6,5,5	5,4,3
17	4,10,4	5,9,5	4,5,4	4,7,5
18	5,9,5	5,10,5	5,5,4	5,5,5
19	4,11,5	4,10,4	5,5,4	4,5,5
20	4,8,4	4,9,5	3,4,4	6,4,4
21	4,8,4	5,8,3	5,3,4	5,5,5
22	4,7,3	4,8,4	3,3,3	4,4,3
23	3,9,4	4,8,5	3,5,4	4,5,4
24	5,9,4	3,10,4	6,4,4	4,5,3
25	5,10,4	4,9,4	6,6,4	4,4,5
26	5,9,4	4,10,5	5,5,4	5,5,5
27	5,11,4	5,11,4	3,5,3	5,5,3
28	5,9,5	4,9,3	5,6,4	4,5,5
29	4,10,4	4,10,4	5,5,6	5,5,4
<b>Mean Values</b>	<b>4.28, 9.17, 4.31</b>	<b>4.14, 8.86, 4.41</b>	<b>4.41, 4.59, 4.21</b>	<b>4.45, 4.79, 4.17</b>

**Table 5.2** Average NOM values for pre-, event-, and post conditions of both Wrist flexion & extension and Tip-pinch

Participant ID	Flexion left	Flexion right	Tip pinch left	Tip pinch right
1	4,9,5	4,11,4	4,5,5	4,6,5
4	5,9,5	4,9,5	5,5,4	4,5,5
6	6,10,5	4,10,6	4,5,5	4,4,4
9	5,10,5	4,6,4	5,3,5	3,4,3
15	4,9,4	5,9,4	5,5,4	4,5,3

**Table 5.3** Set of Average NOM values for pre-event, event and post-event conditions for Left-Handed participants for both wrist flexion & extension and tip-pinch

ID	Tip-pinch left	Tip-pinch right
1	4,5,5	4,6,5
4	5,5,4	4,5,5
6	4,5,5	4,4,4
9	5,3,5	3,4,3
15	5,5,4	4,5,3

**Table 5.4** Average NOM values for pre-, event-, and post conditions of Left-handed participants executing Tip-pinch movement

ID	Tip-pinch left	Tip-pinch right
5	4,5,4	5,3,4
12	4,4,3	4,5,4
20	3,4,4	6,4,4
26	5,5,4	5,5,5
29	5,5,6	5,5,4

**Table 5.5** Average NOM values for pre-, event-, and post conditions of Right-handed(set1) participants executing Tip-pinch movement

ID	Tip-pinch left	Tip-pinch right
8	4,5,5	7,5,5
14	5,5,4	5,4,4
23	3,5,4	4,5,4
24	6,4,4	4,5,3
28	5,6,4	4,5,5

**Table 5.6** Average NOM values for pre-, event-, and post conditions of Right-handed(set2) participants executing Tip-pinch movement

ID	Wrist Flexion/Extension left	Wrist Flexion/Extension right
1	4,9,5	4,11,4
4	5,9,5	4,9,5
6	6,10,5	4,10,6
9	5,10,5	4,6,4
15	4,9,4	5,9,4

**Table 5.7** Average NOM values for pre-, event-, and post conditions of Left-handed participants executing Wrist flexion & extension movement

<b>ID</b>	<b>Wrist Flexion/Extension left</b>	<b>Wrist Flexion/Extension right</b>
11	3,9,4	3,8,4
18	5,9,5	5,10,5
22	4,7,3	4,8,4
26	5,9,4	4,10,5
28	5,9,5	4,9,3

**Table 5.8** Average NOM values for pre-, event-, and post conditions of Right-handed(set1) participants executing Wrist flexion & extension movement

<b>ID</b>	<b>Wrist Flexion/Extension left</b>	<b>Wrist Flexion/Extension right</b>
3	5,11,5	5,10,5
7	5,11,4	5,9,5
13	4,8,5	4,7,5
24	5,9,4	3,10,4
29	4,10,4	4,10,4

**Table 5.9** Average NOM values for pre-, event-, and post conditions of Right-handed(set2) participants executing Wrist flexion & extension movement

## JASP Analysis Tables

### Left Wrist flexion & extension Occurrence

<b>p-values label</b>	<b>Pre-Event</b>	<b>Event-Post</b>	<b>Pre-Post</b>
MS1	mA=0.573, mB=0.881, t(56)=5.93, p.001, d=1.55	mA=0.881, mB=0.684, t(56)=3.89, p.001, d=1.02	mA=0.573, mB=0.684, t(56)=2.39, p=.020, d=0.62
MS2	mA=0.603, mB=0.787, t(56)=4.00, p.001, d=1.05	mA=0.787, mB=0.493, t(56)=6.81, p.001, d=1.79	mA=0.603, mB=0.493, t(56)=2.76, p=.008, d=0.72
MS3	mA=0.503, mB=0.749, t(56)=5.27, p.001, d=1.38	mA=0.749, mB=0.505, t(56)=5.63, p.001, d=1.48	mA=0.503, mB=0.505, t(56)=0.02, p=.977, d=0.007
MS4	mA=0.442, mB=0.628, t(56)=4.07, p.001, d=1.07	mA=0.628, mB=0.446, t(56)=3.71, p.001, d=0.97	mA=0.442, mB=0.446, t(56)=0.07, p=.938, d=0.02

**Table 5.10** P-values for Occurrence parameter of Microstates for Pre-Event, Event-Post and Pre-Post conditions

### Left Wrist flexion & extension Duration

<b>p-values label</b>	<b>Pre-Event</b>	<b>Event-Post</b>	<b>Pre-Post</b>
MS1	U =132, n1=n2=29, z=- 4.47, p.001, two-tailed	U=213.5, n1=n2=29, z=3.21, p=.001, two- tailed	mA=58.815, mB=64.740, t(56)=1.58, p=.118, d=0.41
MS2	mA=59.748, mB=74.771, t(56)=4.90, p.001, d=1.28	mA=74.771, mB=51.526, t(56)=7.43, p.001, d=1.95	mA=59.748, mB=51.526, t(56)=2.24, p=.029, d=0.58
MS3	mA=49.004, mB=75.972, t(56)=, p.001, d=2.02	mA=75.972, mB=55.268, t(56)=6.77, p.001, d=1.77	mA=49.004, mB=55.268, t(56)=1.57, p=.121, d=0.41
MS4	mA=49.759, mB=68.227, t(56)=, p.001, d=1.26	mA=68.227, mB=50.273, t(56)=4.38, p.001, d=1.15	mA=49.759, mB=50.273, t(56)=0.12, p=.902, d=0.03

**Table 5.11** P-values for Duration parameter of Microstates for Pre-Event, Event-Post and Pre-Post conditions

Left Wrist flexion & extension Coverage

<b>p-values label</b>	<b>Pre-Event</b>	<b>Event-Post</b>	<b>Pre-Post</b>
MS1	U=121.5, n1=n2=29, z=-4.64, p.001, two-tailed	mA=7.321, mB=5.485, t(56)=3.77, p.001, d=0.99	U=353.5, n1=n2=29, z=-1.03, p=.301, two-tailed
MS2	mA=4.614, mB=6.060, t(56)=3.56, p.001, d=0.93	mA=6.060, mB=4.804, t(56)=3.54, p.001, d=0.93	mA=4.585, mB=4.804, t(56)=0.52, p=.603, d=0.13
MS3	mA= 3.840, mB=5.573, t(56)=4.54, p.001, d=1.19	mA=5.573, mB=4.689, t(56)=2.12, p=.038, d=0.55	mA=3.840, mB=4.689, t(56)=2.09, p=.041, d=0.54
MS4	mA=3.427, mB=5.267, t(56)=4.55, p.001, d=1.19	mA=5.267, mB=2.880, t(56)=5.48, p.001, d=1.44	mA=3.427, mB=2.880, t(56)=1.62, p=.110, d=0.42

**Table 5.12** P-values for Coverage parameter of Microstates for Pre-Event, Event-Post and Pre-Post conditions

Right Wrist flexion & extension Occurrence

<b>p-values label</b>	<b>Pre-Event</b>	<b>Event-Post</b>	<b>Pre-Post</b>
MS1	U=130.5, n1=n2=29, z=-4.5, p .001, two-tailed	mA=0.878, mB=0.657, t(56)= 3.93, p.001, d=1.03	U=364.5, n1=n2=29, z=0.86, p= .385, two-tailed
MS2	mA=0.556, mB=0.737, t(56)=3.60, p.001, d=0.94	mA=0.737, mB=0.583, t(56)=3.53, p.001, d=0.92	mA=0.556, mB=0.583, t(56)=0.52, p.602, d=0.13
MS3	mA=0.478, mB=0.684, t(56)=4.52, p.001, d=1.18	U=253.5, n1=n2=29, z=2.58, p=.009, two-tailed	U=304, n1=n2=29, z=-1.80, p=.070, two-tailed
MS4	mA=0.413, mB=0.642, t(56)=4.70, p.001, d=1.23	mA=0.642, mB=0.360, t(56)=5.48, p.001, d=1.44	mA=0.413, mB=0.360, t(56)=1.31, p=.195, d=0.34

**Table 5.13** P-values for Occurrence parameter of Microstates for Pre-Event, Event-Post and Pre-Post conditions

Right Wrist flexion & extension Duration

<b>p-values label</b>	<b>Pre-Event</b>	<b>Event-Post</b>	<b>Pre-Post</b>
MS1	mA=59.668, mB=78.342, t(56)=8.80, p.001, d=2.31	mA=78.342, mB=63.468, t(56)=5.52, p.001, d=1.45	mA=59.668, mB=63.468, t(56)=1.27, p=.027, d=0.33
MS2	mA=55.490, mB=76.119, t(56)=6.24, p.001, d=1.63	mA=76.119, mB=58.399, t(56)=5.94, p.001, d=1.56	mA=55.490, mB=58.399, t(56)=0.74, p=.458, d=0.19
MS3	mA=50.526, mB=68.481, t(56)=4.92, p.001, d=1.29	mA=68.481, mB=56.619, t(56)=3.32, p=.002, d=0.87	mA=50.526, mB=56.619, t(56)=1.54, p=.127, d=0.40
MS4	mA=46.956, mB=66.411, t(56)=5.25, p.001, d=1.37	mA=66.411, mB=40.972, t(56)=6.41, p.001, d=1.68	mA=46.956, mB=40.972, t(56)=1.59, p=.116, d=0.41

**Table 5.14** P-values for Duration parameter of Microstates for Pre-Event, Event-Post and Pre-Post conditions

Right Wrist flexion & extension Coverage

<b>p-values label</b>	<b>Pre-Event</b>	<b>Event-Post</b>	<b>Pre-Post</b>
MS1	mA=4.973, mB=7.321, t(56)=5.59, p.001, d=1.46	mA=7.321, mB=5.485, t(56)=3.77, p.001, d=0.99	mA=4.973, mB=5.485, t(56)=1.30, p=.025, d=0.34
MS2	mA=4.614, mB=6.060, t(56)=3.56, p.001, d=0.93	mA=6.060, mB=4.804, t(56)=3.54, p.001, d=0.93	mA=4.585, mB=4.804, t(56)=0.52, p=.014, d=0.13
MS3	mA=3.840, mB=5.573, t(56)=4.54, p.001, d=1.19	mA=5.573, mB=4.689, t(56)=2.12, p.001, d=0.55	mA=3.840, mB=4.689, t(56)=2.09, p=.858, d=0.54
MS4	mA=3.427, mB=5.267, t(56)=4.55, p.001, d=1.19	mA=5.267, mB=2.880, t(56)=5.48, p.001, d=1.44	mA=3.427, mB=2.880, t(56)=1.62, p=.925, d=0.42

**Table 5.15** P-values for Coverage parameter of Microstates for Pre-Event, Event-Post and Pre-Post conditions

Left Tip-pinch Occurrence

<b>p-values label</b>	<b>Pre-Event</b>	<b>Event-Post</b>	<b>Pre-Post</b>
MS1	mA=0.597, mB=0.661, t(56)=1.25, p=.216, d=0.32	mA=0.661, mB=0.663, t(56)=0.03, p=.971, d=0.009	mA=0.597, mB=0.663, t(56)=1.21, p=.229, d=0.32
MS2	mA=0.606, mB=0.610, t(56)=0.09, p=.923, d=0.02	U=306, n1=n2=29, z=1.77, p=.074, two- tailed	U=301, n1=n2=29, z=1.85, p=.063, two- tailed
MS3	mA=0.571, mB=0.538, t(56)=0.58, p=.559, d=0.15	mA=0.538, mB=0.497, t(56)=0.94, p=.351, d=0.24	mA=0.571, mB=0.497, t(56)=1.31, p=.193, d=0.34
MS4	U=339.5, n1=n2=29, z=- 1.25, p=0.208, two-tailed	U=372, n1=n2=29, z=0.74, p=0.452, two- tailed	U=370, n1=n2=29, z=- 0.77, p=.434

**Table 5.16** P-values for Occurrence parameter of Microstates for Pre-Event, Event-Post and Pre-Post conditions

Left Tip-pinch Duration

<b>p-values label</b>	<b>Pre-Event</b>	<b>Event-Post</b>	<b>Pre-Post</b>
MS1	mA=58.637, mB=62.232, t(56)=0.94, p=.347, d=0.24	mA=62.232, mB=66.189, t(56)=1.13, p=.261, d=0.29	mA=58.637, mB=66.189, t(56)=1.85, p=.069, d=0.48
MS2	mA=61.480, mB=62.481, t(56)=0.31, p=.754, d=0.08	U=336, N1=n2=29, z=1.30, p=.193, two- tailed	U=344.5, n1=n2=29, z=1.17, p=.240, two- tailed
MS3	U=380.5, n1=n2=29, z=0.61, p=.539, two- tailed	mA=56.767, mB=51.644, t(56)=1.19, p=.237, d=0.31	U=324, n1=n2=29, z=1.49, p=.136, two- tailed
MS4	mA=47.140, mB=52.213, t(56)=1.24, p=.220, d=0.32	mA=52.213, mB=52.356, t(56)=0.03, p=.971, d=0.01	mA=47.140, mB=52.356, t(56)=1.20, p=.235, d=0.31

**Table 5.17** P-values for Duration parameter of Microstates for Pre-Event, Event-Post and Pre-Post conditions

Left Tip-pinch Coverage

<b>p-values label</b>	<b>Pre-Event</b>	<b>Event-Post</b>	<b>Pre-Post</b>
MS1	mA=4.959, mB=5.481, t(56)=1.21, p=.229, d=0.31	mA=5.481, mB=5.469, t(56)=0.02, p=.978, d=0.007	mA=4.959, mB=5.469, t(56)=1.13, p=.263, d=0.29
MS2	mA=5.027, mB=5.101, t(56)=0.23, p=.819, d=0.06	mA=5.101, mB=4.520, t(56)=1.40, p=.164, d=0.37	mA=5.027, mB=4.520, t(56)=1.30, p=.196, d=0.34
MS3	mA=4.651, mB=4.454, t(56)=0.42, p=.676, d=0.11	mA=4.454, mB=4.011, t(56)=1.18, p=.240, d=0.31	mA=4.651, mB=4.011, t(56)=1.36, p=.177, d=0.35
MS4	U=342.5, n1=n2=29, z=- 1.20, p=.228, two-tailed	mA=3.719, mB=3.487, t(56)=0.63, p=.527, d=0.16	U=390.5, n1=n2=29, z=- 0.45, p=.646, two-tailed

**Table 5.18** P-values for Coverage parameter of Microstates for Pre-Event, Event-Post and Pre-Post conditions

Right Tip-pinch Occurrence

<b>p-values label</b>	<b>Pre-Event</b>	<b>Event-Post</b>	<b>Pre-Post</b>
MS1	mA=0.602, mB=0.696, t(56)=1.79, p=.078, d=0.47	mA=0.696, mB=0.682, t(56)=0.25, p=.799, d=0.06	mA=0.602, mB=0.682, t(56)=1.67, p=.099, d=0.44
MS2	mA=0.611, mB=0.627, t(56)=0.30, p=.765, d=0.07	mA=0.627, mB=0.552, t(56)=1.36, p=.177, d=0.35	mA=0.611, mB=0.552, t(56)=1.35, p=.181, d=0.35
MS3	mA=0.482, mB=0.523, t(56)=0.80, p=.425, d= 0.21	U=350, n1=n2=29, z=1.08, p=.273, two- tailed	U=386.5, n1=n2=29, z=0.52, p=.600, two- tailed
MS4	U=329, n1=n2=29, z=- 1.4, p=0.154, two-tailed	U=251, n1=n2=29, z=2.62, p=.008, two- tailed	mA=0.485, mB=0.434, t(56)=1.02, p=.308, d=0.27

**Table 5.19** P-values for Occurrence parameter of Microstates for Pre-Event, Event-Post and Pre-Post conditions

Right Tip-pinch Duration

<b>p-values label</b>	<b>Pre-Event</b>	<b>Event-Post</b>	<b>Pre-Post</b>
MS1	mA=58.179, mB=63.687, t(56)=1.59, p=.117, d=0.41	mA=63.687, mB=62.365, t(56)=0.47, p=.638, d=0.12	mA=58.179, mB=62.365, t(56)=1.17, p=.244, d=0.30
MS2	mA=60.153, mB=63.056, t(56)=0.74, p=.462, d=0.19	mA=63.056, mB=58.345, t(56)=1.05, p=.295, d=0.27	mA=60.153, mB=58.345, t(56)=0.47, p=.640, d=0.12
MS3	U=414.5, n1=n2=29, z=- 0.08, p=.932, two-tailed	mA=55.278, mB=53.422, t(56)=0.52, p=.600, d=0.13	U=394, n1=n2=29, z=0.40, p=.686, two- tailed
MS4	mA=54.118, mB=58.159, t(56)=1.14, p=.256, d=0.30	mA=58.159, mB=47.058, t(56)=3.18, p=.002, d=0.83	mA=54.118, mB=47.058, t(56)=1.70, p=.094, d=0.44

**Table 5.20** P-values for Duration parameter of Microstates for Pre-Event, Event-Post and Pre-Post conditions

Right Tip-pinch Coverage

<b>p-values label</b>	<b>Pre-Event</b>	<b>Event-Post</b>	<b>Pre-Post</b>
MS1	mA=4.923, mB=5.697, t(56)=1.85, p=.069, d=0.48	mA=5.697, mB=5.610, t(56)=0.21, p=.835, d=0.05	mA=4.923, mB=5.610, t(56)=1.73, p=.088, d=0.45
MS2	mA=4.900, mB=5.236, t(56)=0.77, p=.443, d=0.20	mA=5.236, mB=4.598, t(56)=1.36, p=.178, d=0.35	mA=4.900, mB=4.598, t(56)=0.85, p=.395, d=0.22
MS3	mA=3.982, mB=4.249, t(56)=0.62, p=.532, d=0.16	U=367.5, n1=n2=29, z=0.81, p=.414, two- tailed	U=383.5, n1=n2=29, z=0.56, p=.570, two- tailed
MS4	mA=4.012, mB=4.517, t(56)=1.28, p=.203, d=0.33	U=246.5, n1=n2=29, z=2.69, p=.007, two- tailed	U=325, n1=n2=29, z=1.47, p=.140, two- tailed

**Table 5.21** P-values for Coverage parameter of Microstates for Pre-Event, Event-Post and Pre-Post conditions

Occurrence Parameter values in different MS classes (Wrist flexion & extension)

ID	Occurrence							
	Left Wrist Flexion/Extension				Right Wrist Flexion/Extension			
	MS1	MS2	MS3	MS4	MS1	MS2	MS3	MS4
1	0.44, 0.89, 0.56	0.56, 0.56, 0.72	0.44, 0.67, 0.5	0.39, 0.81, 0.61	0.61, 1.0, 0.94	0.5, 0.56, 0.39	0.33, 1.11, 0.72	0.44, 0.96, 0.17
2	0.28, 0.89, 0.44	0.33, 0.7, 0.5	0.61, 1.11, 0.78	0.44, 0.63, 0.61	0.61, 0.78, 0.33	0.56, 0.85, 0.72	0.72, 0.7, 0.5	0.67, 0.93, 0.83
3	0.56, 1.11, 0.72	0.61, 0.93, 0.56	0.61, 0.78, 0.5	0.83, 0.7, 0.67	0.67, 1.07, 0.78	0.56, 0.59, 0.78	0.56, 1.07, 0.67	0.5, 0.59, 0.44
4	0.5, 0.78, 0.72	0.56, 0.93, 0.44	1.11, 0.63, 0.78	0.39, 0.52, 0.39	0.56, 0.96, 0.72	0.56, 0.63, 0.5	0.56, 0.89, 1.11	0.44, 0.48, 0.39
5	0.61, 0.78, 1.06	0.5, 0.78, 0.44	0.5, 0.56, 0.56	0.44, 0.59, 0.33	0.44, 0.63, 0.5	0.5, 0.44, 0.67	0.44, 0.93, 0.44	0.22, 0.52, 0.56
6	0.78, 1.0, 0.83	0.94, 1.19, 0.67	0.56, 0.48, 0.56	0.61, 0.59, 0.44	0.44, 0.81, 0.44	0.33, 0.85, 0.78	0.72, 0.63, 1.06	0.56, 0.89, 0.5
7	1.0, 1.11, 0.67	0.56, 1.15, 0.33	0.5, 0.56, 0.39	0.39, 0.81, 0.44	0.44, 1.26, 0.94	0.72, 0.48, 0.56	0.56, 0.52, 0.61	0.67, 0.78, 0.33
8	0.44, 0.7, 0.5	0.44, 0.7, 0.61	0.56, 0.81, 0.78	0.17, 0.3, 0.06	0.61, 0.56, 0.39	0.5, 0.67, 0.61	0.56, 0.44, 0.61	0.39, 0.48, 0.28
9	0.56, 1.22, 1.0	0.83, 0.81, 0.44	0.72, 0.67, 0.89	0.5, 0.56, 0.22	0.61, 0.56, 0.39	0.5, 0.67, 0.61	0.56, 0.44, 0.61	0.39, 0.48, 0.28
10	0.44, 0.67, 0.44	0.61, 0.74, 0.67	0.11, 0.59, 0.39	0.33, 0.44, 0.22	0.5, 0.7, 0.67	0.28, 0.85, 0.33	0.39, 0.59, 0.61	0.39, 0.59, 0.22
11	0.5, 1.07, 0.5	0.61, 0.7, 0.33	0.39, 0.7, 0.56	0.22, 0.63, 0.39	0.44, 1.0, 0.56	0.39, 0.56, 0.39	0.5, 0.63, 0.67	0.22, 0.48, 0.22
12	0.39, 0.44, 0.78	0.44, 1.0, 0.28	0.5, 0.85, 0.56	0.39, 0.74, 0.56	0.78, 0.63, 0.67	0.17, 1.07, 0.56	0.67, 0.59, 0.33	0.28, 0.78, 0.28
13	0.5, 0.44, 0.78	0.44, 0.78, 0.44	0.61, 0.74, 0.56	0.61, 0.74, 0.67	0.78, 1.04, 1.11	0.78, 0.63, 1.0	0.17, 0.44, 0.39	0.39, 0.11, 0.11
14	0.67, 0.85, 0.78	0.83, 0.52, 0.28	0.33, 0.89, 0.44	0.5, 0.63, 0.44	0.67, 0.85, 0.72	0.61, 0.7, 0.78	0.33, 0.63, 0.61	0.44, 0.52, 0.44
15	0.28, 0.63, 0.44	0.5, 0.93, 0.72	0.78, 0.81, 0.5	0.33, 0.7, 0.5	0.61, 0.78, 0.44	0.72, 0.81, 0.56	0.56, 0.81, 0.67	0.39, 0.52, 0.33
16	0.89, 1.04, 0.67	0.67, 0.81, 0.56	0.5, 0.85, 0.33	0.28, 0.33, 0.5	0.5, 0.78, 0.5	0.89, 0.59, 0.61	0.22, 0.63, 0.67	0.22, 0.63, 0.5
17	0.5, 0.81, 0.78	0.61, 0.85, 0.44	0.28, 0.81, 0.28	0.44, 0.7, 0.44	0.5, 0.81, 0.78	0.83, 0.67, 0.5	0.83, 0.85, 0.83	0.5, 0.56, 0.28
18	0.67, 0.93, 0.56	0.44, 0.7, 0.67	0.72, 1.0, 0.72	0.5, 0.3, 0.44	0.83, 0.89, 0.72	0.39, 0.85, 0.67	0.5, 0.63, 0.56	0.61, 0.85, 0.39
19	0.5, 0.96, 0.72	0.72, 0.85, 0.44	0.44, 0.67, 0.61	0.56, 1.07, 0.61	0.61, 1.15, 0.78	0.17, 0.7, 0.67	0.5, 0.78, 0.39	0.5, 0.74, 0.17
20	0.67, 1.15, 0.56	0.39, 0.67, 0.61	0.5, 0.7, 0.5	0.28, 0.3, 0.11	0.78, 0.78, 0.94	0.44, 0.78, 0.72	0.33, 0.7, 0.33	0.22, 0.85, 0.61
21	0.72, 0.81, 0.89	0.44, 0.44, 0.33	0.22, 0.7, 0.39	0.72, 0.56, 0.28	0.72, 0.52, 0.33	1.06, 0.93, 0.39	0.5, 0.63, 0.39	0.44, 0.63, 0.39
22	0.61, 0.59, 0.5	0.67, 0.52, 0.33	0.17, 0.74, 0.22	0.44, 0.56, 0.22	0.83, 0.96, 0.78	0.56, 0.74, 0.72	0.5, 0.44, 0.33	0.33, 0.56, 0.11
23	0.28, 0.89, 0.67	0.5, 0.93, 0.72	0.44, 0.44, 0.28	0.22, 0.67, 0.5	0.44, 1.04, 0.67	0.5, 0.56, 0.61	0.17, 0.48, 0.44	0.67, 0.74, 0.61
24	0.72, 0.78, 0.67	0.78, 0.93, 0.5	0.5, 0.81, 0.5	0.33, 0.37, 0.56	0.5, 1.26, 0.78	0.39, 0.78, 0.56	0.39, 0.74, 0.61	0.17, 0.48, 0.22
25	0.83, 1.07, 0.5	0.67, 1.07, 0.39	0.39, 0.63, 0.39	0.39, 0.67, 0.83	0.56, 1.07, 0.61	0.67, 1.04, 0.5	0.39, 0.48, 0.28	0.28, 0.33, 0.39
26	0.39, 0.67, 0.56	0.94, 0.63, 0.44	0.5, 0.89, 0.56	0.56, 0.93, 0.33	0.61, 0.93, 0.89	0.28, 0.81, 0.67	0.72, 0.81, 0.61	0.33, 0.7, 0.39
27	0.78, 1.11, 0.83	0.67, 0.7, 0.39	0.5, 1.0, 0.17	0.5, 0.89, 0.72	0.83, 1.33, 0.5	0.72, 0.93, 0.61	0.28, 0.78, 0.61	0.5, 0.56, 0.11
28	0.67, 1.04, 0.94	0.44, 0.56, 0.56	0.67, 0.7, 0.5	0.67, 0.78, 0.5	0.72, 0.78, 0.61	0.61, 0.85, 0.17	0.56, 0.74, 0.44	0.33, 0.63, 0.44
29	0.44, 1.11, 0.78	0.78, 0.74, 0.5	0.44, 0.93, 0.44	0.39, 0.7, 0.33	0.44, 0.52, 0.56	0.94, 0.78, 0.28	0.33, 0.74, 0.5	0.5, 1.26, 0.44

**Table 5.22** Different MS classes' pre, event, and post condition values for the **Occurrence** parameter for the Wrist flexion & extension exercise

Duration Parameter values in different MS classes (Wrist flexion & extension)

ID	Duration							
	Left Wrist Flexion/Extension				Right Wrist Flexion/Extension			
	MS1	MS2	MS3	MS4	MS1	MS2	MS3	MS4
1	54.33, 78.94, 44.04	69.11, 63.13, 52.56	35.24, 70.0, 56.11	38.93, 88.72, 65.41	51.59, 78.99, 68.59	52.33, 73.22, 43.19	43.33, 80.62, 66.7	42.11, 78.52, 24.44
2	39.67, 75.89, 57.33	34.67, 65.01, 43.0	45.22, 84.45, 66.04	43.07, 59.52, 61.33	51.41, 84.15, 47.22	64.26, 79.02, 54.22	53.0, 73.85, 58.33	41.52, 61.82, 77.19
3	71.67, 85.0, 83.19	62.89, 75.87, 55.78	53.83, 76.44, 40.28	57.83, 65.91, 74.44	63.93, 83.5, 69.22	59.04, 71.43, 61.78	59.26, 77.95, 58.26	52.41, 70.95, 45.26
4	70.56, 78.72, 68.61	48.15, 74.76, 56.56	81.07, 69.56, 78.41	42.74, 55.89, 43.19	53.67, 79.94, 72.0	76.22, 61.59, 52.56	51.7, 83.41, 76.67	42.22, 54.09, 44.89
5	57.96, 60.91, 86.22	62.89, 72.94, 37.93	41.33, 65.7, 52.63	48.33, 82.0, 49.56	56.3, 74.46, 50.78	43.48, 65.07, 41.89	52.89, 78.65, 32.22	28.89, 63.07, 58.67
6	41.06, 87.37, 73.74	83.31, 83.97, 59.15	48.07, 79.11, 62.44	70.11, 70.54, 48.89	47.44, 75.69, 49.44	38.22, 79.54, 60.39	77.3, 74.31, 85.59	71.33, 73.96, 48.0
7	79.3, 89.69, 62.48	69.56, 78.78, 35.22	55.89, 64.63, 42.59	47.56, 83.9, 68.0	67.78, 94.74, 87.63	53.15, 76.0, 72.11	69.74, 83.67, 61.41	57.44, 83.3, 41.56
8	32.13, 91.67, 66.89	50.0, 71.85, 85.56	59.26, 75.14, 81.11	27.11, 44.22, 9.78	55.19, 76.02, 56.67	63.0, 72.61, 46.89	67.07, 43.3, 61.0	36.89, 54.27, 37.11
9	57.56, 77.87, 85.26	80.83, 82.24, 55.11	58.41, 82.17, 62.85	68.11, 72.89, 32.22	55.19, 76.02, 56.67	63.0, 72.61, 46.89	67.07, 43.3, 61.0	36.89, 54.27, 37.11
10	70.78, 87.42, 50.22	41.57, 76.57, 57.0	17.11, 92.81, 31.07	40.33, 56.33, 34.22	64.78, 86.28, 74.81	45.33, 72.32, 47.56	44.0, 73.28, 59.78	50.89, 65.13, 34.22
11	51.7, 80.39, 62.67	53.41, 72.12, 22.83	46.33, 72.55, 56.11	35.56, 75.61, 39.89	47.48, 70.13, 56.5	40.3, 74.56, 58.89	56.11, 69.3, 58.63	29.78, 67.06, 28.22
12	33.44, 55.07, 68.85	66.44, 75.45, 45.78	47.56, 85.15, 62.78	36.04, 74.89, 60.11	69.26, 65.44, 64.07	33.11, 86.02, 68.56	63.0, 56.61, 41.89	23.78, 82.78, 47.56
13	54.11, 68.56, 66.15	31.07, 71.77, 49.22	74.22, 69.78, 68.11	50.33, 66.09, 59.3	72.96, 84.7, 86.52	62.48, 61.44, 69.89	15.33, 44.48, 39.56	45.22, 22.0, 16.22
14	61.67, 70.77, 78.19	59.48, 56.13, 29.89	33.33, 73.19, 56.44	57.63, 78.37, 55.89	68.81, 72.46, 83.81	71.63, 73.85, 73.78	37.41, 62.13, 52.67	50.11, 54.3, 33.78
15	45.33, 71.63, 47.44	51.56, 85.59, 78.85	57.94, 79.56, 49.67	23.96, 44.14, 59.11	53.74, 82.59, 56.11	81.93, 80.37, 51.72	63.15, 78.42, 78.7	52.67, 65.11, 34.11
16	87.33, 84.85, 74.22	59.67, 84.96, 70.7	62.56, 70.8, 55.0	23.33, 41.15, 59.78	57.41, 68.65, 60.67	71.85, 75.48, 58.15	36.22, 65.19, 82.11	39.33, 94.0, 51.96
17	66.11, 71.15, 72.11	75.11, 75.46, 40.89	27.33, 62.74, 56.22	66.33, 85.43, 67.11	50.78, 83.5, 62.32	62.44, 90.0, 66.44	60.44, 70.11, 52.48	67.0, 76.78, 32.67
18	65.85, 75.17, 48.26	61.44, 81.0, 61.07	70.56, 78.7, 73.63	67.44, 55.28, 57.56	74.78, 79.67, 53.37	48.56, 91.97, 62.37	42.67, 61.07, 56.19	51.22, 73.04, 35.0
19	55.52, 85.09, 42.7	81.74, 82.15, 42.11	44.22, 64.93, 65.04	59.52, 85.73, 49.07	62.11, 72.67, 63.52	21.78, 86.81, 78.11	73.33, 76.91, 33.44	60.56, 70.69, 29.11
20	55.81, 83.33, 52.43	41.63, 63.77, 68.81	41.11, 89.0, 59.56	37.11, 56.11, 17.56	76.48, 78.81, 80.67	44.44, 63.59, 50.7	31.33, 68.48, 44.56	41.78, 75.92, 66.22
21	70.52, 90.48, 92.28	59.33, 53.19, 44.56	25.44, 83.96, 42.56	64.89, 68.15, 36.89	58.56, 69.61, 35.56	68.21, 75.56, 56.0	42.07, 56.54, 55.78	58.78, 67.22, 55.56
22	77.56, 43.46, 59.85	58.19, 64.0, 33.0	20.67, 80.26, 29.33	68.33, 62.58, 30.0	73.89, 75.06, 63.74	46.33, 84.22, 54.07	56.89, 56.44, 45.67	37.22, 54.52, 14.22
23	38.89, 84.59, 60.63	52.7, 70.37, 57.26	45.89, 52.41, 40.56	40.89, 66.24, 54.33	46.11, 83.04, 68.22	43.78, 65.07, 74.11	23.33, 67.59, 48.74	80.0, 81.7, 54.78
24	69.74, 62.16, 75.89	66.37, 86.83, 66.0	55.11, 84.74, 62.11	42.89, 41.48, 55.63	43.59, 71.75, 73.89	41.44, 83.22, 66.63	43.78, 91.38, 79.19	33.56, 51.93, 23.44
25	74.69, 75.07, 49.74	55.3, 86.71, 45.33	52.0, 67.54, 48.44	39.56, 75.0, 83.11	67.63, 81.15, 54.33	69.0, 83.25, 75.78	45.67, 59.19, 30.33	36.33, 36.07, 51.56
26	47.67, 69.54, 48.74	85.11, 86.43, 45.78	55.63, 86.19, 50.0	72.33, 87.69, 36.44	50.89, 86.05, 80.93	27.44, 78.69, 77.89	67.56, 75.94, 68.56	46.11, 65.47, 42.44
27	61.93, 72.42, 51.17	54.3, 76.46, 46.67	58.78, 82.69, 26.67	46.41, 80.4, 58.33	65.83, 83.96, 45.17	76.2, 81.29, 67.78	30.33, 61.31, 54.26	48.22, 71.74, 15.33
28	68.89, 84.09, 81.89	51.7, 68.59, 51.78	78.22, 79.26, 66.56	73.22, 83.3, 58.89	65.89, 76.19, 55.15	69.04, 81.42, 19.67	41.93, 76.89, 44.33	36.56, 73.89, 56.56
29	43.85, 76.46, 66.26	65.17, 82.26, 55.85	28.78, 79.74, 60.44	53.11, 71.02, 31.89	56.89, 76.7, 63.0	71.22, 67.24, 35.56	49.33, 75.63, 53.89	62.89, 82.33, 51.0

**Table 5.23** Different MS classes’ pre, event, and post condition values for the **Duration** parameter for the Wrist flexion & extension exercise

Coverage Parameter values in different MS classes (Wrist flexion & extension)

ID	Coverage							
	Left Wrist Flexion/Extension				Right Wrist Flexion/Extension			
	MS1	MS2	MS3	MS4	MS1	MS2	MS3	MS4
1	3.34, 7.14, 4.5	4.91, 3.97, 5.83	3.52, 5.38, 4.23	3.51, 6.99, 5.16	4.66, 7.93, 7.52	4.13, 4.6, 2.99	2.54, 9.01, 5.91	3.58, 8.03, 1.22
2	2.48, 7.5, 3.87	2.93, 5.45, 3.71	4.91, 9.48, 5.81	3.37, 4.85, 4.7	4.9, 6.73, 2.84	4.97, 6.76, 6.14	5.93, 6.03, 4.32	5.16, 7.19, 7.12
3	4.57, 9.49, 6.7	5.0, 7.78, 4.68	4.88, 6.03, 3.72	6.17, 5.84, 5.5	4.74, 8.74, 6.82	4.72, 4.92, 6.26	4.41, 8.64, 5.14	3.96, 4.76, 3.46
4	4.41, 6.64, 6.31	4.23, 7.46, 3.87	8.64, 4.96, 6.13	2.86, 3.8, 2.92	4.34, 7.87, 5.9	5.34, 4.93, 3.96	4.38, 7.47, 8.47	3.49, 4.11, 3.14
5	5.14, 6.3, 9.19	3.99, 6.35, 3.82	3.83, 4.68, 4.48	3.83, 5.47, 2.99	3.89, 5.25, 3.76	4.06, 3.65, 5.04	3.53, 7.42, 3.34	1.86, 4.08, 4.12
6	5.84, 8.5, 6.82	7.9, 9.91, 4.99	4.68, 4.28, 4.49	5.37, 5.21, 3.8	3.82, 6.13, 3.27	2.96, 6.89, 6.14	6.29, 5.06, 8.94	5.04, 7.27, 3.72
7	8.91, 9.78, 5.48	4.32, 9.27, 2.64	4.07, 4.74, 2.94	3.12, 7.14, 3.86	3.97, 11.97, 8.22	5.82, 4.26, 4.5	5.04, 4.3, 4.94	4.9, 6.45, 3.02
8	3.99, 6.32, 4.16	3.34, 5.97, 5.76	4.87, 7.24, 6.57	1.36, 2.44, 0.49	5.28, 4.69, 3.33	4.07, 5.24, 5.03	4.66, 3.44, 5.64	3.2, 3.92, 2.4
9	4.66, 9.41, 8.36	7.43, 6.67, 3.79	5.56, 5.65, 7.21	4.3, 3.88, 1.61	5.28, 4.69, 3.33	4.07, 5.24, 5.03	4.66, 3.44, 5.64	3.2, 3.92, 2.4
10	3.97, 6.32, 3.4	4.56, 5.92, 4.86	0.86, 5.36, 2.7	3.01, 3.24, 1.71	4.14, 6.12, 6.1	2.27, 6.93, 2.38	3.03, 5.1, 4.66	2.97, 4.51, 1.71
11	4.12, 8.5, 3.99	5.07, 5.49, 2.33	3.22, 5.65, 4.66	1.78, 5.14, 2.88	3.26, 7.99, 4.88	3.09, 4.67, 3.32	4.16, 5.13, 5.13	1.49, 4.05, 1.89
12	2.9, 3.13, 6.21	3.71, 8.47, 2.29	4.38, 7.24, 4.49	3.27, 5.62, 4.39	6.09, 5.41, 5.63	1.66, 8.74, 4.77	4.74, 4.36, 2.61	2.03, 6.48, 2.38
13	4.13, 3.59, 6.43	3.08, 6.26, 3.26	4.94, 5.79, 4.81	4.66, 6.27, 5.09	6.39, 8.9, 9.68	6.22, 5.0, 7.9	1.12, 3.54, 2.89	3.24, 0.73, 0.81
14	5.08, 6.85, 6.81	6.39, 3.83, 1.91	2.58, 7.25, 3.69	4.3, 5.33, 3.59	5.9, 7.1, 5.97	5.49, 5.96, 6.52	2.74, 5.12, 4.88	4.12, 4.16, 3.48
15	2.27, 5.04, 4.02	4.79, 7.87, 6.34	7.11, 6.48, 4.56	2.47, 5.52, 3.78	4.83, 6.79, 3.72	6.39, 7.04, 4.09	4.43, 6.39, 6.08	3.52, 4.41, 2.61
16	7.61, 8.75, 5.41	5.23, 6.9, 5.1	4.11, 7.02, 3.19	1.9, 2.5, 4.56	4.13, 6.73, 4.54	7.14, 5.13, 5.51	1.81, 4.64, 5.68	1.97, 5.74, 3.94
17	4.29, 6.46, 6.41	5.77, 7.19, 3.2	2.31, 6.67, 2.81	3.87, 5.72, 3.81	3.94, 6.88, 6.44	6.78, 5.97, 4.39	6.2, 6.76, 6.4	4.41, 4.99, 2.03
18	5.67, 7.96, 4.19	3.92, 5.58, 5.2	5.79, 7.99, 5.99	4.37, 2.86, 3.74	7.09, 7.12, 5.8	3.36, 7.61, 5.41	3.84, 4.98, 4.73	4.54, 7.05, 3.04
19	4.09, 8.19, 5.53	5.88, 7.14, 3.27	3.52, 5.48, 4.51	4.88, 8.89, 4.56	4.79, 9.47, 6.33	1.53, 5.94, 5.79	4.57, 6.69, 2.98	4.48, 5.79, 1.46
20	5.44, 9.44, 4.96	3.13, 5.49, 5.17	3.87, 6.19, 4.56	2.3, 2.64, 0.88	6.84, 6.7, 8.5	3.32, 6.08, 5.71	3.06, 5.67, 2.69	2.09, 7.42, 5.11
21	5.61, 7.2, 8.13	3.34, 3.58, 2.7	1.69, 5.86, 2.97	5.72, 4.21, 2.27	5.76, 4.2, 2.71	8.56, 7.01, 3.18	3.84, 4.77, 3.16	3.94, 4.85, 3.33
22	4.83, 4.65, 4.47	5.13, 4.07, 2.48	1.4, 5.87, 1.47	3.89, 4.38, 1.93	6.97, 7.29, 6.19	4.7, 6.1, 5.94	3.81, 3.93, 2.83	2.7, 4.38, 0.71
23	2.59, 7.54, 5.46	4.03, 7.44, 6.19	3.01, 3.47, 2.66	2.04, 5.12, 4.07	3.83, 8.44, 5.12	4.01, 4.53, 5.2	1.17, 4.16, 3.44	5.33, 6.39, 5.11
24	6.49, 6.09, 5.66	5.8, 8.01, 4.16	4.06, 6.91, 4.01	2.5, 2.8, 4.66	3.99, 10.27, 6.39	2.91, 6.31, 4.66	3.0, 6.36, 6.11	1.68, 3.84, 1.57
25	6.81, 8.99, 4.42	4.7, 9.26, 3.2	2.96, 4.89, 3.53	2.8, 5.01, 6.72	4.28, 8.76, 5.18	5.71, 8.63, 4.83	3.13, 3.8, 1.86	2.26, 2.72, 3.34
26	3.44, 5.21, 4.13	8.01, 5.3, 3.84	4.0, 7.74, 4.26	4.99, 8.01, 2.77	4.6, 8.16, 7.37	2.28, 6.67, 5.83	6.07, 6.95, 5.37	2.76, 5.93, 3.01
27	7.0, 8.96, 6.39	5.59, 5.93, 3.21	4.3, 8.28, 1.33	4.12, 7.24, 5.38	7.17, 11.15, 3.99	6.17, 7.4, 5.18	1.91, 6.24, 4.7	4.0, 4.11, 0.77
28	5.78, 8.99, 7.71	3.4, 4.37, 4.38	5.29, 5.48, 4.39	5.26, 6.63, 3.94	6.11, 6.39, 5.04	4.61, 6.91, 1.5	4.43, 6.6, 3.53	2.86, 5.04, 3.22
29	3.48, 8.58, 6.73	5.86, 6.23, 3.98	3.64, 7.4, 3.88	3.13, 5.83, 2.41	3.24, 4.43, 4.5	7.46, 6.62, 2.11	2.87, 5.62, 3.9	4.6, 10.43, 3.39

**Table 5.24** Different MS classes’ pre, event, and post condition values for the **Coverage** parameter for the Wrist flexion & extension exercise

Occurrence Parameter values in different MS classes (Tip-pinch)

ID	Occurrence							
	Left Tip pinch				Right Tip pinch			
	MS1	MS2	MS3	MS4	MS1	MS2	MS3	MS4
1	0.5, 0.78, 0.67	0.72, 0.78, 0.89	0.5, 0.39, 0.44	0.33, 0.33, 0.44	0.67, 0.78, 1.0	0.67, 0.72, 0.56	0.33, 0.78, 0.5	0.5, 0.5, 0.33
2	0.61, 0.61, 0.33	0.56, 0.39, 0.67	0.56, 0.5, 0.44	0.72, 0.61, 0.61	0.94, 1.11, 0.61	0.61, 0.56, 0.61	0.44, 0.5, 0.56	0.17, 0.67, 0.61
3	0.5, 0.56, 0.94	0.5, 1.0, 0.67	0.78, 0.5, 0.5	0.22, 0.56, 0.39	0.61, 0.61, 0.83	0.5, 0.83, 0.56	0.44, 0.33, 0.44	0.61, 0.61, 0.33
4	0.78, 0.78, 0.94	0.33, 0.78, 0.22	0.61, 0.61, 0.33	0.56, 0.5, 0.56	0.72, 1.11, 0.78	0.33, 0.61, 0.72	0.72, 0.56, 0.56	0.22, 0.44, 0.44
5	0.61, 0.78, 0.56	0.5, 0.72, 0.67	0.5, 0.56, 0.61	0.22, 0.22, 0.33	0.33, 0.33, 0.5	0.89, 0.61, 0.72	0.61, 0.33, 0.44	0.56, 0.28, 0.5
6	0.5, 0.61, 0.83	0.5, 0.5, 0.61	0.56, 0.61, 0.44	0.56, 0.61, 0.72	0.44, 0.67, 0.72	0.61, 0.5, 0.39	0.33, 0.22, 0.44	0.56, 0.44, 0.39
7	0.33, 0.67, 0.56	0.5, 0.56, 0.56	0.5, 0.61, 0.5	0.22, 0.33, 0.44	0.89, 0.78, 0.39	0.56, 0.78, 0.33	0.72, 0.22, 0.44	0.39, 0.67, 0.39
8	0.22, 0.44, 0.94	0.61, 0.83, 0.44	0.33, 0.61, 0.72	0.67, 0.61, 0.61	0.83, 0.89, 0.72	0.78, 0.33, 0.72	0.67, 0.39, 0.39	1.0, 0.94, 0.89
9	0.61, 0.61, 0.83	0.61, 0.33, 0.67	0.94, 0.28, 0.33	0.44, 0.33, 0.56	0.67, 0.39, 0.67	0.56, 0.67, 0.39	0.17, 0.5, 0.22	0.22, 0.44, 0.22
10	0.67, 0.67, 0.72	0.56, 0.67, 0.44	0.56, 0.33, 0.78	0.22, 0.22, 0.17	0.78, 0.67, 0.89	0.44, 0.5, 0.44	0.17, 0.44, 0.28	0.39, 0.5, 0.39
11	0.39, 0.56, 0.5	0.72, 0.39, 0.44	0.39, 0.44, 0.22	0.22, 0.5, 0.28	0.78, 0.67, 0.89	0.44, 0.5, 0.44	0.17, 0.44, 0.28	0.39, 0.5, 0.39
12	0.44, 0.39, 0.28	0.39, 0.61, 0.56	0.44, 0.5, 0.39	0.78, 0.61, 0.33	0.28, 0.61, 0.56	0.5, 0.28, 0.72	0.78, 0.83, 0.56	0.56, 1.0, 0.33
13	0.83, 0.44, 0.78	0.89, 0.67, 1.28	0.33, 0.44, 0.61	0.39, 0.28, 0.28	0.39, 0.78, 0.56	0.72, 1.0, 0.89	0.5, 0.33, 0.39	0.56, 0.78, 0.72
14	0.5, 0.44, 0.61	0.5, 0.78, 0.39	1.0, 0.94, 0.61	0.28, 0.56, 0.33	0.67, 1.0, 0.61	0.89, 0.39, 0.67	0.33, 0.5, 0.5	0.39, 0.28, 0.28
15	0.61, 0.78, 0.72	0.61, 0.72, 0.56	1.0, 0.56, 0.39	0.28, 0.5, 0.5	0.56, 0.61, 0.5	0.5, 0.61, 0.56	0.33, 0.67, 0.44	0.44, 0.56, 0.22
16	1.06, 0.67, 0.61	0.72, 0.56, 0.33	0.78, 0.78, 0.94	0.22, 0.33, 0.44	0.56, 0.72, 0.67	0.61, 0.39, 0.56	0.5, 0.61, 0.39	0.61, 0.33, 0.11
17	0.5, 0.72, 0.67	0.67, 0.67, 0.44	0.39, 0.61, 0.67	0.56, 0.61, 0.44	0.56, 0.94, 0.67	0.33, 0.61, 0.17	0.61, 0.89, 1.0	0.44, 0.83, 0.56
18	0.44, 0.44, 0.72	0.5, 0.72, 0.33	0.78, 0.83, 0.5	0.72, 0.44, 0.33	0.28, 0.33, 0.56	0.94, 1.11, 0.5	0.44, 0.61, 0.61	0.61, 0.56, 0.94
19	0.89, 0.67, 0.67	0.56, 0.67, 0.44	0.39, 0.44, 0.33	0.61, 0.56, 0.44	0.72, 0.56, 1.0	0.72, 1.06, 0.78	0.22, 0.44, 0.44	0.5, 0.61, 0.28
20	0.33, 0.61, 0.44	0.56, 0.39, 0.44	0.39, 0.28, 0.33	0.28, 0.67, 0.78	0.78, 0.83, 0.5	0.67, 0.17, 0.22	0.67, 0.56, 0.61	0.78, 0.44, 0.56
21	0.78, 0.61, 0.89	0.78, 0.39, 0.33	0.39, 0.39, 0.56	0.39, 0.28, 0.28	0.39, 0.61, 0.56	0.78, 0.78, 0.78	0.72, 0.5, 0.61	0.44, 0.56, 0.39
22	0.39, 0.61, 0.56	0.67, 0.33, 0.28	0.11, 0.44, 0.22	0.39, 0.33, 0.39	0.83, 0.67, 0.61	0.61, 0.44, 0.28	0.11, 0.28, 0.33	0.28, 0.67, 0.5
23	0.22, 0.72, 0.67	0.5, 0.5, 0.56	0.44, 0.5, 0.44	0.22, 0.56, 0.56	0.5, 0.61, 0.78	0.44, 0.61, 0.39	0.61, 0.67, 0.39	0.33, 0.44, 0.22
24	1.0, 0.5, 0.89	0.78, 0.44, 0.28	0.83, 0.67, 0.44	0.39, 0.22, 0.17	0.5, 0.83, 0.5	0.61, 0.56, 0.61	0.33, 0.78, 0.39	0.39, 0.5, 0.22
25	0.61, 1.0, 0.28	0.72, 0.72, 0.89	1.11, 0.78, 0.56	0.33, 0.33, 0.5	0.56, 0.5, 0.83	0.61, 0.33, 0.56	0.67, 0.78, 0.56	0.33, 0.39, 0.61
26	0.67, 0.61, 0.72	0.78, 0.61, 0.67	0.5, 0.61, 0.5	0.5, 0.72, 0.22	0.5, 0.78, 1.0	0.56, 0.72, 0.72	0.61, 0.5, 0.33	0.67, 0.5, 0.61
27	0.83, 0.94, 0.44	0.61, 0.67, 0.67	0.11, 0.67, 0.33	0.17, 0.17, 0.22	0.78, 0.89, 0.33	0.61, 0.78, 0.61	0.44, 0.39, 0.33	0.67, 0.44, 0.44
28	0.72, 1.06, 0.56	0.72, 0.56, 0.5	0.56, 0.44, 0.67	0.39, 0.78, 0.5	0.39, 0.39, 0.83	0.67, 0.83, 0.56	0.56, 0.67, 0.83	0.61, 0.44, 0.44
29	0.78, 0.89, 0.89	0.5, 0.72, 0.61	0.78, 0.28, 0.61	0.5, 0.61, 0.89	0.56, 0.5, 0.72	0.56, 0.89, 0.56	0.78, 0.44, 0.56	0.44, 0.78, 0.28

**Table 5.25** Different MS classes’ pre, event, and post condition values for the **Occurrence** parameter for the Tip-pinch exercise

Duration Parameter values in different MS classes (Tip-pinch)

ID	Duration							
	Left Tip pinch				Right Tip pinch			
	MS1	MS2	MS3	MS4	MS1	MS2	MS3	MS4
1	54.11, 61.89, 73.22	77.0, 90.94, 72.07	57.22, 39.89, 36.81	42.67, 41.0, 60.44	76.11, 81.78, 82.72	60.48, 60.22, 84.11	50.11, 67.48, 54.33	58.67, 53.78, 48.44
2	70.11, 56.89, 34.11	49.48, 47.67, 67.67	56.89, 44.96, 48.44	63.78, 62.41, 81.78	84.59, 76.78, 55.59	61.11, 52.48, 69.96	58.22, 66.89, 60.22	18.11, 63.33, 54.81
3	61.11, 48.7, 70.67	51.11, 79.41, 67.89	73.33, 52.52, 51.78	24.89, 53.41, 41.22	62.15, 61.22, 72.17	51.72, 58.85, 45.11	54.44, 42.67, 52.33	51.67, 62.11, 49.67
4	85.52, 53.26, 79.04	36.56, 53.54, 35.56	50.74, 62.44, 24.3	54.11, 58.33, 69.44	82.07, 75.48, 69.44	42.44, 80.41, 81.89	66.52, 66.37, 62.85	35.33, 53.11, 48.0
5	66.67, 73.41, 67.22	46.48, 64.48, 56.41	61.78, 73.56, 52.33	28.78, 38.44, 55.78	43.56, 48.44, 53.7	69.06, 60.3, 57.07	64.59, 47.89, 63.0	51.89, 41.11, 59.0
6	60.0, 72.48, 81.96	57.33, 68.78, 68.89	70.41, 43.67, 54.33	64.67, 50.48, 65.41	67.89, 52.07, 72.89	57.89, 62.81, 43.56	37.11, 33.11, 45.44	66.44, 48.22, 43.56
7	44.11, 72.56, 65.89	62.67, 59.7, 55.11	46.41, 50.67, 69.89	36.89, 55.78, 49.7	78.67, 71.04, 41.93	47.93, 63.85, 38.59	80.44, 31.11, 46.96	38.11, 71.89, 44.22
8	17.56, 62.0, 69.69	64.89, 79.89, 68.56	45.22, 56.0, 60.41	78.41, 70.37, 66.74	77.94, 66.33, 54.59	74.22, 42.22, 66.59	76.33, 40.11, 52.44	79.81, 73.69, 71.11
9	25.94, 50.37, 72.78	71.78, 65.33, 70.7	59.96, 39.78, 30.67	80.0, 43.44, 55.0	62.0, 59.89, 74.0	63.96, 68.89, 52.22	25.11, 62.11, 29.78	26.67, 58.33, 29.44
10	75.93, 76.89, 70.89	49.89, 57.78, 69.56	62.67, 36.78, 56.78	39.33, 27.78, 22.0	62.89, 68.81, 67.09	35.44, 51.89, 69.89	19.0, 47.63, 35.67	37.56, 51.93, 34.11
11	53.0, 40.3, 79.78	62.0, 47.11, 42.44	38.89, 44.74, 16.89	39.33, 43.74, 42.67	62.89, 68.81, 67.09	35.44, 51.89, 69.89	19.0, 47.63, 35.67	37.56, 51.93, 34.11
12	55.22, 54.33, 41.11	48.89, 45.85, 55.26	61.44, 50.33, 44.22	72.33, 70.67, 32.22	51.33, 60.33, 60.37	67.04, 38.22, 61.81	70.44, 86.0, 51.26	49.44, 59.15, 36.89
13	60.0, 34.04, 66.72	67.89, 63.3, 74.58	47.56, 63.78, 87.67	41.44, 44.22, 37.78	53.67, 67.93, 55.17	63.07, 90.09, 81.44	60.89, 43.11, 47.33	68.59, 55.67, 63.89
14	60.33, 49.11, 63.89	50.22, 72.72, 34.3	72.89, 82.78, 71.33	41.11, 70.67, 41.22	47.85, 57.26, 69.33	78.22, 69.56, 69.26	45.22, 50.22, 60.22	51.89, 37.0, 35.0
15	58.41, 65.7, 92.89	72.0, 58.56, 54.67	68.07, 59.44, 40.15	22.07, 66.78, 71.78	44.96, 77.78, 56.22	53.26, 73.3, 47.78	49.11, 68.11, 43.67	44.22, 59.44, 24.0
16	81.76, 62.3, 58.7	62.74, 57.93, 44.67	88.3, 70.85, 77.67	23.22, 50.0, 68.56	55.0, 79.56, 66.11	58.19, 42.67, 74.78	57.19, 49.11, 60.44	75.11, 49.22, 16.22
17	61.22, 59.11, 73.11	59.3, 79.44, 33.78	51.22, 56.67, 68.44	62.81, 50.81, 40.56	42.96, 66.11, 58.89	40.33, 54.94, 19.22	59.48, 69.41, 72.52	55.89, 66.3, 45.22
18	36.93, 49.04, 82.89	47.96, 49.74, 46.89	59.43, 77.59, 59.11	69.89, 43.11, 55.56	30.22, 43.67, 72.33	69.93, 89.26, 77.56	54.0, 60.59, 41.15	75.56, 53.22, 68.3
19	81.07, 70.06, 56.0	65.44, 58.67, 51.0	62.22, 52.11, 43.44	45.5, 59.0, 54.44	82.44, 54.22, 65.33	76.56, 83.26, 75.63	20.74, 41.44, 53.44	64.78, 75.33, 47.78
20	39.11, 64.78, 69.67	49.56, 60.22, 46.56	52.11, 32.89, 42.56	31.78, 71.0, 58.19	68.41, 68.28, 62.56	72.17, 17.0, 32.89	77.56, 65.0, 67.78	58.06, 50.67, 53.7
21	63.59, 63.89, 81.33	80.52, 43.44, 36.89	46.89, 56.56, 67.07	67.11, 47.78, 40.33	25.78, 62.26, 57.22	76.48, 82.59, 53.11	70.19, 66.56, 56.48	70.89, 51.93, 54.44
22	49.41, 63.04, 49.0	59.59, 32.44, 33.89	15.33, 43.78, 23.22	39.93, 55.56, 55.67	53.74, 63.44, 61.93	55.56, 63.0, 29.78	16.44, 33.0, 34.44	45.56, 85.26, 77.22
23	40.22, 61.43, 66.0	71.44, 53.78, 80.44	58.56, 49.11, 44.33	24.78, 56.33, 64.52	36.44, 59.44, 53.96	65.89, 65.33, 45.33	55.15, 63.52, 54.67	42.22, 54.44, 28.33
24	85.81, 73.78, 83.83	75.11, 71.56, 37.0	69.44, 78.89, 51.67	55.56, 32.22, 27.33	57.7, 72.59, 44.78	61.19, 68.56, 45.0	41.56, 85.74, 57.78	61.11, 56.89, 30.78
25	61.04, 79.93, 35.56	67.44, 64.81, 69.83	79.81, 74.63, 52.44	44.22, 35.11, 55.33	51.11, 48.52, 61.57	62.44, 39.44, 54.19	68.33, 68.0, 77.89	45.78, 58.67, 75.56
26	64.0, 53.78, 55.11	72.85, 77.33, 60.44	62.0, 67.04, 48.04	52.11, 49.07, 32.44	53.56, 53.76, 81.09	61.0, 79.85, 71.17	67.89, 57.3, 46.67	65.04, 67.0, 66.44
27	68.0, 74.15, 49.22	65.37, 66.15, 75.85	15.56, 90.0, 34.22	24.22, 25.78, 30.89	65.0, 72.89, 35.22	74.78, 62.22, 64.96	51.78, 35.96, 48.44	78.0, 49.11, 44.22
28	51.07, 84.19, 67.37	64.52, 63.56, 83.0	65.78, 63.44, 70.7	42.44, 79.33, 61.11	41.67, 52.67, 76.74	63.7, 88.67, 51.96	47.81, 55.44, 65.69	70.78, 61.78, 42.67
29	69.22, 73.31, 61.84	72.89, 77.81, 43.04	63.73, 31.33, 68.78	53.67, 61.56, 80.2	64.59, 55.56, 58.56	44.94, 66.85, 57.26	63.44, 51.56, 70.67	44.67, 66.11, 37.56

**Table 5.26** Different MS classes' pre, event, and post condition values for the **Duration** parameter for the Tip-pinch exercise

Coverage Parameter values in different MS classes (Tip-pinch)

ID	Coverage							
	Left Tip pinch				Right Tip pinch			
	MS1	MS2	MS3	MS4	MS1	MS2	MS3	MS4
1	4.02, 6.14, 5.39	5.73, 6.92, 7.43	3.8, 2.78, 3.66	2.63, 2.56, 3.52	5.9, 6.4, 8.2	5.21, 5.62, 4.66	3.06, 6.7, 3.97	3.72, 4.16, 2.42
2	4.69, 5.01, 2.62	4.4, 3.37, 5.64	4.09, 4.06, 3.88	6.03, 4.9, 5.47	7.93, 8.42, 5.03	4.99, 4.49, 5.36	3.93, 4.1, 4.32	1.3, 5.31, 4.96
3	4.43, 4.77, 7.58	4.76, 7.72, 5.66	5.99, 3.8, 3.91	1.67, 4.47, 2.86	4.99, 4.73, 6.64	4.66, 6.41, 4.28	3.52, 2.51, 3.46	4.94, 4.97, 2.88
4	6.58, 6.26, 7.71	2.2, 6.07, 1.78	4.56, 5.11, 2.61	4.54, 4.38, 4.22	6.78, 9.43, 6.14	3.14, 5.7, 6.47	6.11, 4.83, 4.37	1.77, 3.54, 3.2
5	4.63, 6.46, 4.73	4.36, 5.93, 5.57	3.87, 4.71, 4.77	1.91, 1.92, 2.79	2.76, 2.81, 4.58	6.73, 4.98, 6.2	5.13, 2.86, 4.08	4.27, 2.06, 4.44
6	4.49, 5.61, 6.71	4.28, 4.56, 4.67	4.93, 5.01, 3.66	4.74, 4.79, 5.26	3.87, 5.16, 5.87	5.17, 4.18, 3.14	2.63, 1.66, 3.6	5.26, 3.96, 3.02
7	2.72, 5.39, 4.26	4.59, 4.32, 4.62	4.11, 4.58, 4.56	1.84, 2.79, 3.26	6.92, 6.34, 2.89	3.98, 6.33, 2.88	5.9, 2.03, 3.73	2.73, 6.2, 3.11
8	1.68, 3.54, 8.37	5.24, 7.37, 3.97	2.69, 5.39, 5.48	5.64, 5.21, 5.4	6.87, 7.79, 5.97	5.74, 2.63, 6.23	5.6, 2.88, 2.99	8.11, 8.21, 6.88
9	4.72, 4.74, 6.73	5.07, 3.27, 5.36	7.31, 2.53, 2.37	4.0, 2.69, 4.46	5.21, 3.41, 5.67	4.5, 5.3, 3.2	1.26, 4.01, 2.02	1.68, 3.4, 1.99
10	5.64, 5.14, 6.41	4.22, 5.44, 3.9	4.66, 2.8, 6.63	1.97, 1.82, 1.1	6.27, 5.71, 7.3	3.46, 4.06, 3.96	1.47, 3.73, 2.27	3.39, 3.87, 2.92
11	3.16, 5.07, 4.41	5.66, 3.21, 3.48	3.32, 3.81, 1.71	1.97, 4.03, 2.13	6.27, 5.71, 7.3	3.46, 4.06, 3.96	1.47, 3.73, 2.27	3.39, 3.87, 2.92
12	3.66, 3.16, 2.06	3.47, 4.96, 4.64	4.07, 3.79, 3.16	6.24, 4.86, 2.51	2.57, 4.62, 4.47	4.19, 1.91, 5.8	6.33, 7.04, 4.42	4.0, 7.61, 2.89
13	6.33, 3.43, 6.67	7.72, 6.29, 10.14	2.87, 3.62, 5.26	2.89, 2.21, 1.89	3.12, 6.17, 4.46	5.7, 8.67, 7.02	4.08, 2.53, 3.27	5.06, 6.39, 5.97
14	3.8, 3.77, 4.64	3.84, 6.26, 3.0	9.2, 7.68, 5.57	2.06, 4.96, 3.04	4.88, 7.56, 5.28	7.19, 3.48, 5.88	2.69, 3.64, 4.07	2.93, 2.38, 2.26
15	5.29, 6.63, 6.69	4.96, 5.51, 4.42	7.88, 4.81, 2.8	1.93, 4.22, 4.09	4.62, 5.23, 4.13	4.04, 5.68, 4.78	3.0, 5.19, 3.64	4.3, 4.33, 1.69
16	8.63, 5.32, 4.53	5.73, 4.8, 2.73	6.93, 6.31, 7.47	1.59, 3.04, 3.92	4.73, 6.43, 5.47	4.61, 3.02, 4.81	4.22, 4.54, 3.02	5.81, 2.9, 0.81
17	4.5, 6.39, 5.66	5.41, 6.04, 3.27	3.18, 5.18, 5.5	4.54, 4.66, 3.38	4.26, 7.93, 5.86	2.43, 4.97, 1.43	4.9, 7.01, 8.31	3.73, 6.47, 3.81
18	3.62, 3.4, 6.03	4.56, 5.49, 2.77	5.84, 7.09, 3.89	6.14, 3.62, 3.26	2.42, 3.3, 5.07	7.46, 9.84, 4.39	3.6, 4.57, 4.59	5.17, 4.51, 8.27
19	7.18, 5.91, 4.78	4.66, 5.81, 4.03	3.11, 4.0, 2.6	4.92, 4.18, 3.52	6.58, 4.57, 8.54	6.01, 8.97, 6.54	1.82, 3.2, 4.24	4.16, 5.93, 2.39
20	2.89, 5.06, 4.04	4.71, 3.58, 3.71	3.56, 2.47, 2.64	2.02, 5.7, 5.76	6.09, 6.56, 4.58	5.3, 1.29, 1.64	5.82, 4.72, 4.81	5.9, 3.48, 4.36
21	6.39, 4.43, 7.27	6.9, 3.08, 2.82	3.26, 3.29, 4.79	3.36, 2.39, 2.5	3.06, 4.83, 4.73	6.56, 6.47, 6.26	5.53, 4.39, 5.17	4.09, 4.16, 3.2
22	3.46, 5.08, 4.9	5.29, 2.46, 2.31	0.77, 3.59, 1.57	2.79, 2.78, 3.12	6.61, 5.33, 4.98	5.02, 4.2, 2.43	0.82, 2.16, 2.64	2.28, 5.5, 4.33
23	2.01, 5.7, 5.69	3.97, 4.14, 5.08	3.42, 3.67, 3.61	1.78, 3.98, 4.46	4.13, 4.71, 5.5	3.84, 4.92, 2.68	5.1, 5.04, 3.14	2.58, 3.22, 1.82
24	8.44, 4.68, 7.37	6.51, 4.04, 2.23	6.64, 5.3, 3.58	3.93, 1.61, 1.37	4.42, 6.98, 4.19	4.33, 4.96, 5.01	2.59, 7.26, 3.4	3.5, 4.18, 1.97
25	4.91, 8.37, 2.23	5.68, 5.77, 7.07	8.81, 6.61, 4.27	2.71, 2.48, 3.59	4.31, 4.38, 5.98	4.9, 2.92, 4.61	5.18, 6.77, 4.73	2.79, 3.41, 4.96
26	6.47, 4.99, 5.48	6.29, 5.11, 5.92	4.06, 5.5, 3.66	4.01, 5.26, 1.62	3.93, 6.14, 9.21	4.42, 6.27, 5.76	4.74, 4.18, 2.69	5.4, 4.27, 5.1
27	7.17, 7.88, 3.78	5.03, 5.38, 5.58	0.78, 6.02, 2.6	1.21, 1.29, 1.54	5.82, 7.38, 2.69	5.14, 5.57, 5.1	3.48, 3.18, 2.42	5.11, 3.23, 3.42
28	5.6, 9.1, 4.67	6.1, 4.72, 4.63	4.62, 3.6, 5.38	3.03, 6.23, 3.97	2.89, 3.1, 6.26	5.36, 7.31, 4.4	5.03, 4.71, 7.3	5.37, 3.64, 3.68
29	6.7, 7.51, 7.2	4.44, 6.3, 4.66	6.56, 2.06, 4.74	4.06, 4.83, 7.1	4.57, 4.08, 5.69	4.56, 7.64, 4.47	6.47, 4.04, 5.09	3.61, 5.82, 2.33

**Table 5.27** Different MS classes' pre, event, and post condition values for the Coverage parameter for the Tip-pinch exercise

DIFFERENT PARAMETER VALUES AVERAGED ACROSS ALL TRIALS AND ALL SUBJECTS

**Wrist flexion & extension Exercise**

Occurrence Parameter values of left Wrist flexion & extension

States	MS1	MS2	MS3	MS4
Pre	0.57	0.6	0.5	0.44
Event	0.88	0.79	0.75	0.63
Post	0.68	0.49	0.5	0.45

**Table 5.28** Left Wrist flexion & extension averaged values of **Occurrence** parameter

Occurrence comparison for left flexion

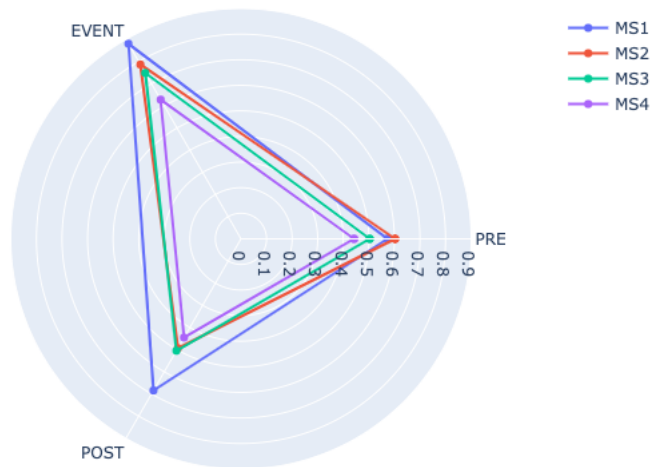


**Figure 5.1** Spider plot Occurrence parameter for left Wrist flexion & extension

Occurrence Parameter values of right Wrist flexion & extension

States	MS1	MS2	MS3	MS4
Pre	0.61	0.56	0.48	0.41
Event	0.88	0.74	0.68	0.64
Post	0.66	0.58	0.57	0.36

**Table 5.29** Right Wrist flexion & extension averaged values of **Occurrence** parameter

Occurrence comparison for right flexion

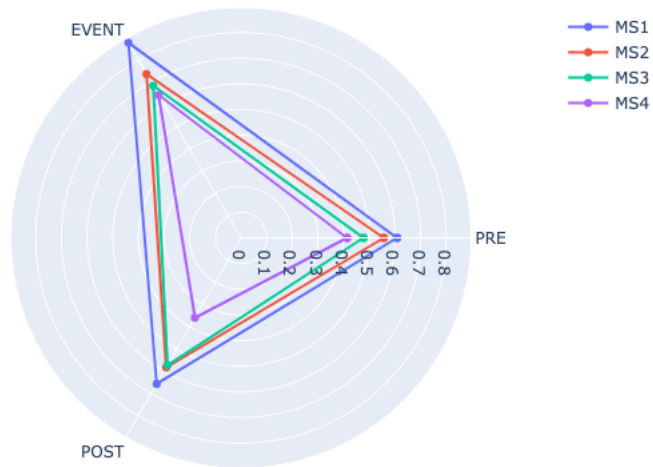


**Figure 5.2** Spider plot Occurrence parameter for right Wrist flexion & extension

Duration Parameter values of left Wrist flexion & extension

States	MS1	MS2	MS3	MS4
Pre	58.81	59.75	49	49.76
Event	76.47	74.77	75.97	68.23
Post	64.74	51.53	55.27	50.27

**Table 5.30** Left Wrist Flexion/Extension averaged values of **Duration** parameter

Duration comparison for left flexion

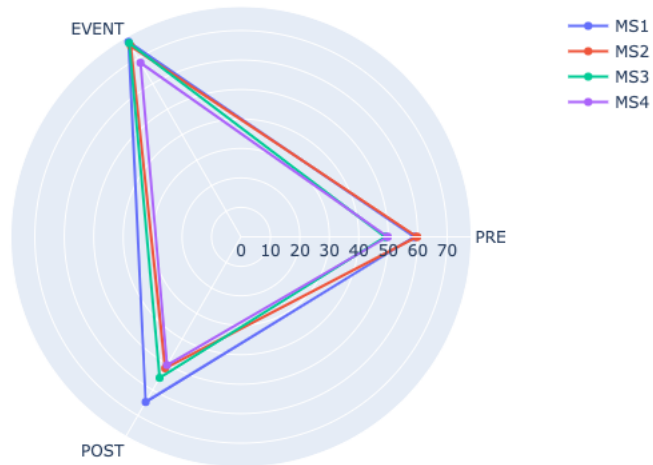


**Figure 5.3** Spider plot Duration parameter for left Wrist flexion & extension

Duration Parameter values of right Wrist flexion & extension

States	MS1	MS2	MS3	MS4
Pre	59.67	55.49	50.53	46.96
Event	78.34	76.12	68.48	66.41
Post	63.47	58.4	56.62	40.97

**Table 5.31** Right Wrist flexion & extension averaged values of **Duration** parameter

Duration comparison for right flexion

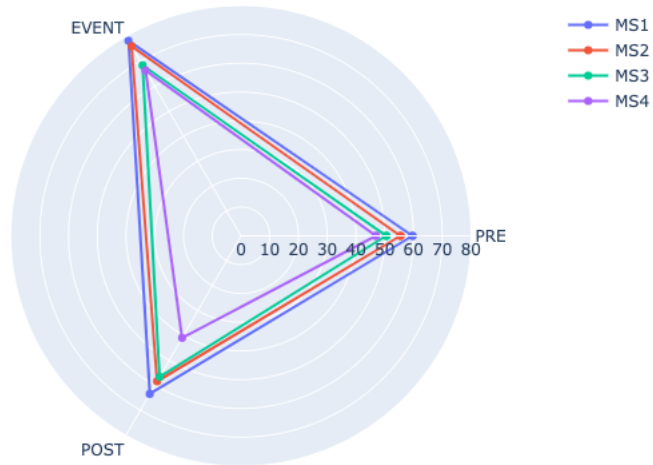


**Figure 5.4** Spider plot Duration parameter for right Wrist flexion & extension

Coverage Parameter values of left Wrist flexion & extension

States	MS1	MS2	MS3	MS4
Pre	4.79	4.88	4.07	3.63
Event	7.29	6.45	6.19	5.12
Post	5.72	4.01	4.14	3.59

**Table 5.32** Left Wrist flexion & extension averaged values of **Coverage** parameter

Coverage comparison for left flexion

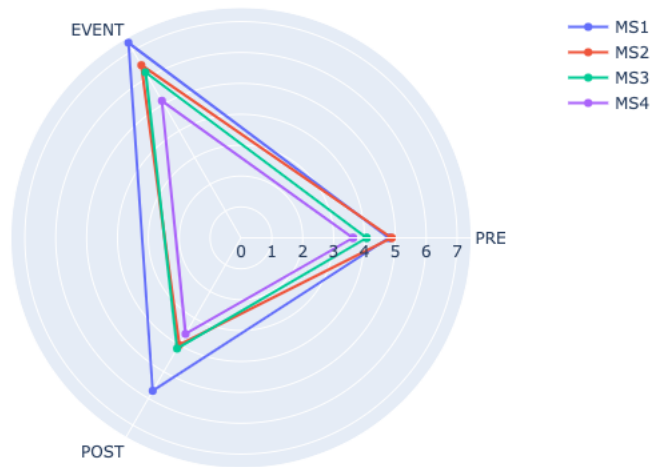


**Figure 5.5** Spider plot Coverage parameter for left Wrist flexion & extension

Coverage Parameter values of right Wrist flexion & extension

States	MS1	MS2	MS3	MS4
Pre	4.97	4.61	3.84	3.43
Event	7.32	6.06	5.57	5.27
Post	5.49	4.8	4.69	2.88

**Table 5.33** Right Wrist flexion & extension averaged values of **Coverage** parameter

Coverage comparison for right flexion

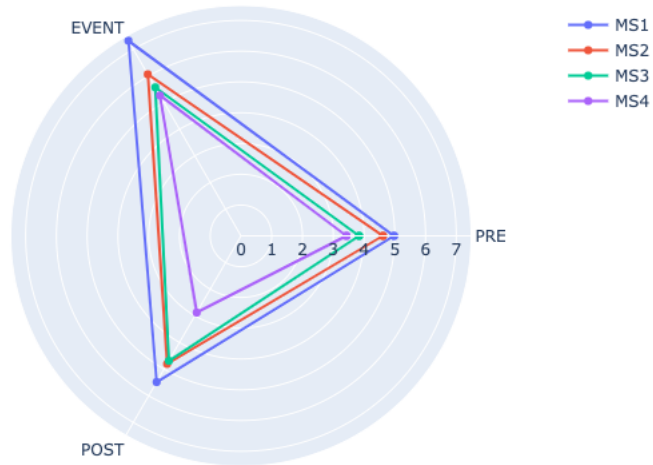


**Figure 5.6** Spider plot Coverage parameter for right Wrist flexion & extension

DIFFERENT PARAMETER VALUES AVERAGED ACROSS ALL TRIALS AND ALL SUBJECTS

**Tip-pinch Exercise**

Occurrence Parameter values of left Tip-pinch

States	MS1	MS2	MS3	MS4
Pre	0.6	0.61	0.57	0.41
Event	0.66	0.61	0.54	0.46
Post	0.66	0.55	0.5	0.44

**Table 5.34** Left Tip-pinch averaged values of **Occurrence** parameter

Occurrence comparison for left tip pinch

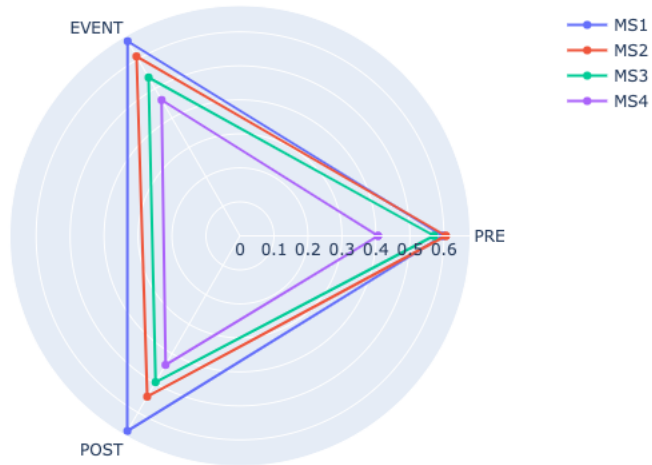


**Figure 5.7** Spider plot Occurrence parameter for left tip-pinch

Occurrence Parameter values of right Tip-pinch

States	MS1	MS2	MS3	MS4
Pre	0.6	0.61	0.48	0.48
Event	0.7	0.63	0.52	0.56
Post	0.68	0.55	0.48	0.43

**Table 5.35** Right Tip-pinch averaged values of **Occurrence** parameter

Occurrence comparison for right tip pinch

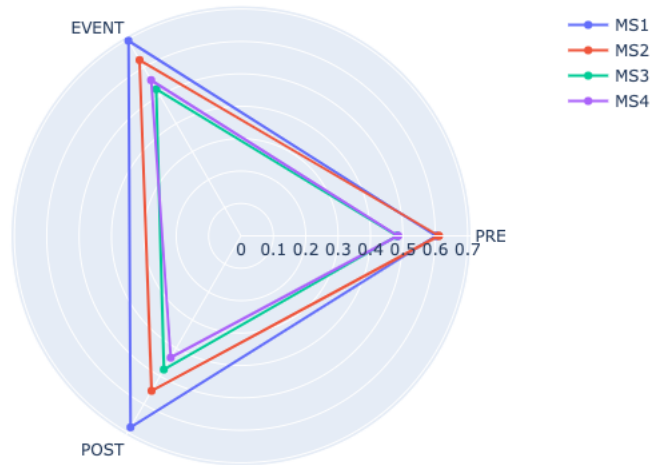


**Figure 5.8** Spider plot Occurrence parameter for right tip-pinch

Duration Parameter values of left Tip-pinch

States	MS1	MS2	MS3	MS4
Pre	58.64	61.48	57.37	47.14
Event	62.23	62.48	56.77	52.21
Post	66.19	56.45	51.64	52.36

**Table 5.36** Left Tip-pinch averaged values of **Duration** parameter

Duration comparison for left tip pinch

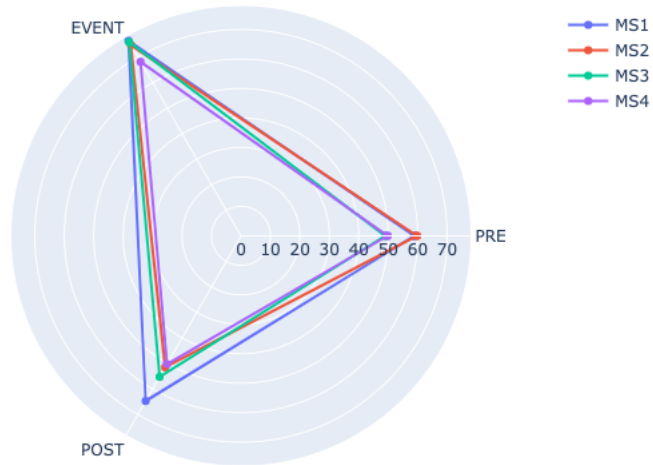


**Figure 5.9** Spider plot Duration parameter for left tip-pinch

Duration Parameter values of right Tip-pinch

States	MS1	MS2	MS3	MS4
Pre	58.18	60.15	52.69	54.12
Event	63.69	63.06	55.28	58.16
Post	62.37	58.35	53.42	47.06

**Table 5.37** Left Tip-pinch averaged values of **Duration** parameter

Duration comparison for right tip pinch

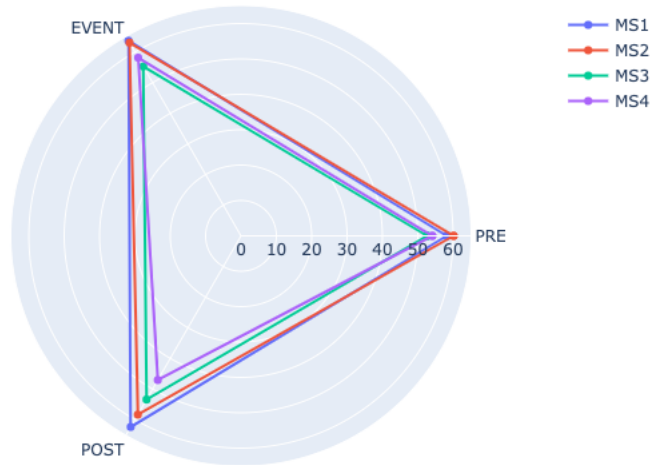


**Figure 5.10** Spider plot Duration parameter for right tip-pinch

Coverage Parameter values of left Tip-pinch

States	MS1	MS2	MS3	MS4
Pre	4.96	5.03	4.65	3.32
Event	5.48	5.1	4.45	3.72
Post	5.47	4.52	4.01	3.49

**Table 5.38** Left Tip-pinch averaged values of Coverage parameter

Coverage comparison for left tip pinch

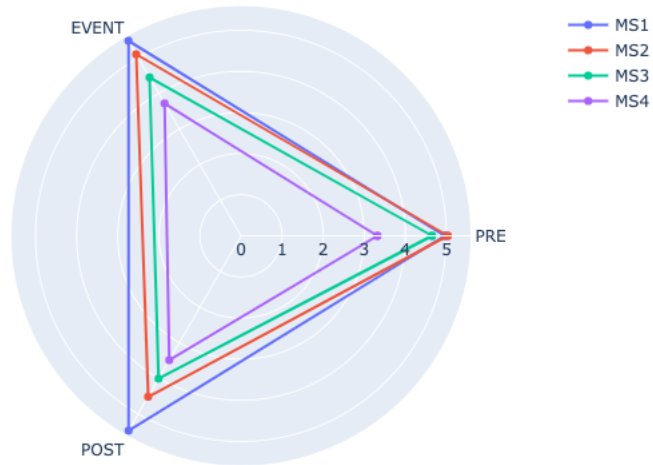


**Figure 5.11** Spider plot Coverage parameter for left tip-pinch

Coverage Parameter values of right Tip-pinch

States	MS1	MS2	MS3	MS4
Pre	4.92	4.9	3.98	4.01
Event	5.7	5.24	4.25	4.52
Post	5.61	4.6	3.93	3.52

**Table 5.39** Right Tip-pinch averaged values of Coverage parameter

Coverage comparison for right tip pinch

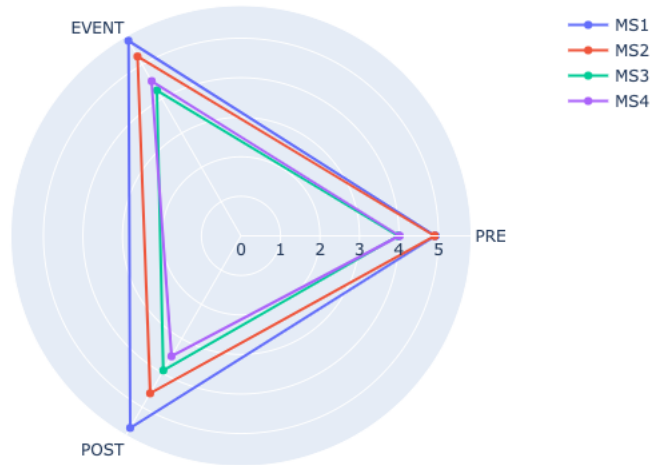


**Figure 5.12** Spider plot Coverage parameter for right tip-pinch

P-values and their descriptives for all microstate parameters

OCCURRENCE				
Motor Task	Microstates	Pre-event—Event	Event—Post-event	Pre-event—Post-event
Left Wrist-Flexion/Extension	MS1 (Left anterior to right posterior – $RS_{MS_b}$ )	m1=0.573	m1 = 0.881	m1=0.573
		m2=0.881	m2 = 0.684	m2 = 0.684
		t(28)=-8.047	t(28) = 4.314	t(28) = -2.830
		p 0.001	p 0.001	p = 0.009
	MS2 (task-specific topography)	m1 = 0.603	m1 = 0.787	m1 = 0.603
		m2 = 0.787	m2 = 0.493	m2 = 0.493
		t(28) = -4.391	t(28) = 7.173	t(28) = 2.570
		p 0.001	p 0.001	p = 0.016
	MS3 (Midline frontal to occipital – $RS_{MS_c}$ )	m1 = 0.503	m1 = 0.749	None
		m2 = 0.749	m2 = 0.505	
		t(28) = -5.531	t(28) = 5.951	
		p 0.001	p 0.001	
MS4 (Midline occipital to frontal – Partially like $RS_{MS_d}$ )	m1 = 0.442	m1 = 0.628	None	
	m2 = 0.628	m2 = 0.446		
	t(28) = -5.243	t(28) = 5.310		
	p 0.001	p 0.001		
Right Wrist-Flexion/Extension	MS1 (Midline occipital to frontal – $RS_{MS_d}$ )	m1 = 0.608	m1 = 0.878	None
		m2 = 0.878	m2 = 0.657	
		t(28) = -5.658	t(28) = 5.689	
		p 0.001	p 0.001	
	MS2 (task-specific topography)	m1 = 0.556	m1 = 0.737	None
		m2 = 0.737	m2 = 0.583	
		t(28) = -3.462	t(28) = 3.270	
		p = 0.002	p = 0.003	
	MS3 (Left anterior to right posterior – $RS_{MS_b}$ )	m1 = 0.478	m1 = 0.684	None
		m2 = 0.684	m2 = 0.572	
		t(28) = -4.965	t(28) = 2.845	
		p 0.001	p = 0.008	
MS4 (Left posterior to right anterior – $RS_{MS_a}$ )	m1 = 0.413	m1 = 0.642	None	
	m2 = 0.642	m2 = 0.360		
	t(28) = -5.960	t(28) = 7.003		
	p 0.001	p 0.001		
Right Tip-pinch	MS1 (Right posterior to left anterior – $RS_{MS_b}$ )	m1 = 0.602	None	None
		m2 = 0.696		
		t(28) = -2.682		
		p = 0.012		
	MS4 (task-specific topography)	None	m1 = 0.555	None
			m2 = 0.434	
		t(28) = 2.976		
		p = 0.006		

Table 5.40 Statistically significant Occurrence values for Wrist flexion & extension and Tip-pinch

DURATION				
Motor Task	Microstates	Pre-event–Event	Event–Post-event	Pre-event–Post-event
Left Wrist- Flexion/Extension	MS1 (Left anterior to right posterior – $RS_{MS_b}$ )	m1 = 58.815	m1 = 76.474	None
		m2 = 76.474	m2 = 64.740	
		t(28) = -5.239	t(28) = 3.585	
		p 0.001	p = 0.001	
	MS2 (task-specific topography)	m1 = 59.748	m1 = 74.771	None
		m2 = 74.771	m2 = 51.526	
		t(28) = -6.174	t(28) = 8.885	
		p 0.001	p 0.001	
	MS3 (Midline frontal to occipital – $RS_{MS_c}$ )	m1 = 49.004	m1 = 75.972	None
		m2 = 75.972	m2 = 55.268	
		t(28) = -7.325	t(28) = 6.564	
		p 0.001	p 0.001	
MS4 (Midline occipital to frontal – Partially like $RS_{MS_d}$ )	m1 = 49.759	m1 = 68.227	None	
	m2 = 68.227	m2 = 50.273		
	t(28) = -6.818	t(28) = 5.113		
	p 0.001	p 0.001		
Right Wrist- Flexion/Extension	MS1 (Midline occipital to frontal – $RS_{MS_d}$ )	m1 = 59.668	m1 = 78.342	None
		m2 = 78.342	m2 = 63.468	
		t(28) = -9.204	t(28) = 6.533	
		p 0.001	p 0.001	
	MS2 (task-specific topography)	m1 = 55.490	m1 = 76.119	None
		m2 = 76.119	m2 = 58.399	
		t(28) = -5.810	t(28) = 6.771	
		p 0.001	p 0.001	
	MS3 (Left anterior to right posterior – $RS_{MS_b}$ )	m1 = 50.526	m1 = 68.841	None
		m2 = 68.841	m2 = 56.619	
		t(28) = -5.449	t(28) = 4.043	
		p 0.001	p 0.001	
MS4 (Left posterior to right anterior – $RS_{MS_d}$ )	m1 = 46.956	m1 = 66.411	None	
	m2 = 66.411	m2 = 40.972		
	t(28) = -6.311	t(28) = 7.729		
	p 0.001	p 0.001		
Right Tip-pinch	MS4 (Centro-parietal to temporal and frontal orientations)	None	m1 = 58.159	None
			m2 = 47.058	
			t(28) = 3.903	
			p0.001	

**Table 5.41** Statistically significant Duration values for Wrist flexion & extension and Tip-pinch

COVERAGE				
Motor Task	Microstates	Pre-event-Event	Event-Post-event	Pre-event-Post-event
Left Wrist- Flexion/Extension	MS1 (Left anterior to right posterior – $RS_{MS_b}$ )	m1 = 4.791	m1 = 7.294	m1 = 4.791
		m2 = 7.294	m2 = 5.719	m2 = 5.719
		t(28) = -7.997	t(28) = 3.926	t(28) = -2.618
		p 0.001	p 0.001	p = 0.014
	MS2 (task-specific topography)	m1 = 4.877	m1 = 6.454	None
		m2 = 6.454	m2 = 4.006	
		t(28) = -4.333	t(28) = 6.720	
		p 0.001	p 0.001	
	MS3 (Midline frontal to occipital – $RS_{MS_c}$ )	m1 = 4.069	m1 = 6.188	None
		m2 = 6.188	m2 = 4.140	
		t(28) = -5.807	t(28) = 6.198	
		p 0.001	p 0.001	
MS4 (Midline occipital to frontal – Partially like $RS_{MS_d}$ )	m1 = 3.626	m1 = 5.123	None	
	m2 = 5.123	m2 = 3.592		
	t(28) = -5.192	t(28) = 4.937		
	p 0.001	p 0.001		
Right Wrist- Flexion/Extension	MS1 (Midline occipital to frontal – $RS_{MS_d}$ )	m1 = 4.973	m1 = 7.321	None
		m2 = 7.321	m2 = 5.485	
		t(28) = -5.582	t(28) = 5.506	
		p 0.001	p 0.001	
	MS2 (task-specific topography)	m1 = 4.614	m1 = 6.060	None
		m2 = 6.060	m2 = 4.804	
		t(28) = -3.464	t(28) = 3.360	
		p = 0.002	p = 0.002	
	MS3 (Left anterior to right posterior – $RS_{MS_b}$ )	m1 = 3.840	None	m1 = 3.840
		m2 = 5.573		m2 = 4.689
		t(28) = -5.002		t(28) = -2.631
		p 0.001		p = 0.014
MS4 (Left posterior to right anterior – $RS_{MS_d}$ )	m1 = 3.427	m1 = 5.267	None	
	m2 = 5.267	m2 = 2.880		
	t(28) = -5.677	t(28) = 7.040		
	p 0.001	p 0.001		
Right Tip-Pinch	MS1 (Right posterior to left anterior – $RS_{MS_b}$ )	m1 = 4.923	None	None
		m2 = 5.697		
		t(28) = -2.877		
		p = 0.008		
	MS4 (task-specific topography)	None	m1 = 4.517	None
			m2 = 3.517	
		t(28) = 2.951		
		p = 0.006		

**Table 5.42** Statistically significant Coverage values for Wrist flexion & extension and Tip-pinch

Highest Microstate class	States	Left flexion	Right flexion	Left tip pinch	Right tip pinch
Occurrence	Pre-event	$MT_{MS2}$	$MT_{MS1}$	$MT_{MS2}$	$MT_{MS2}$
	Event	$MT_{MS1}$	$MT_{MS1}$	$MT_{MS1}$	$MT_{MS1}$
	Post-event	$MT_{MS1}$	$MT_{MS1}$	$MT_{MS1}$	$MT_{MS1}$
Duration	Pre-event	$MT_{MS2}$	$MT_{MS1}$	$MT_{MS2}$	$MT_{MS2}$
	Event	$MT_{MS1}$	$MT_{MS1}$	$MT_{MS2}$	$MT_{MS1}$
	Post-event	$MT_{MS1}$	$MT_{MS1}$	$MT_{MS1}$	$MT_{MS1}$
Coverage	Pre-event	$MT_{MS2}$	$MT_{MS1}$	$MT_{MS2}$	$MT_{MS1}$
	Event	$MT_{MS1}$	$MT_{MS1}$	$MT_{MS1}$	$MT_{MS1}$
	Post-event	$MT_{MS1}$	$MT_{MS1}$	$MT_{MS1}$	$MT_{MS1}$

**Table 5.43** Microstate classes with highest parameter values for all hand movements

## *Appendix A*

### **The role of individual physical body measurements and activity on spine kinematics during flexion, lateral bending and twist tasks in healthy young adults - Comparing marker(less) data**

#### **A.1 Background and Literature Survey**

Trunk Kinematics is crucial to study from a clinical standpoint as it plays a significant role in human activities. Effects of these simple exercises and motor tasks of our daily life causes motion at each of the different trunk segments [91]. Improper trunk activation sequencing may increase the risk of upper extremity joint injury, Parkinson's disease, spinal cord injury, and obesity. Its effect on reaching has also been studied in stroke patients [41]. Spinal column is a vital part of the human trunk and is considered the core section of the body. It is located beneath the Trapezius muscle and aids in bending, flexing, and providing support to the body. The spine's flexibility is attributed to the presence of elastic ligaments in the spinal column which comprises of five sections out of which Cervical, Thoracic and Lumbar are thoroughly investigated. For medical research, many in-vivo and in-vitro procedures have been utilized to explore and study the spinal segments. Both inter-vertebral and intersegmental motion in the spine is seen in general exercises/combined movements, which are motions that occur in tandem with the primary motions, such as flexion-extension, lateral bending, and side-twisting. The range of motion for each spinal segment depends upon the contribution of that segment during spinal motion.

The characterization of kinematics of spine motion includes each of the three segments [164], and with the use of exercises such as flexion, lateral bending, and axial rotations, one may acquire the greatest range of intersegmental motion, that provides us with the individual's degree of flexibility in relation to his or her physical characteristics like BMI, Waist to Hip Ratio and physical activity level. Most of the studies investigating the correlation between BMI and spinal column angles have used flexible curve/ruler [196] to measure these angles which is an unreliable technique [155]. Accordingly, re-investigation of BMI's relationship with spinal column angles is done using a more reliable marker-based method. Moreover, mixed results have been found for BMI and spine flexibility. [137] reported significant relationship between lumbosacral angles and BMI in non-obese Nigerian males while [216]

reported that BMI is not associated with lumbar lordosis in either men or women. Other physical parameters like WHR and physical activity level have not been studied sufficiently with respect to spinal column angles.

Coupled movements are important in detecting intersegmental motion because it might be affected by spinal problems [89]. To study coupled motion it should be quantified as angular displacements of spinal columns. The range of spinal motion or degrees of freedom can be estimated by finding the correlation between the physical parameters and the spine flexibility of an individual. The purpose of this research is to analyze spine kinematics during motion, with an emphasis on the evaluation of multi-segmental kinematic movements of the spine. Changes in the natural structure of a human spine are caused by ageing, injury, and lower back discomfort, all of which induce mobility restrictions. A change at any of the columns affects movement, though symptoms could vary, for example, lower back pain is attributed to stiffness in the lumbar section. Less spinal movements in lumbar and thoracic region were found in chronic low back pain patients performing sit to stand exercise [22]. Less lumbar spine movement was observed in participants with low back pain [64]. Weak correlations were found in upper/lower lumbar during lifting/sit-to-stand and strong correlations during walking and lifting [140]. In addition, flatter upper lumbar angle and greater frontal plane range of motion was found in dancers for the upper lumbar and lower thoracic segments, no lower back pain symptoms were found in any kind of kinematical motion [190]. Another study on the effect of age on thoracic segments of spine [70] found that simultaneous motion of regions and segments of spine in elderly subjects as compared to the young who flexed the lower spine and hips before thorax and distal thoracic segments before proximal. A 2012 meta-analysis of the range of studies and the methods applied for trunk motion analysis [131] showed that only a few studies investigated the whole trunk independently and none focused on spinal columns specifically with an emphasis on intersegmental motion involving the cervical, thoracic, and lumbar segments. Our study focuses on the research gaps highlighted in the aforementioned study.

3D models are required to determine the angular displacements of each section using 3D motion analysis. Estimation of intersegmental spinal motion used techniques such as Magnetic Resonance Imaging, CT scan, X-Ray [160] skin mounted systems. Vicon, Motion Capture systems, Kinect, BTS bioengineering, and optoelectronic systems are some of the systems utilized for motion analysis. A Novel Technique by [222] was developed to record 3D Intersegmental Angular Kinematics during dynamic spine movements and provided increased spatial resolution; it can be further used to detect intersegmental motion patterns, stiffness, and stability. In recent decades, researchers have used optoelectronic motion analysis to examine the neurophysiological and biomechanical underpinnings of human posture and movement in order to create a biomechanical spine model. Opti Track motion capture systems are widely used for biomechanical applications, human motion detection, animations and military purposes. We have used Opti Track motion capture systems to detect motion patterns for Lumbar, Cervical, and Thoracic segments of the Spine as it has emerged as a competitor of the gold standard Vicon [128]. Different optoelectronic technologies have commonly been used to monitor/record trunk kinematics in a variety of methods, with two to nine cameras being used in most cases. Methods to evaluate range of

motion include voluntary patient movements on being instructed by an evaluator (active mobilization) and an examiner moving the specific body parts of the participants to the maximal extent of the joint limit while the participant relaxes the joint that is being explored (passive mobilization). No differences were found between both the mobilization methods while estimating the Range of Motion [120]. Our study is based on the active mobilization approach through Opti Track.

Vertebral motions are widely assumed as a biomechanical factor causing spinal pathology. Cervical spine segments exhibit complex motions in flexion-extension, lateral bending, and axial rotations [191]. Most investigations of coupled motion in the cervical spine focus on intervertebral motion and are confined to MRI and CT imaging. [43] demonstrated that optical motion capture techniques for evaluating cervical range of motion have good repeatability and validity. As the thoracic spine, which serves as a transitional zone between the cervical and lumbar segments, has received less attention in 3D spine kinematics, its examination is essential to have a better understanding of how symptoms appear and the pathophysiology of spinal illnesses. The range of motion of the thoracic segment is less than the range of motion of other spine sections, according to [46]. Intervertebral motion during exercises such flexion-extension, left-right bending, and left-right twisting has been studied for the Lumbar segment [103]. Despite significant advances in our understanding of the individual segments of the human spine during dynamic motions, the intersegmental vertebral motion during dynamic human body activities remains unclear. Except for [221] who investigated the kinematics and muscular activity for the lumbar spine in stooping postures, rarely any research has evaluated realistic and more natural work situations with human volunteers to investigate their biomechanical responses. We are examining how the three spine segments compare in terms of the range of motion in a naturalistic environment using the above-mentioned active mobilization approach.

As motion capture has several limitations, including less mobility, higher costs, longer calibration time, and more setup space, automated marker-less pose estimation methods have been introduced that are less expensive and make experimental sessions faster and simpler. There are two types of markerless techniques: multicamera RGB-D (RGB camera with a depth sensor) and single-camera RGB. Single-camera Markerless approaches have mostly been developed for motion detection and classification. However, because marker-less approaches are not based on anatomical information, their applicability in clinical applications is questionable. We are not aware of any research that has tested and evaluated any 2D, model-based, marker-less technique for estimating spinal column angular displacements and ROM using an optoelectronic marker-based system as the benchmark. Consequently, this study presents a novel approach for spinal kinematics analysis similar to [19] who presented a similar approach for clinical gait analysis.

Real-time approach of multi-Person 3D motion capture using a single RGB camera [111] involves methods such as Resnet convolutional neural network, fully connected neural network and space-time skeletal model fitting. We are proposing RGB as a more cost-effective alternative for Opti track. RGB Camera is used in fundamental computer vision task which can help in motion detection of a human body. With the help of an RGB camera model we can develop a 3D pose estimation which is com-

parable to depth sensors cameras (RGB-D/kinect) but because accuracy of RGB-D is lower than Opti track [150], correction is required on RGB using Opti track. In domains such as Machine Learning and Computer Vision, the state-of-the art deterministic regression models are used for accuracy and precision-based key points detection, human pose reconstruction, [9] automatic estimation of 3D human pose from a single image, [85] model fitting and generating human mesh (Human skeleton). Based on training methodology and a simple network design human mesh reconstruction is done based on 2D key points (human body joints) of an image. Human mesh is used for RGB analysis to estimate range of motion for angular displacements of the three spinal segments as it allows for the rotational and translational motion under 3 degrees of freedom.

By comparing the RGB (product) and Opti-track (Groundtruth) to find out the difference in estimation of angular displacements (error %), we will build an information chart (application) that contains an individual's physical parameters such as height, weight, BMI, waist-to-hip ratio, and physical activity level against their flexibility angles extracted via both Opti-track motion capture and RGB data analysis methods. This chart will assist us in designing an RGB application with Opti track correction, which can be a low-cost alternative to the non-portable and costly Opti track system. Using an Opti-track Motion Capture system and an RGB camera, this study intends to determine the greatest range of spinal motion in a person completing these activities.

The knee is important for the balance and stability of the body's action. Individuals' activity levels have an impact on their load bearing joints, particularly their knees, which differ from other load bearing joints in that soft tissues are the primary stabilizing factors in them, as opposed to articular shape in other load bearing joints [37]. The knee is a vulnerable joint that bears a great deal of stress from everyday activities, such as lifting and kneeling, and from high-impact activities, such as jogging and aerobics [JohnHopkins]. Many knee problems are a result of the aging process and continual wear and stress on the knee joint (such as, arthritis).

The biomechanics of the knee joint are significant in examining daily activities involving the lower limbs as the movement of knee depends on kind of activity, the muscle firing pattern and passive anatomy of the knee joints. Similar to the movement of spine; knee movement also involves coupled motions. Most daily activities (eg, walking and stair climbing) require the synchronous contraction of multiple muscle groups. Only multiple-joint movement exercises such as squatting are able to effectively recruit the necessary muscle groups within a single maneuver [210]. The motion of the knee joint is quantified in terms of angular displacement. Chronic musculoskeletal ailments, diseases, and injuries (such as osteoarthritis, neurodegenerative diseases, ligament sprains, and so on) restrict people's mobility and physical activity. It is feasible to determine or, more specifically, predict locomotion ability in patients by examining and monitoring physical activities over a longer duration of time [162]. Many knee problems are a result of the aging process and continual wear and stress on the knee joint. From a clinical standpoint, measuring knee joint angle is a fundamental and crucial approach for both diagnosing knee deficits and tracking treatment progress. Kneeling and squatting are examples of common

actions that require deep knee flexion [38]. Deep squatting is utilized to gain a better knowledge of knee flexibility and estimate range of motion since it requires both movement and stability [75].

The vector analysis may be used to determine the degree of knee flexion (angle between vectors defined by the adequate location of markers) [162]. If reliable measurements of human knee motion could be acquired via marker-based systems, the scope and clinical relevance of in vitro measurement of human knee motion would be substantially improved. Although clinicians lack the ability to have a reliable and accurate means of quantifying the same types of altered mechanics that researchers use, recent developments in marker less motion capture technology may offer the possibility of such systems becoming available to clinicians in the near future. In the current study, the estimation of knee angular displacements and range of knee motion is done and compared using both marker-less and marker-based systems, as also reported by [169], [20] who calculated knee joint angles, referencing using the distal segment (hip and knee joint) to the proximal as a reference during the squat exercise. Furthermore, the correlation (if any) of angular displacements with physical parameters such as BMI, Waist to Hip Ratio, and physical activity level of individuals enables one to infer an individual's degree of knee flexibility in relation to his or her physical parameters.

## **A.2 Abstract**

Physical exercises and gross motor skills support the spine and the body's lower extremities. This study aimed to categorize the spine and the lumbopelvic-hip segments as a function of body-mass, waist-to-hip ratio and physical activity in healthy young adults while executing a flexion, lateral-bend, twist, and squat movements. The data was compiled from a marker-based optoelectronic motion capture system and a marker-less motion capture system using a RGB camera. Comparing the two techniques on the same data set allows for developing inexpensive diagnostic solutions supported by robust models. A total of Sixty-two subjects (Forty male subjects, mean age =  $21.7 \pm 2.97$  years and twenty-two female subjects, mean age =  $22.5 \pm 3.36$  years) provided the data. The angular displacement of the spine and knee/hip was extracted using vector analysis. There were no significant correlations between BMI and WHR with angular displacements values for all spinal exercises. The physical activity level of male participants is significantly correlated with angular displacements for the spine flexion and spine lateral-bend, and weakly correlated for spine twist exercises. In comparison, physical activity level shows a significant correlation for only the spine flexion in female participants. BMI is negatively correlated in male participants for the squat movement, while WHR and physical activity show positive associations. In the female cohort, a negative correlation with BMI, WHR, and physical activity level is observed for the squat movement. The findings emphasize the critical role of physical activity on musculoskeletal flexibility and role of BMI/WHR load for specific motor movements. The angles estimated from both techniques are comparable. The analysis by considering the kinematics of the whole spine and lumbopelvic-hip segment with physiology and physical activity may benefit sports studies and clinical diagnosis of spine biomechanics.

**Keywords:** spine kinematics, knee/hip joint kinematics, marker-based motion capture, marker-less motion capture, Opti-track motion capture system, markerless motion capture using a single RGB camera, physical parameters and spine kinematics, physical parameters and knee/hip joint kinematics, BMI and spine kinematics, physical activity level and spine kinematics, waist-to-hip ratio and spine kinematics, waist-to-hip ration and knee/hip joint kinematics, BMI and knee/hip joint kinematics, physical activity level and knee/hip joint kinematics.

### A.3 Introduction

The spinal column is a vital part of the human trunk and the core section of the body. It is located beneath the Trapezius muscle and enables bending, flexing, and giving the body structure and support. The spine's flexibility is attributed to elastic ligaments in the spinal column, which comprises five sections of which cervical, thoracic, and lumbar are well investigated. Spine biomechanics (kinetics & kinematics) is crucial to study as it plays a significant role in human activities from gross motor tasks in daily life – bending, moving, sitting, etc.- to complex movements accomplished in sports, gymnastics, yoga, or dance. A 2016 meta-analysis of spine biomechanics studies [131] showed limited studies on the whole trunk focused on inter-intra segmental motion of the cervical, thoracic, and lumbar segments. Understanding the movements as supported by different trunk segments [91], the range of motion (RoM), the coordination between the lumbar-pelvic system, the inter-vertebral and intersegmental movement in the spine are essential for clinical diagnosis [156], test with Aspen collar: [41], lower back pain meta-analysis : [87], [6], [170], Lateral bending : [53]. The kinematics of the lumbar [213], for stooping: [221], thoracic & lumbar [70], cervical [8], [3]; rotation/lateral bend: [72], [71] has been investigated extensively. Understanding spine dynamics is also crucial for medical conditions affecting motor movements, like hemiplegia caused by a stroke, Parkinson's, lower back pain, spine injury, osteoporosis [162], and obesity [135].

In addition to the spine, the hip and knee RoM is essential for body-balance and load-bearing. The knee joint bears a lot of stress from daily activities like lifting, kneeling to high-impact sports, jogging, and aerobics. A multi-joint movement supported workout is squat, which activates the appropriate muscle groups with a single manoeuvre [81], [210], [48]. This technique applies strain on the knee bones, the hip joints and ankles, with improper methods leading to lower back pain [44], [107]. But the body-mass squat exercise also strengthens the muscles after injuries [185], helps diagnosis of age-related degradation of the pelvic and knee boness (example: osteoporosis) or in measuring muscle strength, especially the quadriceps femoris [47] in sports training. Hence, the displacement of the hip segment to identify the role of the lumbo-pelvic-hip-knee system needs to be studied. We used the unrestrained squat as pelvic constraint was shown not to affect the specific lumbar intersegmental level or the whole lumbar spine [90]. Secondly, we aimed for a model that can be used in clinics that do not have access to apparatus or systems to enable restricted movement (for example, hip constraints). Our study's findings can be applied to understand the whole spine displacement in standard flexion, lateral bend,

twist, and squat (pelvic-hip-knee system) modelled with anthropometric indices and physical activity levels. For spine biomechanics, we recorded healthy young adults engaged in four exercises (flexion- in the Frontal axis/ sagittal plane; lateral bending- in the frontal plane about the sagittal axis; twist - in the horizontal plane about a vertical axis and unilateral body-mass load squat in the frontal – horizontal axis) by a motion capture technique and also with a RGB camera. The angular displacement is correlated to individual physiology - BMI, Waist to Hip Ratio (WHR) and self-reported physical activity level (sports, yoga, dance, jogging etc.). For extraction of the angular displacement data, we reviewed the methods proposed in literature and the limitations of each. The spine is a deformable structure with motion dependent on its adjacent segments [174]. Hence, incorrect skin marker placement on the spine impacts its curve measurement and kinematic variability [173]. Minute errors in marker misplacements are usually smoothed out using polynomial fit, which quantifies the quality of spine movement and ensures continuity in the arrangement of the spinal column. The internal spinal alignment was predicted using a cubic polynomial [222], fourth order polynomial [168], fifth order polynomial [154] , [173], and 6th order polynomial [197]. The studies mentioned estimated the shape of the spinal curve using polynomial fit have investigated the changes in the spinal curve due to lower back discomfort [197] and spinal deformity [174] , [70] used cubic polynomial to approximate the s-shaped spinal curve for investigating age-related changes, while [222] applied a similar fit to compare the accuracy of marker-based Opti-track motion capture system and the traditional electromagnetic system. Our study investigated spine biomechanics of 62 young and healthy participants with no reported spinal injury or lower back pain issues and no identified clinical spine deformity. Our participants were healthy (no lower back pain or spinal injuries) and young, hence considering the findings of [222], [101], we assumed an s-shaped spinal curvature. We applied vector analysis to determine the degree of angular displacement, which is the angle between vectors defined by the adequate location of markers [162]. This analysis method can be applied to marker and marker-less systems, as reported by other studies [169], [20].

## **A.4 Measurement Techniques**

[222] devised a method for recording 3D Intersegmental Angular Kinematics during dynamic spine movements with a higher spatial resolution to detect intersegmental motion patterns, stiffness, and stability. They compared it to the electromagnetic method and found that both techniques agree reasonably. Motion capture systems (Opti Track motion capture systems & Vicon) [128] are widely used for biomechanical applications, human motion detection, animations and military purposes and are considered the gold standard. The technique has various limitations, such as less mobility, expensive, high calibration time, space requirement, in addition to trained personnel. [43] demonstrated that optical motion capture techniques for evaluating the cervical range of motion have good repeatability and validity. A 3D pose estimation was presented with depth sensors cameras (RGB-D/kinect) and shown to have comparable accuracy [150]. Automated marker-less pose estimation systems [121] used 3D articulated models in multiple 2D image planes [85] and used human mesh recovery techniques for pose estimation. The

real-time analysis of multi-person 3D motion capture using a single RGB camera [111] involves methods such as *SelecSLS Net* convolutional neural network, fully connected neural network and space-time skeletal model fitting. The state-of-the-art deterministic regression models have resulted in an increase in accuracy and precision-based key points detection, human pose reconstruction [9], automatic estimation of 3D human pose from a single image, [85] model fitting and generating human mesh. Human mesh reconstruction is applied on an image's 2D key points (human body joints) based on training methodology and a simple network design. The mesh is used for RGB analysis to estimate RoM for angular displacements of the three spinal segments. It allows for the rotational and translational motion under 3 Degree of Freedom. [24] developed a system combining marker-less pose estimation with sensors-based motion tracking for the rehabilitation of patients. In our study, a RGB camera capture was analyzed by extraction of 2D poses (key-points) for all frames using the openpose model [17], followed by generation of the 3D skeleton using these 2D poses in the ProHMR model [85].

## **A.5 Scope of the work**

The main focus of our research is the study of spine kinematics from the angular displacement of the three spine segments and the lumbo-pelvic-hip segments in flexion, lateral-bend, twist and squat exercise executed by normal healthy young adults. To generate a reference chart/model, the angular displacement is correlated to an individual's physical parameters such as height, weight, BMI, waist-to-hip ratio, and physical activity level. Our study followed the standard marker set proposed by [107] and other studies from the Institute of Biomechanics ETH Zurich. Comparing the data collected from the same group of participants from two techniques (RGB & marker-based motion capture) would help in better accuracy estimates, error corrections if required, and, significantly, for clinical/human movement science applications with the reference models thus generated. Importantly, the comparison of RGB with motion capture allows for applications of an inexpensive marker-less system for use in clinics backed by robust models.

## **A.6 Marker-based motion capture system using Opti-track cameras**

A three-dimensional marker-based motion capture setup of 6 Opti-track Prime-13w motion tracking cameras capable of capturing 240fps (positional errors less than  $\pm 0.30$ mm; rotational errors less than 0.5 degrees) which can detect active and passive markers was used to capture tracking video. The system uses infra-red reflectors as markers. The Motive Opti-track software controls the motion capture cameras to capture 6 Degree of Freedom (3D position and orientation) data.

## **A.6.1 Methodology**

### **A.6.1.1 Participants**

Ethics approval was provided by the Human Study Ethics Committee of the institute. After providing detailed information about the study, informed consent was obtained from each subject. The participants were further informed that they could exit the study at any time in the event of any discomfort. Forty male subjects (age = 19-33 years; mean = 21.7 years; SD = 2.97 years) and Twenty-Two female subjects (age = 19-30 years; mean = 22.5 years; SD = 3.36 years) volunteered for this study. None of the participants reported being under any medication, especially for pain at the time of the experiment. The participants also had no record of any spine/back injuries in the past.

### **A.6.1.2 Experimental Paradigm**

The tracking video was captured in a room (20x10 ft). The marker set had 12 infrared reflectors arranged along the spinal column's length. The positioning of the markers is as follows: three on the cervical, five on the thoracic, and four on the lumbar region Figure A.1. Additionally, two reflectors each on the knees (one each on the patella and lateral knee), one on each ankle (Fibula), one each on the palm, two on shoulders (approximately the trapezius muscle), just above the hips and in line with the last lumbar segment reflector, two on the upper chest as suggested by [107]. Data collection was preceded by calibration to identify the capture volume by the wand process, to reduce occlusion, setting up of the ground plane and origin as required for the coordinate system in Motive (Optitrack's software). Participants were positioned at a marked spot on the floor with maximum capture volume as determined from the calibration stage. They were asked to wear a skin-tight non-reflective bodysuit to minimize the error margin in motion capture data. The instruction was to perform slow and gradual movements for each exercise to maximize sensor tracking and minimize detection error. Participants performed spine flexion Figure A.1A, lateral bending, twist and the unrestricted unilateral squat exercises and for ecological relevance, no hip constraint was used Figure A.1C. Three self-paced trials of each exercise were executed preceded by a warm-up time. BMI and Waist-Hip Ratio (WHR) was measured and self-report on the Physical Activity Level – for sports, yoga, jogging, dance etc., – was also collected.

### **A.6.1.3 Data Analysis**

The pre-processing steps for the motion capture include the 2D Object Filtering on the frame of the image captured by all six cameras to filter marker noise, removing frames with sudden non-task movements, and identification and labeling of markers. Small gaps in the marker trajectories were filled using the interpolation method. Default setting (Filter Type: Size & Roundness; Min threshold pixels: 4; Max threshold pixels: 2000; circularity: 0.60) was used for 2D object filtering.

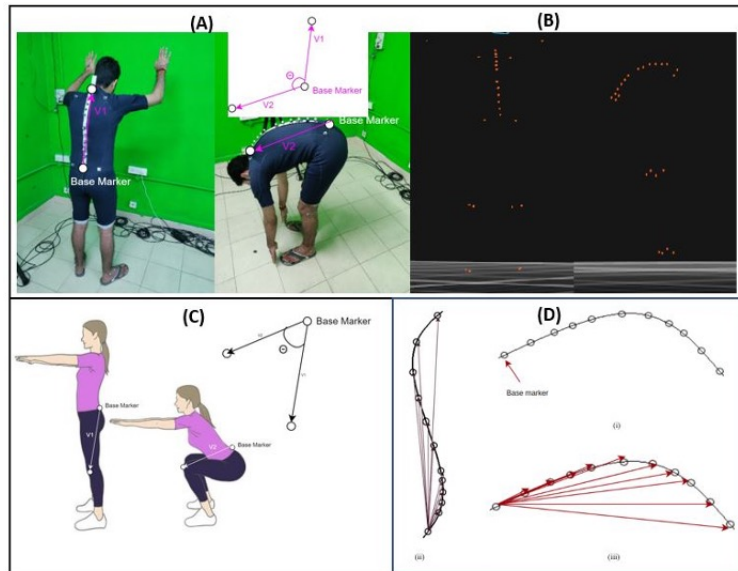


**Figure A.1** (A) Marker placement covering the spine column. A Velcro strip with retro-reflectors affixed was prepared for ease of fixing on the suit. The vectors from the selected base marker are shown in the inset and the estimated angle " $\theta$ " between both positions. (B) The point light capture of the initial position and the flexion exercise. (C) the cartoon representation of the squat exercise and the vector from the spine column to the reflector on the patella of the knee. (D) Approximation of S-shaped spine curvature using vector analysis. Subset images: (i) Last sensor on the lower back as reference (Base) marker (ii) Vectors formed by connecting all the markers with the base marker for the first frame (upright position) (iii) All vectors in the maximum angular displacement frame relative to the first frame in spine flexion exercise (bent position).

#### A.6.1.3.1 Spine Motion Analysis

A vector is drawn to all the marker positions at each time frame for the spine movement analysis, approximating the S-shaped spine curvature. This was done by estimating the three-dimensional cervical, thoracic and lumbar spine angles using the Cardan angles between the current vector (vector formed by connecting all the markers with the base marker at each frame of spinal motion as shown in the Figure A.1D and the base vector (vector which was calculated when the task started as shown in the Figure A.1A in local coordinate system (LCS). The 12th marker of the spine (indicated in Figure A.1A & Figure A.1D) was selected as the reference marker as it shows the least angular and translational displacement while performing the flexion, lateral bend and squat exercises. And the world origin (global coordinate system) was used as the reference point for axial spine rotation. Additionally, having a single reference is advantageous when running a correlational analysis. An exercise starts when the marker's displacement (velocity) changes from zero to positive at each segment with respect to the reference marker in the direction required by the particular spine movement. Subsequently, the end was determined when the marker reached 'zero' displacement, corresponding to the spine's initial vertical position. For example, the base vector V1 at the starting of the exercise and the vector V2 at the ex-

treme bend position i.e., at the ending of the exercise and, the angle " $\theta$ " subtended by those two vectors (shown in Figure A.1A). The time course of angular displacements in the cervical, thoracic, and lumbar regions as distinct segments was determined using the Cardan angles between each frame's base and current vector. For each trial, the maximum angular displacement of each segmental region was extracted for further analysis. Before applying statistical analysis methods, the peak angle values were averaged from the three trials of each participant and spine segment. A representation of the temporal sequence of angles/movements (RoM) for each trial is provided in Figure A.2 for a single participant.

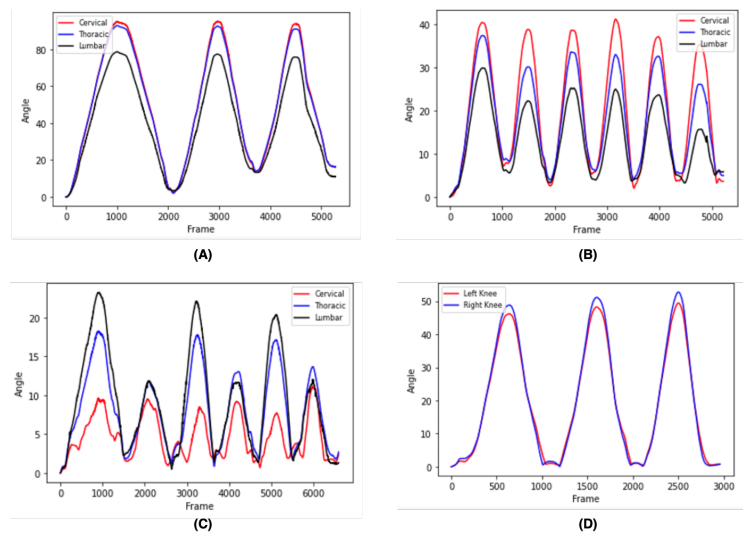


**Figure A.2** Sample of the temporal sequence of the spine movement of a participant for 3 trials with respect to each frame for marker-based motion capture system. (A) Spine Flexion (B) Spine Lateral Bend - left and right- three trails each (C) Spine Side Twist-clock and anticlock wise -three trails each (D) Squat exercise

### A.6.1.3.2 Knee/Hip Motion Analysis

A vector is drawn from the spine base marker to the knee markers for approximating the relative positioning and direction of the knee/hip-joint movement using the estimation of hip segment angle between the current and base vector. The base vector  $V_1$  at the starting of the exercise and the vector  $V_2$  at the final squat position i.e., at the ending of the exercise and, the angle " $\theta$ " subtended by the two vectors is extracted Figure A.1C. The maximum bend displacements of the left and right hip-knee segments from the initial position were noted. Before applying statistical methods, the peak angle values were averaged for three trials and each knee separately. A representation of the angles/movements for each trial is shown in Figure A.2D for a single participant. In addition, squat depth is calculated by estimating the 12th/reference marker's displacement on the spine in the axial plane.

### **A.6.1.3.3 Statistical Analysis**

Shapiro-Wilk test was applied to check the normal distribution of BMI score, WHR, physical activity level, cervical, thoracic, and lumbar angles. The non-parametric Mann-Whitney U test was used to test the group-wise (BMI, WHR, Physical activity) difference. The Spearman's rank correlation analysis examined the relationships between BMI, WHR and physical activity level to angular displacements. Seed-based correlation was used to test if subjects with normal and high BMI, WHR, and level of physical activity form a cluster. The statistical significance level for all tests was set at  $p < 0.05$ .

## **A.6.2 Results**

We first present the movements of spine segments followed by statistical analysis with respect to BMI, WHR, & Physical Activity level separately for male and female groups. The groups were further divided as normal (Males: 20 participants; Female: 15) and overweight (Male: 20 participants; female: 7) as per BMI standards ( $< 24.9$  is normal and  $> 25$  is overweight). Similarly, subjects were categorized into normal and high WHR groups based on established WHO waist-to-hip standards for males (0.90 is normal, number = 15 and  $> 0.90$  is high, number = 25) and females (0.85 is normal, number = 15 and  $> 0.85$  is high, number = 7).

### **A.6.2.1 Descriptive Statistics**

For male participants, Shapiro-Wilk test for spinal column angle data for right side-twist cervical region ( $p = 0.005$ ), left side-twist lumbar region ( $p = 0.021$ ), BMI ( $p < 0.01$ ) and physical activity level ( $p < 0.01$ ) was significant. While for female participants the spinal column angle for spine flexion cervical region ( $p = 0.027$ ), BMI ( $p < 0.01$ ) and physical activity level ( $p < 0.01$ ) was significant, indicating non-parametricity of the data.

#### **A.6.2.1.1 Spine Flexion, lateral Bend and Twist Analysis**

As expected physiologically for the flexion and lateral bend exercises, the cervical segment (neck) displacement is higher than the other two segments Figure A.3 and the scatter plot of the distribution across all participants is presented in the Figure A.7. The mean values and standard deviations for angles of the flexion exercise were comparable for both genders but with a wide distribution of angular displacement (minimum 50 deg and max 90deg). For lateral bend, the dominant side (right, as the majority were right-handed) is evident for both genders Figure A.3c, Figure A.3d. As also observed for flexion exercise, the distribution around the mean is high (stdev  $\pm 9$ ). The distribution of angular displacements of left and right side axial twist Figure A.3e is similar for male participants. In contrast, the distribution of angular displacements of thoracic and lumbar segments for the right-side twist had marginally less dispersion than the left-side twist for female participants Figure A.3f.

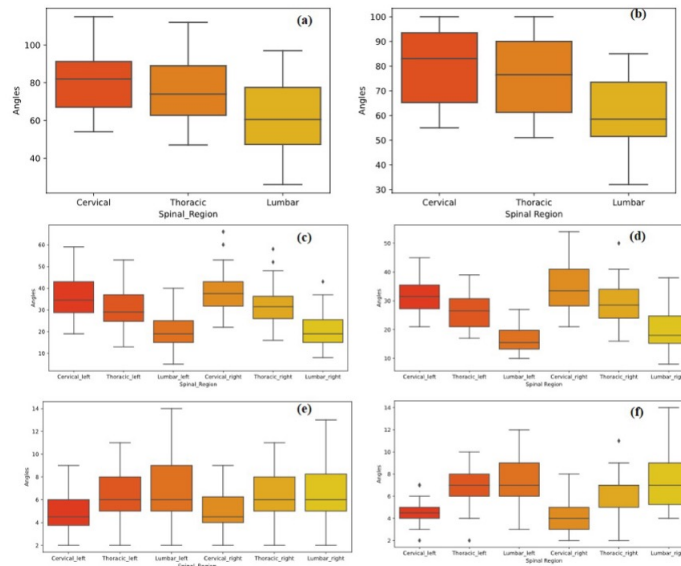


**Figure A.3** The angle estimates for the three spine segments and exercises. Flexion: (a) Male participants, (b) Female participants. Lateral Bend: (c) Male Participants, (d) Female participants. Twist: (e) Male participants, (f) Female participants

### A.6.2.1.2 Hip-knee segment displacement in a squat

The squat had approximately similar angular displacement distribution for all the participants. Female participants show significantly higher angles than the male participants Figure A.4. The squat depth as measured by the reference (12th) marker in male participants was in a range (14.07 - 66.31 cms; average: 32.75 cms), while for female participants, the range was between (15.08 - 65.31 cms; average = 38.5 cms).

### A.6.2.2 Inferential Statistics

#### A.6.2.2.1 Comparative analysis of Angular Displacement in Spine Flexion

In male individuals, cervical angular displacement is similar for both normal (median=83) and overweight (median=82) BMI; however, there are differences in the thoracic and lumbar angular displacement Figure A.8A. For all spinal columns, even though angular displacement of the normal BMI group had more dispersion than those in the overweight category Figure A.8A, the Mann-Whitney test did not show any significant difference. For females, 31.8% had a high BMI; the medians of the high BMI group were higher than the normal group for all three regions Figure A.9A, indicating that the overweight BMI group had more angular displacement. For all three segments, the angular displacement of the high BMI group had more dispersion than the normal group; however, the Mann-Whitney test did not show any significant difference. High WHR was found in 62.5% of males. The medians of both the groups for the cervical and lumbar regions were comparable Figure A.8B, while there were differences in the thoracic

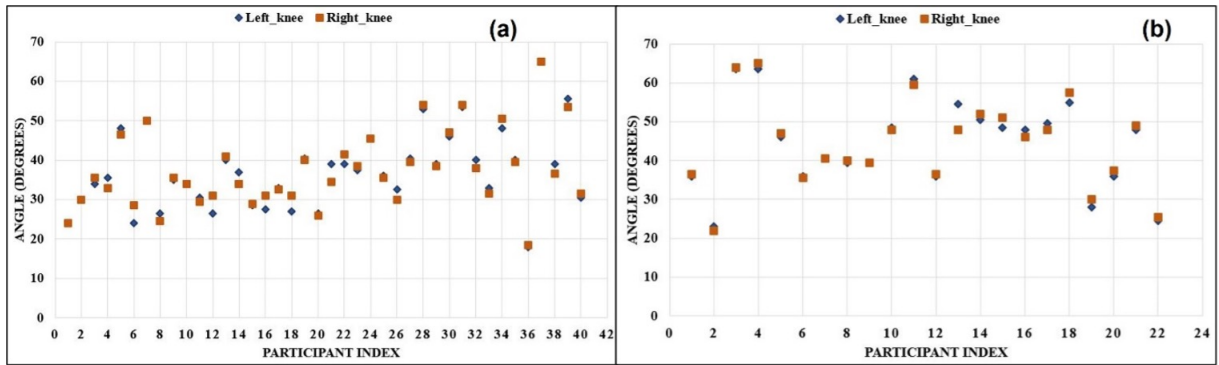


**Figure A.4** The hip-knee segment angle for (a) male and (b) females.

region. Although the Mann-Whitney test did not show any significant difference, the angular displacement of the high WHR group had more dispersion than the normal WHR group. In females, the normal WHR group exhibited significantly higher displacement (median) in all three spinal columns than the high WHR group Figure A.9B. Still, the Mann-Whitney test did not show any significant difference.

#### **A.6.2.2.2 Comparative analysis of Angular Displacement in Spine Lateral Bend**

In male participants, the normal BMI group had larger angular displacement in cervical and thoracic regions in the left lateral-bend Figure A.10A. By contrast, the overweight group's median angular displacement was higher in the right lateral-bend. The overweight BMI group had more dispersion of angular displacement of all three segments for both sides than the normal BMI group; however, the Mann-Whitney test did not show any significant difference. For females, even though the dispersion of angular displacements for both normal and overweight BMI groups were nearly comparable Figure A.11A, the Mann-Whitney test shows significant difference for cervical right lateral-bend (U-value=24, p-value=0.048, n1=15, n2=7, z-score=-1.973, effect-size: -0.543, two-tailed) and lumbar right lateral-bend (U-value=19, p-value=0.0198, n1=15, n2=7, z-score=-2.326, effect-size: -0.638, two-tailed) while thoracic right-lateral bend (U-value=25, p-value=0.057, n1=15, n2=7, z-score=-1.903, effect-size: -0.524, two-tailed) was nearly significant. In male participants, the high WHR group had higher angular displacement for both left and right lateral-bends than the normal WHR group Figure A.10B. The angular displacement of all three segments in the normal WHR group for the left lateral bend had more dispersion than the high WHR group, while the right lateral bend had more dispersion in the high WHR group. Even though the lateral bend showed mixed results in terms of dispersion, the Mann-Whitney test did not show any significant difference. For the female cohort, the normal WHR group had greater angular displacement (median) in all three spinal columns Figure A.11B. The angular displacement of all three segments in the normal WHR group for the left lateral bend had more dispersion, while the right lateral bend had mixed results; however, the Mann-Whitney test did not show any significant difference.

### **A.6.2.2.3 Comparative analysis of Angular Displacement in Spine Side twist**

For both BMI groups in the male cohort, relatively equal angular displacement (median) was observed in all three segments Figure A.12A. The dispersion of angular displacement for both groups was comparable in the cervical region, while the overweight group BMI had more dispersion in the thoracic and lumbar region; however, the Mann-Whitney test did not show any significant difference. In females, approximately equal angular displacement (median) was found for all three segments Figure A.13A. The dispersion of angular displacement for both normal and overweight BMI groups was comparable in the cervical region, whereas the overweight BMI group had more dispersion in the thoracic and lumbar region; however, the non-parametric difference test did not show any significant difference. In the male participants, for the WHR grouping, the angular displacement (median) and dispersion of angular displacement were roughly comparable across all three segments Figure A.12B. For females, the dispersion of angular displacement for both the groups was comparable in the cervical region, whereas the normal WHR group had more dispersion in the thoracic and lumbar region Figure A.13B; however, the Mann-Whitney test did not show any significant difference.

### **A.6.2.2.4 Comparative analysis of Angular Displacement in Squats**

Although the male group in the normal BMI group had more angular displacement (median) and dispersion than the overweight group Figure A.14A and an inverse trend was observed for females Figure A.15A, the Mann-Whitney test did not show any significant difference. For male participants, the high WHR group had more angular displacement (median) than the normal WHR group Figure A.14B, while for females, angular displacement for both WHR groups was comparable Figure A.15B. For both males and females, the normal WHR group had more dispersion of angular displacement than the high WHR group for both the limbs. Though the differences were not significant.

### **A.6.2.2.5 Spearman Correlation of BMI, WHR and physical activity level with angular displacements of spinal columns**

In male participants, physical activity levels were negatively correlated with BMI ( $\rho = -0.18$ ) and WHR ( $\rho = -0.119$ ) values Figure A.17, while for female participants, it was negative for WHR ( $\rho = -0.114$ ) but positive for BMI ( $\rho = 0.29$ ) Figure A.19. BMI and WHR show no correlation with the angular displacement for all the segments in all spinal exercises Figure A.17, Figure A.18, Figure A.19, Figure A.20. BMI was significantly negatively correlated ( $-.352^*$ ) with hip-knee angular displacements for the squat exercise, while WHR showed weak positive correlations (not significant) and physical activity level was positively correlated for male participants Figure A.18. The analysis grouped by gender, BMI, WHR and physical activity level in the female cohort were negatively associated with hip-knee angular displacement Figure A.20, but were not statistically significant. The physical activity level of female participants was significant with only the spine flexion values Table A.1, while for male participants it was positively correlated for flexion and lateral Bend and weakly correlated for spine side-twist Table A.2.

Spinal Column	Flexion	Lateral-bend (L)	Lateral-bend (R)	Sidetwist (L)	Sidetwist (R)
<b>Cervical</b>	.874***	0.229	0.213	0.196	0.317
<b>Thoracic</b>	.879***	0.268	0.197	0.164	0.277
<b>Lumbar</b>	.852***	0.217	0.147	0.037	0.211

**Table A.1** Spearman coefficient (rho) of spine angular displacement with physical activity level for female cohort. The \* indicate the statistically significant associations.

Spinal Column	Flexion	Lateral-bend (L)	Lateral-bend (R)	Sidetwist (L)	Sidetwist (R)
<b>Cervical</b>	.645***	.372*	.488**	-0.064	-0.002
<b>Thoracic</b>	.643***	.324*	.443**	.329*	0.249
<b>Lumbar</b>	.62***	.325*	.411**	.363*	0.288

**Table A.2** Spearman coefficient (rho) of spine angular displacement with physical activity level for the male cohort. The \* indicate the statistically significant associations.

#### A.6.2.2.6 Seed-based correlation analysis of participants

We considered a male participant who was a trained dancer and a female participant who does yoga daily, with great flexibility and good angular displacements of the spinal columns, as references for male and female groups. The Spearman seed-based correlation matrix for all exercises and both genders resulted in a single cluster; that is, the correlational value  $\rho$  was greater than 0.90, signifying minimal variation in participants of both genders as a function of flexibility due to specific motor skills.

## A.7 Marker-less motion capture system using a single RGB camera

### A.7.1 Methodology

#### A.7.1.1 Experimental paradigm

The recording with an RGB camera was captured from the 62 participants wearing track pants and a T-shirt in the mocap studio. The camera angles were adjusted to position the spine in the field view, as shown in Figure A.5. The subjects performed the same exercises for marker-less as were executed for the marker-based motion capture paradigm. Prior to the experiment, participants did warm-up followed by three trials for each exercise.

#### A.7.1.2 Data Extraction

The initial (first frame when the task began) and maximum displacement frames (frames when the participant's spine or knee had the most angular displacement relative to the first frame) for all trials of an exercise for each participant were obtained from the recorded data. Extraction of 2D poses (key-points) for all frames was done using the Open Pose model [17], followed by generation of the 3D

skeleton using these 2D poses in the ProHMR model [85]. By visualizing one of the 3D skeletons with the blender tool (open-source 3D visualization tool) and extracting all the spine and knee coordinates for all 3D skeletons using these indices, twenty-five spine (8 cervical, 14 thoracic, and 5 lumbar) and four knees (2 for each) coordinate indices were identified.

### A.7.1.3 Data Analysis

Using the method applied for marker-based motion capture, the angular displacement for the three spinal columns and hip/knee segments was extracted.

## A.7.2 Results

The 3D skeleton for one participant from the ProHMR model is shown in Figure A.5.

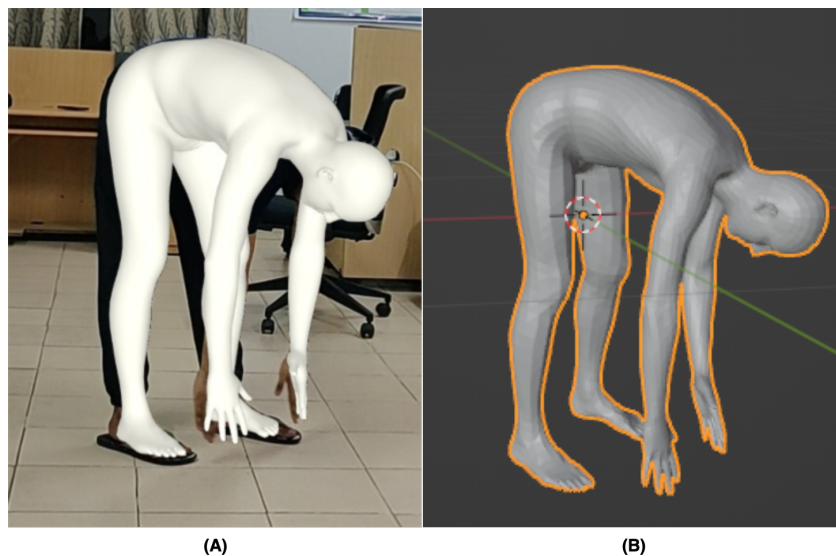


**Figure A.5** Generated 3D Human skeleton for a single participant in spine flexion exercise. (A) Fitted 3D pose from 2D key-points. (B) Consolidated 3D pose visualized in blender tool.

### A.7.2.1 Comparative analysis - marker-less & marker-based data

Spearman's correlation analysis revealed significant and positive correlations between marker-based and marker-less RGB systems angles in spine flexion and squat exercise for both genders Table A.3. Strong positive correlations for spine lateral-bend were discovered in female participants, while weak mixed correlations were found in male participants though the maximum difference was 5.825 degrees. The knee/hip angular displacement Figure A.16 was comparable to the marker-based analysis. Compared to marker-based motion capture, the cervical segment shows the consistent higher angular displacement for the spine flexion Figure A.6 and spine lateral bend exercises.

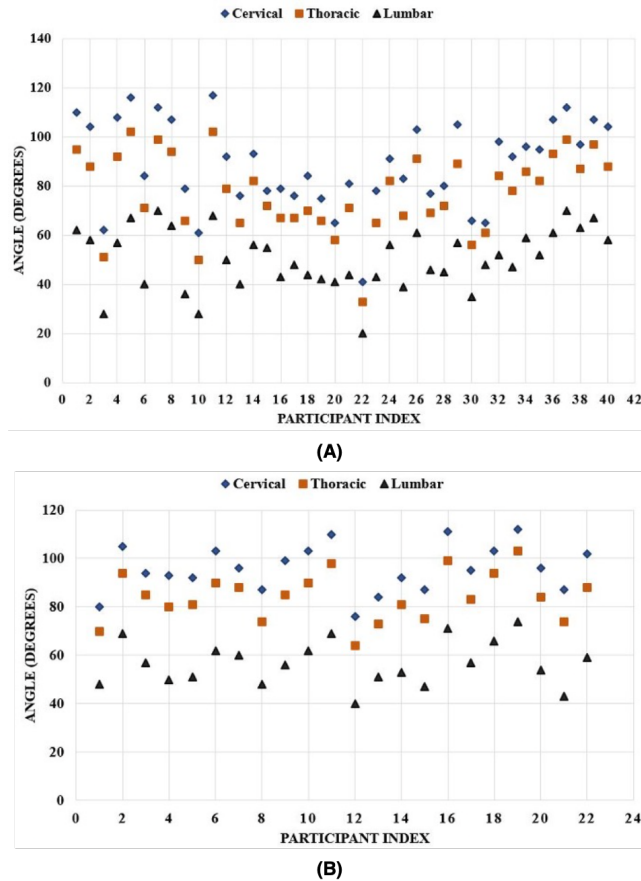


**Figure A.6** Participant wise distribution of spinal column angles extracted from the RGB camera video for spine flexion exercise in (A) Males (B) Females.

## A.8 Discussion

**Spine Kinematics:** Spinal joint centres are challenging to identify using skin-mounted sensors techniques like motion capture due to inherent errors in the identification of the bone landmarks, relatively low intervertebral ranges of motion, and difficulty in comparing to ground truth values from radiographs. The shortcomings have been addressed by a subject-specific spinal alignment of the markers and comparing it to radiographs [167], [173]. But the advantage of techniques that allow for functional imaging like motion capture is the ability to estimate the contributions of the spine columns from the kinematics models of physical activity requiring the engagement of specific segments. Understanding the RoM of each segment is critical for diagnoses of spinal conditions, which requires a detailed understanding of normal vertebral kinematics, which we have attempted by this study.

While there are studies investigating the whole trunk, very few have focused on all the three spinal columns and the intersegmental movement between the cervical, thoracic, and lumbar segments. For example, a local Coordinate System method was applied to extract the relative orientations, say pelvic

Parameter	Spearman $\rho$ value for male participants	Spearman $\rho$ value for female participants
Flexion Cervical	.547***	.634**
Flexion Thoracic	.607***	.624**
Flexion Lumbar	.692***	.583**
Lateral-bend Cervical Left	0.076	.45*
Lateral-bend Cervical Right	0.059	.646**
Lateral-bend Thoracic Left	-0.019	0.398
Lateral-bend Thoracic Right	-0.054	.572**
Lateral-bend Lumbar Left	-0.029	0.335
Lateral-bend Lumbar Right	-0.07	.438*
Squats Left Knee	.409**	.455*
Squats Right Knee	.442**	.513*

**Table A.3** Spearman coefficient (rho) between marker-based and marker-less RGB systems angles for male and female participants. The number of \* indicates statistical significance level ( $p > 0.05$ ).

& thoracic, to generate the kinematics of the lumbar spine [165]. A study [222] closest to the approach considered in this study, used a different reference marker for the thoracic and lumbar spinal columns to measure the angular displacement for each segment individually and compared them using intersegmental and electromagnetic approaches. In contrast, by estimating the angular displacement using a single reference marker and extracting displacement of all points on the spine in our study, we first attempt to address the possible errors due to incorrect identification of the segments and evaluate the role of multi-segments in a full range flexion, bend, twist, and squat movement. This method is particularly relevant when studying the variance due to thoracic kyphosis and lumbar lordosis curves, where identification of the segment demarcation is a challenge. Secondly, by considering a single reference node, we build a model independent of the technique for data collection. A single reference point/base marker is optimal to compare the data collected from a marker-less single RGB camera technique as a skeletal frame extracted from the camera feed represents the spinal column with 27 nodes – at a position approximately from C1 to lumbar/sacrum. In the case of tiny inaccuracy in the estimated 3D human mesh, the error will be higher if three reference frames (for each spinal segment) are considered due to imprecisions in the spine’s S-shape estimate. Thirdly, by using the same reference for unrestricted parallel squat in estimating the hip angle, the contribution of spine movement on the hip/thigh muscles can be inferred.

The three exercises (flexion in the sagittal plane, lateral-bend in the frontal plane and twist in the transverse plane) were executed by engaging all the three segments [164] with maximum range of intersegmental motion. The angular displacement of the lumbar spine for flexion, twist and the lateral-bend [93] was within the reported range [192], [93], [222], review article: [212], but show a substantial inter-subject variability (for flexion in males the range was 50-110 degrees for the thoracic) even in healthy subjects recruited for the study. The angular displacement distribution show more dispersion in female participants than male participants. Previous studies have also reported gender-related differences [MRI method: [122], motion capture method: [70]. However, the range was similar, which could also be due to the sample size (fewer female participants). An additional factor for gender data variability could be the motion capture suit fitted to the body form and skin stretching [118]. In the lateral bending exercise, angles were higher in the right-bend, a dominant side effect as nearly all participants were right-handed.

This finding adds to the discussions on the dominant side effect on the lumbar spinal muscles supporting lateral bend [189].

Comparative analyses based on grouping as a function of BMI or WHR as between-subject parameters for males and females yielded mixed results. For normal and overweight BMI female groups, significant differences were observed only in cervical and lumbar right lateral bends, while male participants had no significant differences. There was also no significant difference when grouped on WHR. In the participants considered for this study, we observed that a significant number of participants with normal BMI also had high WHR, and hence further inferences on the effect of each from the results by this classification require unique groups (high BMI & High WHR/ Normal BMI & Normal WHR). Further investigation with exclusive categorization is important to isolate the role of each factor (WHR or BMI or both) on chronic lower-back pain in the younger population [49]. Secondly, the study does not consider spinal load by computing the muscle forces as a function of body weight and waist circumference, which has been shown to affect flexion exercise [50], [51]. For male participants' physical activity levels were negatively correlated with their BMI and WHR values whereas for female participants' there was a negative correlation with their WHR, and a positive correlation with BMI. The positive correlation between BMI and physical activity level could be due to a more uniform BMI range in the female sample. We observed significant correlations between physical activity level and angular displacements in male subjects in all spinal segments for spine flexion, left and right spine lateral-bend, and few conditions in the spine side-twist. A positive (significant) with physical activity and flexion exercise for all the spine segments was observed in the female group. The absence of statistical significance in the female cohort for certain exercises could be due to smaller sample size and the possibility that flexibility in this cohort is due to higher estrogen levels [21] in the age group considered and, hence, independent of physical characteristics or activity. Overall, the outcomes from the correlations to spine angles are on expected lines, and it can be inferred that flexibility (as measured by the exercise routines) is primarily attributed to age (18-27 years) and physical activity like yoga and sports, which the participants mandated as per curriculum in the college. The seed-based correlation analysis resulted in a single cluster indicating minimal variation across the participants, confirming the role of age and health.

**Knee/hip joint kinematics:** The biomechanics of the hip, thigh muscles and the knee/ankle joints are essential in analyzing daily activities. In particular, the synchronous flexion-extension of several muscle groups ( quadriceps, hamstrings, glutes, abdominals and calves) is required for most daily activities (such as walking, stair climbing, kneeling, and squatting). The engagement of the erector spinae in addition to the hamstring muscles was also reported by [54] when testing runners. Because parallel squatting exercise demands both movement and stability, it is shown to be effective in developing muscle strength [40] and utilized to better understand flexibility by evaluating the RoM. The correlation analysis run on the male participant data showed that BMI was significantly negatively correlated with hip angular displacements, WHR was weakly positively correlated, and physical activity level was positively correlated. While in the female cohort, BMI, WHR, and physical activity level were all neg-

atively correlated with knee angular displacement. There was a difference in male and female's left and right knee angular displacements in the WHR/BMI grouping. This variation could be due to two physiological factors: an individual's center of gravity as a function of body weight and height, and body posture asymmetry. The studies [59] on the role of muscles to execute a squat could explain to a degree the surprising findings of normal BMI group having smaller angular displacements and range of motion than the overweight female group. Thomas et al., (1998) reported that women choose hip and knee movement patterns while men choose spine and knee movement pattern during reaching tasks that necessitate some forward bending of the trunk. Also, it is possible that females and males used different movement strategies as was observed during a single leg squat [55], [211], [219].

**Marker-based vs marker-less Single RGB system:** Clinical instruments such as inclinometer, inertial based sensing system, goniometer, and measuring tape used for measuring RoM require user expertise for data collection. Even the marker-based method necessitates meticulous camera and skeleton calibration procedures, the resulting data is considered as gold standard. But, motion capture systems are unfeasible in the clinical setting and require a large physical space. Practicable alternatives and inexpensive instruments are hence required by the health professionals for the motion assessment. Towards this, our study captured data from a RGB camera and compared the angles extracted from each method. The angle estimates by considering a single reference marker (lower lumbar) to observe the displacement of the cervical, thoracic, and lumbar spinal columns from the two techniques were comparable. This demonstrates that a single RGB camera and post-processing software (application) could be a viable marker-less motion capture technique for clinical applications with age/gender/exercise specific reference models developed using gold-standard techniques. Smartphones with embedded (Inertial, accelerometer, and gyroscope) sensors capable of detecting the joint position, measuring joint RoM, active cervical RoM [58] and active craniocervical RoM [149] have demonstrated robustness [171]. Hence, the RGB camera could be a viable motion capture technique for clinical applications based on clinical-level reference model.

## A.9 Conclusion

The estimated angular displacements measuring intersegmental motion in all three spinal segments and hip-knees segments contribute to the studies on spine biomechanics with data from an Indian population. The findings of this study also include simultaneous RoM of three spine segments, wherein previous studies have focused on a specific column (lumbar or thoracic). By considering a single reference marker to estimate the angular displacement of all other markers along the spine column, we address the problem of marker placement errors, on a suit. The in-depth analysis of physical characteristics and activity helps identify each factor's contribution to the spine/muscle flexibility. The models generated are more robust by analyzing the data captured from two techniques on the same participants. As a future scope, it would be interesting to investigate and extend this study to a larger and more di-

verse population and performing a greater number of trials for each exercise. Other physical parameters such as the torso and leg-length ratio, spine 'S' curvature, and length of the foot (short vs. long) can also be analyzed to understand better the height association with spine and knee/hip angular displacement. Also, with a better algorithm for pose estimation models mainly focusing on spine movement, the accuracies of angular displacements can be improved further.

## A.10 Limitations

A few factors limit this study, the first being that only young and healthy subjects participated in this experiment. Due to covid restrictions, data from older population and non-campus residents could not be collected. Although the angular displacements, estimated by both techniques, were in the predetermined range mentioned in [205], the suit worn by the participants introduces small errors. Increasing the number of mocap cameras could have minimized the marker detection error further. The angular displacements determined employing 3D human reconstruction using an RGB camera were comparable to the marker-based system spinal column angles. It is limited to capturing motion in specific exercises as we could not estimate the motion of spine axial rotations (twists). Lastly, we have used a single metric for physical activity, while a break up into endurance, strength and flexibility training would help identify the effect of each on the spine biomechanics.

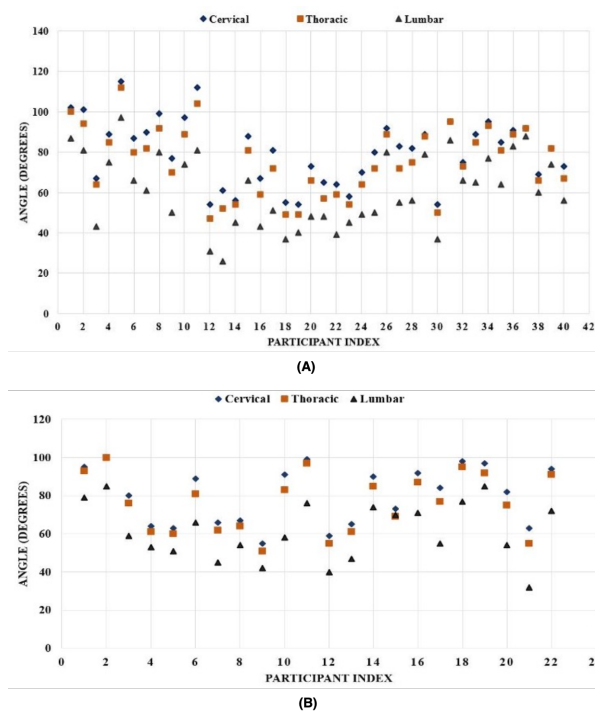


**Figure A.7** Participant wise distribution of spinal column angles using marker-based motion capture for spine flexion exercise in (A) Males (B) Females.

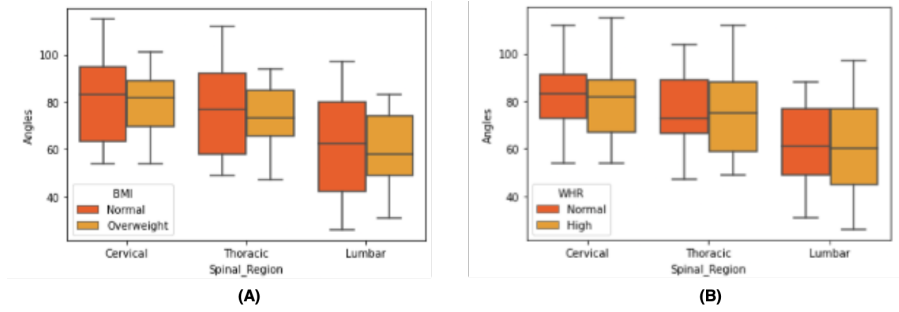


**Figure A.8** Spinal columns' angle distributions for flexion for male participants based on (A) BMI (B) WHR

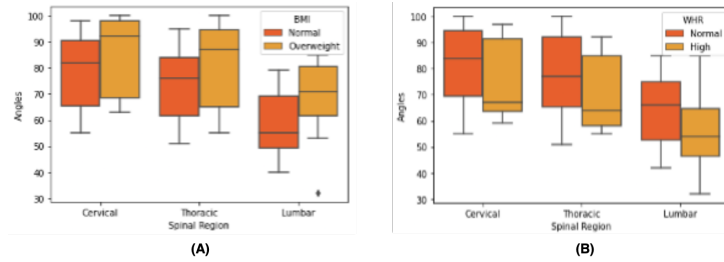


**Figure A.9** Spinal columns' angle distributions for flexion for female participants based on (A) BMI (B) WHR

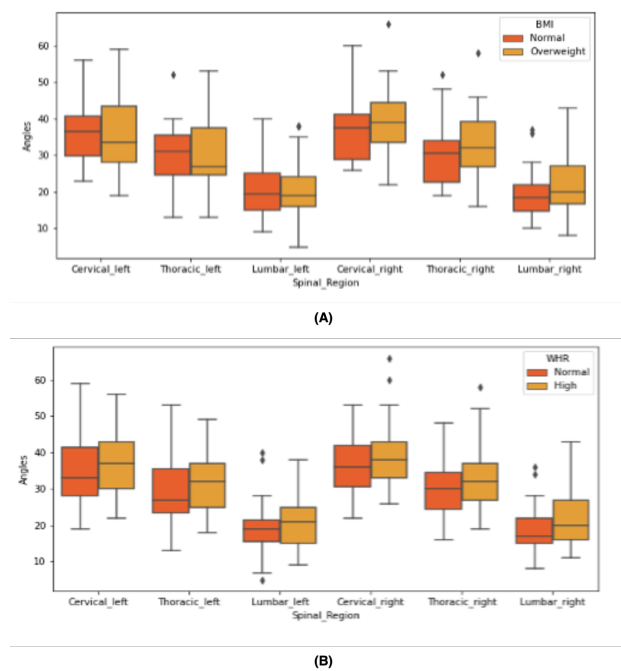


**Figure A.10** Spinal columns' angle distributions for lateral bend for male participants based on (A) BMI (B) WHR

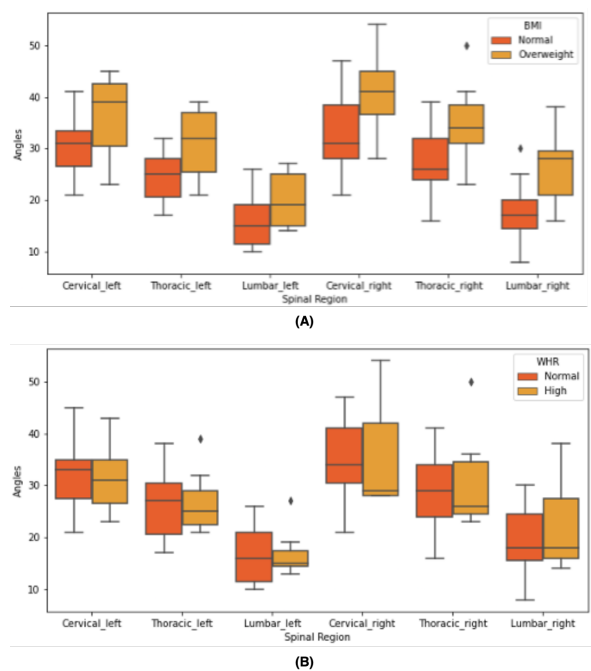


**Figure A.11** Spinal columns' angle distributions for lateral bend for female participants based on (A) BMI (B) WHR

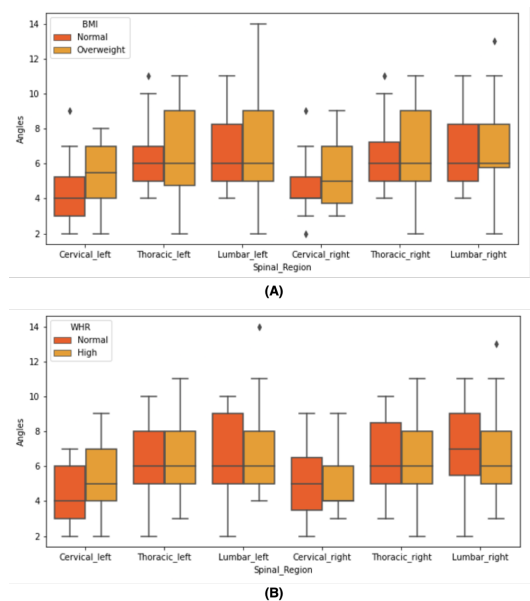
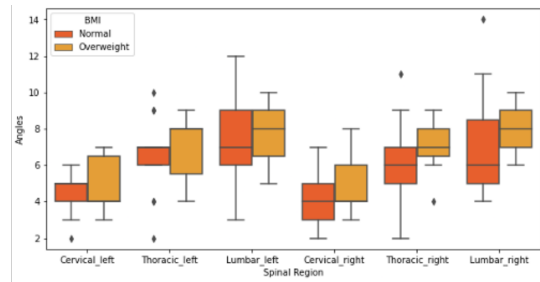
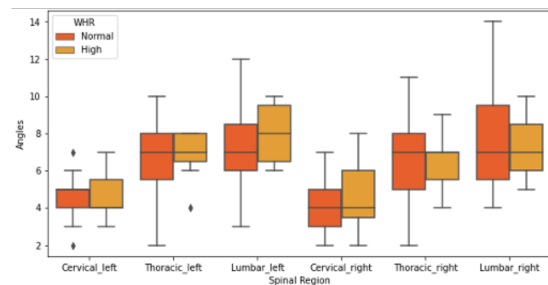


**Figure A.12** Spinal columns' angle distributions for side-twist for male participants based on (A) BMI (B) WHR

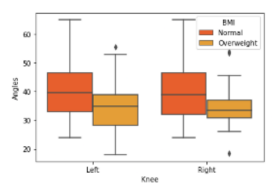


(A)

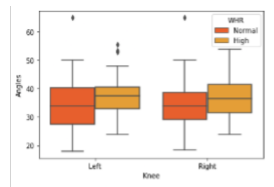


(B)

**Figure A.13** Spinal columns' angle distributions for side-twist for female participants based on (A) BMI (B) WHR

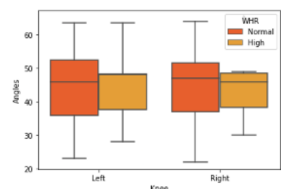


(A)

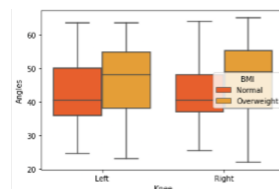


(B)

**Figure A.14** Knee/hip angle distributions for squats for male participants based on (A) BMI (B) WHR



(A)



(B)

**Figure A.15** Knee angle distributions for squats for female participants based on (A) BMI (B) WHR

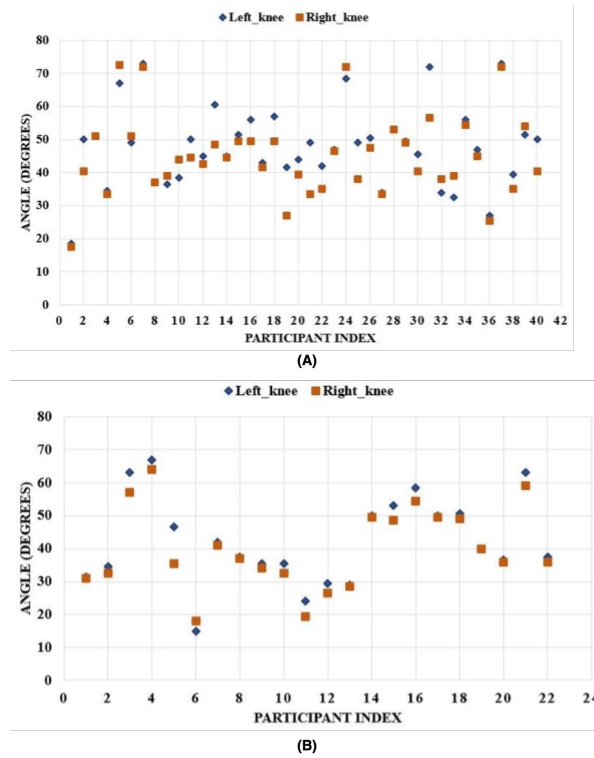


**Figure A.16** Participant wise distribution of knee/hip angles estimated using marker-less RGB motion capture system for squats exercise in (A) Males (B) Females

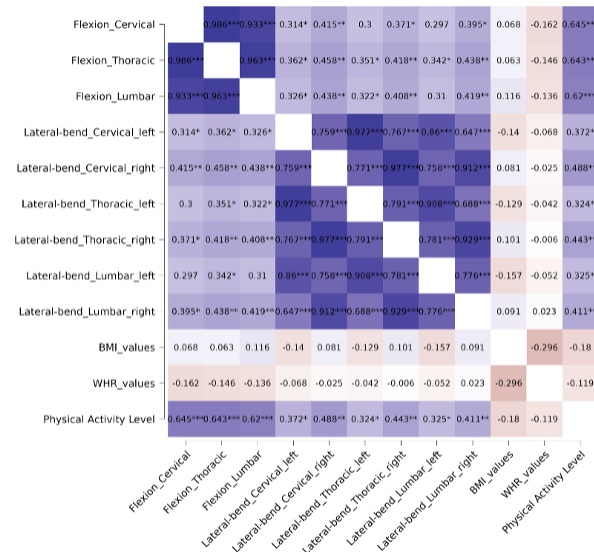


**Figure A.17** Spearman's correlation matrix for spine flexion, lateral-bend and physical parameters for males

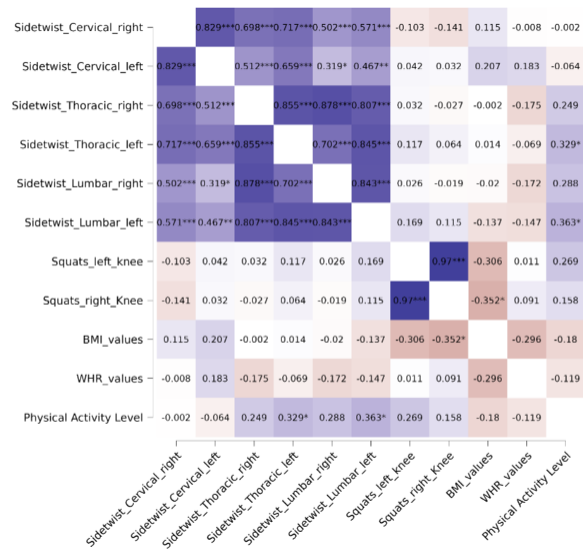


**Figure A.18** Spearman's correlation matrix for spine side-twist, squats and physical parameters for males

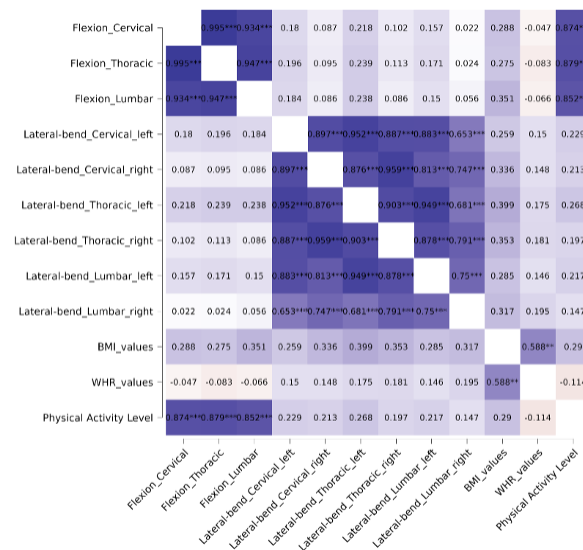


**Figure A.19** Spearman's correlation matrix for spine flexion, lateral-bend and physical parameters for females

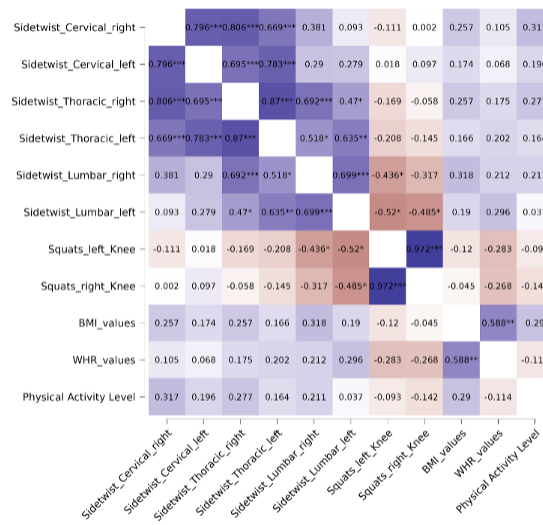


**Figure A.20** Spearman's correlation matrix for spine side-twist, squats and physical parameters for females

## **Response to Reviewers**

### **Thesis Reviews/Suggestions**

#### **Comments/Suggestions by Examiner 1**

**1. EEG Microstates During Motor Movements in case of tip Pinch and Wrist Flexion-Extension is studied.**

**Ans :** To the best of our knowledge, EEG Microstate analysis has been applied on reaching and grasping tasks (including tip-pinch) in literature but not on Wrist flexion and extension. We have studied the EEG microstates for Tip-pinch as well as Wrist flexion & extension motor movement before, during, and after performing the exercises.

**2. Clustering and TFA approaches are used in this study.**

**Ans :** Yes, Clustering procedure was used for extraction of Microstates. TFA methods was applied on EEG signals.

**3. Extra work mentioned in chapter 6 may be moved to appendix or include that in the main work itself.**

**Ans :** Yes, it has been moved to Appendix section.

**4. Publication attempts are fine.**

**Ans :** Thank you sir.

## Comments/Suggestions by Examiner 2

1. **Chapters 2 and 3 combine background literature review and specific Results on the experiments conducted as well. This leads to confusion. Suggestion is to describe the whole pipeline of data pre-processing and microstate extraction adopted in the thesis – the specific choices taken from the various reviewed methods (in Chap 2 and 3), the rationale for the choices, the results obtained and their implications in Chapter 4 where they describe more results. This is a suggestion but please think of another way to distinguish literature review from specific results.**

**Ans :** Yes, we have made the suggested valuable changes to chapters 2 and 3. Chapter 2 has the following content to explain microstate analysis. Sections 2.1 – 2.7 mention established literature on microstates. Section 2.8 comprises the microstate analysis of our dataset based on the literature review. Chapter 3 explains various signal processing techniques applied on EEG signals. Section 3.1 – 3.5 mention established literature on various techniques. Section 3.6 comprises the application of SFF on our dataset.

2. **The citations of references in the main text is non-standard – either follow APA format (name and year format) or IEEE format (numbered references, arranged either alphabetically or order of occurrence)**

**Ans :** Apologies for the mistake, I have made the required changes in the thesis.

3. **Bibliography section needs to be re-organized as per the plan (APA or numbered IEEE), bulleted, unsorted list is not standard format. Many references are incomplete (Journal name missing, etc.). Arhant Jain reference appears twice, similarly Michel & Koenig reference repeats. Please thoroughly check and use latex bib formats where available if you're using Latex for thesis formatting.**

**Ans :** Apologies for the mistake, I have made the required changes in the thesis.

4. **Where figures are reproduced from literature, please indicate this in the caption of the figure (explicitly citing the ref.). Are Figs 2.2 and 2.4 from the literature or your own data? If it's from your data, suggest to move to a later chapter?**

**Ans :** The generated plots/figures are originated from our dataset and have been included only as an example to illustrate the theoretical process of extraction. The figures attached are related to the Chapter 2. However, I have moved Fig 2.4 to section 2.8.1 and added a sentence in thesis for better clarity in case of Fig. 2.2.

5. **Page 5-6: section 1.6 does not include Chapter 6? The thesis seems to focus on EEG microstates for hand movements but suddenly goes into posture and markerless spine kinematics measurement that is not motivated earlier in Chapter 1-3 and not properly connected to the rest of the thesis. These links need to be put make the transition logical and smooth.**

**Ans :** I added the work on spine kinematics in thesis, as this was my core research problem statement – extending to patients & older adults – but it had to be stopped due to covid & the 2-year restrictions on human data collection. The first part of the data was collected on students during the phases when covid restrictions were relaxed a bit. My team member Harsh Sharma submitted this part for his thesis. I added this chapter to show the volume of work done towards my MS thesis. After consulting my guide, I have moved the paper to the Appendix. Also, the spine kinematics paper is published while the microstates paper is under review in a journal. Given the condition for paper publication by the PG Cell, I had to include the spine work to get my thesis to review process.

6. **Current chapter 5 and 6 should be swapped so that the Conclusion chapter is the last chapter. Conclusion chapter needs elaboration. Summary of the two major focus areas of EEG microstates and Spine Kinematics, Major outcomes, Limitations, and Future scope that covers both the focus areas.**

**Ans :** The primary emphasis of this thesis is only on the study of EEG Microstates, with Spine Kinematics being included as an additional work in the appendix. Incorporating the Spine Kinematics study would result in a significant extension of the thesis. Hence, content related to Spine Kinematics is relocated to the Appendix/Supplementary section.

7. **Pg 29: Fig 2.4 is neither referred in the text nor described and discussed in the text.**

**Ans :** It is described and referred to in the section 2.8.1.

8. **Pg 46, Section 3.5.3: Chapter 3 shows several boxplots for various electrode activity over 29 participants for each movement. It's claimed that ipsilateral electrodes show more fluctuations as compared to contralateral side any statistical tests done to support this or are these qualitative observations**

**Ans :** These plots are included to show the inter-subject differences. Only general qualitative observations are made. No statistical tests have been conducted to provide support for this as the major focus is on microstate analysis.

9. **Pg 52: “EEG signals captured for movements have consistent changes in 8-12 Hz (alpha band).” Generally motor activity is found in beta band (15-30 Hz), have they looked at the time-frequency plots to determine which frequency band the power resides in each epoch?**

**Ans :** Yes, most literature reports motor in the 15-30Hz, but we also found it in the 8-12Hz. This has been attributed to the process leading to the execution of the motor task predominantly. But in support of the mentioned statement I hereby attach some corroborating findings :

- **From Arhant's Thesis :** EEG signals captured while performing different types of limb movements like finger tapping, arms moment, flexion, clenching, and natural gestures have shown consistent changes in the 8–12 Hz (alpha band) and 13–28Hz (beta) which were

found using the single-frequency method (introduced by : Yegna et al.). In Arhant's work, the pre-event to post event analysis was not applied. It was taken as one event block.

- **From Wang, T., Deng, J., & He, B. (2004). Classifying EEG-based motor imagery tasks by means of time–frequency synthesized spatial patterns. *Clinical Neurophysiology*, 115(12), 2744-2753 :** “It has been found that planning and execution of movement leads to a short-lasting and circumscribed attenuation in the mu (8–12 Hz) and the central beta (13–28 Hz) rhythm known as event-related (de)synchronization (ERD/ERS) which has played an important role in BCI study (Pfurtscheller and Neuper, 2001).”

10. **Pg 55: Fig 4.3 gives the task structure. It appears that 20 trials of tip-pinch with a 10 sec break followed by 20 trials of wrist movement. Is the order counterbalanced across participants? Do they perform multiple repetitions of the movement within a 2-sec trial? Are these paced similarly across participants? Is wrist flexion a separate trial from wrist extension or this is a combined movement?**

**Ans :** Yes, the order is counterbalanced across the participants. No, they do not perform multiple repetitions of the movement within a 2-sec trial. They perform the exercise only once in the 2-sec window for tip-pinch and 3-sec window for wrist-flexion & extension. Yes, they are paced similarly across participants. Wrist flexion is not a separate trial from Wrist extension, it is a combined movement where execution of flexion is followed by extension only once in the window of 3 seconds.

11. **Pg 56: Time locking of trials was mentioned (6 for pinch and 7 for wrist), how are these epochs time locked to onset of movements as this is critical to identify pre-, during- and post-movement periods.**

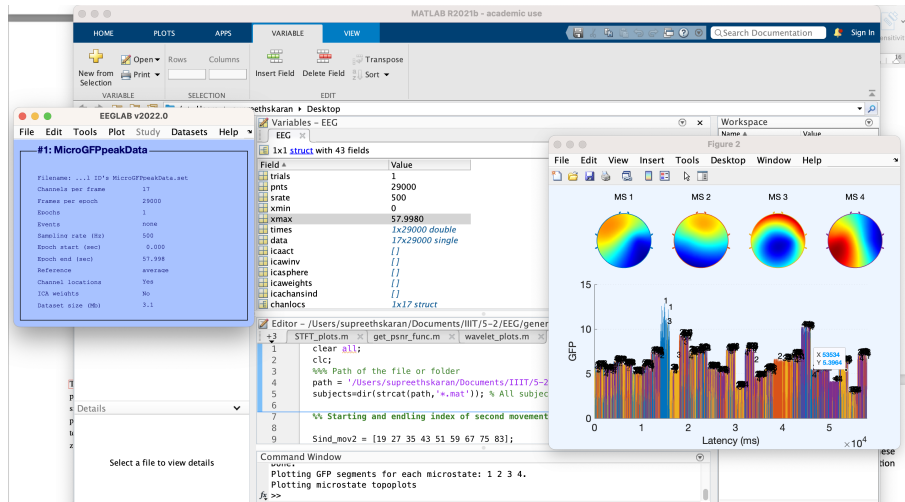
**Ans :** Based on the experimental paradigm, we have aligned the timestamps of each exercise with their corresponding trial durations. The epoch time noted in our observations has been matched with the recorded time for each exercise. For Tip-Pinch of 6s duration – we considered 2s (pre-event), 2s (event), 2s (post-event). For Wrist Flexion & Extension of 7s duration – we considered 2s(pre-event), 3s (event), 2s (post-event). The experimental paradigm with longer duration for executing the movement was designed to serve as a reference model for the purpose of acquiring data from stroke patients.

12. **Pg 60: Fig 4.8 depicts microstates over 60s latency. How are these arrived at what do a-d correspond to (this needs to be written in the caption), why 60s chosen and how does this relate to the trial structure of 6 or 7 secs? The text below distinguishes between states (3) and microstates (4), what are states?**

**Ans :** The label for the pre-event, event post-event is ‘condition’ while states refer to the microstates. Sorry for this confusion, required changes have been done in the thesis. Microstate topographies (A-D) are explained in the caption mentioned below:

Updated caption is : GFP of the active microstates for (a) Left wrist flexion & extension (b)

Right wrist flexion & extension (c) Left Tip-pinch (d) Right Tip-Pinch. The x-axis shows the GFP latency in the entire time range (milliseconds) of the complete EEG motor-task dataset for 29 participants and y-axis shows the peak potential field strength (GFP peaks) of the four active microstates at that time. These values are arrived as shown in the snapshot. The combined epoch



range of 29 participants ranges from 0s(epoch start) - 57.9980s (epoch end). The states are now referred to as conditions. Three conditions are considered (pre-event, event and post-event).

13. **Pg 60:  $RS_{MS}$  resting state microstate is mentioned, how are they defined? Are these defined from the pause between actions or does this correspond to post-action period? These details are not given.**

**Ans :** The  $RS_{MS}$  were not extracted from our data; it is predominantly from Koenig's work. Other studies have confirmed the states and identified more number. The canonical maps for resting state have been defined in the literature by Koenig. We have followed the Koenig's methodology and applied it to motor tasks. In Koenig's paper, 19-electrode (10/20 positions) EEG, with closed eyes resting condition was recorded. We are comparing our motor task microstate topographies with Koenig's established resting state microstate topographies in literature.

14. **What do Figs 4.9-12 depict – X-axis and Y-axis? How are these related to the plots in Fig 4.8?**

**Ans :** In the figures 4.9-12, the Y-axis represents the GEV value of the respective sample in the segmentation at an instant and the X-axis represents the total time of the given epoch. The global explained variance (GEV) is the sum of explained variances of each microstate weighted by the global field power(GFP). The integrated electrical activity in a topographical map of electric potential may be quantified using Global field Power by computing a form of spatial standard deviation. Figure 4.8 shows the GFP values of the active microstates for all motor movements and the figures 4.9-12 show the GEV values for all motor movements.

15. **How is the mapping between various microstates in different actions and Koenig's resting state microstates (shown in the last column) arrived at qualitatively?**

**Ans :** The Motor-tasks topographies/maps obtained in our study and the Resting-state maps already established in the literature are visually inspected and qualitatively contrasted, considering the different intensities (heatmaps). I visually compared the topography of each motor-task to the four canonical resting-state maps to determine if any of them matched. If similarity between the motor-task and the resting-state map could be detected, I classified them as similar.

16. **From Pg 63 till Pg 70 refer to Tables 6.4-6.42 which are in the supplementary. The table numbering needs to change to identify that are not in Chapter 4. Also, now real accessible summary of all these results and their implication is given in the main text.**

**Ans :** Apologies for the mistake, I have made the required changes in the thesis.

17. **It is not clear what actually the several spider plots shown in Chapter 4 depict and how are the values normalized is not clearly explained.**

**Ans :** A Spider plot is generated for each microstate parameter — Occurrence, Duration, and Coverage — for each exercise. Each spider plot illustrates the differences in microstate parameter values of the four microstate classes across pre-event, event, and post-event conditions for an exercise. For instance, the spider plot for the Occurrence Parameter illustrates the differences in the occurrence values across the three conditions for its respective microstate classes. This applies to the Duration and Coverage parameters as well. There is no need for normalisation of microstate parameter values that are plotted in the spider plot because :

(a) We have statistically compared each microstate class's values only across conditions (pre-event, event, post-event) of a parameter for an exercise. For instance, we compared MS1 only across pre-event—event, event—post-event, and pre-event—post-event groups in occurrence parameter for the left wrist flexion/extension.

(b) The scale for all microstate classes MS1, MS2, MS3, MS4 for a parameter (say, occurrence) for an exercise (say, left wrist-flexion/extension) is same.